NORMAL FAULTING, VOLCANISM AND FLUID FLOW, HIKURANGI SUBDUCTION PLATE BOUNDARY, NEW ZEALAND

A thesis submitted in partial fulfilment of

the requirements for the Degree of

Doctor of Philosophy in Geology

in the University of Canterbury by

Hannu Christian Seebeck

Under the supervision of

Prof. Jarg R. Pettinga

Dr. Andy Nicol

Department of Geological Sciences
University of Canterbury

2012

Contents

CHAPTER 1 - Introduction

CHAPTER 2 - Fluid-flow in fault-zones from an active rift

CHAPTER 3 - Structural geometry and kinematics of the Taupo Rift, New Zealand

CHAPTER 4 - Seismicity of the Pacific plate beneath the North Island, New Zealand: The role of faulting in the hydration and dehydration of subducting lithosphere

CHAPTER 5 – Geometry of the subducting Pacific plate along New Zealand's Hikurangi margin since 20 Ma

CHAPTER 6 – Motion of the Australian and Pacific plates in relation to North Island, New Zealand

CHAPTER 7 – Conclusions and future research

APPENDIX

List of Tables

List of Figures

Chapter 1

Chapter 2

Chapter 3

Chapter 4

Chapter 5

Chapter 6

Chapter 7

Appendix

Acknowledgements

I would like to thank Andy for his patience, quiet direction, and guidance in the many years I have worked with him now. He has always had time for my questions, my many, many questions and that I am truly grateful for. I would like to thank Jarg for his understanding and support through challenging times.

Many others have contributed to the successful completion of this thesis, in particular the senior and principal scientists of GNS Science who have kindly contributed their precious time and valuable data to my investigations – Martin Reyners, John Ristau, Dick Beetham, Stephen Bannister, Matt Gerstenberger, Pilar Villamor, John Begg, Dougal Townsend, Julie Lee, Vaughan Stagpoole, John Beavan, Wiebke Heise and Laura Wallace have all helped bring my ideas into the light. Susan Ellis is also thanked for her kind words and support just when they were needed. Des Darby is thanked for his support in getting this thesis started and finished.

The Fault Analysis Group is thanked for their support and direction, the conversations with John Walsh, Marc Giba and Conrad Childs have always been stimulating and enlightening. Much of my real education has taken place on the Taranaki coastline in their company.

Spending time with the volcanologists of UC has also helped broaden my horizons, Ben Kennedy, Darren Gravely, Paul Ashwell, Felix Von Aulock, and Jim Cole have always made me feel welcome even though my visits haven't been as frequent as I would have liked. John and Catherine Ford are thanked for their hospitality and generosity in the field. My friends from VUW, Dan Bassett, Katrina Jacobs and Jess Johnson are thanked for their insights into the dark arts.

There is no question that without the support of my family none of this would have been possible and I'm very fortunate to have them looking after me. My wife Gretta has been by my side throughout this journey, her love, support and patience has been without measure. And of course there was the arrival of August, what a beautiful country he has to explore…

Abstract

This thesis investigates normal faulting and its influence on fluid flow over a wide range of spatial and temporal scales using tunnel engineering geological logs, outcrop, surface fault traces, earthquakes, gravity, and volcanic ages. These data have been used to investigate the impact of faults on fluid flow (chapter 2), the geometry and kinematics of the Taupo Rift (chapter 3), the hydration and dehydration of the subducting Pacific plate and its influence on the Taupo Volcanic Zone (chapter 4), the migration of arc volcanism across the North Island over the 16 Myr and the associated changes in slab geometry (chapter 5) and the Pacific-Australia relative plate motion vectors since 38 Ma and their implications for arc volcanism and deformation along the Hikurangi margin (chapter 6). The results for each of these five chapters are presented in the five paragraphs below.

Tunnels excavated along the margins of the southern Taupo Rift at depths < 500 m provide data on the spatial relationships between faulting and ground water flow. The geometry and hydraulic properties of fault-zones for Mesozoic basement and Miocene strata vary by several orders of magnitude approximating power-law distributions with the dimensions of these zones dependent on many factors including displacement, host-rock type and fault geometries. Despite fault-zones accounting for a small proportion of the total sample length (≤ 15%), localised flow of ground water into the tunnels occurs almost exclusively (≥ 91%) within, and immediately adjacent to, these zones. The spatial distribution and rate of flow from fault-zones are highly variable with typically ≤ 50% of fault-zones in any given orientation flowing. The entire basement dataset shows that 81% of the flow-rate occurs from fault-zones ≥ 10 m wide, with a third of the total flow-rate originating from a single fault-zone (i.e. the golden fracture). The higher flow rates for the largest faults are interpreted to arise because these structures are the most connected to other faults and to the ground surface.

The structural geometry and kinematics of rifting is constrained by earthquake focal mechanisms and by geological slip and fault mapping. Comparison of present day geometry and kinematics of normal faulting in the Taupo Rift (α=76-84°) with intra-arc rifting in the Taranaki Basin and southern Havre Trough show, that for at least the last 4 Myr, the slab and the associated changes in its geometry have exerted a first-order control on the location, geometry, and extension direction of intra-arc rifting in the North Island. Second-order features of rifting in the central North Island include a clockwise ~20° northwards change in the strike of normal faults and trend of the extension direction. In the southern rift normal faults are parallel to, and potentially reactivate, Mesozoic basement fabric (e.g., faults and bedding). By contrast, in the northern rift faults diverge from basement fabric by up to 55° where focal mechanisms indicate that extension is achieved by oblique to right-lateral strike-slip along basement fabric and dip-slip on rift faults.

Hydration and dehydration of the subducting Pacific plate is elucidated by earthquake densities and focal mechanisms within the slab. The hydration of the

subducting plate varies spatially and is an important determinant for the location of arc volcanism in the overriding plate. The location and high volcanic productivity of the TVZ can be linked to the subduction water cycle, where hydration and subsequent dehydration of the subducting oceanic lithosphere is primarily accomplished by normal-faulting earthquakes. The anomalously high heat flow and volcanic productivity of the TVZ is spatially associated with high rates of seismicity in the underlying slab mantle at depths of 130-210 km which can be tracked back to high rates of deeply penetrating shallow intraplate seismicity at the trench in proximity to oceanic fluids. Dehydration of the slab mantle correlates with the location and productivity of active North Island volcanic centres, indicating this volcanism is controlled by fluids fluxing from the subducting plate.

The ages and locations of arc volcanoes provide constraints on the migration of volcanism across the North Island over the last 20 Myr. Arc-front volcanoes have migrated southeast by 150 km in the last 8 Ma (185 km since 16 Ma) sub-parallel to the present active arc. Migration of the arc is interpreted to mainly reflect slab steepening and rollback. The strike of the Pacific plate beneath the North Island, imaged by Benioff zone seismicity (50-200 km) and positive mantle velocity anomalies (200-600 km) is parallel to the northeast trend of arc-front volcanism. Arc parallelism since 16 Ma is consistent with the view that the subducting plate beneath the North Island has not rotated clockwise about vertical axes which is in contrast to overriding plate vertical-axis rotations of $\geq 30^{o}$. Acceleration of arc-front migration rates (~4 mm/yr to ~18 mm/yr), eruption of high Mg# andesites, increasing eruption frequency and size, and uplift of the over-riding plate indicate an increase in the hydration, temperature, and size of the mantle wedge beneath the central North Island from ~7 Ma.

Seafloor spreading data in conjunction with GPlates have been used to generate relative plate motion vectors across the Hikurangi margin since 38 Ma. Tracking the southern and down-dip limits of the seismically imaged Pacific slab beneath the New Zealand indicates arc volcanism in Northland from ~23 Ma and the Taranaki Basin between ~20 and 11 Ma requires Pacific plate subduction from at (or beyond) the northern North Island continental margin from at least 38 Ma to the present. Pacific plate motion in a west dipping subduction model shows a minimum horizontal transport distance of 285 km preceding the initiation of arc volcanism along the Northland-arc normal to the motion vector, a distance more than sufficient for self-sustaining subduction to occur. Arc-normal convergence rates along the Hikurangi margin doubled from 11 to 23 mm/yr between 20 and 16 Ma, increasing again by approximately a third between 8 and 6 Ma. This latest increase in arc-normal rates coincided with changes in relative plate motions along the entire SW Pacific plate boundary and steepening/rollback of the Pacific plate.

Chapter 1

Introduction

1. Introduction and aims of study

The origins of continental intra-arc rifting and associated volcanism and the impact of normal faults on fluid-flow are the focus of this thesis. The Taupo Rift and arc volcanism provide the common threads that run through the thesis, which draws on information from a wide range of scales and over a large geographic area. Rifting and arc volcanism are controlled by subduction processes and a key goal of this thesis is to cast further light on the evolution of subduction beneath the North Island of New Zealand. Improved understanding of subduction is important because it provided a first-order control on the tectonics, sedimentation patterns, and land mass evolution of the North Island for at least the last 30 Myr. In addition to addressing regional plate boundary processes consideration has been given to faults and their role in the flow of fluids. Faults are widely considered to both enhance and retard fluid and gas flow (Wallace & Morris, 1986; Caine et al., 1996; Evans et al., 1997; Cox, 1999; Wibberley et al., 2008; Faulkner et al., 2010; Manzocchi et al., 2010; Ilg et al., 2012), yet in many cases the details of how, where and why this occurs has not yet been resolved. Providing answers to these fundamental questions is of importance to a wide range of industries including; geothermal, oil and gas, CO_2 storage and groundwater. The role of faults in fluid-flow is studied here using a rare dataset in which both fluid-flow rates and fault information are available from tunnels excavated along the margin of the Taupo Rift in the central North Island.

Rifting has occurred in the North Island region since ~12 Ma. The locus of rifting migrated southeast towards the Hikurangi margin front and subducting plate, culminating in the formation of Taupo Rift (Fig. 1). The Taupo Rift is in the central North Island and produced a ~300 km NE-trending regional graben over the last ~2 Ma. The rift is spatially coincident with arc volcanism in the Taupo Volcanic Zone (TVZ), a region that contains one of the most frequently active and productive silicic volcanic arc systems on Earth (Wilson et al., 2008) (Fig. 2). Intra-arc rifting and explosive caldera

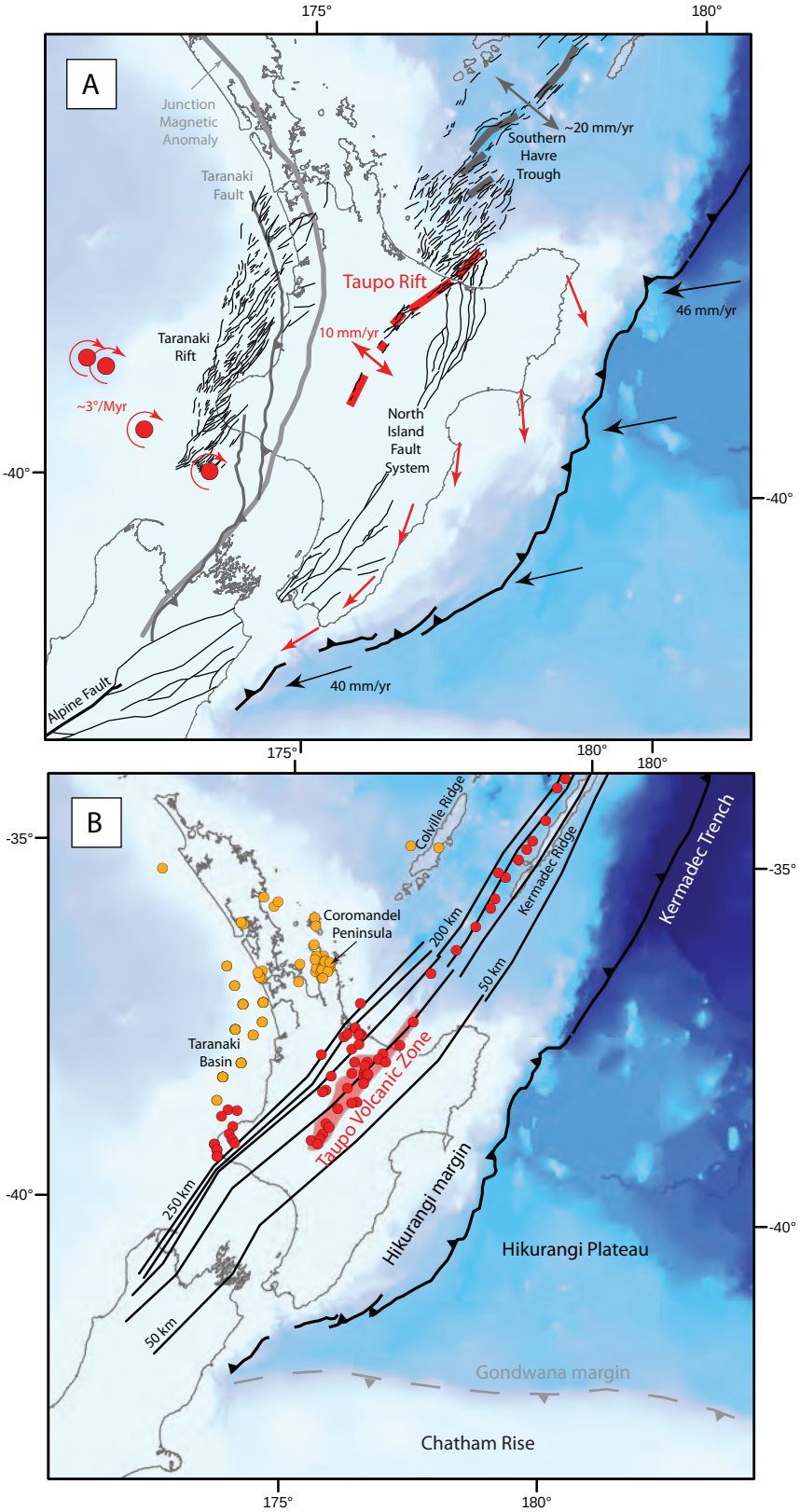

Figure 1. Tectonic and volcanic setting of the Taupo Rift and Taupo Volcanic Zone. A) Intra-arc normal faults of the Taranaki and Taupo Rifts formed over the last 4 Ma with respect to present day poles of rotation (red filled circles) for fore-arc micro-plates of the eastern North Island (Wallace et al., 2012). See chapter 3 for references. B) Arc volcanism in the North Island. Arc volcanism over the last 2 Ma (red filled circles) has similar trends to active arc volcanism between 17-8 Ma (orange filled circles), both of which are sub-parallel to the trend of the underlying slab. See chapter 5 for references.

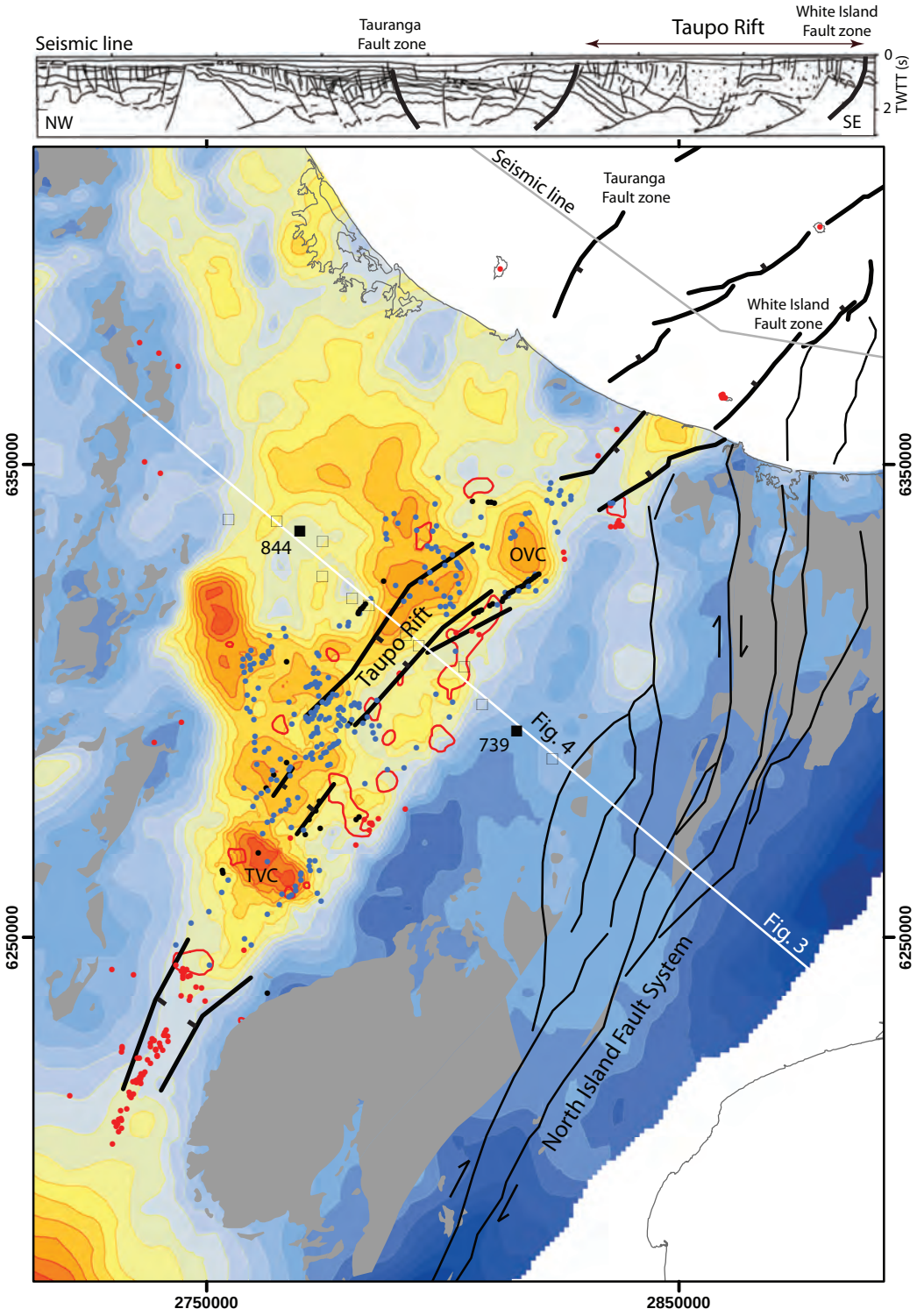

Figure 2. Structure of the Taupo Rift and Taupo Volcanic Zone. Rift bounding faults (heavy black lines) and volcanic vents (andesite/dacite = red filled circles, rhyolite = blue filled circles) super imposed on residual gravity (see chapter 3 for data and methods). Basement depressions < 2 km deep represented by warm colours, near surface Mesozoic besment (grey shading) represented by cool colours. Active rhyolitic calderas (Taupo (TVC) and Okataina (OVC) Volcanic Centres) bound the highly productive and frequently active central rhyolitic segment of the TVZ (Wilson et al., 1995, 2008). High effective heat through geothermal systems (red lines) is mainly focused in the east (Bibby et al., 1995). Asymmetry of the rift (extension rates increasing west to east) is shown by seismic line (grey line) (Davey et al., 1995). Location of Fig. 3 and 4 cross sections shown.

forming arc-volcanism occur in the overriding Australian Plate for over 1000 km along the Tonga-Kermadec trench and the Hikurangi margin. While arc volcanism and intra-arc rifting are spatially coincident and both result from subduction (Fig. 3 and 4), processes associated with their formation and development are often considered independently. The geometric evolution of the subducting slab beneath the North Island, the structural geometry and kinematics of the Taupo Rift in relation to intra-arc rifting over the last 4 Ma, and the high productively of TVZ arc volcanic systems, are all related and presently unresolved questions. Using mainly fault and earthquake constraints, this study focuses on the structural geometry and kinematics of the Taupo Rift and fault-fluid-flow systems associated with the formation of the TVZ.

The main objectives of this study are two fold: i) regional investigations into the key processes resulting in the development and evolution of the Taupo Rift and TVZ and, ii) detailed generic studies of faults and fluid-flow with application to the Taupo Rift and Hikurangi margin. The history of the Taupo Rift and spatially coincident TVZ is broadly known (Wilson et al., 1984; Stern, 1987; Cole, 1990; Wright, 1992; Bibby et al., 1995; Davey et al., 1995; Wilson et al., 1995; Parson & Wright, 1996; Rowland & Sibson, 2001; Acoccella et al., 2003; Carter et al., 2003; Lamarche et al., 2006; Stern et al., 2006; Wilson et al., 2008; Stern, 2009). However, many first-order processes associated with their structural and volcanic evolution are still presently debated. This study mainly employs new and published fault and earthquake data to examine processes relating to the origin and kinematics of the Taupo Rift and Taupo Volcanic Zone. In chapter 2 the relationships between fault-zone architecture, permeability, and fluid-flow properties from two contrasting lithologies are examined using *in situ* measurements from the tunnels of the Tongariro Power Development project in the southern Taupo Rift (Beetham & Watters, 1985). Conceptual models of faults and their permeability structure adopted over recent years (Caine et al., 1996) do not adequately represent the heterogeneity seen in fault-zone structure in Miocene sandstones or Mesozoic basement. Fluid flows from basement fault-zones are highly variable over four orders of magnitude in scale (centimetres to kilometres) and have distributions similar to critically stressed percolation networks (Sanderson & Zhang, 1999).The observations and conclusions of chapter 2 will be of interest to geothermal, CO_2 sequestration and hydrocarbon industries.

Analysis of predominantly normal faulting in this thesis uses constraints from regional and global earthquake catalogues, mapped fault patterns, gravity, geological

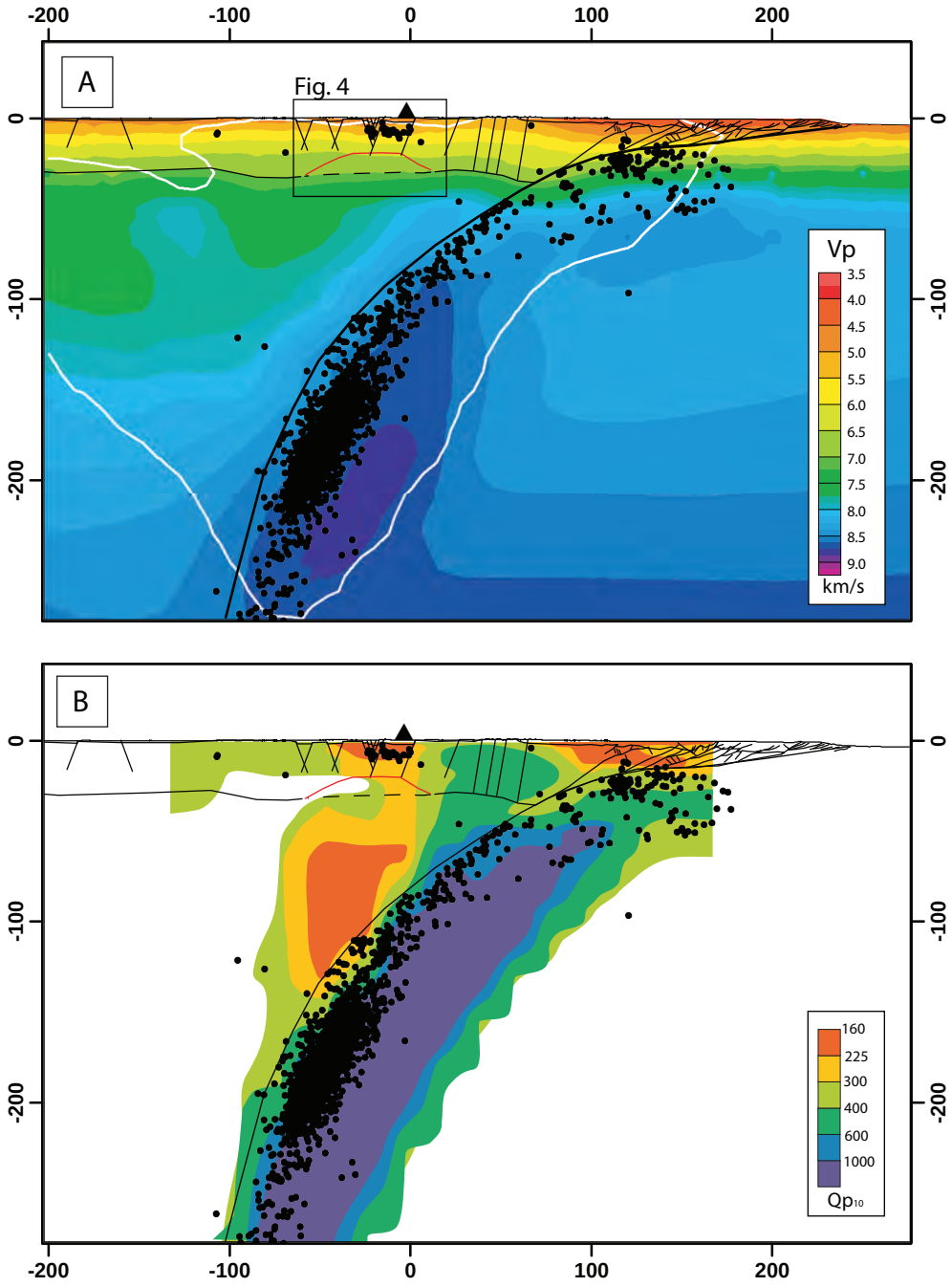

Figure 3. Geophysical cross sections through the central North Island. See Fig. 2 for location of sections. A) P-wave velocity (Vp) of the Hikurangi subduction margin from Eberhart-Phillips et al. (2010) with relocated GeoNet seismicity (black filled circles) and interpretation of crustal structure and faults (thin black lines) derived Bannister et al. (2004), Stern et al. (2006), Townsend et al. (2008), Barnes et al. (2009), Lee et al. (2010), Leonard et al. (2012). B) P-wave attenuation (Qp) structure from Eberhart-Phillips (2008). High Qp (low attenuation) is associated with the cold dense Cretaceous slab while low Qp (high attenuation) features are related to high temperatures and fluid content in the mantle wedge. A strong gradient in Qp indicates a change in the rheology of the mantle wedge coincident with arc front volcanism and rifting.

engineering tunnel logs, and outcrop data collected in the Taupo Rift and beneath the Hikurangi margin. Applied and generic studies here focus on different scales and aspects of faulting directly or indirectly associated with extension in the Taupo Rift and volcanism in the TVZ. For example, arc volcanism and geothermal activity in the TVZ are a direct result of fluid-flows into and out of the subducting slab where faults are considered the primary conduits (Gill, 1981; Kirby et al., 1996; Hacker et al., 2003; Faccenda et al., 2009). Hence, improved understanding for the role of faults in key subduction related processes provides information about the subduction system, intra-arc rifting, and fluid-flow along the Hikurangi margin. Each of the thesis chapters considers different aspects of faulting and these are: chapter 3 determines the structural geometry and kinematics of the Taupo Rift in relation to subduction processes, chapter 4 examines the distribution of earthquakes in the subducting plate in relation to the location and productivity of arc volcanism along the Hikurangi margin, chapter 5 uses constraints from present-day Benioff zone seismicity and volcanic arc age data across the North Island to reconstruct the spatial and temporal evolution of the subducted Pacific Plate, and chapter 6 reviews present tectonic plate reconstructions in relation to subduction beneath the North Island.

The TVZ is New Zealand's primary geothermal energy resource where numerous high temperature (> 300ºC) geothermal systems are located along its eastern boundary, predominantly west of the Taupo Rift (Fig. 2 and 4). The effective heat flow from the central rhyolitic segment of the TVZ is 8 to 14 times greater than through typical continental crust and back-arc rifts (Stern, 2009). In the TVZ recent investment in pre-existing geothermal fields aimed at improving and developing production capacity through targeted drilling (Rosenburg et al., 2009) has begun to focus on the permeability structure of the basement which is predominantly fracture controlled (Braithwaite et al., 2002). This study, which has its main focus on faults and fluid-flow, aims to improve our understanding of the origin and evolution of the Taupo Rift and TVZ, an outcome which could be of significant value to scientific and exploration purposes.

This introductory chapter presents a short summary of previous research on normal faults, details the geological background of the Taupo Rift and TVZ, the data used in this study, and briefly outlines the structure of the thesis.

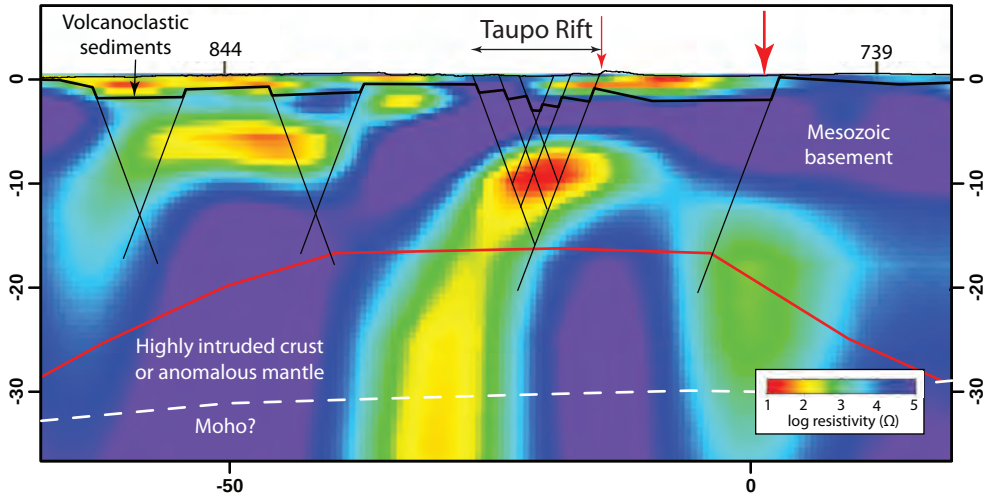

Figure 4. Electrical conductivity across the Taupo Rift. Electrical structure of the central North Island based on magnetotelluric (MT) soundings of Heise et al. (2010). Basement structure based on surface fault traces and gravity data from New Zealand Gravity Station Network complemented with new stations collected in this study and presented in chapter 3. Faults generally dip at > 70º at the surface and are inferred shallow with depth (Villamor & Berryman, 2001). Faults shown here dip 70º. At shallow depths (< 8 km) low resistivities (warm colours) are associated with alteration of volcaniclastic deposits infilling basement depressions. Below the seismogenic crust (> 8 km) low resitivities are interpreted as connected melt (Heise et al., 2010). Geothermal systems (red arrows) (Bibby et al. 1995) are generally located east of active rifting, see Fig. 2 for location. Base of the quartzofeldspathic crust (red line) from Stern et al. (2006).

2. Previous Research

Due to the importance of normal faulting for earthquake processes, mineral and hydrocarbon exploration, previous research includes a vast array of studies ranging from outcrop to plate boundary scales and from fault mechanics to fault-system evolution. Whilst the broad scope of fault research cannot be outlined in this chapter, aspects of normal faulting relevant to this study are briefly introduced below.

2.1 Faults and Earthquakes

Faults and earthquakes are two inter-related phenomena which are widely encountered in plate boundary regions such as New Zealand. Faults record the accumulation of strain during repeated earthquake cycles over millions of years (Nicol et al., 2005; Nicol et al., 2006; Nicol et al., 2010). The spatial and temporal patterns of faults and earthquakes, such as surface traces (chapter 3) or magnitude-frequency relations (chapter 4), provide key information on plate boundary and brittle deformation processes. Fault systems are kinematically coherent (i.e. all faults in the system interact with each other) on geological and earthquake timescales (Walsh & Watterson, 1991; Nicol et al., 2010). A type example for kinematically coherent fault arrays are analogue sand box models of rifting (McClay & White, 1995; McClay et al., 2002). Here, a range of fault orientations and segmentation styles develop in response to different boundary conditions imposed for each model (i.e. the obliquity of extension direction with respect to the rift axis and/or pre-existing structures) (McClay et al., 2002). While displacement (both vectors and magnitude) may be highly variable along individual faults, this variability decreases when considered at the scale of the fault system resulting in coherent and potentially predictable displacement patterns (Marrett & Allmendinger, 1990; Walsh & Watterson, 1991). This type of kinematic coherence has been demonstrated for fault displacement rates in the Taupo Rift for example. Here displacement rates on major faults across the rift are highly variable over short time scales whereas over increasing spatial and temporal scales displacement rates become more uniform (Nicol et al., 2006). The kinematics of the Taupo Rift are investigated over a range of scales in chapter 4.

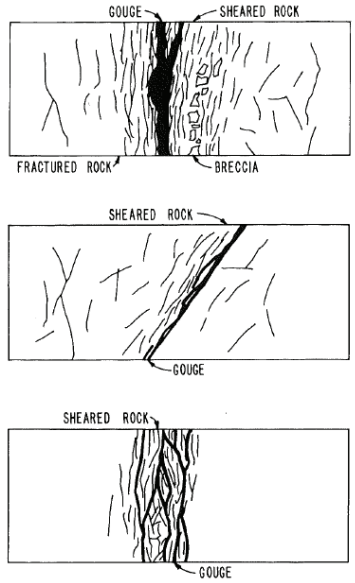

A Wallace & Morris (1986)

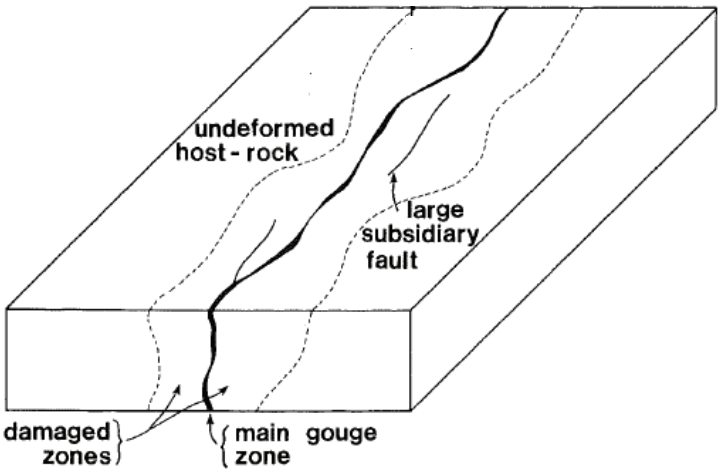

B Chester & Logan (1986)

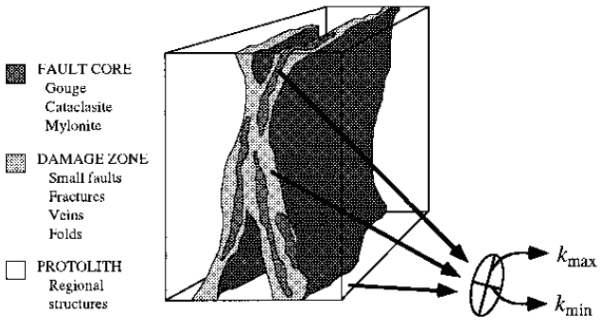

C Caine et al. (1996)

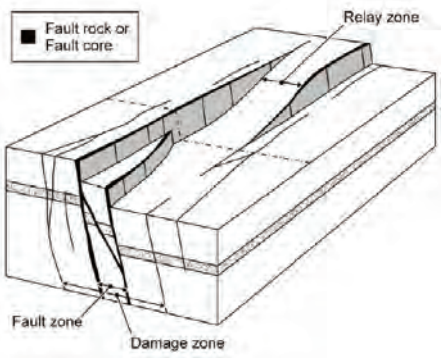

D Childs et al. (2009)

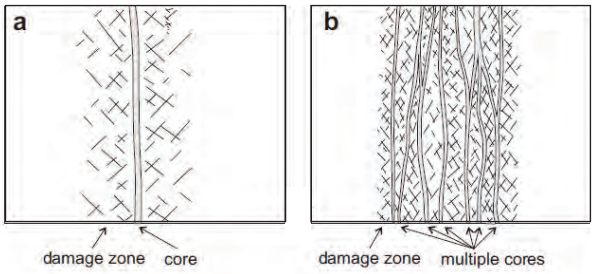

E Faulkner et al. (2010)

Figure 5. Conceptual models of fault-zone structure. A) Subsurface model of Wallace & Morris (1986). B) Mechanical model of Chester & Logan (1986). C) Two component model of Caine et al. (1996). D) Geometric model of Childs et al. (2009). E) Single and multiple strand model of Faulkner et al. (2010).

2.2 Fault-zone architecture

Documenting fault-zone architecture is important for understanding fluid-flow and fault-zone evolution. Faults typically show highly complex internal structures (Wallace & Morris, 1986; Wibberley et al., 2008; Childs et al., 2009; Faulkner et al., 2010) as opposed to comprising a single planar slip surface (Fig. 5 and 6) (Caine et al., 1996) (chapter 2). Irregularities and asperities on fault surfaces are observed on a wide range of scales (Wallace & Morris, 1986) and are considered mainly due to the propagation and linkage of fault segments through mechanically heterogeneous layered sequences (Childs et al., 2009). As displacement accumulates within a fault-zone, the linking and by passing of fault surface irregularities (e.g., relay zones) progressively straightens and localises fault surfaces, resulting in a heterogeneous distribution of finite strain. With increasing displacement, a fault-bound lens incorporated into a fault-zone, for example, will be progressively sheared and comminuted resulting in the formation of fault rock (Childs et al., 2009). The degree of strain rock experiences within a fault-zone determines its macro-scale hydrological properties, for example, a critical fracture density is required before an impermeable rock mass becomes permeable (Zhang & Sanderson, 1998). At very high strains, grain size reduction and mineralogical alteration in fault rock decrease permeability below that of its host lithology (Evans et al., 1997). The processes that produce fault-zone architecture are widely understood, however, descriptions of this architecture are inherently subjective and the terms used to describe fault-zone components differ between publications. This study follows Child et al.'s (2009) definition, which discriminates between fault rock and fault-zones as the main geometric components of a fault (Fig. 5 and 6). The distribution of these fault components in relation to fluid-flow from two contrasting lithologies are considered in chapter 2.

2.3 Faults and Fluid-flow

Faults are important for the exploration and production of geothermal, hydrocarbon, and mineral resources through their control on the distribution and localisation of fluids in the crust (Wallace & Morris, 1986; Caine et al., 1996; Cox, 1999; Sanderson & Zhang, 1999). Fault-zones comprise relatively high and low permeability components which enable them to act as conduits and/or barriers to fluid-flow (Fig. 5) (Caine et al., 1996; Wibberley et al., 2008; Faulkner et al., 2010). Bending-related normal fault-zones in

Figure 6. Outcrop photographs of fault-zone structure. Fault-zones are typically comprised of anastamosing slip surfaces over a range of scales that link and interact. Much of the geometric complexity observed within fault-zones is attributed to fault segment linkage with increasing strain through mechanically hetergeneous layered sequences (Childs et al., 2009).

subducting oceanic crust, for example, promote the deep penetration of water and hydration (serpentinization) of subducting mantle lithosphere (Ranero et al., 2003; Faccenda et al., 2009). Serpentinites (~13 wt% H_2O) are considered a primary reservoir in the subducting slab fluxing the mantle wedge with fluids which leads to melting in the mantle wedge and arc volcanism at the surface (Gill, 1981; Kirby et al., 1996; Schmidt & Poli, 1998; Hacker et al., 2003; Rupke et al., 2004). Fluid-flow in relation to the hydration and subsequent dehydration of the subducting slab via bending-related normal faults is investigated in chapter 3, while fault-zone architecture is examined in chapter 2.

2.4 Fault reactivation

Fault systems can develop by the creation of new faults or the reactivation of pre-existing faults in response to far-field stress (e.g. Fig. 1). In New Zealand, where intensely deformed Mesozoic basement has an important influence on the location and structural geometry of Tertiary deformation, both fault reactivation and new faulting is observed (Nicol et al., 2007; Stagpoole & Nicol, 2008; Giba et al., 2010). During the initial stages of rifting, strain can localise on, and reactivates, pre-existing basement structures (which can be faults, shear zones, cleavage or bedding planes). Reactivation of basement structures has been investigated in many extensional settings (Morley et al., 2004) and numerous analogue models (McClay & White, 1995; McClay et al., 2002) and its importance for rift evolution has been widely recognised. Reactivation of basement structures is widespread throughout New Zealand and its associated offshore continental crust (Nathan et al., 1986; Barnes, 1993; King & Thrasher, 1996; Mortimer, 2004; Ghisetti & Sibson, 2006; Nicol et al., 2007). In the Taranaki Basin, for example, many structures have been reactivated multiple times since ~80 Ma and accommodated reverse and normal displacements at different times (King & Thrasher, 1996; Nicol et al., 2005; Nicol & Wallace, 2007; Giba et al., 2010; Giba et al., 2012). The orientation and size of pre-existing basement structures may affect fault geometry in overlying strata in a variety of ways; (i) the orientation and strength of basement structure may cause local deviations in the stress field (Bell, 1996; Morley, 2010) (chapter 3), ii) the strike and dip of the fault may be controlled by pre-existing structure and depart from the optimum in the reactivating stress regime (Giba et al., 2012) and iii) highly segmented, zig-zag or orthorhombic fault traces may develop above the pre-existing

structure (Fig. 8) (Wright, 1997; Morley et al., 2004; Giba, 2010). The influence of basement structure on the kinematics and structural geometry of the Taupo Rift is investigated in chapter 3.

2.5 Intra- and back-arc rifting

Two principal models for overriding plate extension in a convergent margin setting (Fig. 1) are the rollback of the subduction hinge (slab rollback model) and/or vertical-axis rotations of fore-arc micro-plates (collision model). Slab rollback (or the seaward migration of the subduction hinge) is considered to be one of the primary mechanisms responsible for the development of overriding plate extension associated with subduction and is caused by the negative buoyancy and gravitational instability of the subducting slab as it founders and sinks into the underlying asthenosphere (Molnar & Atwater, 1978; Sdrolias & Muller, 2006). Vertical-axis rotations of the fore-arc induced by the nearby collision of a buoyant indentor with the margin can also result in overriding plate extension (Wallace et al., 2009a). The close temporal and spatial relationships between the collision of a buoyant indentor (e.g. continental crust, oceanic ridges), fore-arc microplate vertical-axis rotation, and overriding plate extension in active and ancient plate boundaries indicates collision along subduction margins may also be a major driver of the evolution and kinematics of back-arc basins (Wallace et al., 2009a). Predictions from these two models are compared to Taupo Rift extension directions in chapter 4 in order to constrain which first-order processes are controlling the location, structural geometry, and kinematics of rifting.

3. Geological background

The Taupo Rift is located in the central North Island of New Zealand and is spatially coincident with arc volcanism in the modern TVZ (> 0.34 Ma) (Fig. 1).The present basin forms part of the overriding Australian plate and is ~200 km west of the Hikurangi Trough where the Pacific Plate is being subducted. Rift faults active over the last 0.1 Myr define a 15-20 km wide NE trending zone extending ~350 km from the southern limit of arc volcanism along the Tonga-Kermadec-Hikurangi trench to the continental margin in the Bay of Plenty. At the continental margin, the southern Havre Trough and northern Taupo Rift form a 45-50 km left-stepping relay zone (Wright,

1992). The total width of the rift basin formed over the last ~2 Ma tapers south from 70 km at the offshore continental margin to 20 km at its southern termination (Wright, 1992; Villamor & Berryman, 2006). The rift contains Pleistocene (1.6 Ma) and younger volcanoclastic sediments up to ~3 km thick (Bibby et al., 1995; Davey et al., 1995; Wilson et al., 1995) which unconformably overlie steeply dipping Jurassic to Cretaceous basement metasediments of multiple accreted terranes (Fig. 2) (Mortimer, 2004). Much of the early history of the Taupo Rift and TVZ prior to 0.5 Ma is buried by more recent volcanic deposits and its temporal evolution prior to this time is poorly constrained. The age of arc volcanoes on the western margin of the TVZ range between 2 and 6 Ma (Briggs et al., 1989; Black et al., 1992). Much of the Paleocene-Miocene cover sequence observed to the east and west of the TVZ is not present at depth with drillholes in the TVZ passing from Pleistocene volcanics directly into basement (Rosenburg et al., 2009). The absence of these Paleocene-Miocene strata may indicate that the central North Island was subject to uplift and erosion prior to the Pleistocene, a possibility that is considered further in chapter 5.

Arc volcanism and intra-arc rifting has occurred continuously across the North Island and offshore Taranaki Basin since ~12 Ma (Fig. 1b). Both rift extension and arc volcanism has increased in magnitude towards the present (Wright, 1992; Adams et al., 1994; Davey et al., 1995; King & Thrasher, 1996; Carter et al., 2003). Contemporaneously with the initiation of intra-arc rifting in the Taranaki Basin around 12 Ma was the development of explosive caldera forming volcanism in the Coromandel Peninsula (King & Thrasher, 1996; Carter et al., 2003; Giba et al., 2010). While no causal relationship is found between the spatial and temporal occurrence of arc volcanism and rifting in the Taranaki Basin (i.e. rifting is not the result of volcanism and vice versa), their mutual evolution is considered the direct result of subduction processes occurring along the Hikurangi margin (Giba et al., 2010). The magnitude of extension in the overriding plate from the southern Havre Trough to the North Island has increased since 7-5 Ma and migrated southeast towards the present (Wright, 1992; Davey et al., 1995; King & Thrasher, 1996; Wright, 1997; Giba et al., 2010). As arc volcanism and intra-arc rifting are both considered manifestations of subduction related processes, the decreasing distance in the locus of faulting and volcanic activity relative to the Hikurangi margin indicate changes have occurred in the relative motions between the overriding Australian and subducting Pacific plates. The evolution and migration of

faulting and volcanism across the North Island and its implications for subduction processes are considered in chapter 5.

Extension in the Taranaki and Taupo Rifts during the last 12 Myr are inferred to have formed in response to subduction along the Hikurangi margin, where the oceanic crust of the Pacific Plate currently subducts obliquely westwards at 40-48 mm/yr (Beavan et al., 2002; De Mets et al., 2010). The kinematics and geometry of Hikurangi subduction appears strongly dependent on the anomalous properties of the Pacific Plate, a 15-20 km thick fragment of a large igneous province (Hikurangi Plateau) (Davy et al., 2008) presently entering the margin (Wallace et al., 2009b; Reyners et al., 2011), and the southward transition from subduction to continental collision and transpression along the Alpine Fault in the South Island (Fig. 1) (Walcott, 1987; Walcott, 1998; Wallace et al., 2004). Subduction may have commenced as early as 40 Ma (Stock & Molnar, 1982; King, 2000; Stagpoole & Nicol, 2008) producing mainly shortening in the North Island prior to ~12 Ma. Following this time, extension and shortening in the North Island occurred synchronously, to the north and south respectively about poles of local rotation at the latitude of the Taranaki Peninsula (King & Thrasher, 1996; Giba et al., 2010). The onset of extension and crustal thinning in the Taranaki Basin is associated with the clockwise rotation of the Hikurangi margin at rates in the eastern North Island of ~3º/Myr. These rotations have been attributed to rollback of the subducting Pacific plate and/or continental collision at the southern end of the Hikurangi margin (refer Fig. 1) (Ballance, 1976; Stern, 1987; Walcott, 1987; Wallace et al., 2004; Mortimer et al., 2007; Nicol & Wallace, 2007; Nicol et al., 2007).

Widespread arc volcanism initiated in the North Island along the NW-SE trending Northland arc around 23 Ma (Herzer, 1995; Hayward et al., 2001). While there has been much debate as to the origin of the volcanism (Ballance, 1976; Brothers, 1984; Hayward et al., 2001; Mortimer et al., 2007; Schellart, 2012), its chemistry is undoubtedly Island arc (Booden et al., 2011) which requires a hydrated slab at depth. From 17 Ma radiometrically dated volcanic centres with Island arc compositions record activity aligned along a NE trend observed from the Taranaki Basin through the Coromandel Peninsula to the Colville Ridge (Fig. 1b) (Bergman et al., 1992; Adams et al., 1994; Mortimer et al., 2010). The mostly low-medium K andesitic compositions of these active centres, their trace element signatures, and NNE-NE alignment indicate that magmas are derived from an underlying subducting Pacific plate (Bergman et al., 1992; King & Thrasher, 1996; Mortimer et al., 2010).

The geometry and regional tectonic setting of the Taupo Rift and TVZ is illustrated by Fig. 2. The locations of the Taupo Rift and TVZ relative to the Hikurangi margin do not have simple 'arc' and 'back-arc' relationships (Wright, 1992). Active rifting dissects many active arc front volcanoes along the rift, with the majority of active volcanic centres bounded to the east and west by active rift faults, hence the term intra-arc rift is appropriate. The regions of highest subsidence in the offshore region are trenchward of the arc front while in the onshore region, maximum basement depths generally coincide with the arc front (Fig. 2). The basement of the Taupo Rift and TVZ is generally considered to be comprised of greywacke basement terranes rifted to half their original thickness (~16 km) (Fig. 2 and 3) (Davey et al., 1995; Stern et al., 2006). Underlying the attenuated quartzo-feldspathic crust are seismic velocities consistent with heavily intruded crust or anomalous mantle (Stern et al., 2006). Melt bodies within the crust, interpreted from magnetotelluric studies, show spatial coincidence with the location of the Taupo Rift (Fig. 4) (Heise et al., 2010). Onshore, the location of the arc front coincides with a rheological boundary in the mantle wedge separating hot, hydrated and convecting mantle to the west from cold, stagnant mantle to the east (Fig. 3b) (Eberhart-Phillips et al., 2008). It is this first-order rheological boundary in the mantle wedge that I consider most likely to determine the locus of rifting and arc front volcanism.

4. Earthquake, Fault and Volcanic datasets

A wide variety of data have been used in this thesis to address the primary goals. Data, which are discussed in detail in sections 4.1 to 4.5, comprise (i) analysis of fault and fluid-flow data mapped in geological tunnel engineering logs, (ii) analysis of surface fault traces along the Taupo Rift, (iii) interpretation of land gravity, (iv) interpretation of earthquakes and focal mechanisms recorded on the GeoNet and Global seismic networks including subsets of relocated events, and (v) interpretation of collated volcanic age data from across the North Island. The extensive fault mapping over the last 20 years and routine collection of earthquake data by GeoNet, complemented by field, gravity, and *in situ* studies of faults, provide an excellent opportunity to investigate subduction and rifting processes in the North Island. In a study with a scope such as the one outlined in this thesis, collaborators are essential. Several data sets have kindly been provided by principal scientists at GNS Science for use in this study.

Engineering geological logs used in chapter 2 were provided by R. D. Beetham. Regional Moment Tensor focal mechanisms used in chapter 3 and 4 were provided by J. Ristau. Relocated GeoNet earthquakes from the Matata earthquake sequence shown in chapter 3 were provided by S. Bannister. B. Davy and T. Powell (Mighty River Power) provided gravity data used in chapter 3. GeoNet earthquakes relocated in the three-dimensional velocity model of New Zealand used in chapter 4 and 5 were provided by M. Reyners.

4.1 Engineering geological logs

In situ fault and fluid-flow data from engineering geological logs produced as part of the Tongariro Power Development project in the southern Taupo Rift are invaluable for examining the bulk hydraulic properties of faults and fault systems (Fig. 3 Chapter 2). Tunnel logs and unpublished engineering geology reports (Hancox, 1975; Hancox & Paterson, 1975; Hegan, 1976; Hegan, 1980) held at GNS Science, Lower Hutt, provide detailed descriptions of fault-zone architecture and fluid-flow from centimetre to kilometres scales. All fault and fluid-flow rate data are taken from 1:240 engineering geological logs constructed at the time of tunnel excavation (1969-1976) to characterise rock mass properties including strength and water flow. Tunnel log description and measurements record structures down to the scale of individual joints in two contrasting lithologies, a porous and permeable Miocene sandstone and low porosity and permeability Mesozoic basement. The dataset comprises 530 basement and 40 Miocene-Recent(?) fault-zones intersected by 3-6 m diameter tunnels excavated 75-500 m below the surface through~34 km of Mesozoic greywacke basement and ~2.5 km through Miocene marine sandstone (Beetham & Watters, 1985). Fault-zone data typically comprise; distance along the tunnel, orientation, displacement (Miocene sandstone), description and thickness of fault rock and fault-zone, rock strength (Mesozoic basement), and the location and rate of any localised groundwater inflow. In chapter 2 data from the logs have been collated to characterise the first-order geometry, distribution, and *in situ* fluid-flow properties of fault-zones.

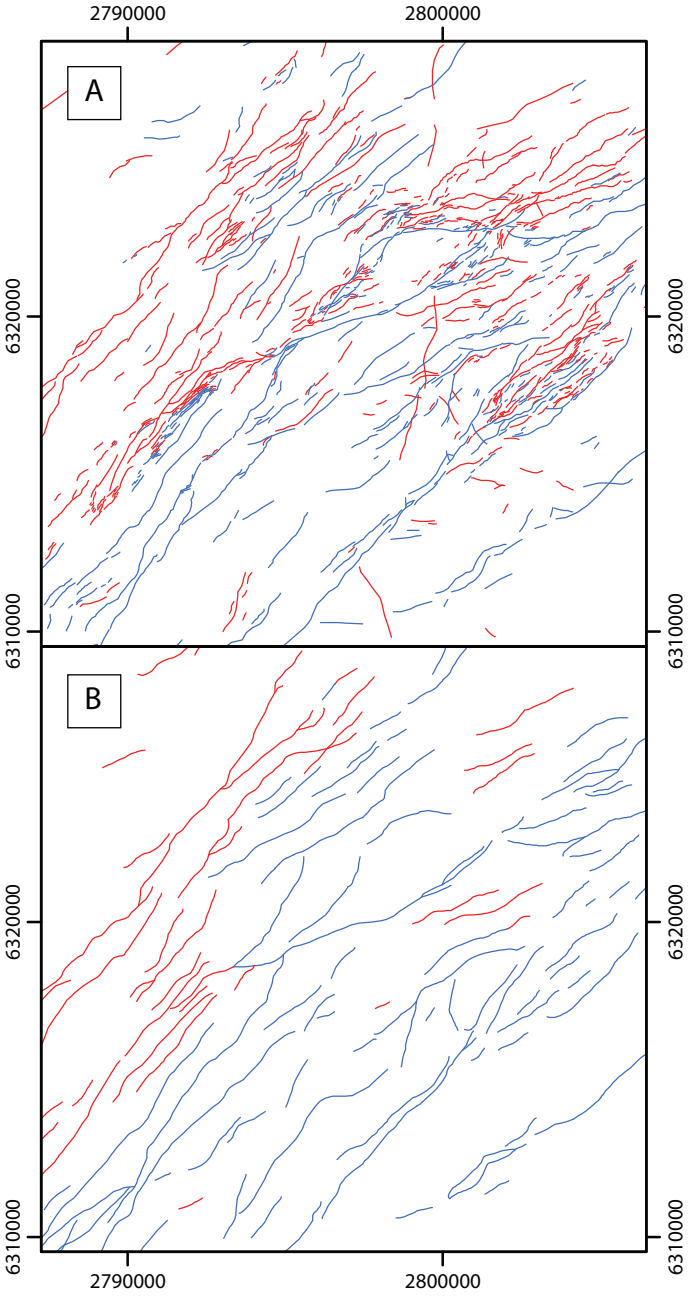

Figure 8. Fault maps from the Taupo Rift. A) Active fault map derived from 1:25 000 and 1:17 000 aerial photographs and field work used in this study. B) Recently published 1:250 000 active fault map from the Taupo Rift (Leonard et al., 2012).

4.2 Surface fault trace data

Data along ~300 km of the NE trending Taupo Rift constrain the kinematics of active faulting and models for rift formation (chapter 3). Active fault data include the GNS Science Active Faults database, supplemented by re-examination of aerial photographs (1:25 000 and 1:17 000 scale) and published geological maps (Fig. 8) (Villamor & Berryman, 2001; Nairn, 2002; Nicol et al., 2006; Townsend et al., 2008; Lee et al., 2010; Leonard et al., 2011). Active fault traces onshore have been confirmed by extensive paleoearthquake studies of displaced dated volcanic and fluvial surfaces typically ≤ 60 ka in age (Villamor & Berryman, 2001; Nicol et al., 2006; Berryman et al., 2010; Begg & Mouslopoulou, 2010). These displaced surfaces range in age up to 0.36 Ma toward the active rift boundaries and < 20 ka towards the rift axes (Villamor & Berryman, 2001; Nicol et al., 2006). Offshore, active fault traces have been identified by seafloor scarps and displacements of a < 20 ka post-last glacial ravinement surface through a network of seismic reflection lines and multibeam bathymetry (Lamarche et al., 2006). I utilise these offshore and onshore data to constrain the location and structural geometry of faulting. Visible surface fault traces are considered to represent the accumulated displacement of earthquakes ≥ M 6 (Villamor & Berryman, 2001) and place constraints on the long-term (thousands to hundreds of thousands of years) regional strain orientation. Geological data is compared to earthquake data over a range of magnitudes and demonstrates the kinematics of faulting is scale invariant in the Taupo Rift over three orders of magnitude.

4.3 Earthquake data

A comprehensive GeoNet catalogue of Benioff zone and crustal earthquakes covers an area of 300 x 700 km and extends to depths of 250-350 km beneath the Hikurangi margin (Fig. 9) (www.GeoNet.cri.nz). This earthquake catalogue forms the basis for the majority of local and regional seismicity studies in the North Island including this one. Subsets of these data have been relocated and used to image subduction zone structure in unparalleled detail (Reyners et al., 2006; Eberhart-Phillips et al., 2008; Eberhart-Phillips et al., 2010). I use earthquakes relocated in the 3D seismic velocity model of New Zealand (3DNZ) (Eberhart-Phillips et al., 2010) kindly provided by M. Reyners of GNS Science to estimate the accuracy of events in the original GeoNet earthquake catalogue when assessing the spatial distribution of earthquakes along the margin

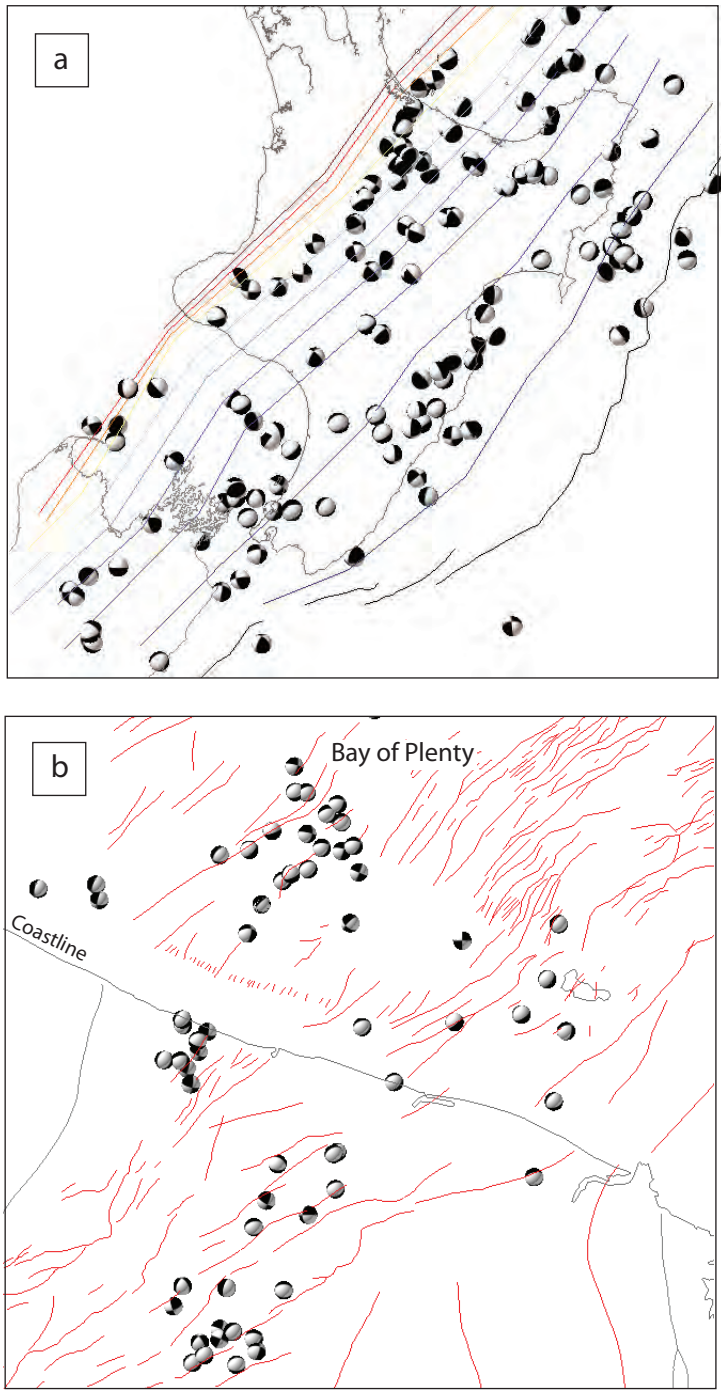

Figure 9. North Island focal mechanisms. (a) RMT focal mechanisms within the subducting Pacific plate along the Hikurnagi margin (Ristau, 2008). Geometry of the slab from chapter 5. (b) Focal mechanisms from the northern Taupo Rift (Anderson & Webb, 1989; Robinson, 1989; Ristau, 2008). Fault map from Lamarche et al. (2006) and Leonard et al. (2012).

(chapter 4), to examine the location of dehydration within the slab (chapter 4), and define the geometry of the slab (chapter 5). These relocated events are the highest accuracy regional catalogue available at present. When combined with 3DNZ they allow the relative hydration of the Pacific plate as it subducts beneath the North Island to be assessed (chapter 4). A relocated subset of events from the Matata region in the Taupo Rift kindly provided by S. Bannister of GNS Science show subsurface fault deformation patterns in unprecedented detail (chapter 3). Regional Moment Tensor focal mechanisms routinely calculated from GeoNet waveform and location data (Ristau, 2008) form the basis for the kinematic analysis in the Taupo Rift (chapter 3) and subducting slab (chapter 4) (Fig. 9). These data combined with Centroid Moment Tensor catalogue (Dziewonski et al., 1981) form a large and consistent catalogue with which to investigate deformation in the overriding and subducting plates. These focal mechanism data have been crucial for determining the style of faulting through the interplate zone (chapter 4), for characterising fluid-flow pathways into and out of the slab (chapter 4), and for the influence of basement on the kinematics and geometry of rifting (chapter 3).

4.4 Gravity data

Gravity data along the rift axis has been collected to delineate better basement trends at > 2 km depth not apparent at the surface (Fig. 2) (chapter 3). Gravity observations in the Taupo Rift were undertaken by the author during two surveys between the 10th February 2009 and the 5^{h} February 2010 using a Lacoste and Romberg gravimeter (serial number G106) where the location and height of each observation was established with a Leica Real-Time Kinematic (RTK) differential GPS system in both real-time and post-processing mode using the New Zealand Geodetic Datum 2000 trig point Waimangu. During the survey 130 new gravity stations were established and tied to Reporoa gravity station 156 (E2801549 N6302170 height 295 m (MSL) 979976.414 mGal), which is part of the New Zealand Primary Network (Robertson & Reilly, 1960). The daily determination of instrumental drift included the occupation of the Primary Gravity Network station at the beginning and end of each day and by looping to local base stations (i.e. repeat readings of previously measured stations). Observations were made along public and private roads. The locations of the surveys and detail of the processing methods can be found in Appendix 1. The design of the surveys was based around two

objectives: filling gaps in the New Zealand Gravity Station Network along the Taupo Rift axis (1-2 km spacing) and a detailed survey normal to the rift axis across the Paeroa Fault (0.25-0.5 km spacing).

4.5 Volcanic age data

The most up to date and precise volcanic age data set has been compiled from the literature (see chapter 5 for references) to document the migration of arc volcanism across the North Island (Fig. 1b). The notable inclusion of the most precise regional age data for volcanism in the Taranaki Basin (Giba et al., 2012) and redating of samples from the Colville Ridge (Mortimer et al., 2010) provide alignments of active arc volcanoes over greater length scale than previous studies (Brothers, 1984; Kamp, 1984). Coupled with the age trends of volcanism, the geochemistry of volcanic samples across the North Island indicate magmas predominantly forming in a hydrated mantle wedge consistent with fluids from a subducting slab. The majority of onshore samples have whole rock chemical analyses and radiometric dates (Ar-Ar, K-Ar) with mean standard errors < ± 0.6 Ma. Radiometric ages from volcanic centres in offshore Northland, offshore Taranaki Basin and the South Fiji Basins are rare. In the offshore Northland and Taranaki Basins the age of volcanic centres is mainly constrained by the age of sedimentary rocks that underlie, onlap, and drape volcanic centres imaged mainly on 2D and 3D seismic-reflection lines (Herzer, 1995; Giba et al., 2010). The ages of stratigraphy that enclose the volcanic centres were determined by correlation of seismic reflectors to wells and typically have uncertainties of ±1-2 Myr (Giba et al., 2010). Where radiometric and stratigraphically correlated ages have been determined for the same location, the maximum age for the onset of volcanism is within error (Bergman et al., 1992; Giba, 2010). As arc front volcanism generally lies ~90-100 km above the subducting slab (Syracuse & Abers, 2006) these data are key for inferring geometric changes in the slab (chapter 5).

5. Thesis outline

Since the chapters in this thesis have been written as manuscripts prepared for journal submission, each dealing with separate generic or regional tectonic topic, it should be possible to read them independently. As a consequence, every chapter includes an

abstract and references. This approach leads to some repetition, particularly in the introduction section of each chapter, and an element of compartmentalization. To counter this focus on discrete topics or questions I have attempted to draw links between each chapter in the introduction and conclusions chapters.

Chapter 2 **combines mapping of water flow rates and fault-zone structure to examine how, where, and why faults impact on fluid-flow.** We examine fault-zone *in situ* fluid-flow in two contrasting lithologies in relation to their structural geometry, architecture and connectivity to the groundwater system. The heterogeneity observed in fault-zone architecture, thickness, and fluid-flow rates indicate that predicting the location of hydraulically conductive high permeability pathways in the crust will be problematic.

Chapter 3 addresses three principle questions associated intra-arc rifting in the central North Island. **Firstly, what are the kinematics of the Taupo Rift? Secondly, what factors are influencing rift kinematics? And thirdly, how are these factors related to processes operating at the plate boundary scale?** The structural geometry and kinematics of the Taupo Rift are defined with fault and earthquake slip data which is placed in context with rifting and volcanism along the southern portion of the Tonga-Kermadec-Hikurangi subduction margin and compared models for extension in the overriding plate. The subducting slab exerts a first-order control on the location and geometry of intra-arc rifting. Second-order changes in the orientation of fault trends and extension direction show how basement anisotropy can influence the geometry and kinematics of rifting.

Chapter 4 **investigates the origin of the heat source driving the exceptionally voluminous volcanism in the central Taupo Volcanic Zone and why arc volcanism extinguishes so abruptly to the south of the TVZ despite the continuity of a seismically active slab for a further ~350 km along strike.** I examine the spatial distribution of earthquakes in the subducting plate in relation to the location and productivity of volcanism along the Hikurangi margin. Benioff zone earthquakes are considered to be the result of high fluid pressures generated by the dehydration of hydrous phases in the subducting lithosphere. Using GeoNet, relocated, and EHB earthquake catalogues the hydration and subsequent dehydration of the slab are documented and the implications for the volcanism and heat flow along the Hikurangi margin discussed.

Chapter 5 **examines how the slab geometry beneath the North Island has changed through time.** I explore the geometric evolution of the subducting Pacific plate over the last 20 Myr using constraints from present-day arc-slab relations defined with relocated Benioff seismicity, a published tomographic model for the location and trend of the deep slab, and a catalogue of volcanic arc age data from across the North Island. The trend of the subducting slab has been approximately parallel to the present-day since 16 Ma which contrasts with the generally accepted evolution of the overriding plate.

Chapter 6 **reviews how relative plate motions constrain the evolution of the subducting Pacific and overriding Australian plates.** I use published poles of rotation to examine relative plate motions for the Hikurangi margin that constrain the direction and rate of subduction. The direction and rate of subduction directly influences the location and timing of arc volcanism and deformation in the North Island in relation to current concepts for back-arc rifting and the evolution of subduction beneath the North Island. This chapter highlights the need for a consistent approach to plate reconstructions in the region.

Chapter 7 summarizes the results of this study and discusses possible lines of future research.

References

Acoccella, V., Spinks, K., Cole, J. & Nicol, A., 2003. Oblique back arc rifting of Taupo Volcanic Zone, New Zealand. *Tectonics*, 22(4), p.1045.

Adams, C.J., Graham, I.J., Seward, D. & Skinner, D.N.B., 1994. Geochronological and geochemical evolution of late Cenozioc volcanism in the Coromandel Peninsula, New Zealand. *New Zealand Journal of Geology & Geophysics*, 37, pp.359-79.

Ballance, P.F., 1976. Evolution of the Upper Cenozoic magmatic arc and plate boundary in northern New Zealand. *Earth & Planetary Science Letters*, 28, pp.356-70.

Barnes, P., 1993. *Structural styles and sedimentation at the southern termination of the Hikurangi subduction zone, offshore Canterbury, New Zealand*. Unpub. PhD Thesis: University of Canterbury.

Beavan, J., Tregoning, P., Bevis, M., Kato, T. & Meertens, C., 2002. Motion and rigidity of the Pacific Plate and implications for plate boundary deformation. *Journal of Geophysical Research*, 107(B10), p.2261. doi:10.1029/2001JB000282.

Beetham, R.D. & Watters, W.A., 1985. Geology of Torlesse and Waipapa terrane basement rocks encountered during the Tongariro Power Development project, North Island, New Zealand. *New Zealand Journal of Geology & Geophysics*, 28, pp.575-94.

Begg, J.G. & Mouslopoulou, V., 2010. Analysis of late Holocene faulting within an actie rift using lidar, Taupo Rift, New Zealand. *Journal of Volcanology & Geothermal Research*, 190, pp.152-67. doi:10.1016/j.jvolgeores.2009.06.001.

Bell, J.S., 1996. In situ stresses in sedimentary rocks (part 2): application of stress measurments. *Geoscience Canada*, 23(3), pp.135-53.

Bergman, S.C., Talbot, J. & Thompson, P.R., 1992. The Kora Miocene submarine andesite stratovolcano hydrocarbon reservior. *Taranaki Basin 1991 New Zealand Oil Exploration Conference Proceedings*, pp.178-206.

Berryman, K., Villamor, P., Nairn, I., Van Dissen, R., Begg, J. & Lee, J., 2010. Late Quaternary surface rupture history of the Paeroa Fault, Taupo Rift, New Zealand. *New Zealand Journal of Geology & Geophysics*.

Bibby, H.M., Caldwell, T.G., Davey, F.J. & Webb, T.H., 1995. Geophysical evidence on the structure of the Taupo Volcanic Zone and its hydrothermal circulation. *Journal of Volcanology & Geothermal Research*, 68, pp.29-58.

Black, P.M., Briggs, R.M., Itaya, T., Dewies, E.R., Dunbar, H.M., Kawasaki, K., Kuschel, E. & Smith, I.E.M., 1992. K-Ar age data and geochemistry of the Kiwitahi Volcanics, western Hauraki Rift, North Island, New Zealand. *New Zealand Journal of Geology & Geophysics*, 35, pp.403-13.

Booden, M.A., Smith, I.E.M., Black, P.M. & Maulk, J.L., 2011. Geochemistry of the Early Miocene volcanic succession of Northland, New Zealand, and implications for the evolution of subduction in the Southwest Pacific. *Journal of Volcanology & Geothermal Research*, 190, pp.25-37. doi:10.1016/j.jvolgeores.2010.10.006.

Braithwaite, R.I., Wood, C.P., Rosenburg, M.D. & Faure, K., 2002. Porosity and permeability in the basement rocks at the Kawerau and Ohaaki geothermal fields, New Zealand. In *Proceedings 24th New Zealand Geothermal workshop*. Auckland, 2002. Auckland University.

Briggs, R.M., Itaya, T., Lowe, D.J. & Keane, A.J., 1989. Ages of the Pliocene-Pleistocene Alexandra and Ngatutura Volcanics, western North Island, New Zealand, and some geological implications. *New Zealand Journal of Geology & Geophysics*, 32, pp.417-27.

Brothers, R.N., 1984. Subduction regression and oceanward migration of volcanism, North Island, New Zealand. *Nature*, 309, pp.698-700.

Caine, J.S., Evans, J.P. & Forster, C.B., 1996. Fault zone architecture and permeability structure. *Geology*, 24(11), pp.1025-28.

Carter, L., Shane, P., Alloway, B., Hall, I.R., Harris, S.E., Harris, S.E. & Westgate, J.A., 2003. Demise of one volcanic zone and the birth of another - a 12 m.y. record of rhyolitic eruptions from New Zealand. *Geology*, 31, pp.493-96.

Childs, C., Manzocchi, T., Walsh, J.J., Bonson, C.G., Nicol, A. & Schopfer, M.P.J., 2009. A geometric model of fault zone and fault rock thickness variations. *Journal of Structural Geology*, 31(2), pp.117-27.

Cole, J.W., 1990. Structural control and origin of volcanism in the Taupo Volcanic Zone, New Zealand. *Bulletin of Volcanology*, 242-257, p.52.

Cox, S.F., 1999. Deformational controls on the dynamics of fluid flow in mesothermal gold systems. In K. McCaffrey, L. Lonergan & J.J. Wilkinson, eds. *Fractures, Fluid flow and Mineralisation*. London: Geological Society Special Publications 155. pp.123-40.

Davey, F.J., Henrys, S.A. & Lodolo, E., 1995. Asymmtric rifting in a continental back-arc environment, North Island, New Zealand. *Journal of Volcanology and Geothermal Research*, 68, pp.209-38.

Davy, B., Horernle, K. & Werner, R., 2008. Hikurangi Plateau: Crustal structure, rift formation, and Gondwana subduction history. *Geochemsitry, Geophysics, Geosystems*, 9, p.Q07004.

De Mets, C., Gordon, R.G. & Argus, D.F., 2010. Geologically current plate motions. *Geophysics Journal International*, 181, pp.1-80.

Dziewonski, A.M., Chou, T.-A. & Woodhouse, J.H., 1981. Determination of earthquake source parameters from waveform data for studies of global and regional seismicity. *Journal of Geophysical Research*, 86, pp.2825-52.

Eberhart-Phillips, D., Reyners, M., Bannister, S., Chadwick, M. & Ellis, S., 2010. Establishing a versatile 3-D seismic velocity model for New Zealand. *Seismological Research Letters*, 81(6), pp.992-1000.

Eberhart-Phillips, D., Ryeners, R., Chadwick, M. & Stuart, G., 2008. Three-dimensional attenuation strucutre of the Hikurangi subduction zone in the central North Island, New Zealand. *Geophysics Journal International*, 174, pp.418-34.

Evans, J.P., Forster, C.B. & Goddard, J.V., 1997. Permeability of fault-related rocks, and implications for hydraulic structure of fault zones. *Journal of Structural geology*, 19(11), pp.1393-404.

Faccenda, M., Gerya, T.V. & Burlini, L., 2009. Deep slab hydration induced by bending-related variations in tectonic pressure. *Nature Geoscience*, 2, pp.790-93. doi:10.1038/NGEO656.

Faulkner, D.R., Jackson, C.A.L., Lunn, R.J., Schlische, R.W., Shipton, Z.K., Wibberley, C.A.J. & Withjack, M.O., 2010. A review of recent developments concerning the structure, mechanics and fluid flow properties of fault zones. *Journal of Structural Geology*, 32, pp.1557-75. doi:10.1016/j.jsg.2010.06.009.

Ghisetti, F.C. & Sibson, R.H., 2006. Accommodation of compressional inversion in north-western South Island (New Zealand): Old faults verses new? *Journal of Structural Geology*, 28, pp.1994-2010. doi:10.1016/j.jsg.2006.06.010.

Giba, M., 2010. *The evolution of Tertiary normal faults in the Taranaki Basin, New Zealand*. Dublin: University College Dublin. unpublished PhD thesis.

Giba, M., Nicol, A. & Walsh, J.J., 2010. Evolution of faulting and volcanism in a back-arc basin and its implications for subduction processes. *Tectonics*, TC4020. doi: 10.1029/2009TC002634.

Giba, M., Walsh, J.J. & Nicol, A., 2012. Segmentation and growth of an obliquely reactivated normal fault. *Journal of Structural Geology*, 39, pp.253-67. doi:10.1016/j.jsg.2012.01.004.

Gill, J., 1981. *Orogenic Andesities and Plate Tectonics*. New York: Springer.

Hacker, B.R., Peacock, S., Abers, G.A. & Holloway, S.D., 2003. Subduction factory, 2. Are intermediate-depth earthquakes in subducting slabs linked to metamorphic dehydration reactions? *Journal of Geophysical Research*, 108(B1), p.2030. doi:10.1029/2001JB001129.

Hancox, G.T., 1975. *Completion report on the engineering geology of the Moawhango Dam*. Unpubl. Engineering Geology Report 213. Lower Hutt: New Zealand Geological Survey Department of Scientific and Industrial Research.

Hancox, G.T. & Paterson, B.R., 1975. *Reappraisal of the Geology and anticipated tunneling conditions in Moawhango Tunnel between Tongariro heading (c.f. 30200') and Moawhango heading (c.f. 26400')*. Unpubl. Engineering Geology Report 233. Lower Hutt: New Zealand Geological Survey Department of Scientific and Industrial Research.

Hayward, B.W., Black, P.M., Smith, I.E.M., Ballance, P.F., Itaya, T., Doi, M., Takagi, M., Bergman, S., Adams, C.J., Herzer, R.H. & Robertson, D.J., 2001. K-Ar ages of Early Miocene arc-type volcanoes in northern New Zealand. *New Zealand Journal of Geology & Geophysics*, 44, pp.285-311.

Hegan, B.D., 1976. *Engineering Geology of the Rangipo tailrace tunnel*. Unpubl. Engineering Geology Report 253. Lower Hutt: New Zealand Geological Survey Department of Scientific and Industrial Research.

Hegan, B.D., 1980. *Engineering Geology of the Moawhango to Tongariro Tunnel*. Unpubl. Engineering Geology Report 343. Lower Hutt: New Zealand Geological Survey Department of Scientific and Industrial Research.

Heise, V., Caldwell, T.G., Bibby, H.M. & Bennie, S.L., 2010. Three-dimensional electrical resistivity image of magma beneath an active continental rift, Taupo Volcanic Zone, New Zealand. *Geophysical Research Letters*, 37, p.L10301. doi:10.1029/2010GL043110.

Herzer, R.H., 1995. Seismic stratigraphy of a buried volcanic arc, offshore Northland, New Zealand and implications for Neogene subduction. *Marine & Petroleum Geology*, 12, pp.511-31.

Ilg, B.R., Hemmings-Sykes, S., Nicol, A., Baur, J., Fohrmann, M., Funnell, R. & Milner, M., 2012. Normal faults and gas migration in an active plate boundary, southern Taranaki Basin, offshore New Zealand. *AAPG Bulletin*, 96(9), pp.1733-56. doi:10.1306/0201.1211.088.

Kamp, P.J.J., 1984. Neogene and Quarternary extent and geometry of the subducted Pacific Plate beneath North Island, New Zealand: implications for Kaikoura tectonics. *Tectonophysics*, 108, pp.241-66.

King, P.R., 2000. Tectonic reconstructions of New Zealand: 40 Ma to present. *New Zealand Journal of Geology & Geophysics*, 43, pp.611-38.

King, P.R. & Thrasher, G.P., 1996. Cretaceous-Cenozoic geology and petroleum systems of the Taranaki Basin. In *Institute of Geological & Nuclear Sciences Monograph 13*. Lower Hutt, New Zealand: Institute of Geological & Nuclear Sciences.

Kirby, S.H., Engdahl, E.R. & Denlinger, R., 1996. Intermediate-depth intraslab earthquakes and arc volcanism as physical expressions of crustal and uppermost mantle metamorphism in subducting slabs. In G.E. Bebout, D. Scholl, S.H. Kirby & J.P. Platt, eds. *Subduction: Top to Bottom*. Geophysical Monograph 96, Washington DC: AGU. pp.195-214.

Lamarche, G., Barnes, P.M. & Bull, J.M., 2006. Faulting and extension rate over the last 20,000 years in the offshore Whakatane Graben, New Zealand continental shelf. *Tectonics*, 25, p.TC4005. doi:10.1029/2005TC001886.

Lee, J., Townsend, D., Bland, K. & Kamp, P.J.J., 2010. *Geology of the Hawke's Bay area: scale 1:250,000*. Institute of Geological & Nuclear Sciences Limited: Institute of Geological & Nuclear Sciences 1:250,000 geological map 8. 86 p.+ 1 folded map.

Leonard, G.S., Begg, J.G. & Wilson, C.J.N., 2011. *Geology of the Rotorua area 1:250 000 geological map*. Lower Hutt, New Zealand: Institute of Geological & Nuclear Sciences. 1 sheet + 99p.

Manzocchi, T., Childs, C. & Walsh, J.J., 2010. Faults and fault properties in hydrocarbon flow models. *Geofluids*, 10, pp.94-113. doi:10.1111/j.1468-8123.2010.00283.x.

Marrett, R. & Allmendinger, R.W., 1990. Kinematic analysis of fault slip data. *Journal of Structural Geology*, 12, pp.973-86.

McClay, K.R., Dooley, T., Whitehouse, P. & Mills, M., 2002. 4-D evolution of rift systems: Insights from scaled physical models. *AAPG Bulletin*, 86(3), pp.935-59.

McClay, K.R. & White, M.J., 1995. Analogue modelling of orthogonal and oblique rifitng. *Marine & Petroleum Geology*, 12, pp.137-51.

Molnar, P. & Atwater, T., 1978. Interarc spreading and Cordilleran tectonics as alternatives related to the age of subducted lithosphere. *Earth & Planetary Science Letters*, 41, pp.330-40.

Morley, C.K., 2010. Stress re-orientation along zones of weak fabrics in rifts: An explanation for pure extension in 'oblique" rift segments. *Earth & Planetary Science Letters*, 297, pp.667-73. doi:10.1016/j.epsl.2010.07.022.

Morley, C.K., Haranya, C., Phoosongsee, W., Pongwapee, S., Kornsawan, A. & Wonganan, N., 2004. Activation of rift oblique and rift parallel pre-existing fabrics during extension and their effect on deformation style: examples for the rifts of Thailand. *Journal of structural Geology*, 26, pp.1803-29. doi:10.1016/j.jsg.2004.02.014.

Mortimer, N., 2004. New Zealand's geological fondations. *Gondwana Research*, 7(1), pp.261-72.

Mortimer, N., Gans, P.B., Palin, J.M., Meffe, S., Herzer, R.H. & Skinner, D.N.B., 2010. Location and migration of Miocene-Quarternary volcanic arcs in the SW Pacific region. *Journal of Volcanology & geothermal Research*, 190, pp.1-10. doi: 10.1016/j.jvolgeores.2009.02.017.

Mortimer, N., Herzer, R.H., Gans, P.B., Laporte-Magoni, C., Clavert, A.T. & Bosch, D., 2007. Oligocene-Miocene tectonic evolution of the South Fiji Basin and Northland Plateau, SW Pacific Ocean: evidence from petrology and dating of dredged rocks. *Marine Geology*, 237, pp.1-24.

Mouslopoulou, V., Nicol, A., Walsh, J.J., Beetham, D. & Stagpoole, V., 2008. Quaternary temporal stability of a regional strike-slip and rift intersection. *Journal of Structural Geology*, 30(4), pp.451-63.

Nairn, I.A., 2002. Geology of the Okataina Volcanic Centre scale 1:50 000. In *Institute of Geological & Nuclear Sciences geological map 25*. Lower Hutt: Institute of Geological & Nuclear Sciences. 1 sheet + 156 p.

Nathan, S., Anderson, H.J., Cook, R.A., Herzer, R.H., Hoskins, R.H., Raine, J.J. & Smale, D., 1986. Cretaceous and Cenozoic sedimentary basins of the West Coast Region, South Island, New Zealand. In *New Zealand Geological Survey Basin Studies 1*. Wellington, New Zealand: Department of Scientific & Industrial Research.

Nicol, A., Mazengarb, C., Chanier, F., Rait, C., Uruski, C. & Wallace, L., 2007. Tectonic evolution of the active Hikurangi subduction margin, New Zealand, since the Oligocene. *Tectonics*, 26, p.TC4002. doi:10.1029/2006TC002090.

Nicol, A. & Wallace, L.M., 2007. Temporal stability of deformation rates: Comparison of geological and geodetic observations, Hikurangi subduction margin, New Zealand. *Earth & Planetary Science Letters*, 258, pp.397-413. doi:10.1016/j.epsl.2007.03.039.

Nicol, A., Walsh, J., Berryman, K. & Nodder, S., 2005. Growth of a normal fault by the accumulation of slip over millions of years. *Journal 0f Structural Geology*, 27, pp.327-42. doi:10.1016/j.jsg.2004.09.002.

Nicol, A., Walsh, J., Berryman, K. & Villamor, P., 2006. Interdependence of fault displacement rates and paleoearthquakes in an active rift. *Geology*, 34(10), pp.865-68. doi:10.1130/GC22335.1.

Nicol, A., Walsh, J.J., Villamor, P., Seebeck, H. & Berryman, K.R., 2010. Normal fault interactions, paleoearthquakes and growth in an atcive rift. *Journal of Structural Geology*, 32, pp.1101-13. doi:10.1016/j.jsg.2010.06.018.

Parson, L.M. & Wright, I.C., 1996. The Lau-Havre-Taupo back-arc basin: A southward-progating, multi-stage evolution from rifting to spreading. *Tectonophysics*, 263, pp.1-22.

Ranero, C.R., Phipps Morgan, J., McIntosh, K. & Reichert, C., 2003. Bending-related faulting and mantle serpentinization at the Middle America Trench. *Nature*, 425, pp.367-73. doi:10.1038/nature01961.

Reyners, M., Eberhart-Phillips, D. & Bannister, S., 2011. Tracking repeated subduction of the Hikurangi Plateau beneath New Zealand. *Earth & Planetary Science Letters*, 311(1-2), pp.165-71. doi:10.1016/j.epsl.2011.09.011.

Reyners, M.E., Eberhart-Phillips, D., Stuart, G. & Nishimura, T., 2006. Imaging subduction from the trench to 300 km depth beneath the central North Island, New Zealand with Vp and Vp/Vs. *Geophysics Journal International,* 165, pp.565-83.

Ristau, J., 2008. Implementation of routine Regional Moment Tensor analysis in New Zealand. *Seismological Research Letters*, 79(3), pp.400-15. doi:10.1785/gssrl.79.3.400.

Rosenburg, M.D., Bignall, G. & Rae, A.J., 2009. The geological framework of the Wairakei-Tauhara Geothermal System, New Zealand. *Geothermics*, 38, pp.72-84. doi:10.1016/j.geothermics.2009.01.001.

Rowland, J.R. & Sibson, R.H., 2001. Extensional fault kinematics within the Taupo Volcanic Zone, New Zealand: soft-linked segmentation of a continental rift system. *New Zealand Journal of Geology & Geophysics*, 44, pp.271-83.

Rupke, L.H., Phipps Morgan, J., Hort, M. & Connolly, J.A.D., 2004. Serpentine and the subduction water cycle. *Earth & Planetary Science Letters*, 223, pp.17-34. doi:10.1016/j.epsl.2004.04.018.

Sanderson, D.J. & Zhang, X., 1999. Critical stress localization of flow associated with deformation of well-fractured rock masses, with implications for mineral deposits. In k. McCaffrey, J.W. Lonergan & J.J. Wilkinson, eds. *Fractures, Fluid Flow and Mineralization*. London: Geological Society Special Publications 155. pp.69-81.

Schellart, W.P., 2012. Comment on "Geochemistry of the Early Miocene volcanic succession of Northland, New Zealand, and implications for the evolution of subduction in the Southwest Pacific" by M.A. Booden, I.E.M. Smith, P.M. Black and J.L. Mauk. *Journal of Volcanology & Geothermal Research*, 211-212, pp.112-17. doi:10.1016/j.jvolgeores.2011.10.010.

Schmidt, M.W. & Poli, S., 1998. Experimentally based water budgets for dehydrating slabs and consequences for arc magma generation. *Earth & Planetary Science Letters*, 163, pp.361-79.

Sdrolias, M. & Muller, R.D., 2006. Controls on back-arc basin formation. *Geochemistry, Geophysics, Geosystems*, 7, p.Q04016. doi:10.1029/2005GC001090.

Seebeck, H.C., Nicol, A., Stern, T.A., Bibby, H.M. & Stagpoole, V., 2010. Fault controls on the geometry and location of the Okataina Caldera, Taupo Volcanic Zone,

New Zealand. *Journal of Volcanology & Geothermal Research,* 190, pp.136-51. doi:10.1016/j.jvolgeores.2009.04.011.

Stagpoole, V. & Bibby, H.M., 1999. *Residual gravity anomaly map of the Taupo Volcanic Zone, New Zealand, 1:250 000*. Institute of Geological & Nuclear Sciences Geophysical Map 13. Lower Hutt: Institute of Geological & Nuclear Sciences Ltd.

Stagpoole, V. & Nicol, A., 2008. Regional structure and kinematic history of a large subduction back thrust: Taranaki Fault, New Zealand. *Journal of Geophysical Research,* 113, p.B01403. doi:10.1029/2007JB005170.

Stagpoole, V., Woodward, D. & Beetham, R., 2005. *Gravity Survey at the Horohoro geothermal prospect, Taupo Volcanic Zone*. Institute of Geological & Nuclear Sciences Client Report 2005/32. Lower Hutt: Institute of Geological & Nuclear Sciences.

Stern, T.A., 1987. Asymmetric back-arc spreading, heat flux and structure associated with Central Volcanic Region, New Zealand. *Earth & Planetary Science Letters,* 85, pp.265-76.

Stern, T.A., 2009. Reconciling short- and long-term measures of extension in continental back-arcs: heat flux, crustal structure and rotations within the central North Island, New Zealand. In U. Ring & B. Wernicke, eds. *Extending a Continent: Architecture, Rheology and Heat Budget*. London, Special Publications 321: Geological Society. pp.73-87. doi:10.1144/SP321.4.

Stern, T.A., Stratford, W.R. & Salmon, M.L., 2006. Subduction evolution and mantle dynamics at a continental margin: Central North Island, New Zealand. *Review of Geophysics,* 44, p.RG4002. doi:10.1029/2005RG000171.

Stock, J. & Molnar, P., 1982. Uncertainties in the relative positions of the Australia, Antarctica, Lord Howe, and Pacific plates since the late Cretaceous. *Journal of Geophysical Research,* 87(B6), pp.4697-717.

Syracuse, E.M. & Abers, G.A., 2006. Global compliation of variations in slab depth beneath arc volcanoes and implications. *Geochemistry, Geophysics, Geosystems,* 7, p.Q05017. doi:10.1029/2005GC001045.

Townsend, D., Vonk, A. & Kamp, P.J.J., 2008. *Geology of the Taranaki area: scale 1:250,000*. Institute of Geological & Nuclear Sciences Limited, New Zealand: Institute of Geological & Nuclear Sciences 1:250,000 geological map 7. 77p + 1 folded map.

Villamor, P. & Berryman, K.R., 2001. A late Quaternary extension rate in the Taupo Volcanic Zone, New Zealand, derived from fault slip data. *New Zealand Journal of Geology & Geophysics*, 44, pp.243-69.

Villamor, P. & Berryman, K.R., 2006. Evolution of the southern termination of the Taupo Rift, New Zealand. *New Zealand Journal of Geology & Geophysics*, 49, pp.23-37.

Walcott, R.I., 1987. Geodetic strain and the deformation history of the North Island of New Zealand during the late Cainozoic. *Philosphical Transactions of the Royal Society London*, A321, pp.163-81.

Walcott, R.I., 1998. Modes of oblique compression: Late Cenozoic tectonics of the South Island of New Zealand. *Reviews of Geophysics*, 36(1), pp.1-26.

Wallace, L.M., Beavan, J., McCaffrey, R. & Darby, D., 2004. Subduction zone coupling and tectonic block rotations in the North Island, New Zealand. *Journal of Geophysical Research*, p.B12406. doi:10.1029/2004JB003241.

Wallace, L.M., Ellis, S. & Mann, P., 2009a. Collisional model for rapid fore-arc block rotations, arc curvature, and episodic back-arc rifting in subduction settings. *Geochemistry, Geophysics, Geosystems*, 10, p.Q05001. doi:10.1029/2008GC0022200.

Wallace, R.E. & Morris, H.T., 1986. Charateristics of faults and shear zones in deep mines. *Pure & Applied Geophysics*, 124(1/2), pp.105-25.

Wallace, L.M., Reyners, M., Cochran, U., Bannister, S., Barnes, P.M., Berryman, K., Downes, G., Eberhart-Phillips, D., Fagereng, A., Ellis, S., Nicol, A. & McCaffrey, R., 2009b. Characterizing the seismogenic zone of a major plate boundary subduction thrust: Hikurangi Margin, New Zealand. *Geochemistry, Geophysics, Geosystems*, 10(10), p.Q10006. doi:10.1029/2009GC002610.

Walsh, J.J. & Watterson, J., 1991. Geometric and kinematic coherence and scale effects in normal fault systems. In A.M. Roberts, G. Yeilding & B. Freeman, eds. *The Geometry of Normal Faults*. Geological Society Special Publication 56. pp.193-203.

Wibberley, C.A.J., Yeilding, G. & Di Toro, G., 2008. Recent advances in the understanding of fault zone internal structure: a review. In C.A.J. Wibberley et al., eds. *The Internal Structure of Fault Zones: Implications for Mechanical and Fluid Flow Properties*. London: Geological Society Special Publications 299. pp.5-33.

Wilson, C.J.N., Gravely, D.M., Leonard, G.S. & Rowland, J.V., 2008. Volcanism in the central Taupo Volcanic Zone, New Zealand: tempo, styles and controls. In T. Thordarson et al., eds. *Studies in Volcanology: The Legacy of George Walker*. Special Publication of IAVCEI 2, London: Geological Society. pp.225-47.

Wilson, C.J.N., Houghton, B.F., McWilliams, M.O., Lanphere, M.A., Weaver, S.D. & Briggs, R.M., 1995. Volcanic and structural evolution of Taupo Volcanic Zone, New Zealand: a review. *Journal of Volcanology & Geothermal Research*, 68, pp.1-28.

Wilson, C.J.N., Rogan, A.M., Smith, I.E.M., Northey, D.J., Nairn, I.A. & Houghton, B.F., 1984. Caldera volcnaoes of the Taupo Volcanic Zone, New Zealand. *Journal of Geophysical Research*, 89(B10), pp.8463-84.

Wright, I.C., 1992. Shallow structure and active tectonism of an offshore continental back-arc spreading system: the Taupo Volcanic Zone, New Zealand. *Marine Geology*, 103, pp.287-309.

Wright, I.C., 1997. Morphology and evolution of the remnant Colville and active Kermadec arc ridges south of 33 30'S. *Marine Geophysical Research*, 19, pp.177-93.

Zhang, X. & Sanderson, D.J., 1998. Numerical study of critical behaviour of deformation and permeability of fractured rocks. *Marine & Petroleum Geology*, 15, pp.535-48.

Chapter 2

Fluid-flow in fault-zones from an active rift

Abstract

The geometry and hydraulic properties of fault-zones have been investigated using data for Mesozoic basement and Miocene strata from ~34 km of tunnels in the southern Taupo Rift, New Zealand. Fault-zones in these contrasting lithologies typically comprise fault-rock, small-scale faults, and fractures. Fault-zone thickness varies by several orders of magnitude approximating power-law distributions with the dimensions of these zones dependent on many factors including displacement, host-rock type and fault geometries. The fault-zones sampled, which are characterized by high shear strains (>10) and high bulk permeability (10^{-12}-10^{-10} m^2) relative to unfaulted host rock, comprise ≤ 15% of the rock. Despite fault-zones accounting for a small proportion of the total sample length, localised flow of groundwater into the tunnels occurs almost exclusively (≥ 91%) within, and immediately adjacent to, these zones. The spatial distribution and rate of flow from fault-zones are highly variable with typically ≤ 50% of fault-zones in any given orientation flowing. There are no simple relationships between fluid-flow and either or, fault strike, hydraulic head and flow-rate. A general positive relationship does however exist between fault size (e.g., fault-zone thickness) and maximum flow-rate. The entire basement dataset, for example, shows that 81% of the flow-rate occurs from fault-zones ≥ 10 m wide, with a third of the total flow-rate originating from a single fault-zone (i.e. the golden fracture). Higher flow-rates on larger faults may arise because these structures have greater dimensions and are more likely (than smaller faults) to be connected to other faults in the system and the surface. While these relationships provide a basis for predicting which fault-zones are likely to have the highest fluid-flow-rates, the system is sufficiently heterogeneous that locating the golden fracture will be challenging.

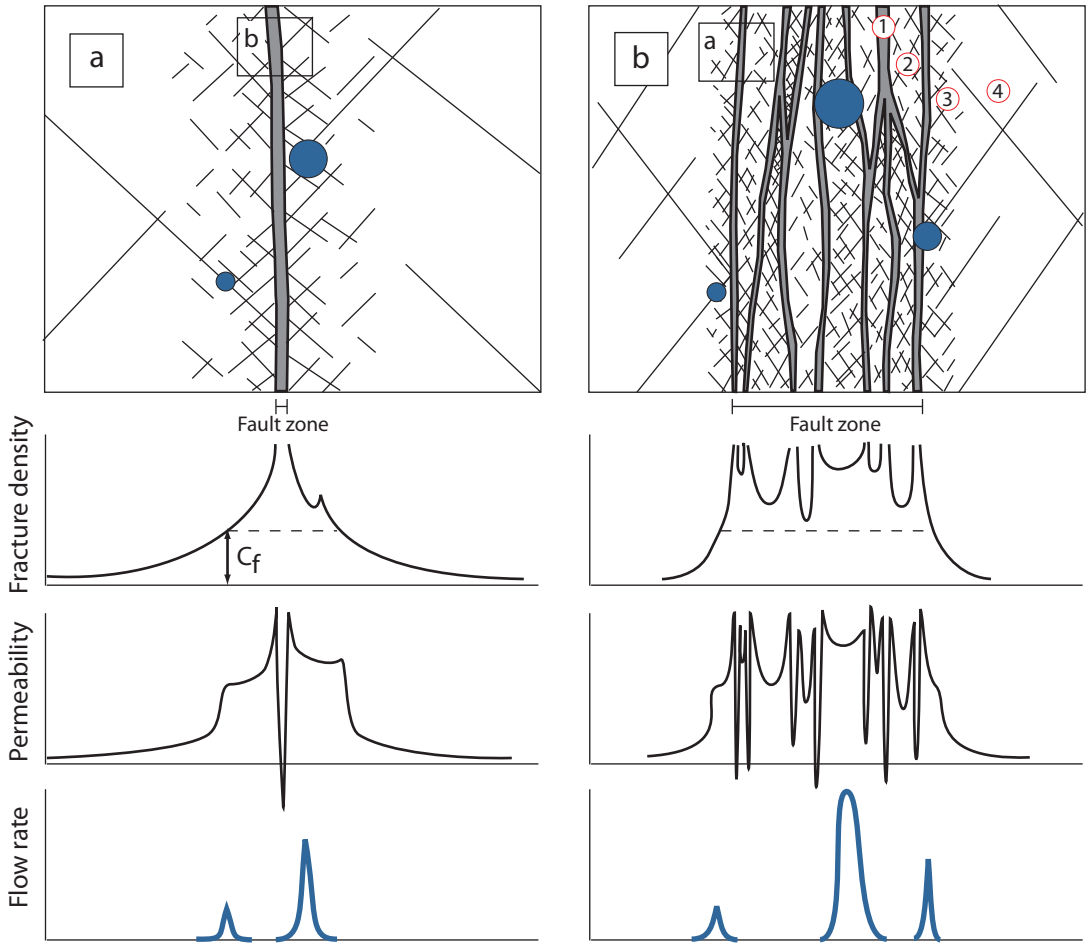

Figure. 1. Schematic hydrogeological properties of fault zone architecture (after Faulkner et al., 2010). (a) A single high strain slip zone surrounded by a lower strain damage zone (e.g. Chester & Logan, 1986). (b) Anastamosing pattern of mulitple high strain slip zones bounding variably strained protolith (e.g. Wallace & Morris, 1986).The bulk physical properties of these two end-members is dependent on the scale of observation. A critical fracture density (C_f) is required before macro-scale permeability occurs. Fault-zone architecture; 1) Fault rock (gouge, breccia, cataclasite), 2) Fault bound lenses of variably strained wall rock, 3) Fractured wall rock and 4) Protolith

1. Introduction

Hydraulic behaviour of fault-zones is difficult to predict due to their spatially variable structure and permeability. Bulk flow-rates through or along a fault-zone are important for many practical applications, including geothermal and hydrocarbon production, and are dependent on a number of factors including permeability variations, structural anisotropy, pressure differentials, and fluid viscosity (Caine et al., 1996; Evans et al., 1997; Cox, 1999; Wibberley et al., 2008; Manzocchi et al., 2010). Assessing the bulk flow characteristics of fault-zones has been hindered by a general lack of *in situ* flow data which can be related to the structure of fault-zones and surrounding rock-mass (Evans et al., 1997; Wibberley et al., 2008; Faulkner et al., 2010). Here I combine mapping of water flow-rates and fault-zone structure to examine how, where, and why faults impact on fluid-flow.

Faults zones exhibit extreme internal complexity and heterogeneous strain distribution which does not lend itself to simplification or generalisation (Childs et al., 2009). It has long been recognised that fault-zones are irregular, branched, and anastomosed over a broad range of scale (mm to km) (Fig. 1). They comprise one or more zones of fault-rock (gouge, breccia, cataclasite) that can bound or sit within a matrix of less sheared and highly fractured rock (Fig. 1) (Wallace & Morris, 1986). Fluid-flow within fault-zones is controlled by their hydraulic properties which are influenced by wall rock lithologies and fault-zone architecture (Wallace & Morris, 1986; Caine et al., 1996; Childs et al., 1996b; Evans et al., 1997; Wibberley et al., 2008; Faulkner et al., 2010). The spatial extent to which faults impact on fluid-flow depends on their size, connectivity (and the connectivity of elements within the zones) and permeability relative to the wall rock (Balberg et al., 1991; Evans et al., 1997; Cox, 1999). Large or highly connected faults or fault-zones with permeabilities which differ significantly, at least two orders of magnitude higher, than the host rock have the greatest potential to modify flow (Bour & Davy, 1997; Evans et al., 1997; Sanderson & Zhang, 1999).

In this paper, I examine *in situ* fluid-flow from tunnels through fault-zones and host rock of very low permeability Mesozoic greywacke basement and relatively permeable Miocene sandstone. The dataset includes information on fault geometries and their spatial relationships to water flowing into the tunnels along the margin of the Taupo Rift, New Zealand. Faults and water flow from engineering geological logs and

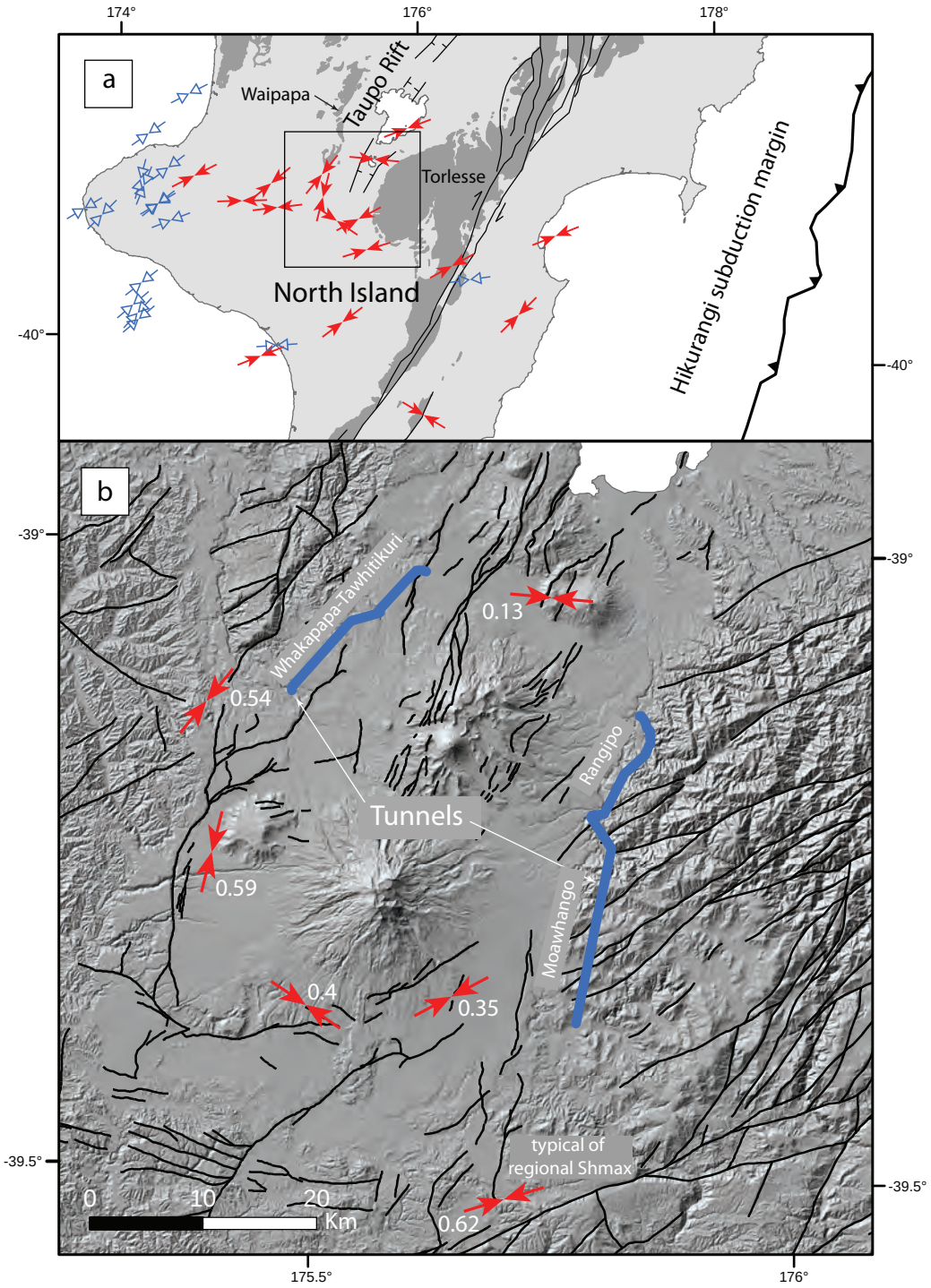

Figure 2. Tectonic setting of the Tongariro Power Development tunnels, southern Taupo Rift, New Zealand. (a) Location of tunnels in relation to the Hikurangi subduction margin, basement terranes (dark grey shading), and rifting. Orientation of SH_{max} and stress ratios in (B) derived from mid-crustal earthquakes (red arrows) (Sherburn et al., 2009) and bore hole breakouts (blue arrows) from the Australasia stress map (www.asprg.adelaide.edu.au/asm/). (b) Shaded relief model overlaid with Tongariro Power development tunnels (thick blue lines) and faults mapped at 1:250 000 (thin black lines) (Townsend et al., 2008; Lee et al., 2012).

reports are used to examine the factors influencing the rates and localisation of groundwater flows in relation to fault-zone architecture and connectivity of the fault-fracture network. The strain distribution, permeability structure, and flow-rates of basement fault-zones are highly heterogeneous, with fault-zone thickness and flow-rates exhibiting power-law distributions. My results may have application to the geothermal (including New Zealand's Taupo Volcanic Zone), hydrocarbon, and CO_2 storage industries however as the fault-fracture network as a whole displays characteristics similar to fracture systems at or above a percolation threshold (i.e. power law flow rates from unpredictable locations), the prediction of high permeability pathways will be problematic.

2. Fault definitions and measurements

Fault and fluid-flow data are from 3-6 m diameter tunnels excavated 75-500 m below the surface during the course of the Tongariro Power Development project in the southern Taupo Rift, North Island, New Zealand (Fig. 2) (Beetham & Watters, 1985). These data form a rather unique data set combining both detailed descriptions of fault zones and the location and rate of ground water flow. Previous descriptions of the tunnels by Beetham & Watters (1985) and various unpublished engineering reports (e.g. Hancox, 1975; Hegan, 1980) provide a general description of the tunnels, basement lithologies, structures (including faults) and the tunnelling conditions encountered during the course of the project. This study uses data from a detailed analysis of fault and fluid-flow-rate data taken from 1:240 engineering geological logs constructed at the time of tunnel excavation (1969-1976) to characterise rock-mass properties including strength and water flow (Fig. 3) (Hegan, 1980). The logs have been collated here to describe the first order geometry, distribution, fluid-flow properties of fault-zones over scales of centimetres to kilometres.

The dataset comprises 530 basement and 40 Miocene-Recent fault-zones intersected by ~34 km of tunnels excavated through Mesozoic greywacke basement and by ~2.5 km of tunnels through a Miocene marine sandstone, respectively (Fig. 2) (Beetham & Watters, 1985; Townsend et al., 2008). Fault-zone data typically comprise; distance along the tunnel, orientation, displacement (Miocene sandstone), description and thickness of fault-rock and fault-zone, rock strength (Mesozoic basement), and the location and rate of any localised groundwater inflow (Fig. 3).

Fault-zone and fault-rock thicknesses have been measured from tunnel sections through normal faults in Miocene strata and probable normal faults in basement. As with all studies of fault-zone and fault-rock dimensions these measurements carry an element of subjectivity and may vary depending on how these terms are defined. Here, fault-zone has been defined as a system of related fault segments that are kinematically related (i.e. they link or interact) and are restricted to a relatively narrow band or volume (Peacock et al., 2000). This definition can be applied to fault-zones within the tunnels which are generally defined by slip-surfaces containing fault-rock and/or by marked changes in rock strength (a function of fracture density) in the case of large basement fault-zones (Hancox, 1975; Hegan, 1980). Similarly, fault-rock which typically comprise gouge, crush zones and breccia, are generally well defined (e.g. Fig. 3). In this study all fault-zone thicknesses are measured between planar surfaces containing or bounding fault-rock (e.g. Fig. 3). The displacement required to discriminate fault-zone bounding slip surfaces from minor faults outside these zones cannot be rigidly defined since it depends on factors such as fault style, fault density or the scale of observation (Childs et al., 2009). Although difficult to estimate, it is possible that in some cases volumes of small (e.g. < 5%) fault-related strains have been excluded from our measurements. The concept of fault-zones comprising a high strain, low permeability fault core surrounded by a low strain, high permeability damage zone (Caine et al., 1996), do not adequately describe the variety of fault-zone geometries observed in the tunnels and has not been employed here.

Faults within the Miocene strata displace centi- to decimetre bedding with measured normal separations up to 3 m (i.e. tunnel height) (Fig. 3a). Fault-zones typically comprise numerous steeply dipping (73 ± 12°) slip zones of silty clay fault-rock (gouge) that separate relatively undeformed lenses of host rock (i.e. minor jointing and rotation). Fault-zones in Miocene strata are generally separated by thicknesses of undeformed wall rock at least as wide as the zone itself. In the rare instances where fault-zone definition becomes subjective (i.e. high frequencies of low displacement faults occurring over a broad thickness), subdivision of faulting into smaller zones makes little difference to displacement-thickness ratios (Childs et al., 2009) or to the general conclusions of this paper.

Although steeply dipping (68 ± 17º) basement faults typically have no displacement markers, their size (e.g. length and maximum displacement) can be inferred from fault-zone width. Large fault-zones ≥ 10 m in width typically contain, and

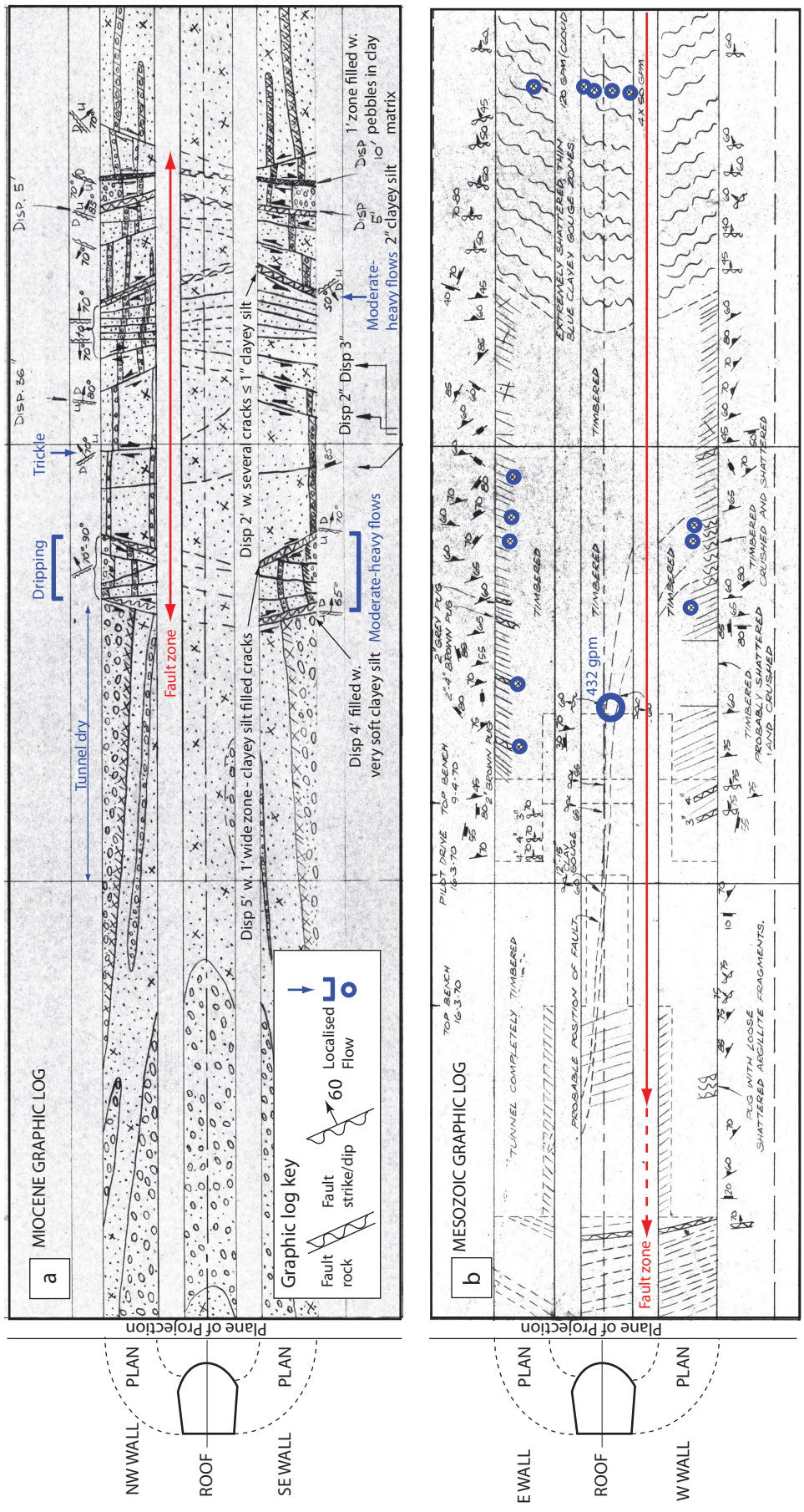

Figure 3. Graphic engineering geological logs from the Tongariro Power Development tunnels. Graphic logs represent ~100 m (300 ft) long sections. Flow locations and fault rock thickness not recorded directly on graphic log included for reference. (a) Example of a fault zone in Miocene sandstone. (b) Example of fault zone in Mesozoic basement. Locations of flows highlighted by blue open circles, brackets, and arrows. Fault zone dimensions shown by red arrows.

are bounded by, numerous sub-parallel slickensided slip surfaces which define lenses of variously sheared, jointed, shattered, and/or crushed rock (Fig. 3b). Small fault-zones (i.e. ≤ 1 m) are well defined, almost planar zones of crushed rock within a matrix of plastic silty clay (gouge). Grading analysis of typical fault-rock (i.e. gouge, breccia, and/or cataclasite) shows it to comprise ~50% sand or larger grain sizes (Hegan, 1980).

Regions of highly fractured rock bounding one or both margins of basement fault-zones are common, though not universal. Highly fractured rock (fracture spacing ≤ 5 cm) represents the lowest strain component of fault-zones which may be bounded by fault-rock or located between fault-rock and wall rock. For example, many highly fractured regions approaching the margins of fault-zones contain minor clay slickensided fault surfaces (Hegan, 1980) from which it is inferred that these regions accrued a small percentage of the total shear strain. As there is little or no pore space remaining in the basement host lithologies (Allis et al., 1993; Wood et al., 2001), it is these highly fractured zones predominantly within and adjacent to fault-zones that produce the majority of porosity and bulk permeability in the basement. At the resolution of the logs, water flow also occurs directly from basement fault-rock containing mixtures of gouge with fractured and crushed rock.

3. Geological setting

The tunnels are located on the margins of the southern Taupo Rift in the central North Island, New Zealand. Rifting formed over the last 2 Ma and is spatially coincident with arc volcanism and high temperature geothermal systems (Bibby et al., 1995; Wilson et al., 1995), although neither were intersected by the tunnels. Basement greywacke rocks of the North Island comprise a series of imbricate tectono-stratigraphic terranes accreted along the Gondwana subduction margin during the Permian to Cretaceous, two of which are intersected by the tunnels (Waipapa and Torlesse) (Fig. 2) (Beetham & Watters, 1985; Mortimer, 2004). These basement rocks have undergone multiple episodes of faulting, including the most recent episode of rifting (Beetham & Watters, 1985; Walcott, 1987; King & Thrasher, 1996; Nicol et al., 2007) which accommodated NW-SE oriented extension of the central North Island (Hurst & McGinty, 1999; Acoccella et al., 2003; Hayes et al., 2004; Villamor & Berryman, 2006; Reyners, 2010) (chapter 3).

Basement rocks intersected by tunnels are indurated, Mesozoic sedimentary rocks (initially formed as deep water turbidites) which have been subject to low-grade

metamorphism (Beetham & Watters, 1985; Mortimer, 2004). Basement comprises three dominant lithologies with bedding thicknesses ranging between 0.1 m to ≥ 100 m; a muddy fine to medium quartzo-feldspathic sandstone, a fissile mudstone (argillite), and an argillite that typically contains thin discontinuous beds or lenses of sandstone (Hegan, 1980; Beetham & Watters, 1985). These rocks have been folded with beds generally dipping steeply (> 60°) and striking north-northeast. Moderate-high angle (70-90º dips) joints with variable lengths and spacing are ubiquitous throughout basement and cross-cut less common and older moderate-low (30-50º) quartz and epidote veins (Hancox, 1975; Hegan, 1980). Low permeabilities outside basement fault-zones are indicated by very low or no groundwater seepage in unfaulted sections of tunnel. Basement has primary porosities typically < 10% (Brathwaite et al., 2002) and intrinsic permeabilities (for an equivalent lithology from drill core in the Taranaki Basin) ranging between 10^{-15}-10^{-17} m^2 (Higgs et al., 2012). Unconformably overlying basement is a Mid-Miocene age silty fine sandstone, interbedded with conglomerate lenses, with gentle (<10°) bedding dips towards the south (Townsend et al., 2008). Drill core samples from the Mt Messenger formation in the Taranaki Basin, which is of similar age and provenance to the Miocene sequence encountered here, show a general positive correlation between porosity (15-25%) and intrinsic permeability (10^{-15}-10^{-13} m^{-2}) (Higgs et al., 2012).

Fluid-flow data from Mesozoic basement and Miocene strata are primarily sourced from engineering geological logs (Fig. 3). The exception are basement fault-zones with large fluid-flows where tunnel conditions were poor, these data are sourced from engineering geological reports detailing fault-zone dimensions, properties, and flow-rates (Hancox & Paterson, 1975). Concentrated localised groundwater flow into the tunnels reflects fault parallel (in-plane) flow. I shall refer to these groundwater inflows as “localised flow” or “flow”. While there is sparse anecdotal evidence that some faults compartmentalize the groundwater system (e.g. Fig. 3a) similar to that described in other fault systems (Wallace & Morris, 1986; Evans et al., 1997), no data are available from the tunnel logs to assess across fault flow-rates. Within the Miocene sequence, all flow occurred from within fault-zones where individual faults were identified and described as the source of flow, though the exact locations were not shown (e.g. Fig. 3a). Within Mesozoic basement, the location of fluid-flow is generally recorded as a point source with an assigned flow-rate measurement (Hancox & Paterson, 1975). Basement flow-rates were measured quantitatively (i.e. gallons per

minute) while in the Miocene sequence flow-rates where typically given descriptive terms (i.e. trickle, moderate, heavy). In some cases descriptive terms and measured rates were given for the same flow, and these were used to calibrate flow-rates for the descriptors. Flow-rates were recorded at the time of logging which generally occurred between 5-15 days after excavation. Flow-rates decrease with time from tunnel excavation. Repeat flow-rate measurements at three sites suggest groundwater flow-rates decayed exponentially reducing to a half and one third of their initial values after 15 and 30 days, respectively. Therefore, the time the sample was taken relative to tunnel excavation probably accounts for no more than a factor of 2 variation in flow-rates.

4. Relationships between faults and fluid-flow

The vast majority of fluid-flow into the tunnels is associated with fault-zones. Within basement for example, 91% of the total number of instances of localised flow come directly from fault-zones or within 10 m of fault-rock. These flows account for ~99% of the total localised flow-rate measured in the tunnels through basement. Not all fault-zones are, however, associated with flow. In the basement only around a quarter of fault-zones $\geq$ 0.1 m thick are associated with localised flows. Within Miocene strata, all localised water flow occurs from fault-zones though only about a half of the fault-zones have flow associated with one or more slip zones. Understanding the factors that govern whether a fault-zone is associated with flow, and where that flow occurs in relation to fault-zone architecture, are discussed in this section.

4.1 Fault-zone geometry

Permeability across and along fault-zones is governed by their spatial distribution of rock deformation products (e.g. fault-gouge and fractures) in three dimensions. Fault-rock containing gouge can act as barriers to across fault flow, while open fractures can promote along fault flow (Caine et al., 1996; Evans et al., 1997; Cox, 1999; Wibberley et al., 2008; Faulkner et al., 2010; Manzocchi et al., 2010). The widths of both fault-zones and fault-rock can change significantly over a few metres. Fault-gouge thickness can, for example, vary by up to a factor of four between tunnels walls (~ 3 m) in basement. These variations are associated with bifurcation and truncation of slip zones which are widely observed in many fault systems (Childs et al., 2009). I examine the geometry of hydraulically conductive faults in the Mesozoic basement and Miocene

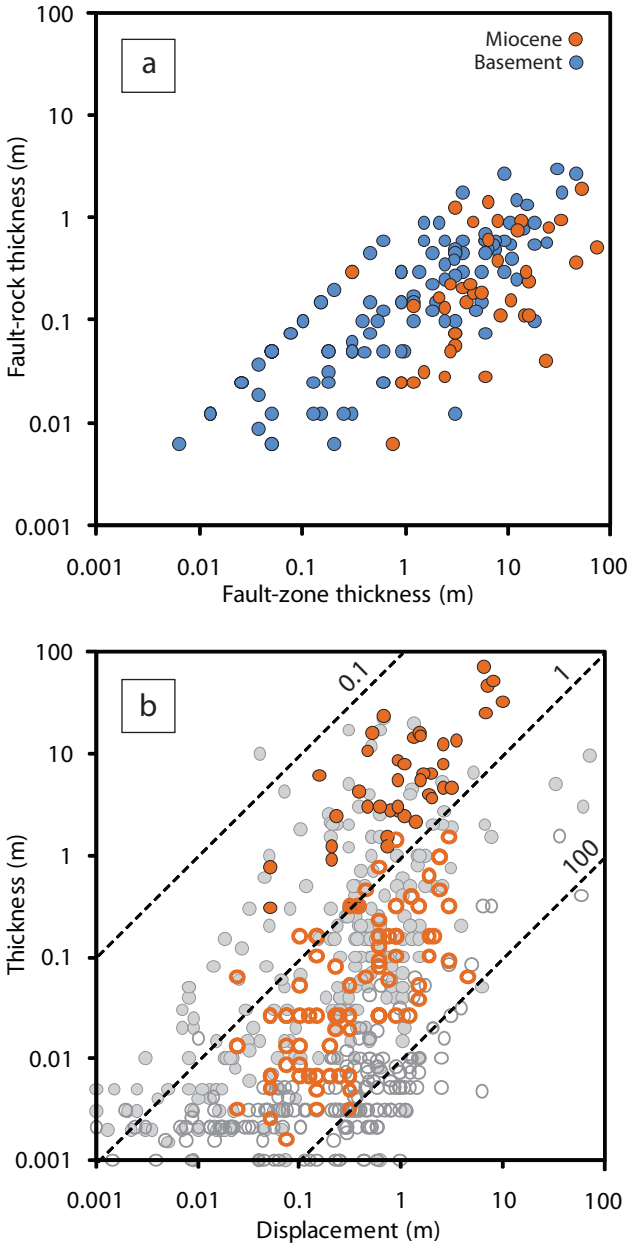

Figure 4. Fault-zone architecture. (a) Fault-rock thickness in relation to fault-zone thickness in Miocene strata (orange filled cirles) and Mesozoic basement (blue filled circles). (b) Relations between Miocene fault-zone (filled circles) and fault-rock (open circles) thickness and displacement. Data from this study (orange) superimposed on outcrop data from equivalent lithologies in Taranaki Basin (grey filled circles = fault zones and grey open circles = fault rock). Taranaki data from Childs et al. (2009).

sequence to understand better what factors control the location and rate of flow into the tunnels. First I describe the main geometric elements of fault-zones in each lithology, examine these in relation to global compilations and general properties of fault populations, then look at the main relationships between fault-zones and fluid-flow.

Fault-zones in the Miocene sequence comprise two main architectural units, fault-rock (Gouge) and fault-bound lenses of generally undeformed (at the resolution of the logs) or sparsely jointed host rock (Fig. 3). In contrast, basement fault-zones are comprised of four main architectural units. The three main types of fault-rock (Gouge, Crush, and Shear zones) and zones of fractured rock (Shatter zones) were typically discriminated within basement fault-zones in the engineering geological logs. These four fault-zone components reflect decreasing strain intensity (from gouge to fractured rock respectively) through decreases in fracture density and clay content associated with increasing grain size (Hegan, 1980). Zones of fractured rock, while generally associated with fault-rock, are not exclusive to fault-zones. Combinations of gouge and variable amounts of rock fragments (termed crush zones in the logs), which are typically centimetres to metres wide, constitute the majority of fault-rock observed in the tunnels through basement.

The heterogeneity of fault-gouge thickness and its positive relationship to fault-zone thickness are illustrated for basement and Miocene in Fig. 4. Fault-gouge thicknesses (contained in single or multiple slip zones) are 10-100% of the fault-zone thickness in circumstances where the latter ranges between 0.1 and 1 m. Fault-zones encountered within the Miocene sequence typically comprise 2 and 8 slip zones each containing fault gouge (e.g. Fig. 3a). Smaller fault-zones in basement (< 1 m thickness) may be associated with a single slip zone, however, as fault-zone thickness increases, so generally does the number of slip zones. For fault-zone widths in basement > 10 m only the widest thicknesses of fault-rock were measured due to the increasing numbers of minor slip zones and the presence of tunnel supports (e.g. Fig. 3b). Faults in basement and Miocene strata show a general positive relationship between total fault-rock and fault-zone thicknesses (Fig. 4). In the Miocene sequence positive relationships between fault-rock and fault-zone thickness with displacement also exist and are consistent with the global compilation Childs et al. (2009).

Faults in both basement and Miocene strata display one-dimensional power-law scaling relationships. These relationships for displacement (d), thickness (t), and flow-rate (f) populations are determined from normalized cumulative frequency distributions,

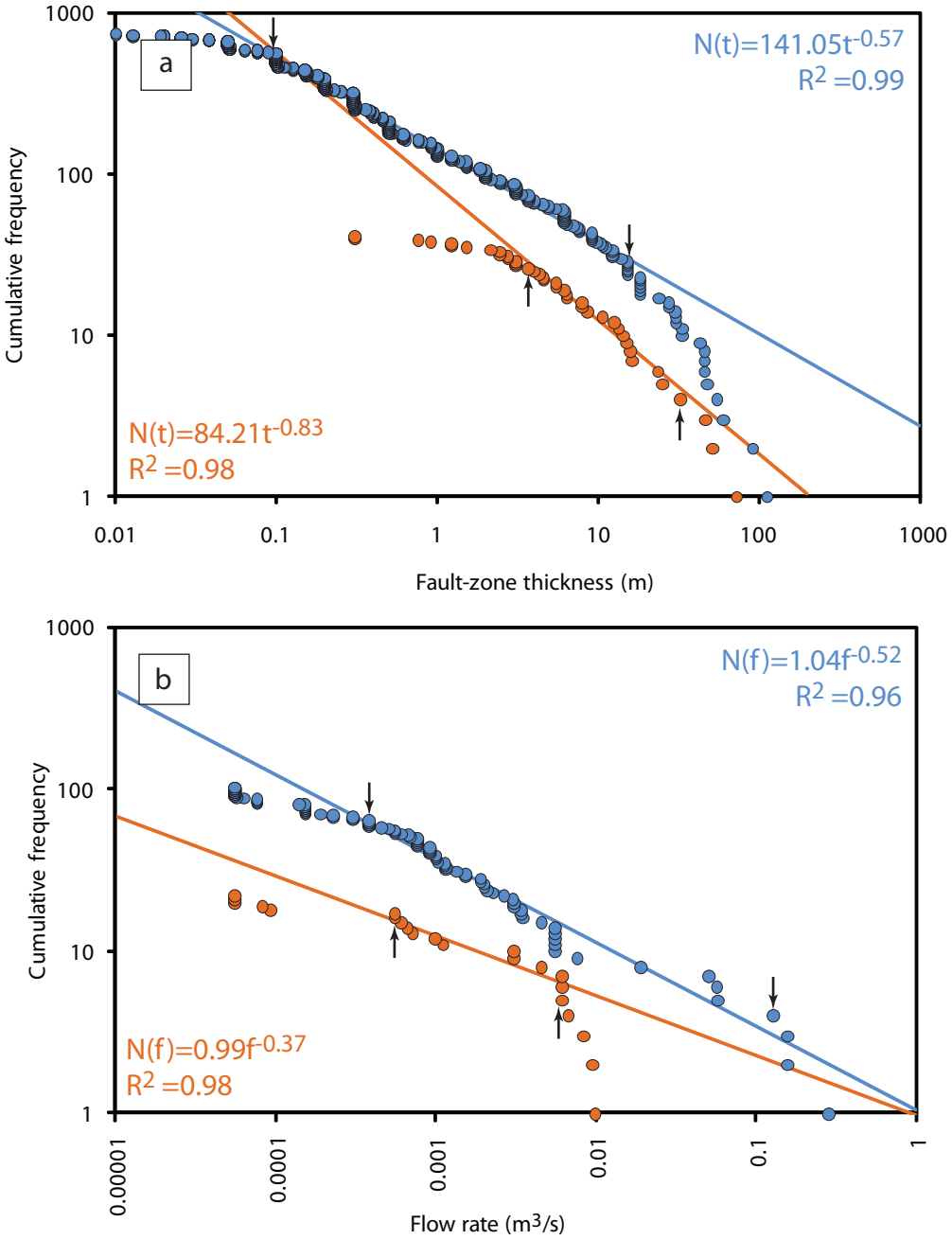

Figure 5. Fault-zone thickness and flow-rate one-dimensional populations. (a) Fault-zone thicknesses from Miocene strata (orange filled circles) and Mesozoic basement (blue filled circles). (b) Flow rates from fault-zones, key as in (a). Best fit power law trends (coloured lines) derived from the central segment (defined between arrows) of each population.

N(d, t, f) (i.e. thickness in metres greater or equal to t). In log-log plots, where a straight line indicates a power-law distribution with an exponent, a, given by the slope of the graph (Walsh & Watterson, 1992; Gillespie et al., 1993):

$$N(d, t, f) \approx (d, t, f)^{-a}$$

Resolution effects at the upper and lower ends of these distributions are a common feature of natural data and only the maximum slope of the central segment over at least one order of magnitude is considered here (Walsh & Watterson, 1992; Nicol et al., 1996). Power-law distributions are commonly referred to as 'self-similar' or fractal (i.e. scale independent) and indicate a high degree of variability in the quantity measured.

Consistent with other measures of fault-zone size, such as displacement or length (Walsh & Watterson, 1992; Kim & Sanderson, 2005), fault-zone thicknesses also display power-law distributions with exponents ranging from -0.57 for the aggregate basement dataset (Fig. 5a) to between -0.8 and -1.0 for well constrained tunnel sections 2.5-5 km in length (e.g. Miocene in Fig 5a). Deviation from the power-law trends at fault-zones thicknesses < 0.1 m in basement and < 1m in Miocene is interpreted to indicate under sampling of fault-zone thicknesses below these values.

Flow-rates in the tunnels are highly variable and range over four orders of magnitude (10^{-5} to 10^{-1} m^3/s) (Fig. 5). Flow-rates in Miocene and basement rocks approximate power-law distributions over at least one order of magnitude with exponents of -0.37 and -0.52, respectively. Deviation from the power-law trend at flow-rates < 5 x10^{-4} m^3/s indicate under sampling of flows below this value. Basement fault-zones show a broader range of flow-rates than the Miocene sequence which is probably, at least in part, due to differences in sample size and the corresponding increase in maximum fault size in basement. The inference that flow rates are positively related to fault size is supported by the power-law exponents for fault-zone thickness and flow-rates in basement which are similar. Fault-zone thickness and flow-rates in Miocene strata have different power-law exponents and may in part be due to the limited sample size range which is significantly less than for basement.

Fault-zones, including fractured wall rock adjacent to fault-rock in basement, account for the vast majority of localised flow entering the tunnels. No systematic entry location (with respect to the tunnel axis) is observed between adjacent (and sometimes within) fault-zones in either Miocene or basement rocks as might be expected if, for example, flow locations were controlled by a local or regional topographic gradient. In basement at the resolution of the tunnel logs, flow typically occurs from within or

immediately adjacent to fault-rock and from lenses of variably strained host rock bounded by fault-rock. Fault-rock in basement typically contains variable proportions of breccia and clay and flow is inferred to be mainly occurring within breccia dominated zones. In the Miocene sequence, the majority of flow occurs within fault-zones adjacent to fault-rock typically 0.01-1 m in thickness. Occasionally this flow was observed to emanate from joints within fault-zones. In many cases, not all fault-rock was associated with nearby flow. For example, along a 1.5 km tunnel section in the Miocene sequence, 52 of 111 fault-rock zones were associated with flow. This contrasts with the undeformed Miocene host rock either within or adjacent to fault-zones, from which only minor (< 1%) (mainly associated with conglomerate units) or no seepage occurred.

By contrast, flows occur from fractured wall rock within, and adjacent to fault-zones in basement. Flow associated with small basement fault-zones (i.e. < 1 m wide) occur directly from fault-rock crush zones or from fractured rock adjacent to the fault-zone (i.e. typically ≤ 2 m). Flows associated with larger fault-zones (i.e. > 1 m thick) occur directly from fault-rock or from variably sheared/fractured zones within or adjacent to the fault-zone. Where there is clear distinction between zones of gouge and highly fractured and/or sheared rock within a fault-zone, flow occurs from the later. In general, fractured rock throughout the basement appears to support moderate to low flow-rates ($\leq 5 \times 10^{-3}$ m^3/s) typically adjacent to or within fault-zones (see below). As noted previously (Wallace & Morris, 1986), rare instances of moderate to low flow occurring from fractured zones not associated with a fault-zone are found. High flow-rates ($\geq 5 \times 10^{-3}$ m^3/s) occur exclusively from sheared and fractured rock in proximity to gouge thicknesses > 1 m thick within basement fault-zones typically ≥ 10 m wide.

Fracture density may influence basement fault-zone flow-rates. In specific examples where high flow-rates ($> 1 \times 10^{-2}$ m^3/s) occur within, and moderate-low flow-rates ($\leq 5 \times 10^{-3}$ m^3/s) occur adjacent to fault-zones. Fracture densities derived from drillcore through multiple basement fault-zones ≤ 1 m in thickness indicate the number of fractures increase from background values of ~1-10 m^{-1} to ~100 m^{-1} adjacent to fault-zones, increasing to > 100-1000 m^{-1} within fault-zones (Hegan, 1976). These high flow-rates may have been facilitated by high densities of open fractures (e.g. 100-1000 fractures/m) which are common in wider fault-zones. It is not possible, however, to correlate high flow-rates to individual fractures or to estimate fracture apertures from tunnel logs.

In summary, fault-zones in Miocene strata and Mesozoic basement typically comprise an anastomosing system of intersecting fault segments (both synthetic and antithetic) which bound lenses of variably fractured wall rock. The location and rates of flow from within and adjacent to fault-zones are highly variable. Within medium-high porosity and permeable Miocene sandstones, all localised flow is associated with fault-zones. Within low porosity and permeability Mesozoic basement, localised flow is fracture controlled and predominantly occurs from within and adjacent to fault-zones where fracture densities are highest. Given the time scales flow occurs over in this study (days to weeks) and the porosity and permeability of the host lithologies, I suggest that the hydraulically conductive faults are the primary reservoirs associated with flow into the tunnels. In general, the majority of flow occurs from fault-zones where the intrinsic permeability/porosity structure of the host lithology appears to have little influence on the flow properties of the faults. In the following sections I examine factors such as fault orientation with respect to the local and regional stress field and/or the connectivity of the fault-fracture network that may account for the highly variable distribution and rate of flow.

4.2 Fault orientations and stress regime

The permeability of faults and fractures is believed to be strongly controlled by their orientation relative to the present day stress field (Barton et al., 1995; Morris et al., 1996; Ferrill et al., 1999; Sanderson & Zhang, 1999; Townend & Zoback, 2000). Under anisotropic stress conditions, critically stressed faults and fractures (i.e. those close to failure) are considered more likely to be permeable or hydraulically conductive than those that are not (Barton et al., 1995; Townend & Zoback, 2000; Evans et al., 2005). Critically stressed faults, for example, have resolved shear stress (τ) acting on their surfaces that equals or exceeds their frictional resistance to sliding (F), where frictional resistance is proportional to the effective normal stress (σ_n) acting on those surfaces: $F \leq \tau = \mu\sigma_n$ where μ is the coefficient of static friction (Jaeger & Cook, 1979; Barton et al., 1995; Morris et al., 1996). Faults and fractures in optimal orientation for failure or with high slip tendencies (T_s) in an ambient stress field have $T_s \geq \tau/\sigma_n \geq 0.6$ (Byerlee, 1978; Morris et al., 1996; Townend & Zoback, 2000). Faults and fractures striking sub-parallel to the trend of the maximum stress are therefore the most likely structures to be hydraulically conductive under the Coulomb failure criterion. The dilation of fractures,

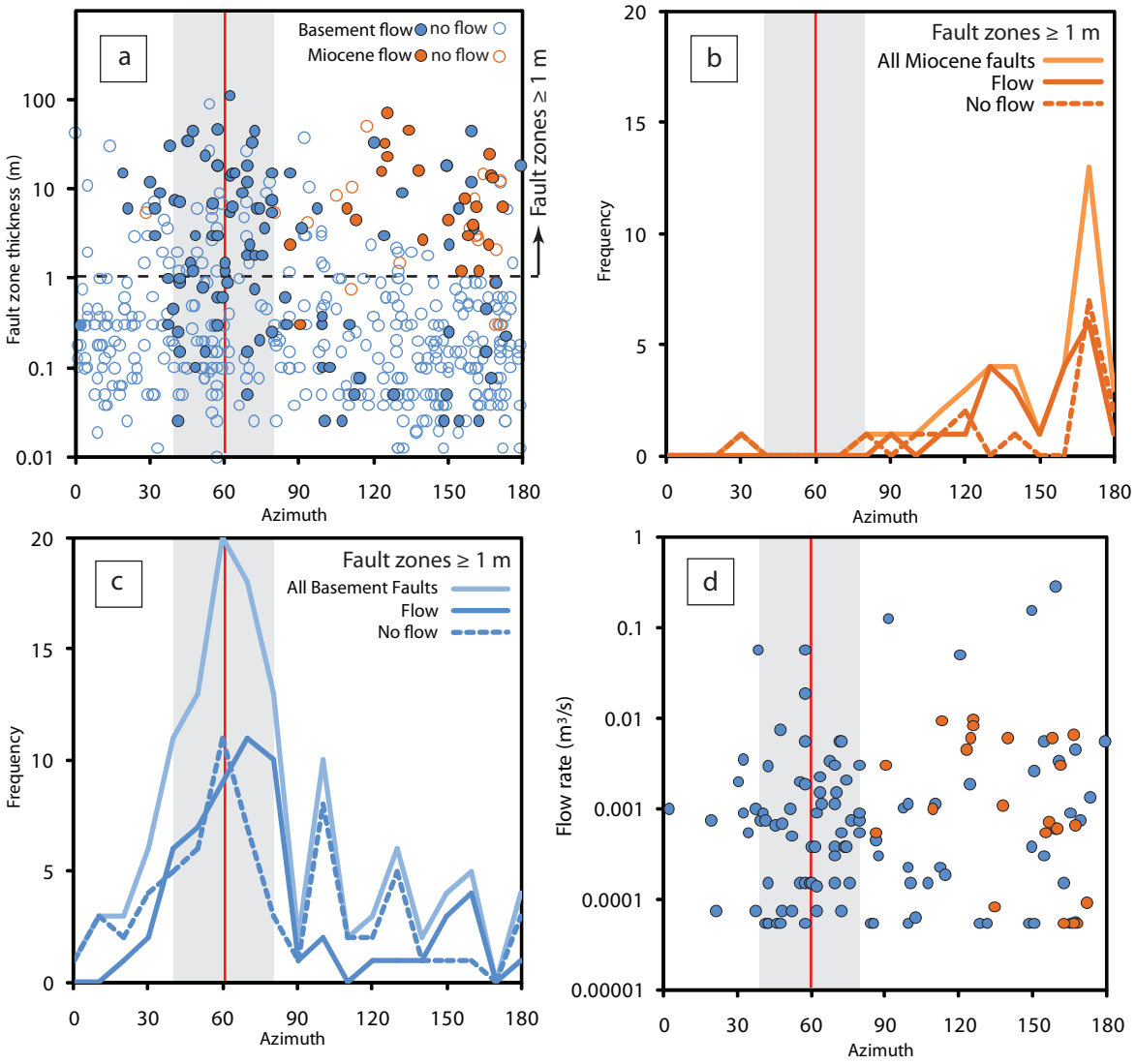

Figure 6. Fault-zone flow data. (a) Hydraulically conductive and non-conductive fault-thickness orientation. (b) Miocene sequence fault zones ≥ 1 m with and without flow. (c) Basement fault zones ≥ 1 m with and without flow. (d) Fault-zone orientation verses flow rate. Regional Shmax trend (red line) with ± 20 º variability (grey shading) observed across central North Island, see Fig. 2 for location and references. The majority of basement fault zones < 1 m are not associated with flow, those that are only account for ~3% of the total flow rate, and therefore we restrict our analysis to faults zones ≥ 1 m in thickness.

largely controlled by effective normal stress, can also influence permeability (Ferrill et al., 1999). The normal stress a fracture experiences depends on the orientation and magnitude of the principal stresses in relation to that plane. The permeability or the ability of a fracture to dilate and transmit fluid is directly related to its aperture, which in turn is a function of the effective normal stress acting upon it (Ferrill et al., 1999). *In situ* studies of crustal permeability from deep boreholes (2-9 km) indicate that, in general, the crust has near hydrostatic pore pressures to depth that are maintained by high bulk permeability (~10^{-17} to 10^{-16} m^2 over scales of 1-10 km) induced by critically stressed faults and fractures (Townend & Zoback, 2000).

Within Miocene strata on the western margin of the Taupo Rift, the mode for normal fault strike is ~170º (Fig. 6a), sub- normal to the regional maximum horizontal stress (Shmax) (refer Fig. 3) and approximately parallel with the underlying basement fabric (Townsend et al., 2008). The frequency and orientations of hydraulically conductive and non-conductive fault-zones within Miocene rocks are approximately equivalent (Fig. 6b). In contrast to the Miocene sequence, the basement faults strike predominantly parallel to the regional Shmax orientation and to regional faults mapped above the eastern tunnels (Lee et al., 2010) from where the majority of basement data originate (Fig. 6a and c). Again, approximately equal numbers of hydraulically conductive and non-conductive faults are observed around the peak strike ~060º (Fig. 6c). Approximately 75% of large basement fault-zones ≥ 10 m and sub-parallel to Shmax (040-080º) are hydraulically conductive with a wide range of flow-rates (10^{-5} to 10^{-2} m^3/s) (Fig. 6d). However, high flow-rates (> 10^{-2} m^3/s) occur across a range of azimuths in basement, the highest occurring on faults orientated perpendicular to Shmax.

The optimal orientation of faults in the prevailing stress field cannot account for the variability in the distribution and rate of flow occurring on faults within the tunnels 100-500 m below the surface. The observations that only half of optimally oriented faults within basement are associated with flow, that the largest flow-rates occur from a basement fault-zone striking normal to the regional Shmax and that most of the hydraulically conductive faults in Miocene strata also strike at a high angle (60-90º) to Shmax, suggest factors other than stress also influence the hydraulic properties of fault-zones in this study. There are two main interpretations of these observations. Firstly, fault-stress orientation relations control fault permeability but either regional Shmax is not a good predictor or local Shmax and/or that not all slip surfaces/fractures within

fault-zones are parallel to the general fault strike. Secondly, factors other than (or in addition to) stress and fault strike influence fault permeability (e.g. fracture density and connectivity, or fluid source).

In the southern Taupo Rift the local stress field can deviate significantly from the regional trend over distances of no more than 15-20 km (Fig. 2). Determination of Shmax orientation and stress ratios (σ_1-σ_2/ σ_1-σ_3) from clusters of mid crustal focal mechanisms by Sherburn et al. (2009) show deviations of up to 80º from regional trends observed across the central North Island. Stress ratios in the southern Taupo Rift also show a high degree of variability (from 0.1 ($\sigma_1 \approx \sigma_2$) to 0.67 ($\sigma_2 \approx \sigma_3$) (Sherburn et al., 2009). These local variations in the stress field could account for flow associated with non-optimally orientated faults. Deviation of the local stress field from the regional Shmax orientation could also occur in proximity to recently active faults (Barton & Zoback, 1994; Brudy et al., 1997) some of which are close to, or intersected by, the tunnels (Villamor & Berryman, 2006).

Alternatively, complex fracture patterns within a fault-zone may result in fracture sets optimally oriented with respect to the maximum principal stress and/or Shmax even though the general trend of the fault is not. Minor faults and fractures in basement fault-zones, for example, may vary in strike more than 60º from each other or from the overall strike of the fault. Such variations could produce fault slip surfaces or fractures within the zone that strike parallel to Shmax. Departures in the strike of faults and fractures within fault-zones from the general fault strike will be common at relays or bends in fault surfaces (Childs et al., 1996b; Cox, 1999; Kim et al., 2004; Childs et al., 2009). These are likely to be sites of large numbers of small-scale faults and wide fault-zones and could represent favoured locations of fluid-flow (Childs et al., 1996a; Fossen et al., 2005; Ilg et al., 2012). Numerical modelling of pervasively fractured rock (at depths equivalent to this study) also show significant variations in deformability and permeability that are functions of fracture geometry (density, length, anisotropy) and orientation within a stress field (Zhang & Sanderson, 2001). In these models where Shmax is parallel to fracture sets (i.e. critically stressed), dilation is observed, otherwise dilational shear deformation modes develop, within which sliding, opening and block rotation occurs at fracture intersections resulting in highly localised power-law flow-rates (Zhang & Sanderson, 2001).

Within the near surface tunnels in this study the orientation of faults with respect to the regional or local principal stress directions does not appear to be a good indicator

of their hydraulic conductivity. While out of scope of this study, this raises a question about what depth principal stress orientations do begin to significantly influence flow anisotropy? Fault controlled flow anisotropy at Yucca Mountain, for example, is consistent with predictions based on slip and dilation tendency analysis from depths of ~400 m (Ferrill et al., 1999) whereas orientation of faults in this study at depths between 100-500 m depth shows little influence on flow direction or rate. Disparity between our results and those of previously published suggest that further work is required to determine under what conditions slip and dilation tendency might prove fruitful for predicting when and where faults will enhance fluid flow.

4.3 Fluid-flow Model

Fault-zones controlling flow into the tunnels (and potentially the hydrostatic fluid regime) comprise ≤ 8% of the rock encountered by the tunnels, yet they account for ≥ 90% of the flow. The majority of fluid-flow into the tunnels comes from fault-zones where fracture densities are high. Faults with widely varying strikes accommodate fluid-flow and it is not possible to predict which faults will flow based on their strike. Fault-zones are fluid reservoirs which contain highly localised conduits for water flow. Moderate to low flows ($\leq 5 \times 10^{-3}$ m^3/s) occur as point sources from, or immediately adjacent, to fault-rock or from fracture zones associated with fault-zones. The highest flows occur from the biggest faults as these are the most connected to the surface and other faults. High flow-rates ($\geq 5 \times 10^{-3}$ m^3/s) generally occur across areas within fault-zones that suggest these sheared, fractured, or crushed zones have properties similar to a porous medium. Because of the relationship between fault size and flow-rates, power-law scaling properties of the two variables are similar.

Fluid-flow pathways in the crust are influenced by the permeability of the rock-mass over a variety of spatial and temporal scales, and by fluid pressure gradients that depart from hydrostatic (Cox, 1999). Many *in situ* studies, including this one, highlight the highly localised nature of fluid-flow through fractured media (Wallace & Morris, 1986; Palliet et al., 1987; Levens et al., 1994; Tsang & Neretnieks, 1998; Cox, 1999; Evans et al., 2005). Numerical models of rock deformation consistent with these studies show highly non-linear behaviour and flow localization are features of a wide range of natural well-connected critically stressed fracture networks (Sanderson & Zhang, 1999). Similar to these studies, a small fraction of the elements within the fault-fracture

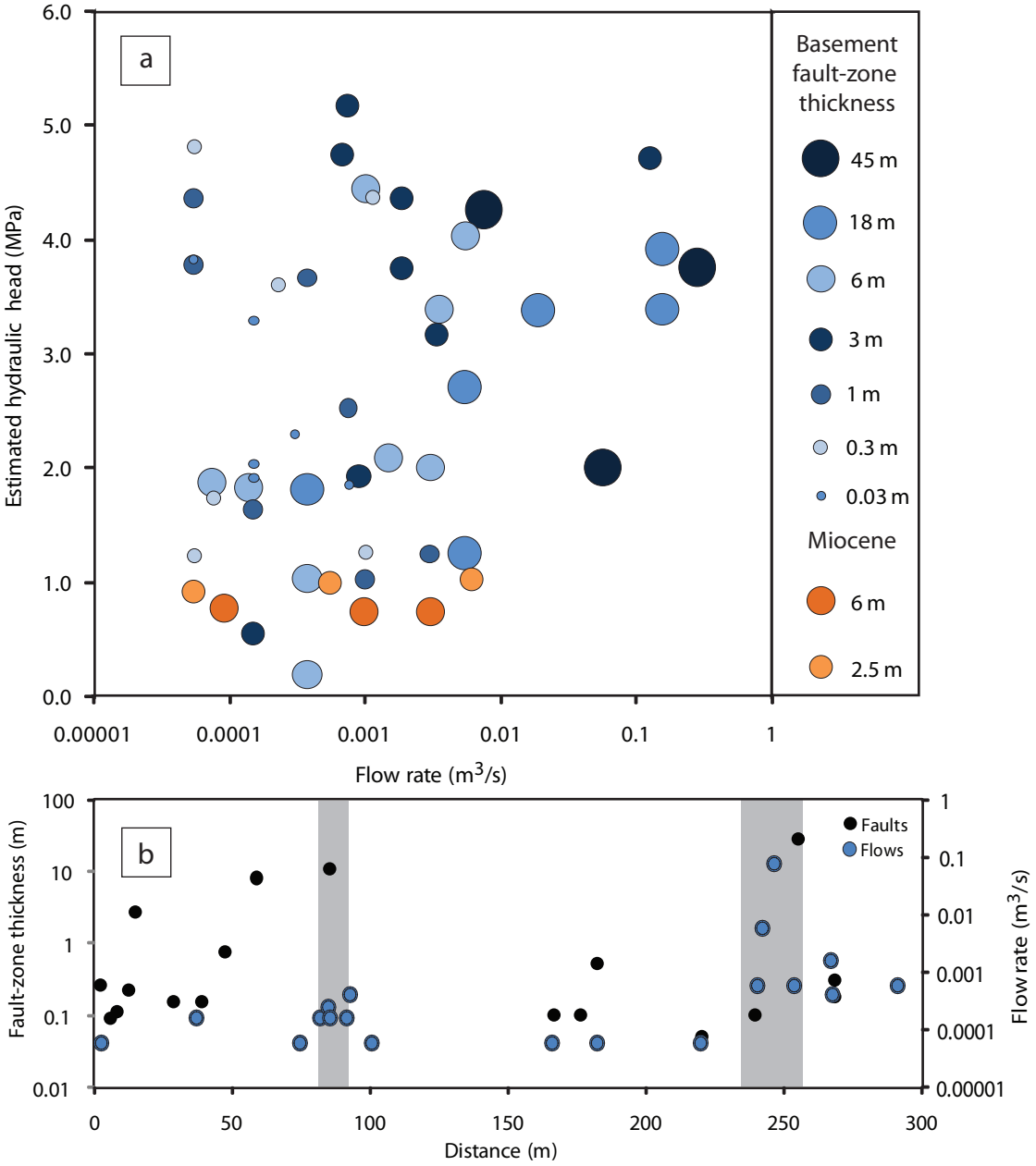

Figure 7. (a) Fault-zone flow-rate verses estimated hydraulic head. The hydraulic head driving flow is approximated by height of topography above the tunnels (Hegan, 1976; Hegan, 1980). (b) Example of variable flow from fault-zones along a basement tunnel section (Moawhango heading 24368-25334'). The height of topography above the tunnel, and therefore estimated fluid pressure driving flow, are approximately constant. Fluid flow locations (blue filled circles) in relation to basement fault zones (black filled circles). Grey shading represents fractured and sheared fault-zone rock.

network in this study are associated with the majority of flow. For example, basement fault-zones > 10 m thick (N = 23) representing < 3% of the total tunnel length account for ~80% of the localised flow-rate entering the tunnels, and one fault-zone accounts for 33% (Fig. 8). I also highlight the similarities in flow properties between fault-zones in two lithologies that contrast in both physical properties (porosity and permeability) and deformation history under similar fluid pressure differentials. The flow properties of fault-zones, which is of primary interest to industry, are highly variable both in distribution and rate (under relatively low stress and driving pressures). The spatial distribution and rate of flow associated with basement fault-zones suggests the rock-mass has properties similar to that of a fracture network at or above a percolation threshold where flow is governed principally by fracture connectivity. In these terms, the prediction of highly permeable fluid pathways for reservoir modelling or targeted drilling for example becomes problematic.

Comparison of flow-rates relative to fault-zone thickness and estimated hydrostatic pressure indicates that the connectivity of permeable zones within and/or adjacent to a fault-zone must be variable or that sub-hydrostatic fluid pressures are driving flow (Fig. 7). Consistent with groundwater studies at the time of excavation, flows are assumed to enter the tunnel under pressures equal to the full hydraulic head approximated by height of topography above the tunnel (Hegan, 1976; Hegan, 1980). The contribution of these fault-zones to the bulk permeability of the system appears to depend on how (or if) they are connected to the surface and/or other hydraulically conductive faults. Flow-rates may be lower where a fault-zone is connected by relatively low permeability pathways or not connected directly or indirectly to the surface (e.g. Fig. 7b). In the same way that across fault flow is dependent on the continuity of fault-gouge (i.e. the weakest point) (Lunn et al., 2008), in-plane flow-rates should be governed by the lowest permeability (Long & Witherspoon, 1985) and average pressure differential encountered along a connected pathway.

The connectivity of fault-zones to the groundwater system is a key determinant for flow. The connectivity of a fault to other faults in the system will be influenced by its length (Bour & Davy, 1997). In the basement there is no direct measure of either fault length or displacement, however, given the broad positive relationships between fault-zone thickness & displacement (i.e. the Miocene sequence; refer Fig. 4) and displacement & length relationships (Kim & Sanderson, 2005; Childs et al., 2009), I would expect fault-zone thickness also to have a general positive correlation to fault

length. Therefore, the widest fault-zones are likely to also be the longest faults with the greatest potential to extend to the ground surface and to be hydraulically conductive. In support of this model many large basement fault-zones (10-50 m thick) within the tunnels are associated with prominent lineations mapped or inferred at the surface (Hancox & Paterson, 1975; Beetham & Watters, 1985). Because there are few of these large fault-zones connected to the surface there is not a strong positive relationship between estimated hydraulic head and flow-rate (Fig. 7a).

In a simple Darcian flow model, a column of water with direct hydraulic connection from the surface to the tunnel (with negligible friction losses) has a greater pressure differential under high topographic elevations, and therefore higher flow-rate, than under low elevations (all other parameters remaining constant). Here, the inflow-rates for a given fault-zone thickness are largely insensitive to the estimated hydraulic head driving fluid-flow. This insensitivity arises because the majority of small basement faults (< 1 m thick) (Fig. 6a) are not connected to the fault network maintaining hydrostatic fluid pressures. In contrast, the largest flows occur on basement fault-zones typically > 10 m thick indicate these are flowing in response to hydrostatic or near hydrostatic fluid pressures (Fig. 9). It must be remembered that not all large fault-zones are associated with flow, and some that are, have flows characteristic of much smaller fault-zones (Fig. 9a). Much of the variability in the distribution and rate of flow observed in the tunnels can be accounted for if the system is considered at or close to a percolation threshold (Balberg et al., 1991; Cox, 1999; Sanderson & Zhang, 1999).

Percolation theory provides insights into the development of hydraulic connectivity and the partitioning of fluid-flow amongst elements of a network of permeable faults and fractures in an otherwise impermeable medium (Cox, 1999). Percolation networks can be described in terms of three types of elements: backbone elements that connect one side of the system to the other and support the majority of flow through the network, dangling or deadend elements that branch from the flow backbone, and isolated elements which are disconnected from other system elements (Balberg et al., 1991; Cox, 1999). A percolation threshold is reached when enough elements connect to allow fluid-flow across the entire width of the network and the medium becomes permeable (Zhang & Sanderson, 1998). Small basement fault-zones (< 1 m thick) not associated with flow could be considered isolated elements in that respect (Fig 6a). Further, fault or individual slip zones not associated with flow have the same architectural elements as those that are hydraulically conductive, which in some

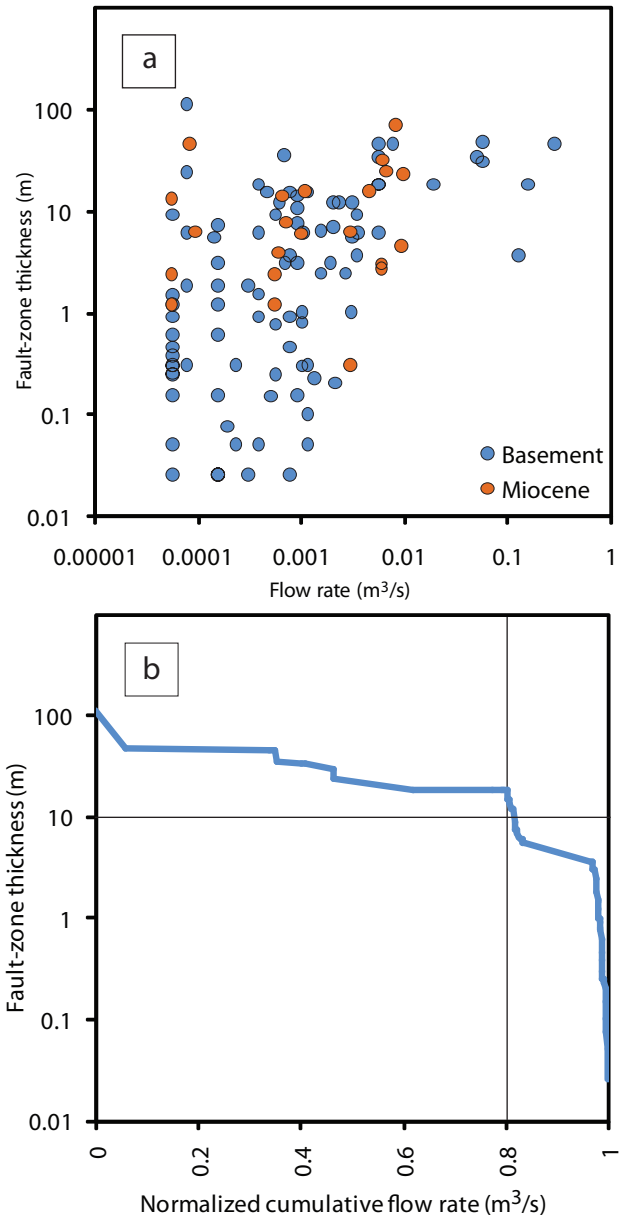

Figure 8. Fault-zone thickness and flow-rate. (a) Flow-rate verses fault-zone thickness. (b) Proportion of localised flow carried by basement fault zones. Illustrates ~80% of total cumulative flow-rate occur on < 3% of basement faults which typically have zones > 10 m wide. Note one fault accounts for ~33% of total flow-rate entering basement tunnels.

cases, are only separated by 10's of metres between fault-zones (e.g. Fig 7b) and 10's of centimetres within fault-zones, indicating highly variable fault and fracture density. The distribution of highly variable flow-rates observed in the basement tunnels approximates a power-law (Fig. 5b), a property of fault-fracture systems at or above the percolation threshold (Sanderson & Zhang, 1999).

5. Discussion

Within the TVZ many high temperature geothermal systems originate from Mesozoic basement rocks at depths > 1 km (Bibby et al., 1995) similar to those in this study and where bulk permeability is largely unconstrained. Previous estimates at depths > 0.5 km from geothermal mass transport (~10^{-14} m^2) (Allis et al., 1993) are consistent with a power-law decrease with depth from near surface values detailed in this study (Fig. 9) (Manning & Ingebritsen, 1999). Direct measures of permeability within drill holes and estimates from fault-zones within the tunnels indicates that the permeability structure of the basement is highly variable over 4 orders of magnitude in scale (1 – 10^4m).

For many practical applications (e.g. geothermal and petroleum exploration or production), knowledge of the bulk permeability of a rock-mass and fault-zones is desirable. While many studies focus on the sealing qualities across faults (Yeilding et al., 1997; Walsh et al., 1998), in plane permeability of fault-zones may also provide important information for reservoir modelling (Manzocchi et al., 2010). Bulk in plane fault-zone permeabilities can be estimated using Darcy's Law for flow through a porous medium:

$$Q = -\frac{kA(\nabla P)}{\mu L} \quad (1)$$

where flow-rate (Q m^3/s) is dependent on the permeability (k m^2) of the medium, the area (A m^2) of flow in the plane of observation, the hydraulic head gradient (∇P Pa), the dynamic viscosity of the fluid (μ Pa s), and the length (L m) the pressure differential occurs over. For comparison with *in situ* hydraulic tests, permeability is related to hydraulic conductivity (K m/s) by:

$$k = K\frac{\mu}{\rho g} \quad (2)$$

where ρ is the density of the fluid (kg/m^3) and g is the acceleration due to gravity (m/s^2). While the highest fault-zone flow-rates are likely to be above those associated

with laminar flow, equations 1 and 2 provide simple first order estimations for their bulk permeability.

To estimate bulk fault-zone permeability from equation (1) I assume the minimum distance flow is occurring over (*L*) is the height of topography above the tunnel (~100-500 m), the maximum area (*A*) flow occurs across is the tunnel circumference multiplied by the tunnel distance or fault-zone thickness, and a minimum area (A) of flow is estimated from the engineering geological logs. At the kilometre scale, average flow-rates measured at tunnel portals (Hegan, 1980) both in basement and the Miocene sequence indicate near surface bulk permeabilities of ~1 x 10^{-12} m^2 (1 Darcy), the majority of which originates directly from fault-zones. Basement fault-zones typically comprise 5-15% of the rock-mass which suggests minimum bulk fault-zone permeabilities of 10^{-12} m^2 to 10^{-10} m^2 when flow frequency is considered. At the scale of individual hydraulically conductive fault-zones (0.08 to 45 m in thickness) bulk permeabilities are estimated at 10^{-12} m^2 to 10^{-9} m^2 for flow-rates of 5.7 x 10^{-5} m^3 s^{-1} to 1.3 x 10^{-1} m^3 s^{-1} (high permeabilities are associated with high flow-rates). I find bulk permeability estimated over a wide range of scales using these simple parametres are consistent with those measured *in situ* from hydraulic conductivity tests in bore holes (Hancox, 1975).

My estimates of fault-zone permeability compare reasonably well to existing data. *In situ* hydraulic conductivities (K) measured from packer tests in basement drill holes (10-70 m depth range) indicate permeability (k) variations ranging over three orders of magnitude (10^{-13} to 10^{-10} m^2) (Fig. 9). No such data is available for the Miocene sequence. The background permeability of near surface basement ranges between 10^{-13}-10^{-12} m^2, increasing to 10^{-12}-10^{-11} m^2 adjacent to fault-zones, and 10^{-11}-10^{-10} m^2 within fault-zones. Variations in permeability over three orders of magnitude can occur over distances as small as 10 m (Hancox, 1975; Hegan, 1976). No data presently exists for the permeability of basement fault-gouge however other studies indicate fault-gouges have low permeabilities (typically 10^{-17}-$10^{-20}$$m^2$) (Evans et al., 1997; Wibberley & Shimamoto, 2003) which are similar to or lower than the host rock (Higgs et al., 2012). These permeability ranges are consistent with observations made during tunnel excavation in basement where flows weren't generally encountered until the clay gouge zones had been breached, suggesting that the flow system was compartmentalised by fault gouge (Hegan, 1980).

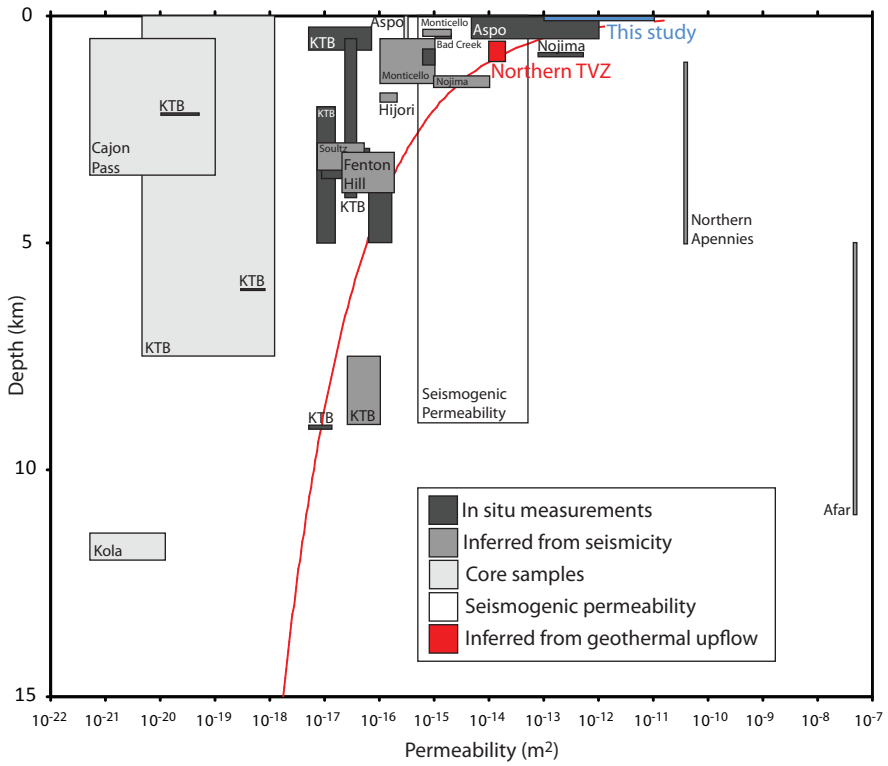

Figure 9. Crustal bulk permeability. Data from core samples, in situ hydraulic tests, and induced seismicity after Townend & Zoback (2000). See Townend & Zoback (2000) for original references in addtion to the following: inferred from seismicity - Noir et al. (1997), Tadokoro et al. (2000), Miller et al. (2004); in situ - Hancox (1975), Kitagawa et al. (1999), Molinero et al. (2002); inferred from geothermal upflow - Allis et al. (1993); Geothermal/metamorphic curve - Manning & Ingebritsen (1999).

Scale is of fundamental importance when considering fault-zone permeability. Direct measurements suggest the bulk permeability structure of a fault-zone can be considered either heterogeneous or homogeneous dependent on the scale of observation. Talawani et al. (1999) present permeability variations over 2 orders of magnitude (10^{-15}-10^{-13} m^2) derived from *in situ* hydraulic conductivities measured in boreholes intersecting a 1 m wide shear zone in granitic gneiss. The permeability estimated from same shear zone using lake level fluctuations however was more homogeneous (10^{-15} m^2) with respect to its hydraulic properties over time scales of days and distances of a kilometre (Talwani et al., 1999). In a similar situation to this study, Molinero et al. (2002) model groundwater inflows induced by excavation into the Äspö Hard Rock Laboratory. Permeabilities derived from *in situ* hydraulic conductivities vary by up to 5 orders of magnitude (e.g. 10^{-13}-10^{-8} m^2) across fracture zones ranging in width from 5-50 m. The geometric mean of these permeability ranges (10^{-15}-10^{-12} m^2), 2-5 orders of magnitude higher than the granitic basement (~10^{-17} m^2), approximated values required to model the majority of flow-rate into the facility (Molinero et al., 2002). Core samples taken across the Median Tectonic Line by Wibberley & Shimamoto (2003) show 5 orders of magnitude variation in permeability (10^{-21}-10^{-15} m^2 at confining pressures of 100 MPa) over distances < 0.1 m adjacent to the primary slip zone. Over distances of a few hundred metres either side of the primary slip zone, where evidence for fluid-flow is observed, permeabilities are however on average 2-3 orders higher (10^{-17}-10^{-16} m^2) than the protolith on either side (~ 10^{-19} m^2). These data, including this study, suggest that an average permeability at least 2 orders of magnitude higher than the intrinsic permeability of the host rock may be adequate to represent in-plane fault-zone permeability.

The prediction or location of high permeability pathways associated with fault-zones will become increasingly important for the exploration and production of hydrocarbon (Manzocchi et al., 2010; Ilg et al., 2012) and geothermal systems (Rosenberg et al., 2009). For example, while many studies have focused on the potential for fault-zones to impede fluid-flow, understanding how fault-zones, and the high permeability pathways they contain, influence fluid migration pathways will lead to more focused exploration and production strategies. Many high temperature geothermal systems originate from basement in the central North Island where faults are likely to be the high permeability conduits and fluid pressure gradients are similar to those considered here. Taking into account the variability of fault size, orientation and flow-

rate observed in the tunnels, and the connectivity within the rock-mass these components imply, flow paths at depth are likely to be highly convoluted. While active fault intersections and relay zones observed at the surface are a likely location for enhanced vertical permeability (Rowland & Sibson, 2001), the presence of pre-existing basement faults in orientations other than active regional trends may significantly influence flow pathways. While this study shows a positive correlation between fault size and flow-rate, not all large faults have flow and the ones that do have highly variable rates. If these data do approximate a fracture network near a percolation threshold, predicting the location and rate of flow at any given point in the system will be problematic.

6. Conclusions

Localised groundwater flow from tunnels at the southern end of the Taupo Rift typically occur from within, and at the margins of fault-zones. Fault-zones in two contrasting lithologies show similarities in the rate and distribution of flow. In medium-high porosity and permeable Miocene sandstones, localised flow occurs exclusively from fault-zones. In low porosity impermeable Mesozoic basement, localised flow occurs from within fault-rock (breccia in a clay matrix) and fractured and sheared zones within and adjacent to fault-rock. The rate of flow is highly variable, approximating a power-law distribution, and occurs from less than half of all fault-zones. Fault-zone thicknesses also approximate power-law distributions indicating scale invariant fault-length distributions. The orientation of fault-zones with respect to the regional stress show approximately equal numbers of fault-zones $\geq$ 1 m with and without flow both perpendicular and parallel to the regional Shmax direction. A general positive relationship is found between fault-zone thickness and maximum flow-rate whereas no correlation is found between these parameters and the estimated fluid pressure driving flow. Larger faults that are longer and/or more connected to other faults are likely to have higher flow-rates. The flow characteristics of basement fault-zones are similar to those of a fracture network close to a percolation threshold (i.e. power-law flows from unpredictable locations) and as such, predicting the location of highly permeable hydraulically conductive faults will be challenging.

References

Acoccella, V., Spinks, K., Cole, J. & Nicol, A., 2003. Oblique back arc rifting of Taupo Volcanic Zone, New Zealand. *Tectonics*, 22(4), p.1045.

Allis, R.G., Christenson, B.W., Nairn, I.A., Risk, G.F. & White, S.P., 1993. The natural state of Kawerau geothermal field. In *Proceedings 15th NZ Geothermal Workshop*. Auckland, 1993. Auckland University.

Balberg, I., Berkowitz, B. & Drachsler, G.E., 1991. Application of a percolation model to flow in fractured hard rocks. *Journal of Geophysical Research*, 96(B6), pp.10015-21.

Barton, C.A. & Zoback, M.D., 1994. Stress perturbations associated with active faults penetrated by boreholes: Possible evidence for near-complete stress drop and a new technique for stress magnitude measurement. *Journal of Geophysical Research*, 99(B5), pp.9373-90.

Barton, C.A., Zoback, M.D. & Moos, D., 1995. Fluid flow along potentially active faults in crystalline rocks. *Geology*, 23(8), pp.683-86.

Beetham, R.D. & Watters, W.A., 1985. Geology of Torlesse and Waipapa terrane basement rocks encountered during the Tongariro Power Development project, North Island, New Zealand. *New Zealand Journal of Geology & Geophysics*, 28, pp.575-94.

Bibby, H.M., Caldwell, T.G., Davey, F.J. & Webb, T.H., 1995. Geophysical evidence on the structure of the Taupo Volcanic Zone and its hydrothermal circulation. *Journal of Volcanology & Geothermal Research*, 68, pp.29-58.

Bour, O. & Davy, P., 1997. Connectivity of random fault networks following a power law fault length distribution. *Water Resources Research*, 33(7), pp.1567-83.

Brathwaite, R.I., Wood, C.P., Rosenberg, M.D. & Faure, K., 2002. Porosity and permeability in the basement rocks at the Kawerau and Ohaaki geothermal fields, New Zealand. In *Proceedings 24th New Zealand Geothermal workshop*. Auckland, 2002. Auckland University.

Brudy, M., Zoback, M.D., Fuches, K., Rummel, F. & Baumgartner, J., 1997. Estimation of the complete stress tensor to 8 km depth in the KTB scientific drill holes: implications for crustal strength. *HJournal of Geophysical Research* , 102(B8), pp.18453-75.

Byerlee, J.D., 1978. Friction of rocks. *Pure & Applied Geophysics*, 116, pp.615-26.

Caine, J.S., Evans, J.P. & Forster, C.B., 1996. Fault zone architecture and permeability structure. *Geology*, 24(11), pp.1025-28.

Chester, F.M. & Logan, J.M., 1986. Implications for mechanical properties of brittle faults from observations of the Punchbowl Fault Zone, California. *Pure & Applied Geophysics*, 124(1/2), pp.79-106.

Childs, C., Manzocchi, T., Walsh, J.J., Bonson, C.G., Nicol, A. & Schopfer, M.P.J., 2009. A geometric model of fault zone and fault rock thickness variations. *Journal of Structural Geology*, 31(2), pp.117-27.

Childs, C., Nicol, A., Walsh, J.J. & Watterson, J., 1996a. Growth of vertically segmented normal faults. *Journal of Structural Geology*, 18, pp.1387-97.

Childs, C., Walsh, J.J. & Watterson, J., 1996b. A model for the structure and development of fault zones. *Journal of the Geological Society*, 153, pp.337-40.

Cox, S.F., 1999. Deformational controls on the dynamics of fluid flow in mesothermal gold systems. In K. McCaffrey, L. Lonergan & J.J. Wilkinson, eds. *Fractures, Fluid flow and Mineralisation*. London: Geological Society Special Publications 155. pp.123-40.

Evans, J.P., Forster, C.B. & Goddard, J.V., 1997. Permeability of fault-related rocks, and implications for hydraulic structure of fault zones. *Journal of Structural geology*, 19(11), pp.1393-404.

Evans, K.F., Genter, A. & Sausse, J., 2005. Permeability creation and damage due to massive fluid injections into granite at 3.5 km at Soultz: 1. Borehole observations. *Journal of Geophysical Research*, 110, p.B04203. doi:10.1029/2004JB003168.

Faulkner, D.R., Jackson, C.A.L., Lunn, R.J., Schlische, R.W., Shipton, Z.K., Wibberley, C.A.J. & Withjack, M.O., 2010. A review of recent developments concerning the structure, mechanics and fluid flow properties of fault zones. *Journal of Structural Geology*, 32, pp.1557-75. doi:10.1016/j.jsg.2010.06.009.

Ferrill, D.A., Winterle, J., Wittmeyer, G., Sims, D.C.S. & Armstrong, A., 1999. Stressed rock strains groundwater at Yucca mountain, Nevada. *GSA Today*, 9(5), pp.1-8.

Fossen, H., Johansen, T.E.S., Hesthammer, J. & Rotevatn, A., 2005. Fault interaction in porous sandstone and implications for reservoir management: Examples from southern Utah. *AAPG Bulletin*, 89(12), pp.1593-606. doi:10.1306/07290505041.

Gillespie, P.A., Howard, C.B., Walsh, J.J. & Watterson, J., 1993. Measurement and characterisation of spatial distributions of fractures. *Tectonophysics*, 226, pp.113-41.

Hancox, G.T., 1975. *Completion report on the engineering geology of the Moawhango Dam*. Unpubl. Engineering Geology Report 213. Lower Hutt: New Zealand Geological Survey Department of Scientific and Industrial Research.

Hancox, G.T. & Paterson, B.R., 1975. *Reappraisal of the Geology and anticipated tunneling conditions in Moawhango Tunnel between Tongariro heading (c.f. 30200') and Moawhango heading (c.f. 26400')*. Unpubl. Engineering Geology Report 233. Lower Hutt: New Zealand Geological Survey Department of Scientific and Industrial Research.

Hayes, G., Reyners, M. & Stuart, G., 2004. The Waiouru. New Zealand, earthquake swarm: Persistent mid-crustal activity near an active rift. *Geophysical Research Letters*, 31, p.L19613. doi:10.1029/2004GL020709.

Hegan, B.D., 1976. *Engineering Geology of the Rangipo tailrace tunnel*. Unpubl. Engineering Geology Report 253. Lower Hutt: New Zealand Geological Survey Department of Scientific and Industrial Research.

Hegan, B.D., 1980. *Engineering Geology of the Moawhango to Tongariro Tunnel*. Unpubl. Engineering Geology Report 343. Lower Hutt: New Zealand Geological Survey Department of Scientific and Industrial Research.

Higgs, K.E., Strogen, D., Griffin, A., Ilg, B. & Arnot, M., 2012. *Reservoirs of the Taranaki Basin, New Zealand*. Data series No. 2012/13a. Lower Hutt: GNS Science.

Hurst, A.W. & McGinty, P.J., 1999. Earthquake swarms to the west of Mt Ruapehu preceding its 1995 eruption. *Journal of Volcanology & Geothermal Research,* 90, pp.19-28.

Ilg, B.R., Hemmings-Sykes, S., Nicol, A., Baur, J., Fohrmann, M., Funnell, R. & Milner, M., 2012. Normal faults and gas migration in an active plate boundary, southern Taranaki Basin, offshore New Zealand. *AAPG Bulletin*, 96(9), pp.1733-56. doi:10.1306/0201.1211.088.

Jaeger, J.C. & Cook, N.G.W., 1979. *Fundementals of rock mechanics*. 3rd ed. London, United Kingdom: Chapman & Hall.

Kim, Y.-S., Peacock, D.C.P. & Snaderson, D.J., 2004. Fault damage zones. *Journal of Structural Geology*, 26, pp.503-17. doi: 10.1016/j.jsg.2003.08.002.

Kim, Y.-S. & Sanderson, D.J., 2005. The relationship between displacement and length of faults: a review. *Earth-Science Reviews*, 68, pp.317-34. doi:10.1016/j.earscirev.2004.06.003.

King, P.R. & Thrasher, G.P., 1996. Cretaceous-Cenozoic geology and petroleum systems of the Taranaki Basin. In *Institute of Geological & Nuclear Sciences Monograph 13*. Lower Hutt, New Zealand: Institute of Geological & Nuclear Sciences.

Kitagawa, Y., Koizumi, N., Notsu, K. & Igarashi, G., 1999. Water injection experiments and discharge changes at the Nojima Fault in Awaji Island, Japan. *Geophysical research Letters*, 26(20), pp.3173-76.

Lee, J., Townsend, D., Bland, K. & Kamp, P.J.J., 2010. *Geology of the Hawke's Bay area: scale 1:250,000*. Institute of Geological & Nuclear Sciences Limited: Institute of Geological & Nuclear Sciences 1:250,000 geological map 8. 86 p.+ 1 folded map.

Levens, R.L., Williams, R.E. & Ralston, D.R., 1994. Hydrogeologic role of geologic structures; Part 1, The paradigm. *Journal of Hydrology*, 156, pp.227-43.

Long, J.C.S. & Witherspoon, P.A., 1985. The relationship of the degree of interconnection to permeability in fracture networks. *Journal of Geophysical research*, 90(B4), pp.3087-98.

Lunn, R.J., Shipton, Z.K. & Bright, A.M., 2008. How can we improve estimates of bulk fault zone hydraulic properties? In C.A.J. Wibberley et al., eds. *The Internal structure of Fault Zones: Implications for Mechanical and Fluid-Flow properties*. London: Geological Society Special Publications 299. pp.231-37. doi:10.114/SP299.14.

Manning, C.E. & Ingebritsen, S.E., 1999. Permeability of the continental crust: implications of geothermal data and metamorphic systems. *Reviews of Geophysics*, 37(1), pp.125-50.

Manzocchi, T., Childs, C. & Walsh, J.J., 2010. Faults and fault properties in hydrocarbon flow models. *Geofluids*, 10, pp.94-113. doi:10.1111/j.1468-8123.2010.00283.x.

Miller, S.A., Collettini, C., Chiaraluce, L., Cocco, M., Barchi, M. & Klaus, B.J.P., 2004. Aftershocks driven by a high-pressure CO2 source at depth. *Nature*, 427, pp.724-27. doi:10.1038/nature02251.

Molinero, J., Samper, J. & Juanes, R., 2002. Numerical modeling of the transient hydrogeological response produced by tunnel construction in fracture rocks. *Engineering Geology*, 64, pp.369-86.

Morris, A., Ferrill, D.A. & Henderson, D.B., 1996. Slip-tendency analysis and fault reactivation. *Geology*, 24(3), pp.275-78.

Mortimer, N., 2004. New Zealand's geological fondations. *Gondwana Research*, 7(1), pp.261-72.

Nicol, A., Mazengarb, C., Chanier, F., Rait, C., Uruski, C. & Wallace, L., 2007. Tectonic evolution of the active Hikurangi subduction margin, New Zealand, since the Oligocene. *Tectonics*, 26, p.TC4002. doi:10.1029/2006TC002090.

Nicol, A., Walsh, J.J., Watterson, J. & Gillespie, P.A., 1996. Fault size distribution - are they really power law? *Journal of structural Geology*, 18(2/3), pp.191-97.

Noir, J., Jacques, E., Bekri, S., Adler, P.M., Tapponier, P. & King, G.C.P., 1997. Fluid flow triggered migration of events in the 1989 Dobi earthquake sequence of Central Afar. *Geophysical Research Letters*, 24(18), pp.2335-38.

Palliet, F.L., Hess, A.E., Cheng, C.H. & Hardin, E., 1987. Characterization of fracture permeability with high-resolution vertical flow measurements during borehole pumping. *Groundwater*, 25(1), pp.28-40.

Peacock, D.C.P., Knipe, R.J. & Sanderson, D.J., 2000. Glossary of normal faults. *Journal of Structural Geology*, 22, pp.291-305.

Reyners, M., 2010. Stress and strain from earthquakes at the southern termination of the Taupo Volcanic Zone, New Zealand. *Journal of Volcanology & Geothermal Research*, 190(1-2), pp.82-88.

Rosenberg, M.D., Bignall, G. & Rae, A.J., 2009. The geological framework of the Wairakei-Tauhara Geothermal System, New Zealand. *Geothermics*, 38, pp.72-84. doi:10.1016/j.geothermics.2009.01.001.

Rowland, J.R. & Sibson, R.H., 2001. Extensional fault kinematics within the Taupo Volcanic Zone, New Zealand: soft-linked segmentation of a continental rift system. *New Zealand Journal of Geology & Geophysics*, 44, pp.271-83.

Sanderson, D.J. & Zhang, X., 1999. Critical stress localization of flow associated with deformation of well-fractured rock masses, with implications for mineral deposits. In k. McCaffrey, J.W. Lonergan & J.J. Wilkinson, eds. *Fractures, Fluid Flow and Mineralization*. London: Geological Society Special Publications 155. pp.69-81.

Sherburn, S., Townend, J., Arnold, R. & Woods, L., 2009. *EQC Project 08/550 - Establishing a Spatiotemporal Benchmark for Ongoing Crustal Stress monitoring in the Southern Taupo Volcanic Zone*. GNS Science Consultancy Report 2009/185. Lower Hutt: GNS Science.

Tadokoro, K., Ando, M. & Nishigami, K., 2000. Induced earthquakes accompanying the water injection experiment at the Nojima fault zone, Japan: Seismicity and its migration. *Journal of Geophysical Research*, 105(B4), pp.6089-104.

Talwani, P., Cobb, J.S. & Schaeffer, M.F., 1999. In situ measurements of hydraulic properties of a shear zone in northwestern South Carolina. *Journal of Geophysical Research*, 104(B7), pp.14993-5003.

Townend, J. & Zoback, M.D., 2000. How faulting keeps the crust strong. *Geology*, 28(5), pp.399-402.

Townsend, D., Vonk, A. & Kamp, P.J.J., 2008. *Geology of the Taranaki area: scale 1:250,000*. Institute of Geological & Nuclear Sciences Limited, New Zealand: Institute of Geological & Nuclear Sciences 1:250,000 geological map 7. 77p + 1 folded map.

Tsang, C.-T. & Neretnieks, I., 1998. Flow channeling in heterogeneous fractured rocks. *Reviews of Geophysics*, 36(2), pp.275-98.

Villamor, P. & Berryman, K.R., 2006. Evolution of the southern termination of the Taupo Rift, New Zealand. *New Zealand Journal of Geology & Geophysics*, 49, pp.23-37.

Walcott, R.I., 1987. Geodetic strain and the deformation history of the North Island of New Zealand during the late Cainozoic. *Philosphical Transactions of the Royal Society London*, A321, pp.163-81.

Wallace, R.E. & Morris, H.T., 1986. Charateristics of faults and shear zones in deep mines. *Pure & Applied Geophysics*, 124(1/2), pp.105-25.

Walsh, J.J. & Watterson, J., 1992. Populations of faults and fault displacements and their effects on estimates of fault-related regional extension. *Journal of Structural Geology*, 14(6), pp.701-12.

Walsh, J.J., Watterson, J., Heath, A.E. & Childs, C., 1998. Representation and scaling of faults in fluid flow models. *Petroleum Geoscience*, 4, pp.241-51.

Wibberley, C.A.J. & Shimamoto, T., 2003. Internal structure and permeability of major strike-slip fault zones: the Median Tectonic Line in Mie Prefecture, Southwest Japan. *Journal of Structural Geology*, 25, pp.59-78.

Wibberley, C.A.J., Yeilding, G. & Di Toro, G., 2008. Recent advances in the understanding of fault zone internal structure: a review. In C.A.J. Wibberley et al., eds. *The Internal Structure of Fault Zones: Implications for Mechanical and Fluid Flow Properties*. London: Geological Society Special Publications 299. pp.5-33.

Wilson, C.J.N., Houghton, B.F., McWilliams, M.O., Lanphere, M.A., Weaver, S.D. & Briggs, R.M., 1995. Volcanic and structural evolution of Taupo Volcanic Zone, New Zealand: a review. *Journal of Volcanology & Geothermal Research*, 68, pp.1-28.

Wood, C.P., Braithewaite, R.L. & Rosenberg, M.D., 2001. Basement structure, lithology and permeability at Kawerau and Ohaaki geothermal fields, New Zealand. *Geothermics*, pp.461-81.

Yeilding, G., Freeman, B. & Needham, D.T., 1997. Quantitative fault seal prediction. *American Association of Petroleum Geologist Bulletin*, 81, pp.897-917.

Zhang, X. & Sanderson, D.J., 1998. Numerical study of critical behaviour of deformation and permeability of fractured rocks. *Marine & Petroleum Geology*, 15, pp.535-48.

Zhang, X. & Sanderson, D.J., 2001. Evaluation of instability in fractured rock masses using numerical analysis methods: Effects of fracture geometry and loading direction. *Journal of Geophysical Research*, 106(B11), pp.26671-87.

Chapter 3

Structural geometry and kinematics of the Taupo Rift, New Zealand

Abstract

The kinematics of the continental intra-arc Taupo Rift has been investigated mainly using a large catalogue of new and published focal mechanisms (N=186) and geological fault-slip (N=73) data. The average extension direction is approximately orthogonal to the average trend of the rift and its constituent faults (α=76-84°). A small amount of right-lateral strike-slip is also common on faults throughout the rift, accommodating a minor amount (<1.5 mm/yr) of the total margin-parallel plate motion. Contemporary crustal-scale normal faults that border the eastern rift margin are sub-parallel to the strike of the subducted slab and located along the crest of the mantle wedge. These relationships indicate that the underlying subducting plate provides a first-order control on the location and geometry of faulting. Fault strike and extension direction change in unison by up to 20º across an abandoned kinematic boundary indicating a relationship between fault orientation and extension direction. In the southern part of the rift normal faults are parallel to, and probably reactivate, Mesozoic basement fabric (e.g., faults and bedding). By contrast, in the northern part of the rift faults diverge from basement fabric by up to 55° and may have formed since rift initiation 1-2 Ma ago. Focal mechanisms from the northern rift indicates oblique to right lateral strike-slip on steeply dipping basement fabric and dip-slip on newly formed rift faults. The trend and kinematics of the Taupo Rift are comparable to intra-arc rifting in the Taranaki Basin and southern Havre Trough, suggesting that the northeast strike of the subducting plate remained uniform for at least 4 Ma.

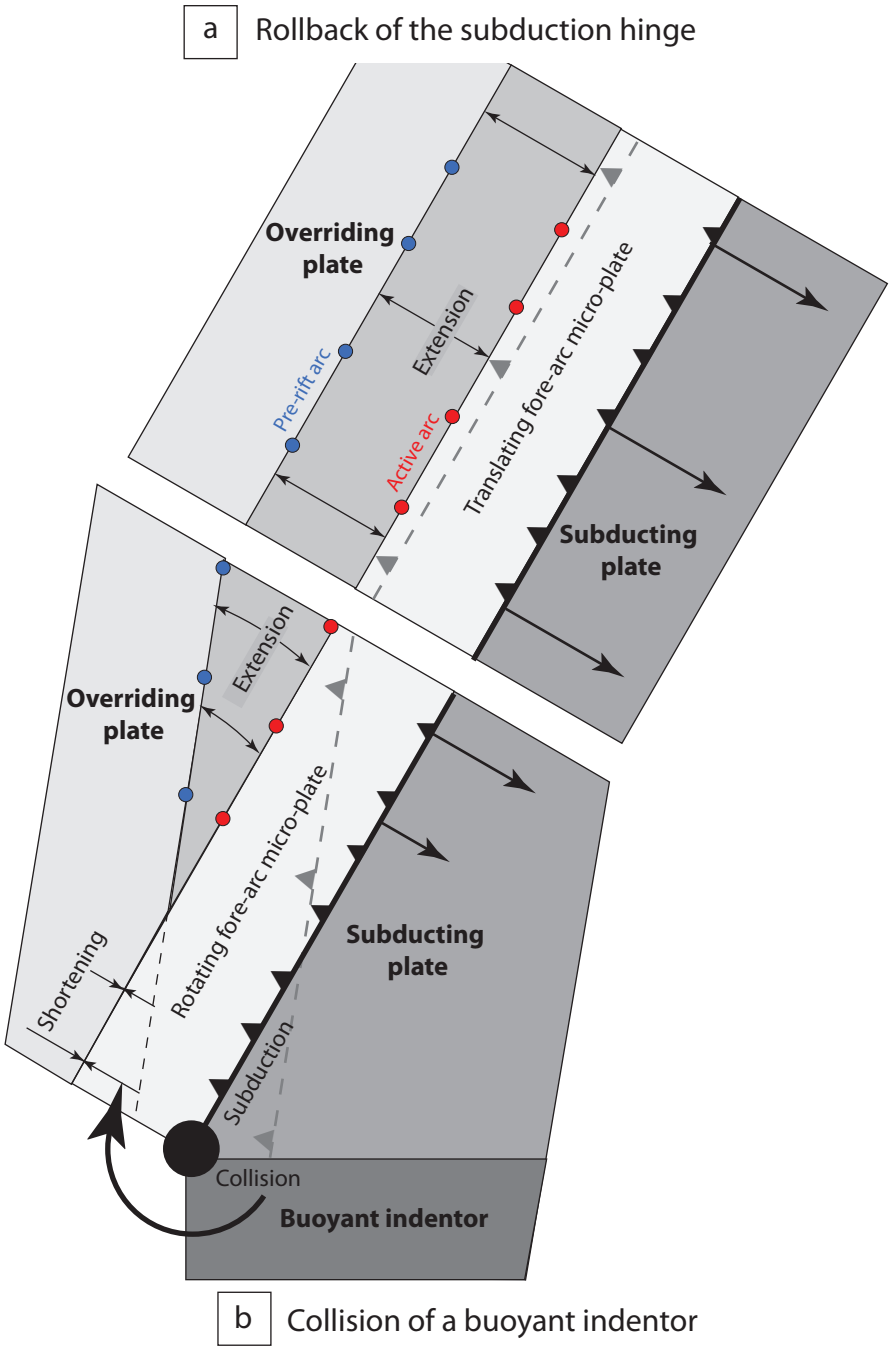

Figure 1. Schematic models for the formation of intra- and back-arc rifts. (a) Rollback or "retreat" of the subduction hinge results in the seaward translation of the forearc through 'trench suction' forces resulting in extension of the overriding plate (e.g. Molnar & Atwater, 1978: Sdrolias & Muller, 2006). Along with seaward migration of the fore-arc, the distance of arc volcanism (blue and red filled circles) from the trench remains approximately constant if no change in slab dip occurs during rollback. (b) The torque exerted on the crustal blocks by the transition from subduction to collision causes rapid tectonic block rotations relative to the bounding tectonic plates (Wallace et al., 2004; 2009). In proximity to the collision point a net landward migration or "advance" of the trench occurs, away from the collision point the subduction hinge will either remain fixed (i.e. "slab anchor") or "retreat" seaward as in (a). Refer to original publications for further details.

1. Introduction

Intra-arc and back-arc rift systems form in response to subduction processes. At present our understanding of the relationship between the geometry and kinematics of subduction and rifting (and ultimately spreading) in the over-riding plate is incomplete. Many models for what is commonly referred to as back-arc extension have been proposed (Molnar & Atwater, 1978; Jarrard, 1986; Lallemand et al., 2005; Sdrolias & Muller, 2006; Wallace et al., 2009). A widely held view is that slab rollback, or the seaward migration of the subduction hinge, is the primary cause for over-riding plate extension (Fig. 1a) (Sdrolias & Muller, 2006). Alternatively, it has been proposed that back-arc extension results from vertical-axis rotations arising from subduction of buoyant indentors (e.g. continental crust, oceanic ridges or sea mount chains), hundreds of kilometres from the termination of these systems (Fig. 1b) (Wallace et al., 2009). A prerequisite for determining the processes that produce intra- and back-arc rifts is an understanding of their structural geometry and kinematics.

In this paper the structural geometry and kinematics of the Taupo Rift and their relationships to subduction processes have been examined to determine what drives intra-arc extension. Taupo Rift is an intra-arc continental rift developed in association with oblique convergence along the Hikurangi margin, New Zealand (Fig. 2). It is located in a transition zone from oceanic-oceanic subduction to continental collision and transpression at the southern end of the Tonga-Kermadec-Hikurangi subduction margin (Walcott, 1987; Walcott, 1998). Consensus has not been reached regarding the underlying cause for extension of the Taupo Rift and the exceptional volcanic productivity associated with the spatially coincident Taupo Volcanic Zone (Stern, 1986; Wilson et al., 1995; Parson & Wright, 1996; Wallace et al., 2004; Reyners et al., 2006; Stern et al., 2006; Wilson et al., 2008). Along with vertical-axis rotation and slab rollback (Wallace et al., 2004; Wallace et al., 2009), models involving clockwise rotation of the arc, delamination of the mantle lithosphere, and uplift of the over-riding plate have been proposed to account for the high heat flow and apparent wedge shaped opening of the central North Island (Stern, 1986; Stern et al., 2006; Stern, 2009). Additional models, including slab rollback and/or steepening have been proposed to account for the easterly migration of a northeast-southwest trending arc and rift systems across the North Island (Brothers, 1984; Kamp, 1984; King & Thrasher, 1996; Giba et al., 2010). To the north of New Zealand, intra- and back-arc rifting in the Havre Trough

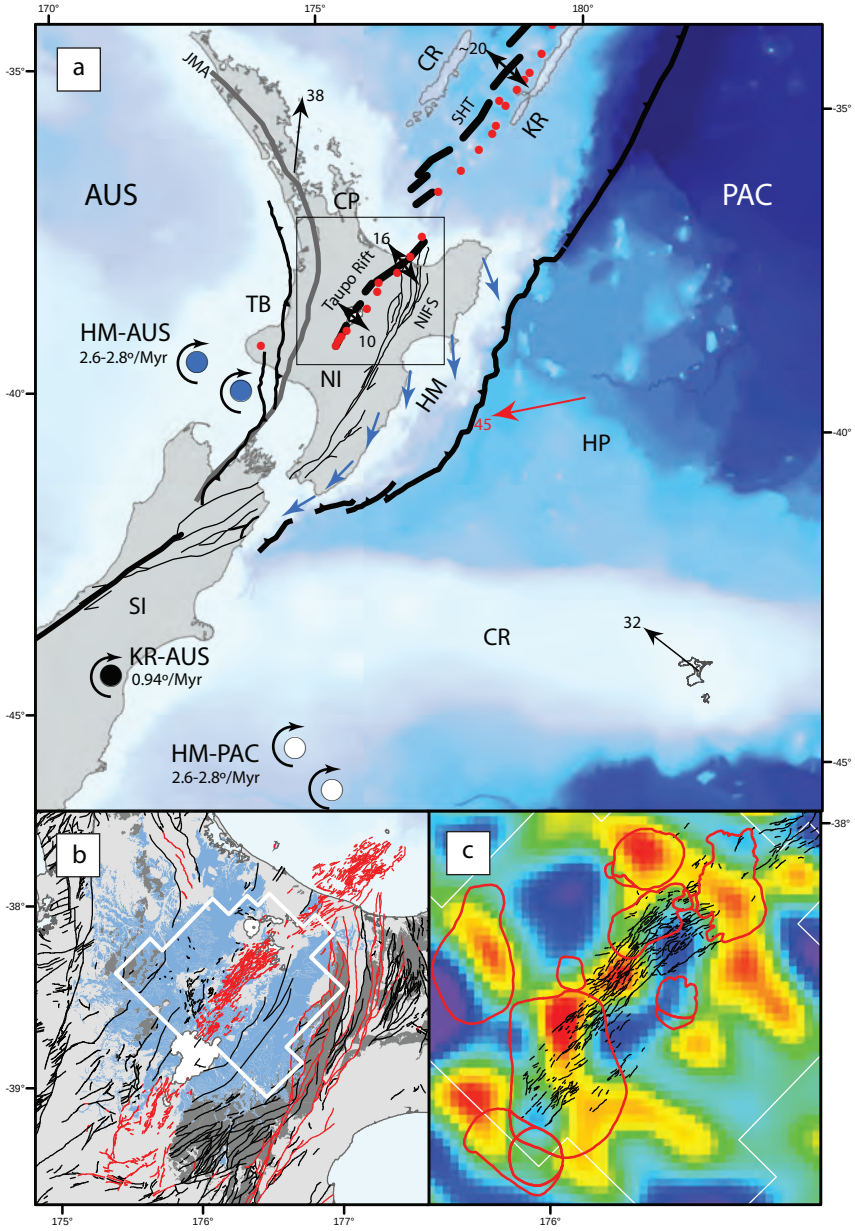

Figure 2. (a) Tectonic setting of the Taupo Rift. The Pacific plate subducts obliquely westwards beneath the Australian plate in the North Island, New Zealand. Clockwise rotation of the Hikurangi margin (HM) (blue arrows) is accommodated by intra-arc extension in Taupo Rift and strike-slip along the North Island Fault System (NIFS) (Wallace et al., 2004). Arc volcanoes (red filled circles) (Wright et al., 1993; Wilson et al., 1995; Campbell et al., 2007), Hikurangi Plateau (HP), Chatham Rise (CR), Taranaki Basin (TB), Junction Magnetic Anomaly (JMA), Coromandel Peninsula (CP), Colville Ridge (CR), Kermadec Ridge (KR), and southern Havre Trough (SHT) shown for reference. Relative (red arrow) and absolute (black arrow) plate motions from Beavan et al. (2002). Local poles of rotation for the Hikurangi margin (white and blue filled circles) from Wallace et al. (2012) and Kermadec Ridge (black filled circle) from Yan & Kroenke (1993). (b) Geology and faults of the central North Island (geology blue = ignimbrite, grey = basement) (faults red = active, black = inactive) (Edbrooke, 2005; Townsend et al., 2008; Lee et al., 2010; Leonard et al., 2012). 3D magnetulleric (MT) inversion model boundaries in (c) shown by white line. (c) Deep electrical resistivity structure from MT soundings (Heise et al., 2010) at the inferred base of the quartz-feldspathic crust (~18 km depth) beneath active rift faults (black lines) and caldera structures (red lines) (Wilson et al., 1995). Warm colours indicate low resistivities interpreted as connected melt (Heise et al., 2010).

and Lau Basins are generally considered to be the result of changes in the Pacific slab geometry (dip and/or strike) relative to the stable Australian plate (Walcott, 1987; van der Hilst, 1995; Sdrolias & Muller, 2006).

In this paper I examine the kinematics of a continental intra-arc rift using fault and earthquake slip data together with published geodetic and stress tensors from across the North Island (see Table 1 for references to all data sources used in this study). I address three principal questions. Firstly, what are the kinematics of the Taupo Rift? Secondly, what factors are influencing rift kinematics? And thirdly, how are these factors related to processes operating at the plate-boundary scale? The structure and kinematics of the Taupo Rift are examined using maps of active fault traces both onshore and offshore, gravity, and a catalogue of published (see Table 1 for references) and unpublished earthquake focal mechanisms (Ristau, 2008) and geological fault-slip indicators (Beanland et al., 1989; Rowland & Sibson, 2001; Acocella et al., 2003). The kinematics of faulting show that the Taupo Rift is a predominantly orthogonal intra-arc rift (α = 76-84°), the location of which is coincident with the crest of the underlying mantle wedge and the strike of the slab, respectively. Similarities between the structural geometry and kinematics of intra-arc rifting in the Taranaki Basin and southern Havre Trough to the present day Taupo Rift indicates the driving mechanism for extension has been uniform for at least 4 Ma, migrating progressively southeast with time sub-parallel to the strike of the underlying slab. I conclude that the geometry and rollback of the underlying slab is exerting a first-order control on the location, structural geometry, and extension direction of intra-rifting in the North Island.

2. Data and geological setting

The northeast-southwest trending Taupo Rift lies within the Taupo Volcanic Zone (TVZ) and is located at the present southern limit of arc volcanism and rifting ~200 km west of the Tonga-Kermadec-Hikurangi trench in the SW Pacific in the North Island, New Zealand (Fig. 2) (Parson & Wright, 1996). Towards the southern termination of the Tonga-Kermadec-Hikurangi trench the thickness and composition of the subducting and over-riding plate changes. Along the Kermadec trench, normal Cretaceous oceanic crust of the Pacific plate is being subducted obliquely westwards beneath the active Kermadec, and extinct Colville, Island arcs of the Australian plate (Parson & Wright, 1996; Downey et al., 2007; De Mets et al., 2010). Further south along the Hikurangi

margin, thickened oceanic crust of a large igneous province, the Hikurangi Plateau, is subducting beneath continental crust of the North Island (Davy & Wood, 1994; Davy et al., 2008; Bassett et al., 2010). At the southern end of the Hikurangi margin in the South Island, subduction gives way to continental collision and transpression along the Alpine Fault (Norris et al., 1990; Walcott, 1998).

The general strike of the subducting slab swings from 020-030º beneath the southern Havre Trough (Syracuse & Abers, 2006) to 040-050° beneath the North Island (chapter 5) and is accompanied by a general southward shallowing of slab dip (Ansell & Bannister, 1996; Barker et al., 2009; Reyners et al., 2011). Beneath the North Island the subducting slab is segmented with inflections of 15-20º in slab strike occurring at depths between 50-300 km along the Hikurangi margin (Reyners, 1983; Robinson, 1986; Eberhart-Phillips et al., 2010). Tertiary subduction along the Hikurangi margin, a segment of the relict Gondwana subduction margin, commenced in the Late Eocene to Oligocene (~40-24 Ma) (Stock & Molnar, 1982; Walcott, 1987; King, 2000; Stagpoole & Nicol, 2008; Sutherland et al., 2009). Deep intra-slab earthquakes and seismic tomography indicate the subducted Pacific plate extends to depths of at least 600 km at the latitude of the Taupo Rift (Boddington et al., 2004; Li et al., 2008). The subducting slab steepens with increasing depth and, for a given depth, from south to north along the margin (Reyners et al., 2011).

Subduction is associated with 40-48 mm/yr of westward relative plate motion (273º), ~50° oblique to the strike of the underlying slab (040-050º) and arc front volcanism (036º) (Fig. 2) (Beavan et al., 2002; De Mets et al., 2010). Plate convergence (i.e. arc-normal motion) is primarily accommodated on the subduction interface, while the remainder of arc-normal motion (≤ 20%) and most of the arc-parallel motion (≥ 60%) accommodated in the overriding plate through a combination of reverse and strike-slip faulting, and by clockwise vertical-axis rotations of ~3°/Myr (Webb & Anderson, 1998; Wallace et al., 2004; Nicol & Beavan, 2003; Nicol et al., 2007; Nicol & Wallace, 2007).

The Taupo Rift and TVZ is the southern limit of arc volcanism and intra-arc rifting that dissects both andesitic strato-volcanoes and rhyolitic calderas along the length of the Kermadec-Hikurangi subduction margin (Fig. 2) (Cole et al., 1995; Wright, 1993; Wilson et al., 1995; Campbell et al., 2007). The locus of active rifting transitions southward from a back-arc position in the intra-oceanic Havre Trough to an intra-arc position in the continental North Island (Wright, 1992) (Fig. 2). The rift is the

present location of intra-arc extension within the North Island where the crust has thinned by approximately half (thickness ~16 km) (Davey et al., 1995; Stern et al., 2006). Prior to the development of the TVZ and Taupo Rift around ~ 2 Ma (Houghton et al., 1995; Wilson et al., 1995; Briggs et al., 2005), arc volcanism and intra-arc rifting was located 100-150 km to the northwest in the Taranaki Basin and Coromandel Peninsula (Adams et al., 1994; King & Thrasher, 1996; Booden et al., 2010; Giba et al., 2010). Rates of extension measured by GPS and Late Quaternary fault displacements decrease southwards along the Taupo Rift from 13-19 mm/yr in the offshore Bay of Plenty to ≤ 5 mm/yr towards the southern limit of rifting (Villamor & Berryman, 2001; Wallace et al., 2004; Lamarche et al., 2006; Villamor & Berryman, 2006; Begg & Mouslopoulou, 2010). Active volcanism and rifting over the last ~0.5 Myr has occurred along a northeast-southwest trending 15-20 km wide zone variously referred to as the modern TVZ (Wilson et al., 1995; Leonard et al., 2011) and Taupo Rift (Nicol et al., 2006; Villamor & Berryman, 2006).

Volcanism in the modern TVZ (referred to hereafter at the TVZ) has been divided into three segments along its length: a central segment dominated by explosive rhyolitic caldera forming volcanic centres bounded to the north and south by regions containing andesite-dacite strato-volcanoes (Fig. 3) (Wilson et al., 1995). The central rhyolitic region is presently the most frequently active and most productive silicic volcanic systems on Earth producing an estimated ≥ 6000 km^3 of magma at rates of 3.8-12.8 km^3/kyr (Wilson et al., 2008). The central region has high heat flows (700 mW/m^3) through numerous high temperature geothermal systems coincident, and to the east of, active rift faults (Bibby et al., 1995). Recently active rhyolitic calderas (Taupo and Okataina) are coincident with the active rift (Wilson et al., 1984; Nairn, 2002). A plume-like structure of high conductivity, derived from magnetotelluric soundings and interpreted as an interconnected melt zone, rises from >35 km depth beneath the axis of the rift (Fig. 2) (Heise et al., 2010). Seismic activity associated with extension along the Taupo Rift indicates the depth to the brittle-ductile transition is 7-9 km in the central rhyolitic region which increases to 10-15 km to the north and south (Bibby et al., 1995; Hurst & McGinty, 1999).

Earthquake swarms are typical of seismicity in the Taupo Rift (Bibby et al., 1995; Hurst et al., 2008). The Matata earthquake sequence (Hurst et al., 2008; Mouslopoulou & Hristopulos, 2011), for example, occurred along the Rurima Ridge and coastal region in the northern onshore TVZ over a period of 49 months (January

2005 to January 2009) and comprised 2083 earthquakes M_L 2.3- 4.7 recorded by the national seismic network (www.GeoNet.org.nz) and two portable seismograms. Here, relocated hypocentres (by S. Bannister of GNS Science) delineate a detailed image of the sub-surface fault structure where the spatial and temporal characteristics of the earthquake sequence are interpreted as tectonic in origin (Mouslopoulou & Hristopulos, 2011). Recent large earthquakes (> M 6) occurring in the same region show predominantly normal faulting focal mechanisms (Webb & Anderson, 1998) as do the majority of geological fault-slip indicators (Beanland et al., 1989; Rowland & Sibson, 2001; Acocella et al., 2003). This study focuses on faulting processes that have occurred in the Taupo Rift over the last 0.3 Myr and predominantly over the last 60 kyr. Although rifting and volcanism are broadly coincident in space and time, outside the main active volcanic centres faulting is primarily tectonic and not driven by volcanism (Nicol et al., 2006; Seebeck & Nicol, 2009; Mouslopoulou & Hristopulos, 2011).

3. Geometry of Rifting

Taupo Rift faults active over the last 0.3 Myr define a 15-20 km wide northeast trending zone extending ~300 km from the southern limit of arc volcanism to the North Island continental margin in the Bay of Plenty (Fig. 3). The rift is predominantly asymmetric with the largest fault displacements observed along the eastern rift margins. Quaternary extension rates are highest on active eastern rift border faults and diminish westwards across the rift (Villamor & Berryman, 2001; Lamarche et al., 2006; Mouslopoulou et al., 2008; Begg & Mouslopoulou, 2010), consistent with displacement patterns over the last ~1.6 Ma observed in a regional seismic-reflection line (Davey et al., 1995). These eastern rift border faults, the ~045º trending Paeroa Fault and ~041º trending White Island Fault (Fig. 3a), are the longest continuous structures in the rift at ~30-40 km in length (i.e. approximate thickness of pre-rift crust) (Villamor & Berryman, 2001; Bannister et al., 2004; Lamarche et al., 2006). These two large faults are parallel to an interpretation of the rift axes defined by changes in fault dip direction onshore (Fig. 3 and 4), and are parallel to the strike of the underlying subducting plate (chapter 5). The longest fault towards the southern termination of the rift, the ~025º trending Waihi Fault, is slightly oblique to the underlying slab (~20º). The steep dips of normal faults observed at the surface (≥ 70º) are inferred to shallow to more moderate dips (≥ 50º) at seismogenic depths (Villamor & Berryman, 2001).

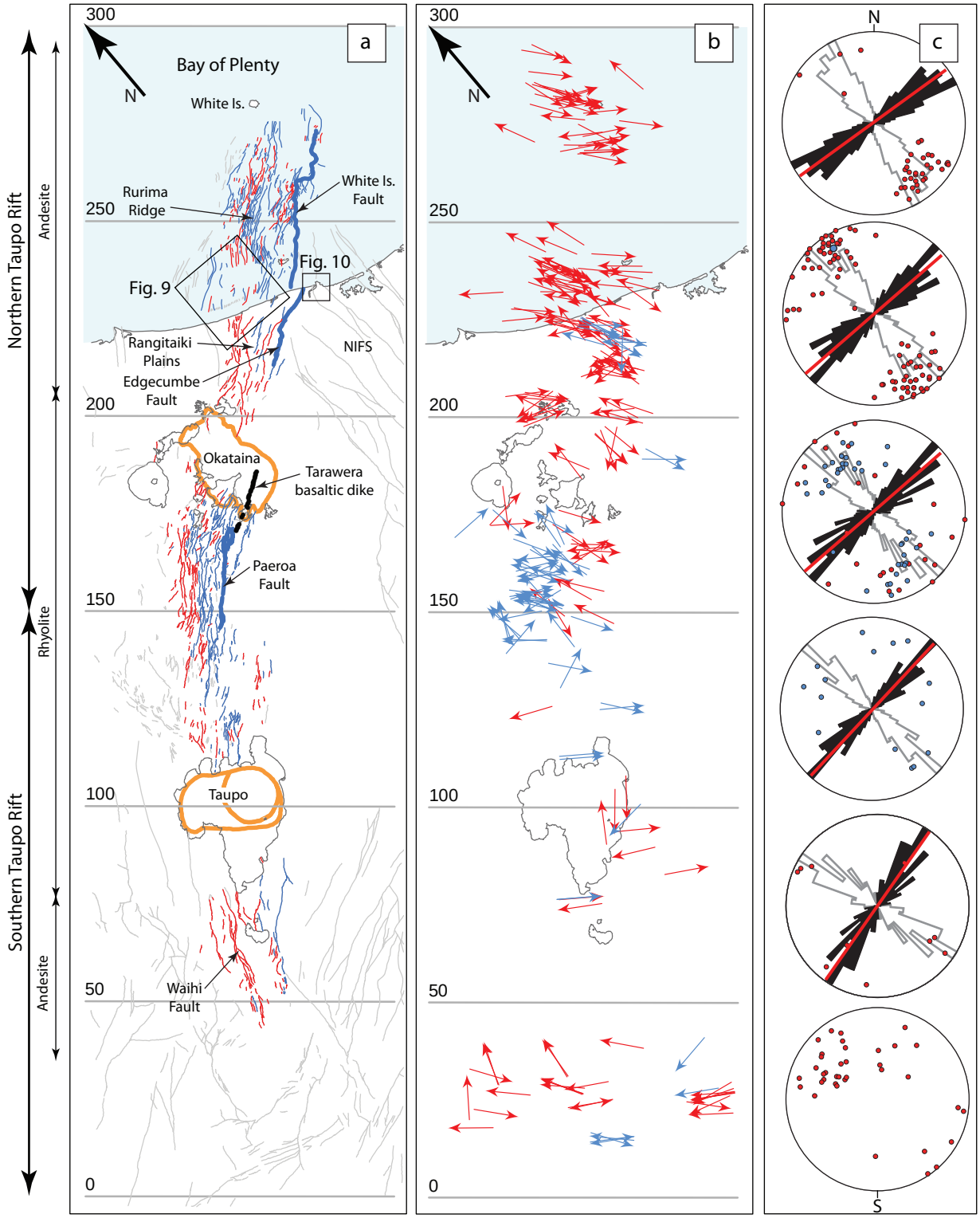

Figure 3. Taupo Rift geometry and kinematics. (a) Active rift faults with colours showing dip direction (red lines = east, blue lines = west), faults outside the rift shown in light grey. Active rhyolitic calderas (Taupo and Okataina) (thick orange lines) and vents of the AD 1886 Tarawera basaltic dike (black filled circles) also shown (Davy & Caldwell, 1998; Nairn, 2002). NIFS = North Island Fault System. Dominant volcanic compositions from Wilson et al. (1995). (b) Kinematic extension directions from focal mechanisms (red arrows) and geological fault-slip data (blue arrows), see text for references. Measured location at foot of arrow. (c) Rose diagrams summarise fault orientations for each 50 km section (black fill fault trends and white fill fault dip direction). Red and blue filled circles show trend and plunge of extension directions on lower hemisphere equal area stereonet for focal mechanisms and geological fault-slip data, respectively.

The geometry of the rift is defined by GNS Science Active Faults database, supplemented by re-examination of aerial photographs (1:25 000 and 1:17 000 scale) and published geological maps (Fig. 3) (Villamor & Berryman, 2001; Nairn, 2002; Lamarche et al., 2006; Nicol et al., 2006; Townsend et al., 2008; Lee et al., 2010; Leonard et al., 2011). Active fault traces onshore have been confirmed by extensive paleoearthquake studies of displaced dated volcanic and fluvial surfaces typically ≤ 60 ka in age (Villamor & Berryman, 2001; Nicol et al., 2006; Berryman et al., 2010; Begg & Mouslopoulou, 2010; Nicol et al., 2010). These displaced surfaces range in age up to 0.36 Ma toward the active rift boundaries and < 20 ka towards the rift axes (Villamor & Berryman, 2001; Nicol et al., 2006). Offshore, active fault traces have been identified by seafloor scarps and displacements of a < 20 ka post-last glacial ravinement surface through a network of seismic-reflection lines and multibeam bathymetry (Lamarche et al., 2006). This study utilised these offshore and onshore data on the location and geometry of faulting which have been augmented by residual gravity data along the onshore rift axis (Stagpoole & Bibby, 1999; Stagpoole et al., 2005; Mouslopoulou et al., 2008; Seebeck et al., 2010) (New Zealand Gravity Station Network, This study).

To capture the local variability in fault trend along strike of the Taupo Rift the orientation of individual active traces have been measured within 1 km^2 regions in a grid aligned parallel to the regional trend of arc front volcanism and underlying slab (040°). Previous interpretations averaged faults in regions determined by inferences about rift structure and segmentation (Rowland & Sibson, 2001; Acocella et al., 2003). Our method allows the fault orientation measured across and along the rift to be treated as a continuous function from which kinematic boundaries within the rift can be determined. Surface trace orientations within 1 km^2 sample regions are weighted equally resulting in larger faults being sampled proportionally more often due to their greater lengths. High densities of short (e.g. 1-4 km) segmented faults are generally observed in young volcanic and fluvial surfaces (i.e. towards the rift axes) whereas long continuous (e.g. 20-30 km) faults are more typical of older volcanic surfaces and/or where basement is relatively shallow (i.e. towards the rift shoulders). Fault-trace orientation have variations of ± 10-20° (1σ) across 1 km wide rift normal sections (minimum 5 fault traces) and mean variations of ± 7° (1σ) between adjacent along strike 1 km wide rift normal sections. For comparison, the same method applied to scaled models of rifting by McClay et al. (2002) show variability in rift normal fault

orientation associated with orthogonal and oblique extension averages ± 7-11° (1σ) and ± 10-14° (1σ) respectively.

The regional trend of active fault-traces is 047 ± 23º, where 69% of the fault data come from distances of 150-300 km along strike (Table 1), and is sub-parallel to the strike of the underlying slab (040-050º) (Reyners et al., 2006; Eberhart-Phillips et al., 2010). Fault trends averaged along 25-50 km segments show a general northward swing in mean fault trend from 035º to 054º (Fig. 3 and Table 1). Systematic variations in mean fault trend of ~10º over wavelengths of ~20 km occur along the active rift, with the largest change of ~20º occurring immediately south of the Okataina Volcanic Centre between 150-165 km along strike distance (Fig. 3). This swing in mean fault trend is accommodated by the inter-fingering of two dominant fault sets (030-040º and 050-060º) (Fig. 3) which are parallel to negative residual gravity contours (-40—50 mGal) representing basement structure at depths of 2-3 km (Fig. 4) (Seebeck et al., 2010) (see Appendix 1 for gravity methods and data). This change in mean fault orientation is approximately coincident with a ~25º rotation in the trend of basement structures and fabric observed across the North Island (Nicol et al., 2007). This rotation axis marked an important kinematic boundary prior to the development of the Taupo Rift (Nicol & Wallace, 2007) and is discussed further in section 5 of this chapter. For the purposes of this paper, I divide the Taupo Rift into southern and northern sections at this rotation boundary where mean fault and basement trends change (Fig. 3). This location also marks important changes in rift kinematics discussed in the next section.

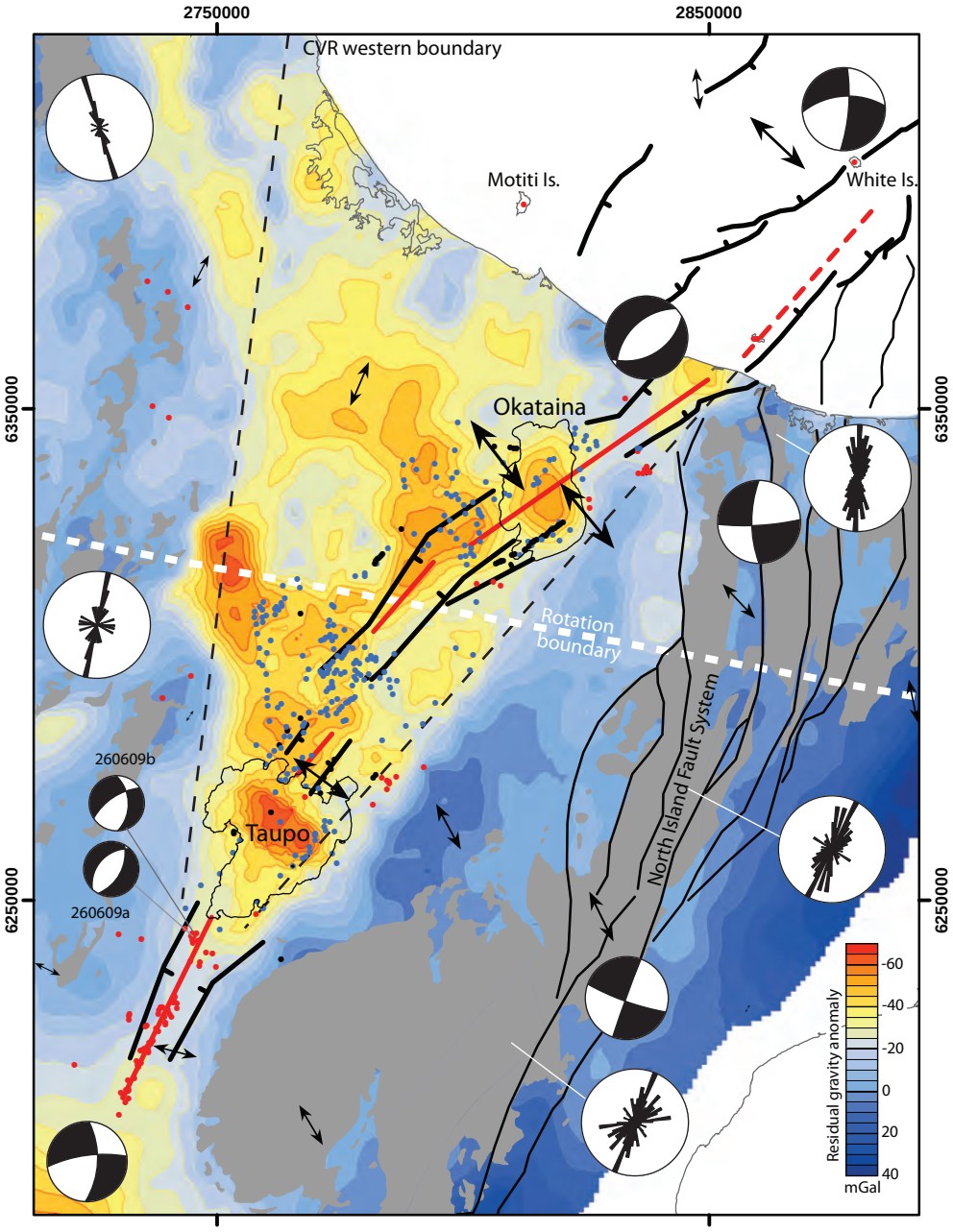

Figure 4. Volcano-tectonic summary of the Taupo Rift superimposed on residual gravity. Due to the high density contrast between volcanic infill and basement, residual gravity highlights structural depressions (black lines = active rift border faults, red lines = rift axes) and rhyolitic calderas where warm colours represent basement at depths of > 2 km and cool colours for near surface basement and grey shading for Mesozoic basement. See appendix 1 for methods and references. Offshore faults from Wright (1992) and Lamarche et al. (2006). Alignments of volcanic vents (black filled circles = basalt, red filled circles = andesite and dacite, blue filled circles = rhyolite) are generally parallel to active rift boundaries (Townsend et al., 2008; Leonard et al. 2010; Lee et al. 2012). Composite TVZ focal mechanisms detailed in Table 1. RMT focal mechanisms from Ristau (2008). Kinematic axes of the North Island Fault System from Mouslopoulou et al. (2007). Geodetic extensional strain directions (black arrows) from Beavan et al. (2007); size of arrows proportional to magnitude of extension. Central Volcanic Region (CVR) boundaries (black dashed line) from Stern et al. (2006). Rotation boundary from Nicol et al. (2007) (white dashed line) represents ca. 25° bend in the steeply dipping basement fabric which is shown by rose diagrams plotting basement bedding (Edbrook et al., 2005; Townsend et al., 2008; Lee et al, 2010; Leonard et al., 2012).

Location	Distance km	Focal mechanism/Fault-slip P	T	B	N	Stress Inversion σ_1	σ_3	FM SH_{max}	Borehole Breakout	GPS PHS/PHE	Faults Mean Az.
Ngatoro Basin	340-370	151/77	305/10	036/5	22						
White Island	250-300	231/34	131/4	022/53	32					223/133	$054 \pm 18_{(250\text{-}275km)}$
NTR	150-250	073/86	323/1	233/3	105	160/70[1]	328/20[1]	060		230/140	$047 \pm 17_{(250\text{-}225km)}$
Matata	225-250	025/60	142/15	239/35	28	090/78[2]	322/7[2]			232/142	$050 \pm 21_{(225\text{-}200km)}$
Edgecumbe[b]	228	052/77	148/2	238/13	1						$050 \pm 29_{(175\text{-}200km)}$
Edgecumbe[d]	228	011/72	153/14	246/10	1						$049 \pm 23_{(150\text{-}175km)}$
Edgecumbe[a]	228	156/75	313/13	045/5	1						
Edgecumbe[c]	210-230	093/83	328/3	237/5	27						
Taupo	75-100	221/16	128/11	4/70	5					216/126	
STR	0-50					052/38[4]	142/0[4]				$045 \pm 27_{(125\text{-}150km)}$
STR	0-50					033/28[3]	296/12[3]				$038 \pm 14_{(100\text{-}125km)}$
STR	0-150	219/34	315/7	056/54	35	050/13[5]	316/14[5]	071 ± 32	058 ± 21	194/104	$035 \pm 30_{(50\text{-}75km)}$
TR FM	0-250	192/85	323/3	053/3	149					234/144 ± 22	$047 \pm 23_{(0\text{-}250km)}$
TR FM	0-300	239/65	140/4	048/24	186						
TR FS[e]	0-225	137/68	313/22	044/1	73						
Taranaki FS[f]		324/83	131/6	221/1	103						

Table 1. Stress and strain indicators from across the central North Island. Azimuths in °N, see Fig. 3 and 11 for location. Composite focal mechanisms derived from published sources; (a) Dziezwonski et al. (1981), (b) Anderson & Webb (1989), Richardson (1989), (c) Robinson (1989), (d) Webb & Anderson (1998), Hurst & McGinty (1999), Hayes et al. (2004), Hurst et al. (2002), Hurst et al. (2008), Ristau (2008), Reyners (2009). Fault-slip data (e) from Beanland et al. (1989), Acocella et al. (2003) and unpublished data, (f) from Giba et al. (2010). Stress Inversions use the method of Robinson & McGinty (2000) to invert first motion polarities for optimum stress axes under Coloumb failure criteria; (1) Hurst et al. (2002), (2) Hurst et al. (2008) Matata sequence, (3) Hayes et al. (2004) Waiouru sequence, (4) Sherburn & White (2005) Mid-crustal earthquakes, (5) Reyners (2009) all STR mid-crustal earthquakes. SH_{max} directions from 3D cluster analysis of focal mechanisms by Sherburn et al. (2009). Borehole breakout in exploration wells from Australasian Stress Map (http://asprg.adelaide.edu.au/asm/). Principal Horizontal Shortening/Extension direction (PHS/PHE) derived from GPS by Beavan et al. (2007). Average strike of active rift faults in 25 km long segments from north to south derived from GNS active faults database (http:/data.gns.cri.nz/af/) and Begg & Mouslopoulou (2010) onshore and from Lamarche et al. (2006) offshore. Regional trend of PHS and SH_{max} through central North Island ~55/235°.

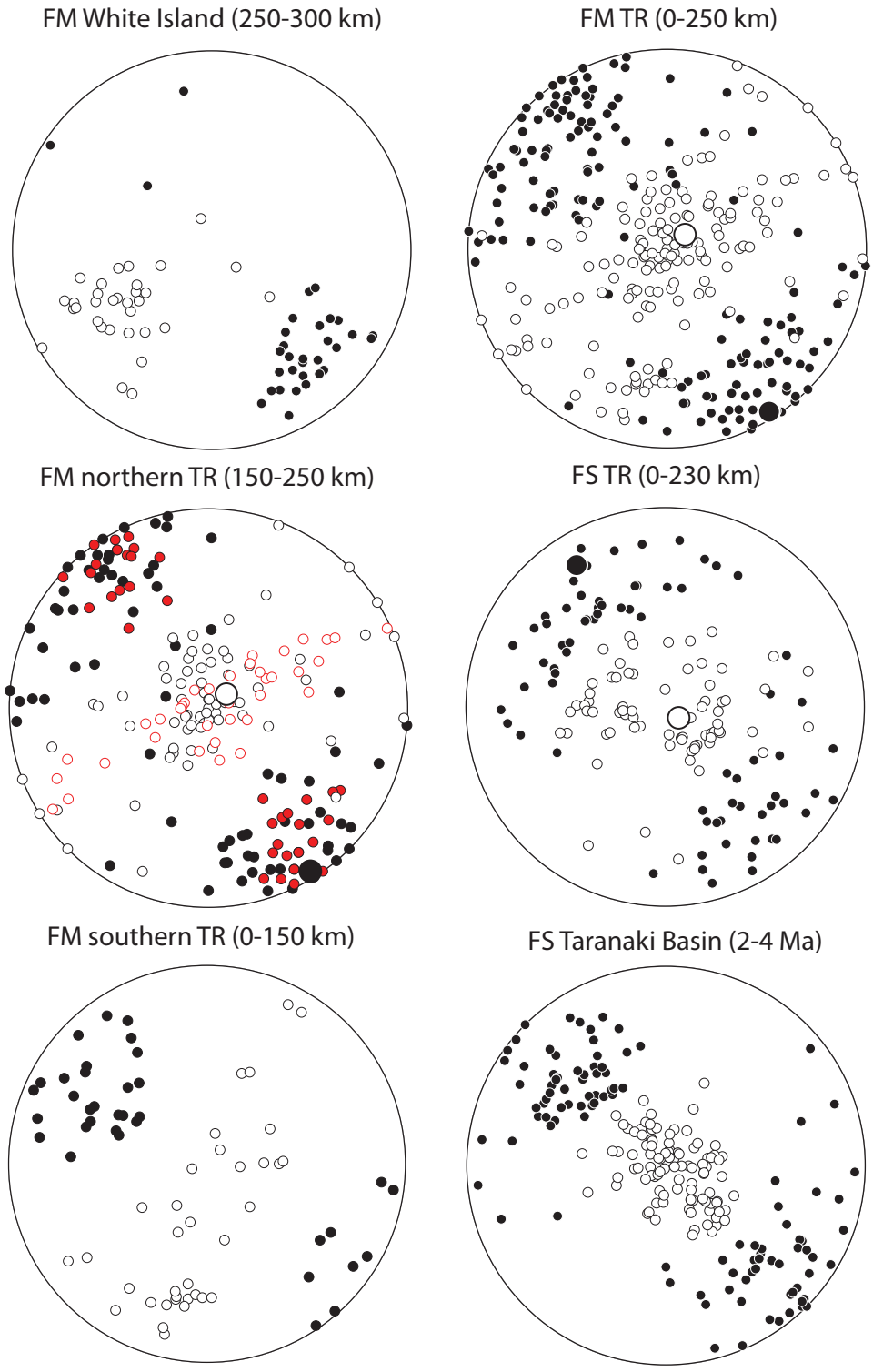

Figure 5. Taupo Rift (TR) earthquake kinematics. Shortening (P) (white filled circles) and extension (T) (black filled circles) axes from earthquake focal mechanisms (FM) and geological fault-slip (FS) data shown on lower hemisphere equal area stereonets. See text for references. Larger symbols associated with M_W 6.5 Edgecumbe earthquake. Red symbols in northern Taupo Rift are associated with the Matata sequence shown in Fig. 9. White Island data representing oblique-strike-slip faulting has been excluded from Taupo Rift compilation as not presently representative of normal faulting further south and is discussed further in the text. Fault slip data from the Taranaki Basin representing faulting in the western North Island 2-4 Ma ago (Giba et al., 2010) for comparison with present day Taupo Rift.

4. Kinematics of Rifting

Faults at the ground surface in the Taupo Rift have predominantly normal dip-slip (Beanland et al., 1989; Villamor & Berryman, 2001; Rowland & Sibson, 2001; Acocella et al., 2003). Many studies have concluded that the TVZ accommodates a component of strike-slip either as oblique-slip vectors on normal faults or partitioned onto strike-slip faults and volcanic intrusions (Nairn & Cole, 1981; Smith & Webb, 1986; Webb & Anderson, 1998; Acocella et al., 2003; Lamarche et al., 2006). In order to constrain better the kinematics of rifting, I have collated kinematic indicators from earthquake focal mechanisms and geological field studies from 300 km along the active rift.

All kinematic axes and sources of data used in this study can be found in Table 1 and Fig. 5. Kinematic data are from unpublished Regional Moment Tensor (RMT) focal mechanisms (N = 94) calculated using local network data for earthquakes $\geq M_W$ 3.4 in New Zealand since 2004 (Ristau, 2008) and published focal mechanisms (N = 124) from 1977 to 2008 which are generally comparable to RMT solutions (Fig. 5) (Anderson & Webb, 1989; Richardson, 1989; Robinson, 1989; Hurst & McGinty, 1999; Hayes et al., 2004; Hurst et al., 2002; Hurst et al., 2008; Reyners, 2010). In the northern Taupo Rift the 3-9 km depth of earthquakes contrasts to the 11-35 km depth at the southern termination of the rift. Earthquake focal mechanism slip data have been augmented by surficial fault-slip data (N = 79) from offset landforms and fault-plane striae (Beanland et al., 1989; Rowland & Sibson, 2001; Acocella et al., 2003) (refer to the original publications for methods) and unpublished data from this study reduced to kinematic strain axes (i.e. P and T axes) using the method of Marrett & Allmendinger (1990) (Fig. 5). For comparison with rifting to the west of the Taupo Rift in the Taranaki Basin I use fault-striation data similarly reduced to kinematic axes collected along the Taranaki coast by Giba et al. (2010) (Fig. 5). Taupo Rift fault data are sampled from layered pyroclastic deposits younger than 0.3 Ma, while some slip data were recorded from active faults that accrued slip in the last 10 kyr. The majority of kinematic data come from the northern Taupo Rift, a region that straddles the boundary between central rhyolitic and andesitic volcanic regions (Wilson et al., 1995) (Fig 3.) and the intersection with the strike-slip faults of the North Island Fault System (NIFS) (150-250 km along strike distance) (Mouslopoulou et al., 2007) (Fig. 3b). Visible surface fault traces are considered to represent the accumulated displacement of

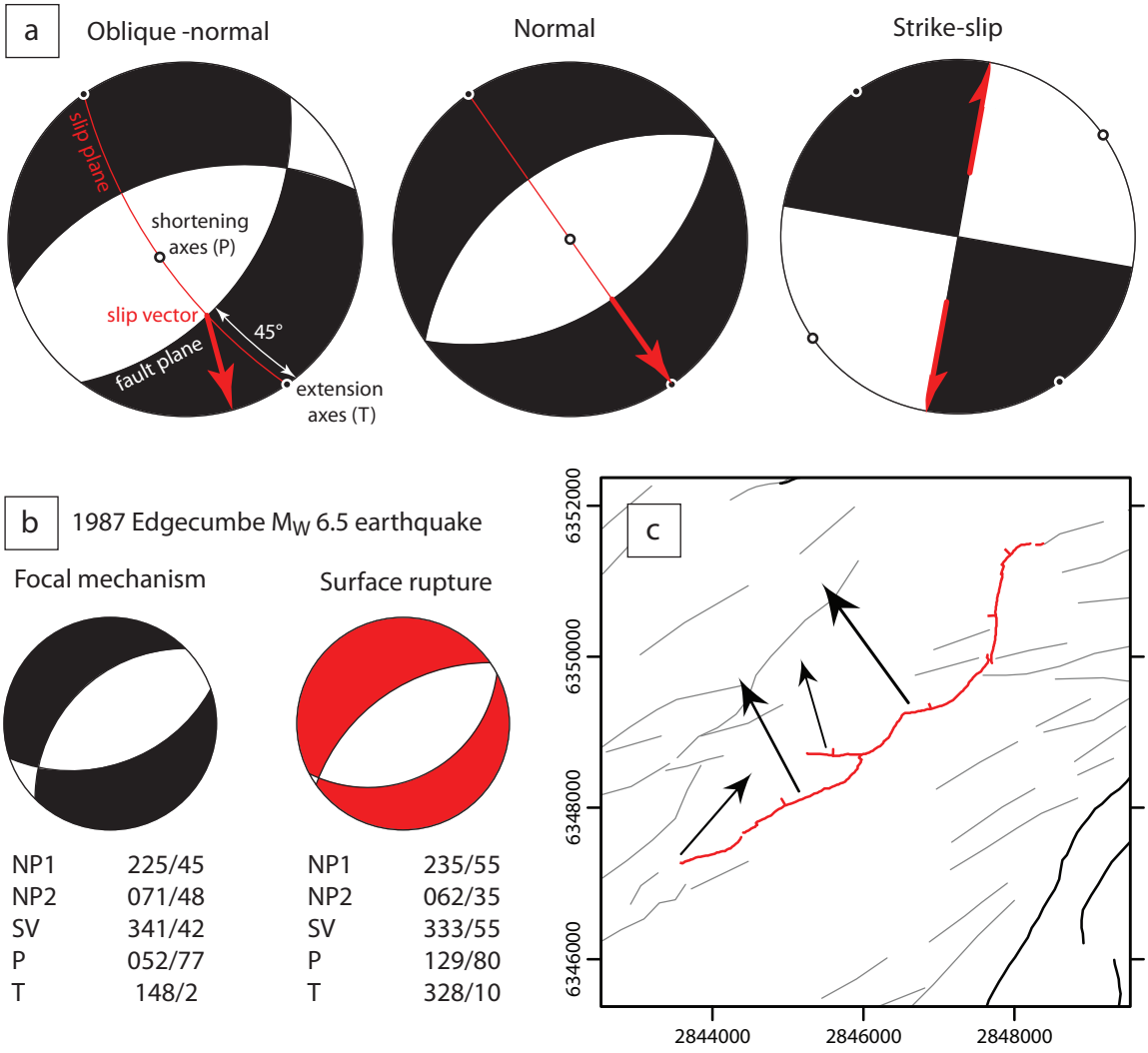

Figure 6. (a) Relationships between fault geometry, slip vector or rake, and kinematic axes (after Marrett & Allmendinger, 1999). Shortening and extension kinematic axes (in lower hemisphere stereographic projection) derived from geologic data (e.g. striae or slickenlines) are equivalent to P and T axes from focal mechanism solutions . Illustration of fault kinematics with uniform extension axes where the shortening axes changes from vertical (normal faulting) to horizontal (strike-slip faulting). (b) 1987 M_W 6.5 Edgecumbe earthquake. Focal mechanism solution at ~8 km depth (Anderson & Webb, 1989) compared to that derived from the surface rupture (Beanland et al., 1989) showing equivalent horizontal extension directions (T axes). (c) Map of the Edgecumbe earthquake surface rupture and slip vectors calculated from offset cultural markers (Beanland et al., 1989)

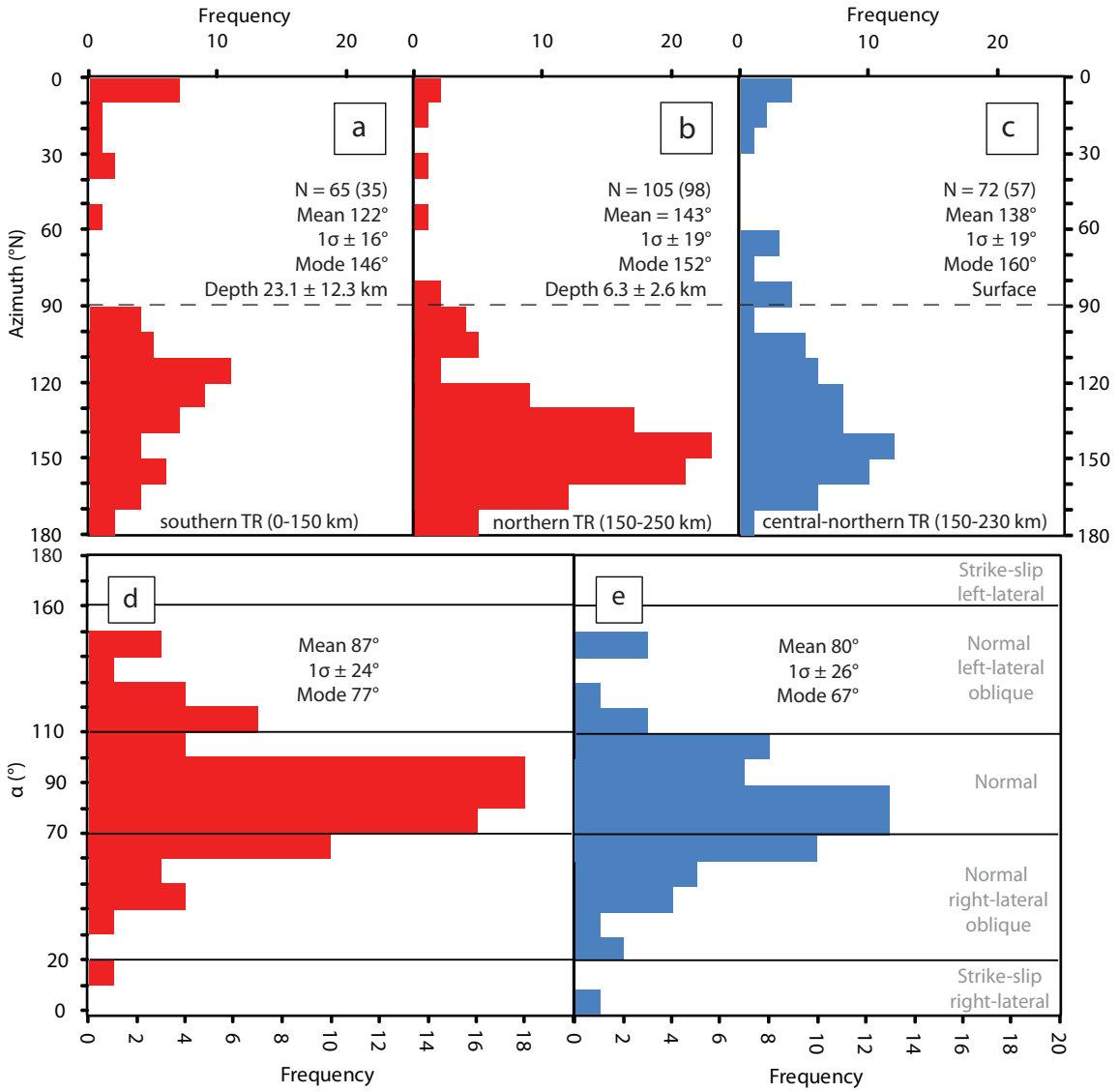

Figure 7. Extension direction frequency histograms for the Taupo Rift. (a) Focal mechanism T axes fom the southern Taupo Rift. (b) Focal mechanism T axes from the northern Taupo Rift. (c) Extension directions derived from fault kinematic data (Beanland et al., 1989; Rowland & Sibson, 2001; Acocella et al., 2003) from central-northern Taupo Rift. See Fig. 3 for locations of focal mechanism and geological fault-slip data. Mean extension direction calculated from directions approximately normal to fault trends (i.e. 90-180°) with the number of data used in brackets. (d) Focal Mechanism extension directions relative to mean fault strike along the rift. (e) Surface fault extension directions relative to mean fault strike along the rift.

earthquakes ≥ M 6 (Villamor & Berryman, 2001) and place constraints on the long-term (thousands to hundreds of thousands of years) regional strain orientation.

To determine the direction of principal horizontal extension (which I will simply refer to as the extension direction) in the Taupo Rift, I examine extension axes orientations from earthquake focal mechanisms and geological data. The kinematic axes of the incremental strain tensor for a fault lie in the "slip plane" containing the slip vector and the pole to the fault-plane, and makes angles of 45º with each of these vectors (Fig. 6) (Marrett & Allmendinger, 1990). Kinematic axes are an alternative representation of the original fault-slip vector and are equivalent to focal mechanism P and T axes (Marrett & Allmendinger, 1990) and, as such, I use these terms interchangeably. Detailed studies of the 1987 M_W 6.5 Edgecumbe earthquake show the consistency between kinematic axes estimated from focal mechanism and field data (Fig. 6) as do previous studies from other localities (Anderson & Webb, 1989; Beanland et al., 1989; Marrett & Allmendinger, 1990). The similar extension direction distributions for focal mechanisms (i.e. small faults or small slip earthquakes, < 1 m) and geological observations (large earthquakes or slip during surface rupturing events, > 1 m) indicate that the slip and extension data are scale invariant (Table 1). This is further supported by comparison of strain axes for M_W 3-4 earthquakes (e.g. N = 30) from the Matata region and those derived for the M_W 6.5 Edgecumbe earthquake (Table 1).

4.1 Regional Extension directions

Extension axes from northern Taupo Rift earthquakes consistent over a magnitude range 3.5-6.5 for a twenty year period (Table 1). Mean extension (T) axes for the Matata sequence M_W 3.4- 4.7 (N =28) (142 ± 8º) show a near identical extension direction to the fault-plane solutions for M_W 6.5 Edgecumbe earthquake (144 ± 10º) and M_W 2.9-4.0 earthquakes associated with its aftershock sequence (148 ± 22º) (Table 1 and Fig. 5). This extension direction is also parallel to that inferred for the Tarawera basaltic dike intrusion (147º) in AD 1886 that erupted along a 17 km fissure system in the Okataina Volcanic Centre 50 km to the southeast of Matata (Fig. 3) (Nairn & Cole, 1981; Rowland & Sibson, 2001). Further, the girdle formed by the variability of P axis orientations in the Matata and Edgecumbe earthquake aftershock sequences contain the principal horizontal shortening axis (237-239º) (refer Fig. 5) which is parallel to the

central graben faults (055-061º) (Beanland et al., 1989; Lamarche et al., 2006; Begg & Mouslopoulou, 2010) and the trend of the AD1886 basaltic dike (057º) (Nairn & Cole, 1981).

On a regional scale, the extension direction is approximately normal to the rift. The frequency of extension directions between 090-180º (i.e. approximately normal to the rift) are comparable between earthquake and geological data showing mean azimuths of 143 ± 19º (1σ) and 138 ± 19º (1σ) respectively (Fig. 7). These extension directions are comparable to the average of 135 ± 7º (1σ) derived from regional GPS (Beavan et al., 2007). The average extension direction for the active rift from all earthquake data is comparable to the eigenvector representing the extension axis for all northern Taupo Rift earthquakes (143º) (Table 1). Towards the southern termination of the Taupo Rift (0-50 km along strike distance) the mean extension direction of 122 ± 16º (1σ) is consistent with an counter-clockwise swing in the mean fault trend (Fig. 7). The few kinematic data that occur between distances of 50-150 km along the rift indicate an extension direction predominantly orthogonal to mean fault orientation (Table 1 and Fig. 3b). I use the eigenvectors (maximum eigenvalues) detailed in Table 1 to represent mean kinematic extension (T) and shortening (P) axes from this point.

The obliquity of the extension direction to the rift boundary determines the pattern of faulting (the orientation, linkage and interaction of fault segments) accommodating biaxial (orthogonal rifting) or triaxial (oblique rifting) strain (McClay & White, 1995; Dewey et al., 2008). Consistent with previous studies along the TVZ and southern Havre Trough (Lamarche et al., 2006; Campbell et al., 2007), the obliquity of rifting is defined by the angle α between the eastern active rift boundary and the extension direction: $\alpha = 90^{\circ}$ corresponds to pure orthogonal extension; $\alpha < 90^{\circ}$ (clockwise direction) corresponds to a component of right lateral shear and $\alpha > 90^{\circ}$ (counter-clockwise direction) corresponds to a component of left-lateral shear (Fig. 8).

For a mean Taupo Rift fault trend of 047º with a mean extension direction of 143º, the mean obliquity is $\alpha = 84^{\circ}$ (Fig. 8) indicating predominantly orthogonal extension with a minor component of right-lateral strike-slip (6º clockwise from mean down dip direction). If the extension direction with respect to arc front is considered (representing the crest of the mantle wedge), the obliquity is $\alpha = 76^{\circ}$. The obliquity between the mean fault trend and the extension direction from focal mechanisms at a given distance along the rift also show predominantly normal extension (mean α = 87 ±

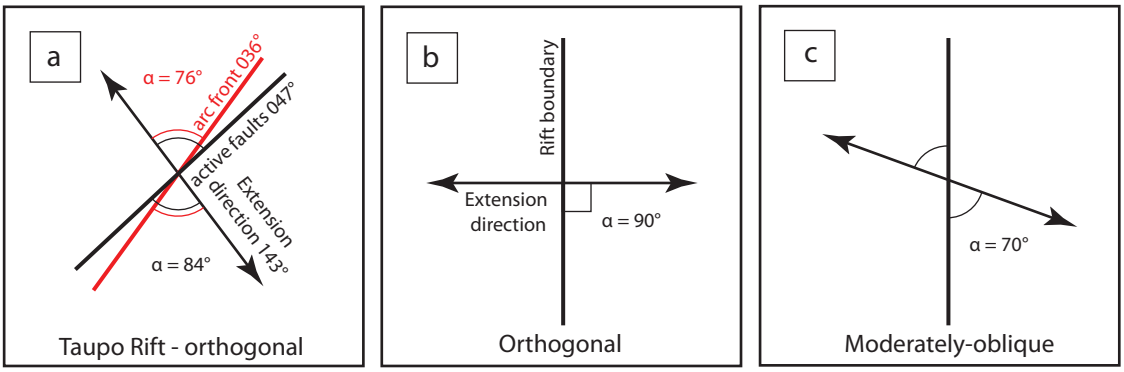

Figure 8. Style of Taupo Rift extension. The relationship between normal fault strike and extension direction in the Taupo Rift (a) in comparison with (b) orthogonal extension, α = 90º and (c) moderately oblique extension α = 70º.

24º) with minor right lateral strike-slip (Fig. 7). Active eastern border faults have α = 78-82º to the mean extension direction (143º) (along strike distance 145-275 km). The largest fault in southern Taupo Rift, the Waihi Fault, is approximately normal to the extension directions of recent nearby Mw 4.2-4.4 earthquakes (α = 80-84º) (Fig. 4). The unweighted geological fault data and GPS inversion (Beavan et al., 2007) shows similar results with mean values of α = 80 ± 26º and 91 ± 7º, respectively. Extension direction frequency distributions show a minor dextral component is a feature of both data sets (e.g. mode α = 77º and 67º for earthquake and geological data respectively), however, given that the majority of extension directions are within 20º of the mean fault dip direction (81% and 62% for earthquake and geological data respectively) (refer Fig. 7), the faults are considered to be predominantly dip-slip.

Changes of up to 15-20º can occur in the extension direction along strike over distances < 50 km (Table 1). Along with these small variations in extension direction, larger variations (i.e. up to 90º) occur in the trend of the shortening direction, changing the faulting style from predominantly normal to strike-slip to varying degrees in both northern and southern Taupo Rift (Fig. 5). The resulting variation in the plunge of the shortening axes typically occur about a girdle normal to the extension direction and contains the direction of maximum horizontal shortening which is parallel with mean fault trends. Previous interpretations of small earthquakes with strike-slip mechanisms in the Taupo Rift (Smith & Webb, 1986) involved a model with a complex array of faults similar that proposed by Hill (1977). In this model, en echelon dip-slip normal faults striking parallel to principal shortening direction and/or Shmax are linked via obliquely trending strike-slip faults. The spatial distribution and focal mechanisms of earthquakes associated with the Matata sequence (Fig. 9) shows that a model involving a complex array of faults is appropriate.

Despite evidence to suggest that fault-slip directions change locally, the kinematic data do not appear to support suggestions that the rift can be divided into orthogonal and obliquely extending segments with different extension directions as proposed by Acocella et al. (2003). Changes in mean fault strike occur in unison with changes in the extension direction which results in predominantly normal faulting along strike (refer Fig. 7). The consistency of the extension direction in the offshore Bay of Plenty and northern onshore Taupo Rift through the Okataina Volcanic Centre show that significant changes in extension direction (or fault trend) do not occur across

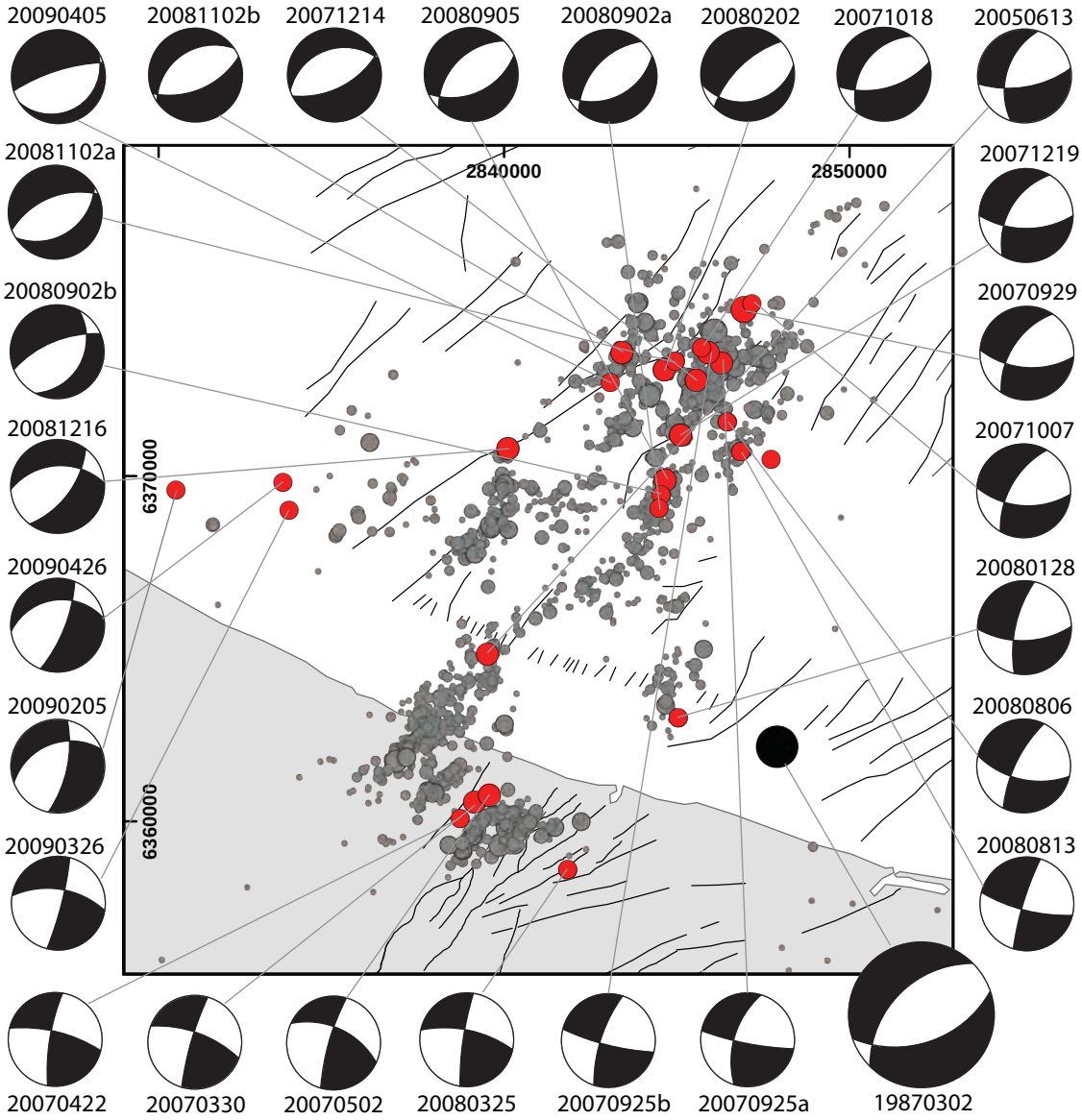

Figure 9.Focal mechanisms and relocated seismicity associated with the Matata earthquake sequence. Relocated seismicity (2007-2009) (grey filled circles) and RMT focal mechanism solutions (2005-2010) (red filled circles) (Ristau, 2008) from the Rurima Ridge. Mapped active faults (grey lines) from Begg & Mouslopoulou (2010) onshore and Lamarche et al. (2006) offshore. 1987 M_W 6.5 Edgecumbe earthquake focal mechanism and location (black filled circle) from Anderson & Webb (1989).

previously inferred segment boundaries (Acocella et al., 2003), between predominantly rhyolitic and andesitic segments (Spinks et al., 2005), or the intersection with the active NIFS (Mouslopoulou et al., 2007). Future models accounting for variation in the structure and evolution of the Taupo Rift, and possibly the style and productivity of volcanism in the TVZ, will be constrained by the kinematics presented here. In the following section I examine variations in the kinematics of the rift to identify first and second-order controls on extension along the Hikurangi subduction margin.

4.2 Influence of basement

Within the northern Taupo Rift faulting varies from normal to strike-slip for a uniform extension direction (Fig. 5). While the shortening axes of the Matata earthquake sequence, and other earthquakes from the region, are predominantly vertical and consistent with surface fault trace data, approximately half have sub-horizontal to moderately plunging P axes (< 60^{o}) representative of oblique- strike-slip earthquakes on steeply dipping north-south or east-west fault-planes (Fig. 9). Strike-slip focal mechanisms occur in the source region of the M_W 6.5 Edgecumbe normal faulting earthquake across to the Rurima Ridge, on the western margin of the active rift. Focal mechanisms and surface fault-trace in this region show that strike-slip and normal faults coexist in the same rock volume which is in contrast to present models for oblique extension (Dewey et al., 2008). Toward White Island strato-volcano oblique- strike-slip earthquakes are the predominant style of faulting (Fig. 5, see Fig. 3 for location).

Comparison between focal mechanism fault-plane solutions, faults (of unknown age) and fabric orientations in basement from the Matata region are consistent with two predominant orientations of faults, one parallel with the observed northeast-southwest strike of normal faults at the surface and the second consistent with strike-slip faulting along a north-south trending basement fabric parallel trend (Fig. 10). The continental crust of the North Island is comprised of a steeply dipping imbricate tectono-stratigraphic assemblage of alternating indurated sandstone and argillite units (Mortimer, 2004) which trends north-south in the Matata region (Leonard et al., 2011). The inferred basement controls on strike-slip is consistent with slip on steeply dipping bedding planes exposed along the Bay of Plenty coastline (Fig. 10). It is inferred that earthquakes near White Island, directly north of the dextral strike-slip North Island Fault System, indicate steeply north-south basement fabric is presently being reactivated

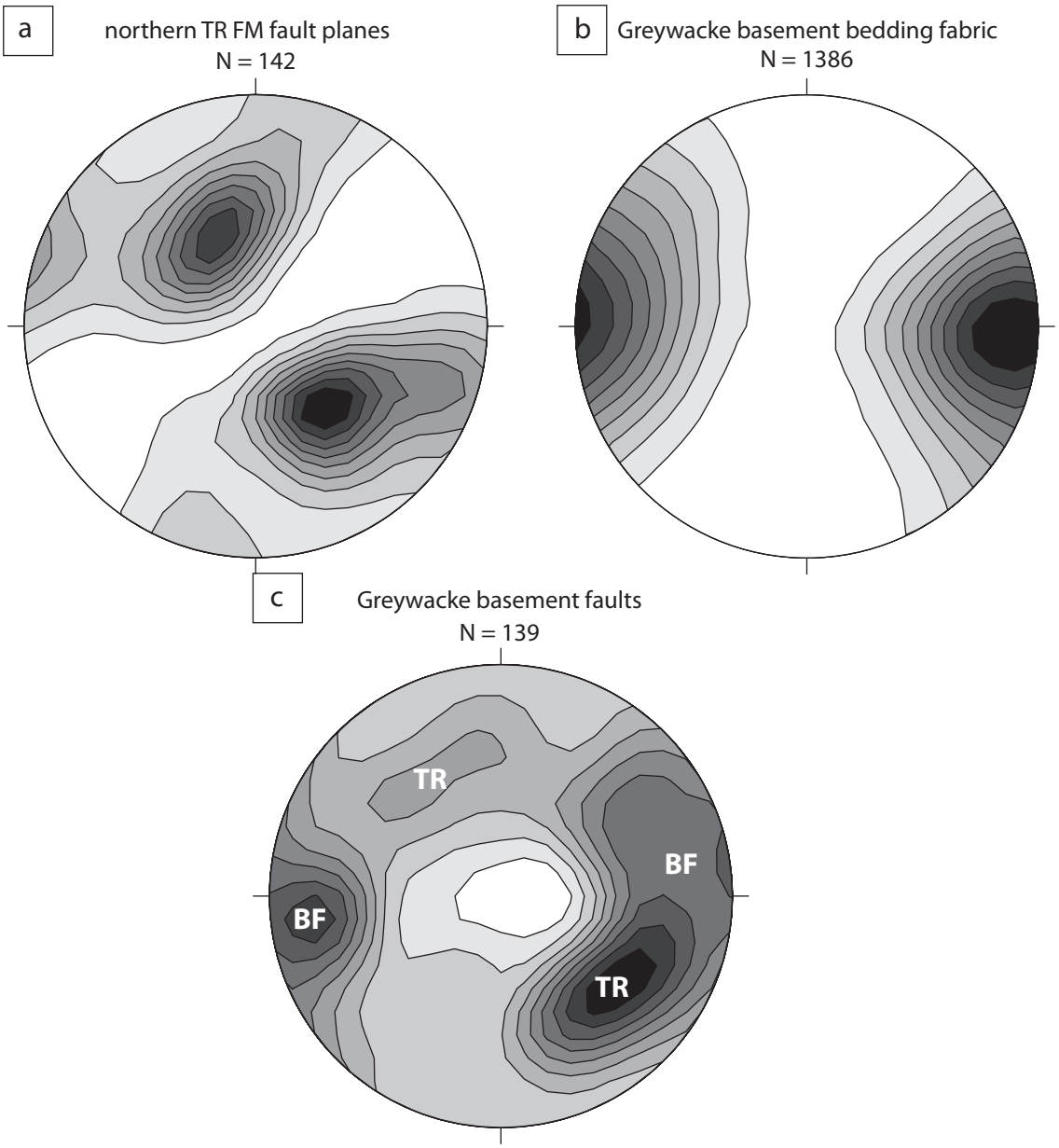

Figure 10. Equal area lower hemisphere density distributions for poles to basement faulting in the northern Taupo Rift. (a) Fault planes from Matata earthquake focal mechanisms have three predominant strikes (see Fig. 9 for data); moderately dipping NE-SW Taupo Rift strikes, and steeply dipping N-S and E-W strikes. (b) Greywacke basement bedding fabric in outcrop on the eastern rift margin and NIFS has a steeply dipping N-S strike. Bedding measurements from Leonard et al. (2012). (c) Greywacke basement faults measured in outcrop on the eastern rift margin at the Bay of Plenty coast (see Fig. 3 for location) have two dominant strikes, NE-SW rift faults that cut across basement fabric (TR) and N-S bedding parallel faults (BF).

to accommodate a component of margin parallel motion (the amount of which is presently undetermined).

The trend of basement fabric could influence fault strike and extension direction at the scale of the rift. The 15-20º rotation in trends of rift faults and extension direction at 150-165 km along strike distance is coincident with a vertical-axis rotation boundary trending approximately east-west across the central North Island where a clockwise ca. 25º bend occurs in the basement fabric and Miocene to active faults (i.e. Taranaki Fault and NIFS) (refer Fig. 4) (Nicol et al., 2007). To account for the change in trend of the rift and extension direction south of this rotation boundary I propose that the rift is utilizing pre-existing basement structure. To the north of the rotation boundary, new faults formed at high angles to basement fabric (~55º) and normal to the extension direction with minor strike-slip on basement fabric (Fig. 4). South of the rotation boundary rifting is parallel to basement fabric and may reactivate a boundary/suture between two tectono-stratigraphic greywacke terranes (Beetham & Watters, 1985; Mortimer, 2004) which is parallel to the basement terranes and bedding either side of the rift (Fig. 4). Both the rift trend and extension direction in the southern Taupo Rift are rotated 10-20º anticlockwise of their orientations north of the rotation boundary (Table 1). These rotations are attributed to weak basement anisotropy in the south.

The notion that stress and strain field may be influenced by pre-existing strength anisotropy is supported by previous work (Bell, 1996; Amadei & Stephansson, 1997; Morley, 2010). For simple cases, changes in the geomechanical properties (e.g. strength anisotropy, competency contrasts, and variations in elastic properties) of rocks can affect the orientation of stresses in the following way: where the strength anisotropy is weak the maximum principal stress will trend sub-parallel to strength anisotropy, where the strength anisotropy is relatively strong the maximum principal stress will deflect sub-normal to the strength anisotropy (Fig. 11) (Bell, 1996; Morley, 2010). These studies support the hypothesis that 15-20º variations in extension direction observed along strike of the Taupo Rift to the Ngatoro Basin (Table 1) are attributed to the orientation of steeply dipping anisotropic basement fabric with respect to the regional extension direction. The main implication of stress deflections by pre-existing fabric is that extensional fault trends oblique to the regional extensional direction, which in some cases are assumed to exhibit a component of oblique-slip (Acocella et al., 2003) may actually be approximately pure dip-slip as I have shown (Morley, 2010).

Another somewhat speculative possibility is that variations in rift trend are controlled by second-order variation in the strike of the subducting slab. Examination of Benioff zone seismicity relocated with the 3D velocity model of New Zealand beneath the North Island (Eberhart-Phillips et al., 2010) support previous interpretations that the subducting slab is divided into 100-200 km long variably oriented (030º to 050º) segments (Fig. 12) (Reyners, 1983; Robinson, 1986). Beneath the Havre Trough the subducting slab is only presently constrained to a first-order (Syracuse & Abers, 2006) and it is unclear whether the slab beneath this region is also segmented. If extension in the overriding plate is directly related to the geometry of the subducting slab, the oblique subduction of variably striking slab segments could account for the 15-20º variability in fault trends and extension directions observed at the surface. Testing this hypothesis will require that the geometry of the slab more precisely defined than is presently the case.

5. Subduction controls on Extension

Models for overriding plate extension in a convergent margin setting include rollback of the subduction hinge (slab rollback model) and/or vertical-axis rotations of fore-arc micro-plates (collision model) (refer Fig. 1). Slab rollback (or the seaward migration of the subduction hinge) causes upper plate extension by the negative buoyancy and gravitational instability of the subducting slab as it founders and sinks into the underlying asthenosphere (Molnar & Atwater, 1978; Sdrolias & Muller, 2006). Several studies have concluded that extension in the overriding plate associated with subduction correlates strongly with absolute motion of the overriding plate away from the trench where the age of the subducting lithosphere is > 55 Ma (Jarrard, 1986; Heuret & Lallemand, 2005; Lallemand et al., 2005; Sdrolias & Muller, 2006). In the North Island, the absolute motion of the Australian plate has been away from the Pacific plate (in a hotspot reference frame or relative to Antarctica) from at least 20 Ma (chapter 6) (Sdrolias & Muller, 2006), which would be consistent with extension being driven by rollback.

Vertical-axis rotations of the fore-arc induced by the nearby collision of a buoyant indentor with the margin can also result in overriding plate extension (Fig. 1) (Wallace et al., 2009). In the collision model extension arises because the indentor locally inhibits subduction and imposes a torque on the overriding plate which produces

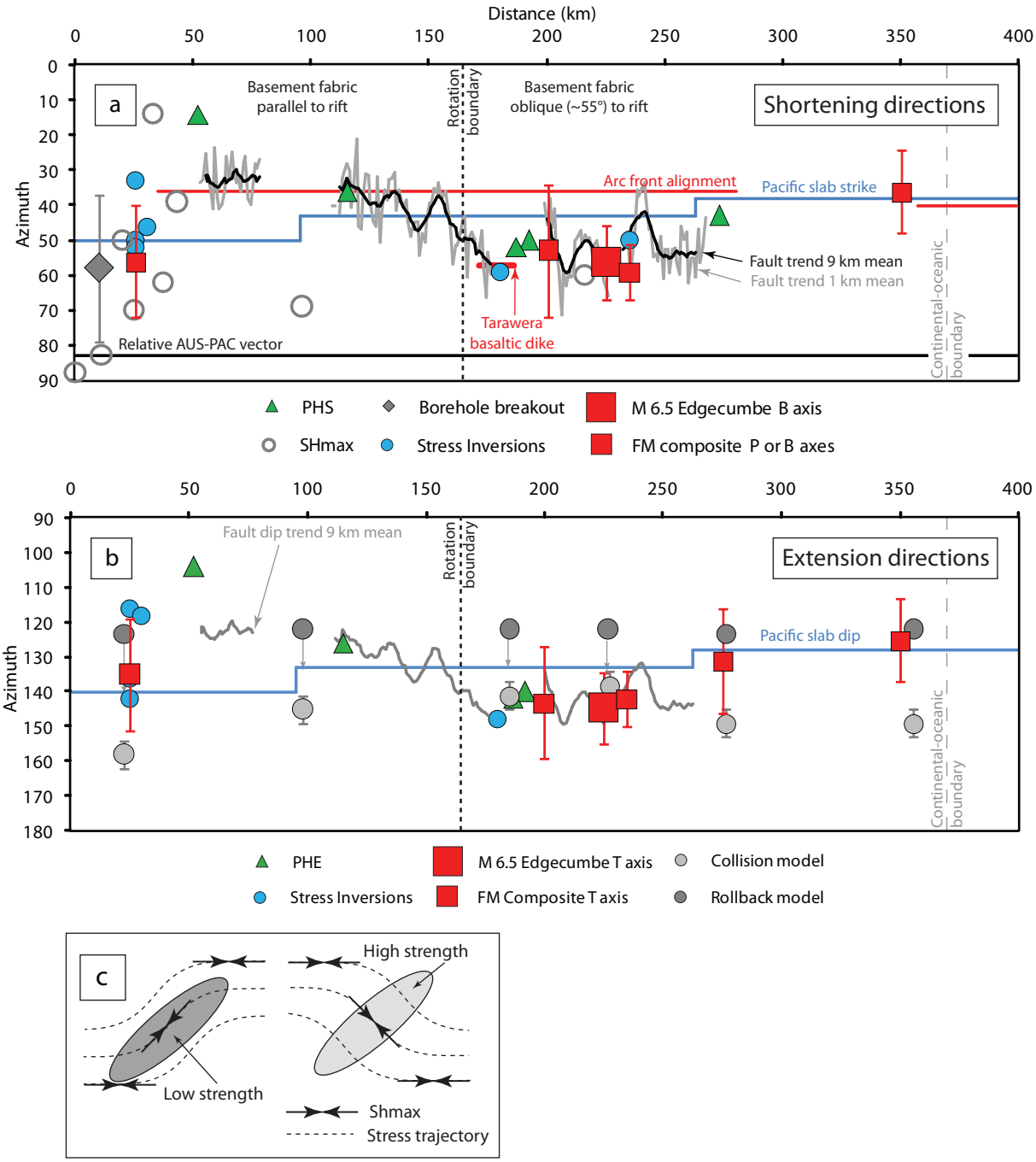

Figure 11. Summary of strain orientations along the Taupo Rift. (a) Shortening directions relative to mean fault trends, strike of the subducting slab and the alignment of arc front volcanoes. (b) Extension directions relative to the mean dip direction of rift faults and the underlying subducting slab. Note rollback model points associated with rollback of a ~026º striking slab beneath the Kermadec arc (Yan & Kroenke, 1993), arrows show the inferred extension direction expected with the slab rolling parallel to its dip direction beneath Taupo Rift. See text for methods and references associated with collision and rollback models. (c) Schematic illustration of the deflection of the maximum horizontal stress direction (Shmax) by sub-vertical elastic moduli contrasts (after Bell, 1996; Morley, 2010). Refer to Table 1 for data and references of stress and strain orientation. See Fig. 4 for location of rotation boundary relative to strike of basement fabric and Appendix Fig. 3 for stress and strain data locations.

vertical-axis rotations and extension (Wallace et al., 2009). It is worth noting that the two models generally use data from contrasting locations along subduction zones. The majority of global compilations of subduction zone parameters and overriding plate extension exclude, for example, locations where collision of anomalous crust is occurring (Lallemand et al., 2005; Sdrolias & Muller, 2006).

At present, fore-arc microplates of the eastern North Island are rotating relative to the subducting Pacific plate about poles of rotation adjacent to the collision point between the unsubductable Chatham Rise and Australian plate in the South Island (Fig. 2) (Wallace et al., 2004). The detailed kinematics of Taupo Rift extension reflect the relative motion between microplates of the North Island fore-arc and the Australian plate which are determined by two main factors: (1) the relative motion between the Pacific and Australian plates, determined by larger-scale plate tectonic processes and (2) the relative motion between the eastern North Island and the Pacific plate, dictated by the changing subduction zone boundary conditions (e.g. increases in interplate coupling and decreases in subduction rate) near the collision point (Wallace et al., 2004). The rollback of the Pacific plate subduction hinge relative to a stable Australian plate along the Tonga-Kermadec trench may also induce the migration of the forearc relative to the stable overriding plate through "trench suction" forces whereby the forearc maintains its position relative to the trench resulting in intra- and back-arc extension (Sdrolias & Muller, 2006; Wallace et al., 2009). The "collision resistance" of the thickened oceanic crust of the Hikurangi Plateau and continental crust of the Chatham Rise combine with "trench suction" forces associated with slab rollback to effectively exert a torque on the eastern North Island causing it to rotate about a nearby axis (refer Fig. 2) (Wallace et al., 2004). The spatial distribution of these forces along the Hikurangi margin in relation to extension in the overriding plate are unclear.

The extension direction along the Taupo Rift predicted by slab rollback and vertical-axis rotations of fore-arc micro-plates differ by 20-40º (Fig. 11b). Extension directions for these models have been compared with the extension direction derived from earthquake data to constrain better the dominant process responsible for rifting. The extension direction was estimated assuming rollback normal to the strike of the slab. The orientation and rate of extension associated with a rollback model along the southern Havre Trough-Taupo Rift is based on restoration of the eastern Havre Trough/Kermadec Ridge towards the Colville Ridge over the last 1.8 Ma by Yan & Kroenke (1993) using magnetic anomalies from Malahoff et al. (1982). The finite pole

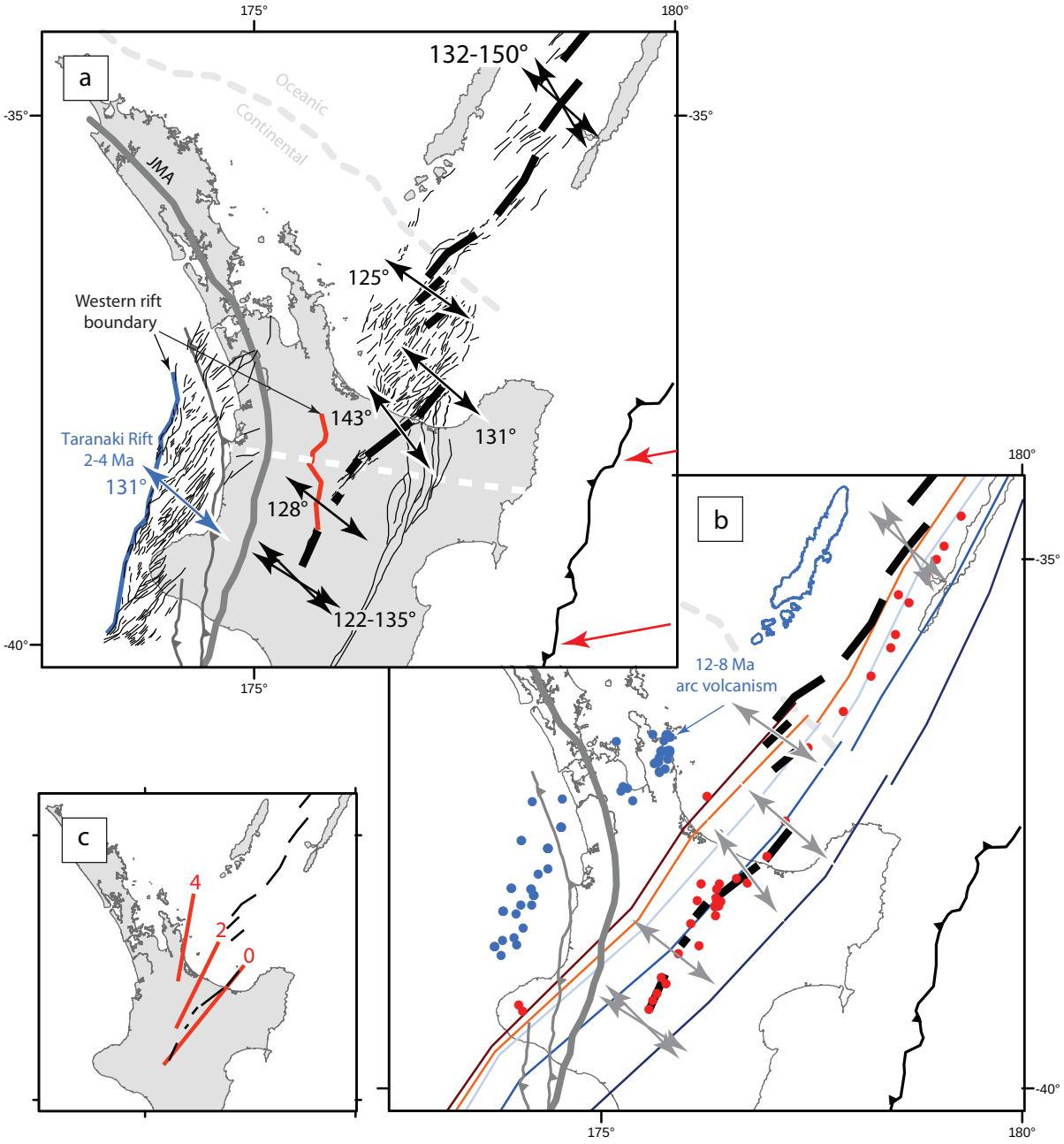

Figure 12. Intra-arc extension along the southern Havre Trough to Taupo Rift. (a) Rift trends and extension directions from this study, Wright (1993), Lamarche & Barnes (2005), Lamarche et al. (2006), Bonnardot et a. (2007), Campbell et al. (2007), Giba et al. (2010) and New Zealand Active Faults database (http://data.gns.cri.nz/af/). Note the parallel trends of the western rift boundaries in the Taranaki Basin and Taupo Volcanic Zone with passive markers in the basement (i.e. Junction Magnetic Anomaly - JMA). (b) Distribution of arc volcanism and extension with respect to the geometry of the subducting Pacific Plate. See chapter 5 for references relating to volcanism and slab geometry. (c) Fan-shaped migrating arc model of Stern et al. (2006).

of rotation closing the southern Havre Trough with respect to the North Island calculated by Yan & Kroenke (1993) lies in the central of the South Island (Fig. 2) where clockwise rotations of 0.94º/Myr predict extension rates of 14 to 29 mm/yr from the Taupo Rift to the northern limit of the southern Havre Trough respectively along an extension direction 122 ± 1º (i.e. approximately arc normal) (Fig. 11). The orientation and rate of extension in the Taupo Rift associated with the collision model are based on the kinematic block model of Wallace et al. (2012) constrained by GPS and fault-slip data. The finite poles of rotation associated with fore-arc blocks bounding the eastern margin of the Taupo Rift (AXIR and RAUK) with respect to the Australian plate are located in the western North Island (Fig. 2) where clockwise rotations of 2.6-2.8º/Myr predict extension rates of 8-19 mm/yr oriented 158º-138º (from south to north along the Taupo Rift).

The kinematic block rotation (collision) model of Wallace et al. (2012) shows good agreement with kinematic shortening and extension directions estimated for the Taupo Rift between 150 km and 300 km along strike (i.e. rotation boundary to continental margin) (Fig. 11b). South of 150 km and north of 300 km, the kinematic block model shows an increasing mismatch with the observed extension direction. In addition, the kinematic block model for the North Island is unlikely to extend into the southern Havre Trough (i.e. the northeastern North Island and Kermadec Ridge cannot be a continuous microplate rotating about a common pole) as extension rates predicted by the block model at the northern end of the southern Havre Trough are approximately double current estimates (Parson & Wright, 1996).

Extension directions for the rollback model fit the data better than the kinematic block model extension directions. Extension directions predicted by a rollback model fit the trend of rift extension derived from earthquakes in the southern Taupo Rift and southern Havre Trough. The direction of extension predicted by the rollback model is within the uncertainty bounds of extension directions observed along the Taupo Rift (Fig. 11b) and the direction of σ_3 in the southern Havre Trough inverted from focal mechanisms (132º) (Bonnardot et al., 2007) (Fig. 11). In addition, rates of extension predicted from the rollback model of Yan & Kroenke (1993) approximately match the predicted rates of extension along the Taupo Rift-southern Havre Trough (Parson & Wright, 1996).

6. Discussion

Rift geometries and kinematics within the North Island and along the southern Havre Trough indicate the subducting slab has exerted a first-order control on the orientation and magnitude of extension over the last 4 Myr (Fig. 12). Rift faults in the eastern Taranaki Basin active between 4-2 Ma have comparable trends (041-048º) (Giba et al., 2010) to intra-arc rift faults along the Taupo Rift to southern Havre Trough (Fig. 12) (Wright, 1992; Wright, 1997; Campbell et al., 2007). The orientation of principal strain in the Taranaki Basin is supported by kinematic data from fault exposures along the Taranaki coastline which indicate extension axes parallel to the present southern Taupo Rift (131º) (Fig. 5) (Giba et al., 2010) and border faults along the Colville Ridge (127º) (Wright, 1997). These kinematic data from the North Island are therefore consistent with the extension direction associated with the initial and continued separation of the Colville and Kermadec Ridges over at least the last 4 Ma (Wright, 1997).

The data support a model in which slab steepening and/or rollback beneath the western and central North Island provided an important control of the location, strike, and extension direction for normal faults formed over at least the last 4 Ma. Normal faults in the Taranaki and Taupo Rifts are approximately parallel to each other and to the present strike of the slab (Fig. 12). The similarity of fault strike and the eastward migration of rifting are consistent with the southeast migration of arc volcanism (Fig. 12b) (Stipp, 1968; Brothers, 1984; Adams et al., 1994; King & Thrasher, 1996; Mortimer et al., 2007; Giba et al., 2010; Mortimer et al., 2010). Both rifting and volcanism suggest steepening and/or rollback with no discernable change in slab strike since 4 Ma.

The parallelism of the northeast-southwest striking Taranaki and Taupo Rifts seems inconsistent with the northerly trend of the western margin of the Central Volcanic Region (CVR) (Stern et al., 2006) (Fig. 4 and 12c). This boundary is primarily defined by gravity data and has been interpreted to mark the western margin of fan-shaped opening of the CVR associated with clockwise vertical axis rotation of the eastern North Island (Walcott, 1987; Stern et al., 2006; Stern, 2009). As noted by Wilson et al. (1995), the western margin of the CVR cuts across all observable tectonic and geophysical elements oriented at high angles to the inferred boundary (e.g. Fig. 4). In the fan-shaped opening model, the inferred western boundary of the CVR defines location and trend of arc volcanism at 4 Ma which subsequently rotates clockwise by

~30º to its present manifestation as the TVZ (Stern et al., 2006; Stern, 2009). In the central Bay of Plenty ~50 km east of the western CVR boundary, Motiti Island, an eroded andesitic volcanic centre active between 4.3 to 3.4 Ma (Henry, 1991) is presently inconsistent with this model (Fig. 4). Implicit in the CVR opening model is the requirement that the rift faults in the central North Island initially had an approximate north-south strike and that faults along the eastern margin of the CVR rotated clockwise to their present northeast-southwest strike (Fig. 12c). Neither of these inferences are supported by the apparent uniform strike of rift faults and extension direction over at least the last 4 Ma. Instead, it is proposed that the north-south trend of the western CVR is parallel to, and reactivates underlying basement fabric (Fig. 12a). By contrast, the eastern margin of the CVR, which is partly coincident with the Taupo Rift, is defined by a combination of basement fabric in the south and newly formed faults in the north. A similar interplay between reactivated late Cretaceous faults and newly formed Late Miocene-Pliocene rift faults is also observed along the western and eastern margins of the Taranaki Rift (Giba et al., 2010). In the basement reactivation model the absolute extension of the CVR is significantly less ($\leq$ 50%) than the distance between its margins defined by the residual gravity data (Fig. 4).

7. Conclusions

The subducting slab controls the first-order structural geometry and kinematics of the Taupo Rift. Intra-arc rifting is predominantly normal (6º clockwise from mean down dip direction) where extension directions are consistent with the southeast rollback of the slab parallel to its dip direction. Rift faults are sub-parallel to the trend of the underlying slab where swings of up to 20º in mean fault trend and extension direction occur in unison along strike. The coincidence of a 15-20º clockwise rotation in mean fault trend and extension with a similar counter-clockwise rotation in the trend of basement fabric indicates strength anisotropy may control the second-order geometry and kinematics of rift. In the southern rift, weak basement fabric sub-parallel to the shortening direction causes a reactivation of pre-existing faults. This contrasts with the new faults formed in the northern rift where basement fabrics are at a high angle the shortening direction. The extension direction in the northern Taupo Rift, consistent over earthquake magnitudes of M_W 3.5-6.5, is uniform between rhyolite and andesite volcanic segments of the Taupo Volcanic Zone and the intersection of the rift with the

North Island Fault System. In detail, the trend of basement fabric also exerts a third-order control on faulting where minor oblique- and strike-slip faulting occurs along steeply dipping north-south aligned basement bedding planes within the same rock volume as the predominant northeast-southwest striking dip-slip rift faults. The consistency in the structural geometry and kinematics of the Taupo Rift with rifting in the Taranaki Basin and southern Havre Trough indicates the geometry and rollback of the subducting slab has controlled the location of intra-arc rifting over at least the last 4 Ma.

References

Acocella, V., Spinks, K., Cole, J. & Nicol, A., 2003. Oblique back arc rifting of Taupo Volcanic Zone, New Zealand. *Tectonics*, 22(4), p.1045.

Adams, C.J., Graham, I.J., Seward, D. & Skinner, D.N.B., 1994. Geochronological and geochemical evolution of late Cenozioc volcanism in the Coromandel Peninsula, New Zealand. *New Zealand Journal of Geology & Geophysics*, 37, pp.359-79.

Amadei, A. & Stephansson, O., 1997. *Rock stress and its measurement*. London: Chapman & hall.

Anderson, H. & Webb, T., 1989. The rupture process of the 1987 Edgecumbe earthquake, New Zealand. *New Zealand Journal of Geology & Geophysics*, 32, pp.43-52.

Ansell, J.H. & Bannister, S.C., 1996. Shallow morphology of the subducted Pacific Plate along the Hikurangi Margin, New Zealand. *Physics of Earth & Planetary Interiors*, 93, pp.3-20.

Bannister, S., Bryan, C.J. & Bibby, H.M., 2004. Shear wave velocity variation across the Taupo Volcanic Zone, New Zealand, from receiver function inversion. *Geophysics Journal International*, 159, pp.291-310. doi:10.1111/j.1365-246X.2004.02384.x.

Barker, D., Sutherland, R., Henrys, S. & Bannister, S., 2009. Geometry of the Hikurangi subduction thrust and upper plate, North Island, New Zealand. *Geochemistry, Geophysics, Geosystems*, 10(2), p.Q02007. doi:10.1029/2008GC002153.

Bassett, D., Sutherland, R., Henrys, S., Stern, T., Scherwath, M., Benson, A., Toulmin, S. & Henderson, M., 2010. Three-dimensional velocity structure of the northern Hikurangi margin, Raukumara, New Zealand: Implications for the growth of continental crust by subduction erosion and tectonic underplating. *Geochemistry Gephysics Geosystems*, 11(10), p.Q10013. doi:10.1029/2010GC03137.

Beanland, S., Berryman, K.R. & Blick, G.H., 1989. Geological investigations of the 1987 Edgecumbe earthquake, New Zealand. *New Zealand Journal of Geology & Geophysics*, 32, pp.73-91.

Beavan, J., Ellis, S., Wallace, L. & Denys, P., 2007. Kinematic constraints from GPS on oblique convergence of the Pacific and Australian Plates, Central South Island, New Zealand. In D. Okaya, T. Stern & F. Davey, eds. *A Continental Plate Boundary: Tectonics at South Island, New Zealand*. Geophysical Monograph 175, Washington DC: American Geophysical Union. pp.75-95.

Beavan, J., Tregoning, P., Bevis, M., Kato, T. & Meertens, C., 2002. Motion and rigidity of the Pacific Plate and implications for plate boundary deformation. *Journal of Geophysical Research*, 107(B10), p.2261. doi:10.1029/2001JB000282.

Beetham, R.D. & Watters, W.A., 1985. Geology of Torlesse and Waipapa terrane basement rocks encountered during the Tongariro Power Development project, North Island, New Zealand. *New Zealand Journal of Geology & Geophysics*, 28, pp.575-94.

Begg, J.G. & Mouslopoulou, V., 2010. Analysis of late Holocene faulting within an actie rift using lidar, Taupo Rift, New Zealand. *Journal of Volcanology & Geothermal Research*, 190, pp.152-67. doi:10.1016/j.jvolgeores.2009.06.001.

Bell, J.S., 1996. In situ stresses in sedimentary rocks (part 2): application of stress measurments. *Geoscience Canada*, 23(3), pp.135-53.

Berryman, K., Villamor, P., Nairn, I., Van Dissen, R., Begg, J. & Lee, J., 2010. Late Quaternary surface rupture history of the Paeroa Fault, Taupo Rift, New Zealand. *New Zealand Journal of Geology & Geophysics*.

Bibby, H.M., Caldwell, T.G., Davey, F.J. & Webb, T.H., 1995. Geophysical evidence on the structure of the Taupo Volcanic Zone and its hydrothermal circulation. *Journal of Volcanology & Geothermal Research*, 68, pp.29-58.

Boddington, T., Parkin, C.J. & Gubbins, D., 2004. Isolated deep earthquakes beneath the North Island of New Zealand. *Geophysics Journal International*, 158, pp.972-82.

Bonnardot, M.-A.R.M., Ruellen, E., Christova, C. & Tric, E., 2007. Seismicity and state of stress within the overriding plate of the Tonga-Kermadec subduction zone. *Tectonics*, 26, p.TC5017. doi:10.1029/2006TC002044.

Booden, M.A., Smith, I.E.M., Mauk, J.L. & Black, P.M., 2010. Evolving volcanism at the tip of a propagating arc: The earliest high-Mg andesities in northern New Zealand. *Journal of Volcanology & Geothermal Research*, 190, pp.83-96.

Briggs, R.M., Houghton, B.F., McWilliams, M. & Wilson, C.J.N., 2005. 40Ar/39Ar ages of silicic volcanic rocks in the Tauranga-Kaimai area, New Zealand: dating the transition between volcanism in the Coromandel Arc and Taupo Volcanic Zone. *New Zealand Journal of Geology & Geophysics*, 48, pp.459-69.

Brothers, R.N., 1984. Subduction regression and oceanward migration of volcanism, North Island, New Zealand. *Nature*, 309, pp.698-700.

Campbell, M.E., Rowland, J.V., Wright, I.C. & Smith, I.E.M., 2007. Obilque rifting along the central and southern Kermadec Arc front (30-36S), SW Pacific. *Geochemisrty Geophysics Geosystems*, 8(1). doi:10.1029/2006GC001504.

Cole, J.W., Darby, D.J. & Stern, T.A., 1995. Taupo Volcanic Zone and Central Volcanic Region: Backarc structures of North Island, New Zealand. In B. Taylor, ed. *Back Arc Basins: Tectonics and Magmatism.* New York: Plenum Press. pp.1-28.

Davey, F.J., Henrys, S.A. & Lodolo, E., 1995. Asymmtric rifting in a continental back-arc environment, North Island, New Zealand. *Journal of Volcanology and Geothermal Research*, 68, pp.209-38.

Davy, B.W. & Caldwell, T.G., 1998. Gravity, magnetic and seismic surveys of the caldera complex, Lake Taupo, North Island, New Zealand. *Journal of Volcanology & Geothermal Research*, 81, pp.69-89.

Davy, B., Horernle, K. & Werner, R., 2008. Hikurangi Plateau: Crustal structure, rift formation, and Gondwana subduction history. *Geochemsitry, Geophysics, Geosystems*, 9, p.Q07004.

Davy, B. & Wood, R., 1994. Gravity and magnetic modelling of the Hikurangi Plateau. *Marine Geology*, 118, pp.139-51.

De Mets, C., Gordon, R.G. & Argus, D.F., 2010. Geologically current plate motions. *Geophysics Journal International*, 181, pp.1-80.

Dewey, J.F., Taylor, T.R. & Monastero, F.C., 2008. Transtension in the Brittle Field: The Coso Region, Southern California. *International Geology Review*, 50, pp.193-217. doi:10.2747/0020-6814.50.3.193.

Downey, N.J., Stock, J.M., Clayton, R.W. & Cande, S.C., 2007. History of the Cretaceous Osborn spreading center. *Journal of Geophysical Research*, 112, p.B4102. doi:10.1029/2006JB004550.

Eberhart-Phillips, D., Reyners, M., Bannister, S., Chadwick, M. & Ellis, S., 2010. Establishing a versatile 3-D seismic velocity model for New Zealand. *Seismological Research Letters*, 81(6), pp.992-1000.

Eberhart-Phillips, D., Ryeners, R., Chadwick, M. & Stuart, G., 2008. Three-dimensional attenuation strucutre of the Hikurangi subduction zone in the central North Island, New Zealand. *Geophysics Journal International*, 174, pp.418-34.

Edbrooke, S.W., 2005. *Geology of the Waikato area: scale 1:250,000*. Institute of Geological & Nuclear Sciences Limited: Institute of Geological & Nuclear Sciences geological map 4. 68p. + 1 folded map.

Giba, M., Nicol, A. & Walsh, J.J., 2010. Evolution of faulting and volcanism in a back-arc basin and its implications for subduction processes. *Tectonics*, TC4020. doi: 10.1029/2009TC002634.

Hayes, G., Reyners, M. & Stuart, G., 2004. The Waiouru. New Zealand, earthquake swarm: Persistent mid-crustal activity near an active rift. *Geophysical Research Letters*, 31, p.L19613. doi:10.1029/2004GL020709.

Heise, V., Caldwell, T.G., Bibby, H.M. & Bennie, S.L., 2010. Three-dimensional electrical resistivity image of magma beneath an active continental rift, Taupo Volcanic

Zone, New Zealand. *Geophysical Research Letters*, 37, p.L10301. doi:10.1029/2010GL043110.

Henry, M.A.C., 1991. *The volcanic geology of Motiti Island*. Hamilton, New Zealand: University of Waikato. unpublished MSc Thesis.

Heuret, A. & Lallemand, S., 2005. Plate motions, slab dynamics and back-arc deformation. *Physics of the Earth and Planetary Interiors*, 149, pp.31-51. doi:10.1016/j.pepi.2004.08.022.

Hill, D.P., 1977. A model for earthquake swarms. *Journal of Geophysical Research*, 82(8), pp.1347-52.

Houghton, B.F., N, W.C.J., McWilliams, M.O., Lamphere, M.A., Weaver, S.D., Briggs, R.M. & Pringle, M.S., 1995. Chronology and dynamics of a silicic magmatic system: Central Taupo Volcanic Zone, New Zealand. *Geology*, 23(1), pp.13-16.

Hurst, A.W., Bannister, S., Robinson, R. & Scott, B., 2008. Characteristics of three recent earthquake sequences in the Taupo Volcanic Zone, New Zealand. *Tectonophysics*, 452, pp.17-28. doi:10.1016/j.tecto.2008.01.017.

Hurst, A.W., Bibby, H.M. & Robinson, R., 2002. Earthquake focal mechanisms in the Taupo Volcanic Zone and their relation to faulting and deformation. *New Zealand Journal of Geology & Geophysics*, 45, pp.527-38.

Hurst, A.W. & McGinty, P.J., 1999. Earthquake swarms to the west of Mt Ruapehu preceding its 1995 eruption. *Journal of Volcanology & Geothermal Research*, 90, pp.19-28.

Jarrard, R.D., 1986. Relations among subduction parameters. *Reviews of Geophysics*, 24(2), pp.217-84.

Kamp, P.J.J., 1984. Neogene and Quarternary extent and geometry of the subducted Pacific Plate beneath North Island, New Zealand: implications for Kaikoura tectonics. *Tectonophysics*, 108, pp.241-66.

King, P.R., 2000. Tectonic reconstructions of New Zealand: 40 Ma to present. *New Zealand Journal of Geology & Geophysics*, 43, pp.611-38.

King, P.R. & Thrasher, G.P., 1996. Cretaceous-Cenozoic geology and petroleum systems of the Taranaki Basin. In *Institute of Geological & Nuclear Sciences Monograph 13*. Lower Hutt, New Zealand: Institute of Geological & Nuclear Sciences.

Lallemand, S., Heuret, A. & Boutelier, D., 2005. On the relationships between slab dip, back-arc stress, upper plate absolute motion, and crustal nature in subduction zones. *Geochemistry, Geophysics, Geosystems*, 6(Q09006). doi: 10.1029/2005GC000917.

Lamarche, G. & Barnes, P.M., 2005. *Fault characterization and earthquake source identification in the Offshore Bay of Plenty. Commercial report to the Environment Bay*

of Plenty Regional Council. NIWA Client Report WLG2005-51. Wellington: National Institute of Water & Atmospheric Research (NIWA) Ltd. 105 p..

Lamarche, G., Barnes, P.M. & Bull, J.M., 2006. Faulting and extension rate over the last 20,000 years in the offshore Whakatane Graben, New Zealand continental shelf. *Tectonics*, 25, p.TC4005. doi:10.1029/2005TC001886.

Lee, J., Townsend, D., Bland, K. & Kamp, P.J.J., 2010. *Geology of the Hawke's Bay area: scale 1:250,000*. Institute of Geological & Nuclear Sciences Limited: Institute of Geological & Nuclear Sciences 1:250,000 geological map 8. 86 p.+ 1 folded map.

Leonard, G.S., Begg, J.G. & Wilson, C.J.N., 2011. *Geology of the Rotorua area 1:250 000 geological map*. Lower Hutt, New Zealand: Institute of Geological & Nuclear Sciences. 1 sheet + 99p.

Li, C., van der Hilst, R.D., Engdahl, E.R. & Burdick, S., 2008. A new global model for P wave speed variations in Earth's mantle. *Geochemsitry, Geophysics, Geosystems*, 9(Q05018). doi: 10.1029/2007GC001806.

Malahoff, A., Feden, R.h. & Fleming, S., 1982. Magnetic anomalies and tectonic fabric of marginal basins north of New Zealand. *Journal of Geophysical Research*, 87, pp.4109-25.

Marrett, R. & Allmendinger, R.W., 1990. Kinematic analysis of fault slip data. *Journal of Structural Geology*, 12, pp.973-86.

McClay, K.R., Dooley, T., Whitehouse, P. & Mills, M., 2002. 4-D evolution of rift systems: Insights from scaled physical models. *AAPG Bulletin*, 86(3), pp.935-59.

McClay, K.R. & White, M.J., 1995. Analogue modelling of orthogonal and oblique rifitng. *Marine & Petroleum Geology*, 12, pp.137-51.

Molnar, P. & Atwater, T., 1978. Interarc spreading and Cordilleran tectonics as alternatives related to the age of subducted lithosphere. *Earth & Planetary Science Letters*, 41, pp.330-40.

Morley, C.K., 2010. Stress re-orientation along zones of weak fabrics in rifts: An explanation for pure extension in 'oblique'' rift segments. *Earth & Planetary Science Letters*, 297, pp.667-73. doi:10.1016/j.epsl.2010.07.022.

Mortimer, N., 2004. New Zealand's geological fondations. *Gondwana Research*, 7(1), pp.261-72.

Mortimer, N., Gans, P.B., Palin, J.M., Meffe, S., Herzer, R.H. & Skinner, D.N.B., 2010. Location and migration of Miocene-Quarternary volcanic arcs in the SW Pacific region. *Journal of Volcanology & geothermal Research*, 190, pp.1-10. doi: 10.1016/j.jvolgeores.2009.02.017.

Mortimer, N., Herzer, R.H., Gans, P.B., Laporte-Magoni, C., Clavert, A.T. & Bosch, D., 2007. Oligocene-Miocene tectonic evolution of the South Fiji Basin and Northland Plateau, SW Pacific Ocean: evidence from petrology and dating of dredged rocks. *Marine Geology*, 237, pp.1-24.

Mouslopoulou, V. & Hristopulos, D., 2011. Patterns of tectonic fault interactions captured through geostatistical analysis of microearthquakes. *Journal of Geophysical Reseacrh*, 116, p.B07305. doi:10.1029/2010JB007804.

Mouslopoulou, V., Nicol, A., Little, T.A. & Walsh, J.J., 2007. Displacement transfer between intersecting regional strike-slip and extensional fault systems. *Journal of Structural Geology*, 29(1), pp.100-16.

Mouslopoulou, V., Nicol, A., Walsh, J.J., Beetham, D. & Stagpoole, V., 2008. Quaternary temporal stability of a regional strike-slip and rift intersection. *Journal of Structural Geology*, 30(4), pp.451-63.

Nairn, I.A., 2002. Geology of the Okataina Volcanic Centre scale 1:50 000. In *Institute of Geological & Nuclear Sciences geological map 25*. Lower Hutt: Institute of Geological & Nuclear Sciences. 1 sheet + 156 p.

Nairn, I.A. & Cole, J.W., 1981. Basaltic dikes in the 1886 Tarawera Rift. *New Zealand Journal of Geology & Geophysics*, 32, pp.1-13.

Nicol, A. & Beavan, J., 2003. Shortening of an overriding plate and its implication for slip on a subduction thrust, central Hikurangi Margin, New Zealand. *Tectonics*, 22(6), p.1070. doi:10.1029/2003TC001521.

Nicol, A., Mazengarb, C., Chanier, F., Rait, C., Uruski, C. & Wallace, L., 2007. Tectonic evolution of the active Hikurangi subduction margin, New Zealand, since the Oligocene. *Tectonics*, 26, p.TC4002. doi:10.1029/2006TC002090.

Nicol, A. & Wallace, L.M., 2007. Temporal stability of deformation rates: Comparison of geological and geodetic observations, Hikurangi subduction margin, New Zealand. *Earth & Planetary Science Letters*, 258, pp.397-413. doi:10.1016/j.epsl.2007.03.039.

Nicol, A., Walsh, J., Berryman, K. & Villamor, P., 2006. Interdependence of fault displacement rates and paleoearthquakes in an active rift. *Geology*, 34(10), pp.865-68. doi:10.1130/GC22335.1.

Nicol, A., Walsh, J.J., Villamor, P., Seebeck, H. & Berryman, K.R., 2010. Normal fault interactions, paleoearthquakes and growth in an atcive rift. *Journal of Structural Geology*, 32, pp.1101-13. doi:10.1016/j.jsg.2010.06.018.

Norris, R.J., Koons, P.O. & Cooper, A.F., 1990. The obliquely-convergent plate boundary in the South Island of New Zealand: implications for ancient collision zones. *Journal of Structural Geology*, 12(5/6), pp.715-25.

Parson, L.M. & Wright, I.C., 1996. The Lau-Havre-Taupo back-arc basin: A southward-progating, multi-stage evolution from rifting to spreading. *Tectonophysics*, 263, pp.1-22.

Reilly, W.I., 1970. *Topographic-isostatic Gravity Corrections for New Zealand*. Department of Scientific and Industrial Reseach Bulletin 203. Wellington: Department of Scientific and Industrial Reseach.

Reilly, W.I., 1972. New Zealand Gravity Map series. *New Zealand Journal of Geology & Geophysics*, 15(1), pp.3-15.

Reyners, M., 1983. Lateral segmentation of the subducted plate at the Hikurangi Margin, New Zealand: Seismological evidence. *Tectonophysics*, 96, pp.203-23.

Reyners, M., 2010. Stress and strain from earthquakes at the southern termination of the Taupo Volcanic Zone, New Zealand. *Journal of Volcanology & Geothermal Research*, 190(1-2), pp.82-88.

Reyners, M., Eberhart-Phillips, D. & Bannister, S., 2011. Tracking repeated subduction og the Hikurangi Plateau beneath New Zealand. *Earth & Planetary Science Letters*, 311(1-2), pp.165-71. doi:10.1016/j.epsl.2011.09.011.

Reyners, M.E., Eberhart-Phillips, D., Stuart, G. & Nishimura, T., 2006. Imaging subduction from the trench to 300 km depth beneath the central North Island, New Zealand with Vp and Vp/Vs. *Geophysics Journal International*, 165, pp.565-83.

Richardson, W.P., 1989. The Matata earthquake of 1977 May 31: a recent event near Edgecumbe, Bay of Plenty, New Zealand. *New Zealand Journal of Geology & Geophysics*, 32, pp.17-30.

Ristau, J., 2008. Implementation of routine Regional Moment Tensor analysis in New Zealand. *Seismological Research Letters*, 79(3), pp.400-15. doi:10.1785/gssrl.79.3.400.

Robertson, E.I. & Reilly, W.I., 1960. The New Zealand Primary Gravity Network. *New Zealand Journal of Geology & Geophysics*, 3, pp.41-68.

Robinson, R., 1986. Seismicity, structure and tectonics of the Wellington region, New Zealand. *Geophysical Journal of the Royal Astromoical Society*, 87, pp.379-409.

Robinson, R., 1989. Aftershocks of the 1987 Edgecumbe earthquake, New Zealand: seismological and structural studies using portable seismographs in the epicentral region. *New Zealand Journal of Geology & Geophysics*, 32, pp.61-72.

Rowland, J.R. & Sibson, R.H., 2001. Extensional fault kinematics within the Taupo Volcanic Zone, New Zealand: soft-linked segmentation of a continental rift system. *New Zealand Journal of Geology & Geophysics*, 44, pp.271-83.

Sdrolias, M. & Muller, R.D., 2006. Controls on back-arc basin formation. *Geochemistry, Geophysics, Geosystems*, 7, p.Q04016. doi:10.1029/2005GC001090.

Seebeck, H. & Nicol, A., 2009. Dike intrusion and displacement accumulation at the intersection of the Okataina Volcanic Centre and Paeroa Fault zone, Taupo Rift, New Zealand. *Tectonophysics*, 475, pp.575-85. doi:10.1016/j.tecto.2009.07.009.

Seebeck, H.C., Nicol, A., Stern, T.A., Bibby, H.M. & Stagpoole, V., 2010. Fault controls on the geometry and location of the Okataina Caldera, Taupo Volcanic Zone, New Zealand. *Journal of Volcanology & Geothermal Research*, 190, pp.136-51. doi:10.1016/j.jvolgeores.2009.04.011.

Sherburn, S., Townend, J., Arnold, R. & Woods, L., 2009. *EQC Project 08/550 - Establishing a Spatiotemporal Benchmark for Ongoing Crustal Stress monitoring in the Southern Taupo Volcanic Zone*. GNS Science Consultancy Report 2009/185. Lower Hutt: GNS Science.

Sherburn, S. & White, R.S., 2005. Crustal seismicity in Taranaki, New Zealand using accurate hypocentres from a dense network. *Goephysics Journal International*, 162, pp.494-506. doi:10.1111/j.1365-246X.2005.02667.x.

Smith, E.G.C. & Webb, T.H., 1986. The seismicity and related deformation of the Central Volcanic region, North Island, New Zealand. In I.E.M. Smith, ed. *Late Cenozoic Volcanism in New Zealand*. Royal Society New Zealand Bulletin 23. pp.112-33.

Spinks, K.D., Acocella, V., Cole, J.W. & Bassett, K.N., 2005. Structural control of volcanism and caldera development in the transtensional Taupo Volcanic Zone, New Zealand. *Journal of Volcanology & Geothermal Reseach*, 144, pp.7-22.

Stagpoole, V. & Bibby, H.M., 1999. *Residual gravity anomaly map of the Taupo Volcanic Zone, New Zealand, 1:250 000*. Institute of Geological & Nuclear Sciences Geophysical Map 13. Lower Hutt: Institute of Geological & Nuclear Sciences Ltd.

Stagpoole, V. & Nicol, A., 2008. Regional structure and kinematic history of a large subduction back thrust: taranaki Fault, New Zealand. *Journal of Geophysical Research*, 113, p.B01403. doi:10.1029/2007JB005170.

Stagpoole, V., Woodward, D. & Beetham, R., 2005. *Gravity Survey at the Horohoro geothermal prospect, Taupo Volcanic Zone*. Institute of Geological & Nuclear Sciences Client Report 2005/32. Lower Hutt: Institute of Geological & Nuclear Sciences.

Stern, T.A., 1979. Regional and Residual gravity fields, Central North Island, New Zealand. *New Zealand Journal of Geology & Geophysics*, 479-485, p.22.

Stern, T.A., 1986. Geophysical studies of the upper crust within the central volcanic region, New Zealand. In I.E.M. Smith, ed. *Cenozoic Volcanism*. Royal Society of New Zealand Bulletin 23. pp.92-111.

Stern, T.A., 2009. Reconciling short- and long-term measures of extension in continental back-arcs: heat flux, crustal structure and rotations within the central North

Island, New Zealand. In U. Ring & B. Wernicke, eds. *Extending a Continent: Architecture, Rheology and Heat Budget*. London, Special Publications 321: Geological Society. pp.73-87. doi:10.1144/SP321.4.

Stern, T.A., Stratford, W.R. & Salmon, M.L., 2006. Subduction evolution and mantle dynamics at a continental margin: Central North Island, New Zealand. *Review of Geophysics*, 44, p.RG4002. doi:10.1029/2005RG000171.

Stipp, J.J., 1968. *The geochronology and petrogenesis of the Cenozoic volcanics of North Island, New Zealand*. Canberra, Australia: Australian National University. Unpublished PhD Thesis.

Stock, J. & Molnar, P., 1982. Uncertainties in the relative positions of the Australia, Antarctica, Lord Howe, and Pacific plates since the late Cretaceous. *Journal of Geophysical Research*, 87(B6), pp.4697-717.

Sutherland, R., Stagpoole, V., Uruski, C., Kennedy, C., Bassett, D., Henrys, S., Scherwath, M., Kopp, H., Field, B., Toulmin, S., Barker, D., Bannister, S., Davey, F., Stern, T. & Flueh, E.R., 2009. Reactivation of tectonics, crustal underplating, and uplift after 60 Myr of passive subsidence, Ruakumara Basin, Hikurangi-Kermadec fore arc, New Zealand: Implications for growth and recycling of continents. *Tectonics*, 28, p.TC5017. doi:10.1029/2008TC002356.

Syracuse, E.M. & Abers, G.A., 2006. Global compliation of variations in slab depth beneath arc volcanoes and implications. *Geochemistry, Geophysics, Geosystems*, 7, p.Q05017. doi:10.1029/2005GC001045.

Townsend, D., Vonk, A. & Kamp, P.J.J., 2008. *Geology of the Taranaki area 1:250 000 geological map*. Lower Hutt, New Zealand: Institute of Geological & Nuclear Sciences. 1 sheet + 77p.

van der Hilst, R.D., 1995. Complex morphology of subducted lithosphere in the mantle beneath the Tonga trench. *Nature*, 374, pp.154-57. doi:10.1038/374154a0.

Villamor, P. & Berryman, K.R., 2001. A late Quaternary extension rate in the Taupo Volcanic Zone, New Zealand, derived from fault slip data. *New Zealand Journal of Geology & Geophysics*, 44, pp.243-69.

Villamor, P. & Berryman, K.R., 2006. Evolution of the southern termination of the Taupo Rift, New Zealand. *New Zealand Journal of Geology & Geophysics*, 49, pp.23-37.

Walcott, R.I., 1987. Geodetic strain and the deformation history of the North Island of New Zealand during the late Cainozoic. *Philosphical Transactions of the Royal Society London*, A321, pp.163-81.

Walcott, R.I., 1998. Modes of oblique compression: Late Cenozoic tectonics of the South Island of New Zealand. *Reviews of Geophysics*, 36(1), pp.1-26.

Wallace, L.M., Barnes, P., Beavan, J., Van Dissen, R., Litchfield, N., Mountjoy, J., Langridge, R., Lamarche, G. & Pondard, N., 2012. The kinematics of a transition from subduction to strike-slip: An example from the central New Zealand plate boundary. *Journal of Geophysical Research*, 117, p.B02405. doi:10.1029/2011JB008640.

Wallace, L.M., Beavan, J., McCaffrey, R. & Darby, D., 2004. Subduction zone coupling and tectonic block rotations in the North island, New Zealand. *Journal of Geophysical Research*, p.B12406. doi:10.1029/2004JB003241.

Wallace, L.M., Ellis, S. & Mann, P., 2009. Collisional model for rapid fore-arc block rotations, arc curvature, and episodic back-arc rifting in subduction settings. *Geochemistry, Geophysics, Geosystems*, 10, p.Q05001. doi:10.1029/2008GC0022200.

Webb, T.H. & Anderson, H., 1998. Focal mechanisms of large earthquakes in the North Island of New Zealand: slip partitioning at an oblique active margin. *Geophysics Journal International*, 134, pp.40-86.

Wilson, C.J.N., Gravely, D.M., Leonard, G.S. & Rowland, J.V., 2008. Volcanism in the central Taupo Volcanic Zone, New Zealand: tempo, styles and controls. In T. Thordarson et al., eds. *Studies in Volcanology: The Legacy of George Walker*. Special Publication of IAVCEI 2, London: Geological Society. pp.225-47.

Wilson, C.J.N., Houghton, B.F., McWilliams, M.O., Lanphere, M.A., Weaver, S.D. & Briggs, R.M., 1995. Volcanic and structural evolution of Taupo Volcanic Zone, New Zealand: a review. *Journal of Volcanology & Geothermal Research*, 68, pp.1-28.

Wilson, C.J.N., Rogan, A.M., Smith, I.E.M., Northey, D.J., Nairn, I.A. & Houghton, B.F., 1984. Caldera volcanoes of the Taupo Volcanic Zone, New Zealand. *Journal of Geophysical Research*, 89(B10), pp.8463-84.

Wright, I.C., 1992. Shallow structure and active tectonism of an offshore continental back-arc spreading system: the Taupo Volcanic Zone, New Zealand. *Marine Geology*, 103, pp.287-309.

Wright, I.C., 1993. Pre-spread rifting and heterogeneous volcanism in the southern Havre Trough back-arc basin. *Marine Geology*, 113, pp.179-200.

Wright, I.C., 1997. Morphology and evolution of the remnant Colville and active Kermadec arc ridges south of 33 30'S. *Marine Geophysical Research*, 19, pp.177-93.

Yan, C.Y. & Kroenke, L.W., 1993. A Plate Tectonic reconstruction of the Southwest Pacific, 0-100 Ma. In Berger, W.H., Kroenke, L.W., Mayer, L.A. & al., e. *Proceedings of the Ocean drilling Program Scientific Results vol. 130*. pp.697-709.

Chapter 4

Seismicity of the Pacific plate beneath the North Island, New Zealand: The role of faulting in the hydration and dehydration of subducting lithosphere

Abstract

The Taupo Volcanic Zone (TVZ) is currently one of the most frequently active and productive silicic volcanic systems on Earth. The location and high volcanic productivity of the TVZ can be linked to the subduction water cycle, where hydration and subsequent dehydration of the subducting oceanic lithosphere is primarily accomplished by earthquakes. Analysis of regional and global earthquake catalogues indicates the location, geometry, deformation, and dehydration of the subducting Pacific plate. Shallow intraplate earthquakes (e.g., ≤ 50 km) are predominantly normal dip-slip and formed due to bending. The magnitude and frequency of these shallow intraplate earthquakes are greatest where the overriding plate changes from oceanic to continental crust and decreases southwards along the margin. The high rates of seismicity associated with plate bending in proximity to oceanic fluids promote local hydration of the subducting plate east of the TVZ. Hydration of the subducting plate decreases to the south where 'bending' earthquakes occur mainly beneath continental crust of the North Island, 100-200 km west of and distal from oceanic fluids. The anomalously high heat flow and volcanic productivity of the TVZ is spatially associated with high rates of seismicity in the underlying slab mantle at depths of 130-210 km. Benioff-zone seismicity is inferred to reflect dehydration embrittlement of the previously hydrated slab. Dehydration of the slab crust provides insufficient fluid flux into the mantle wedge to induce 'wet' partial melting resulting in arc volcanism. In contrast, dehydration of the slab mantle correlates with the location and productivity of active North Island volcanic centres. South of the TVZ the subducting plate has not experienced the same degree of hydration as further north and, as a consequence, expels less fluid. In this model, hydration of the subducting plate varies spatially and is an important determinant for the location of arc volcanism in the overriding plate.

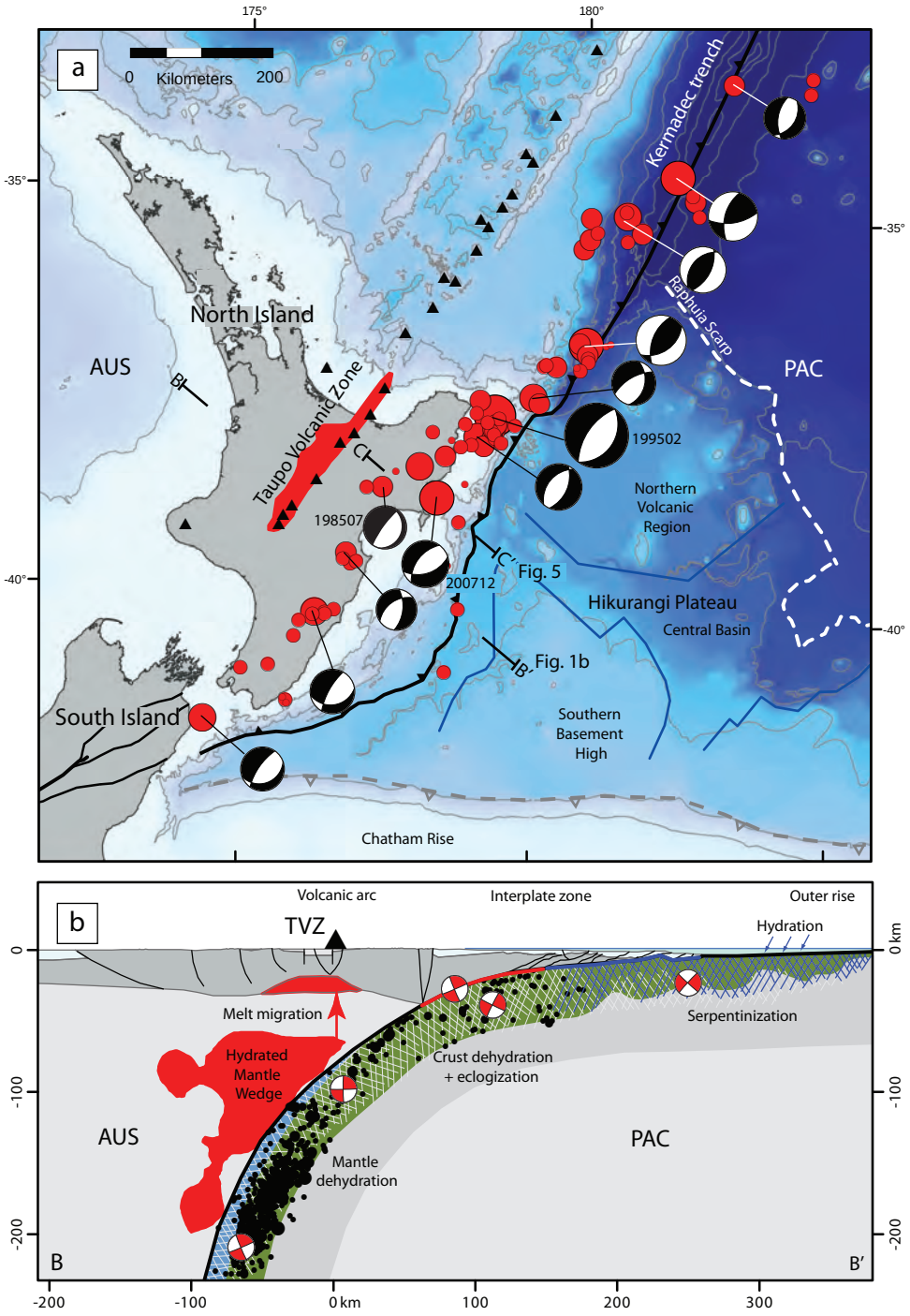

Figure 1. (a) Pacific plate bending-related normal-faulting earthquakes (M_W 5-7) along the Kermadec-Hikurangi subduction margin. EHB catalogue (1977-2007) ≤ 50 km depth (Engdahl et al., 1998) (red filled circles) with associated CMT focal mechanisms (Dziewonski et al., 1981). Arc volcanoes of the North Island and southern Havre Trough (black triangles) and outline of modern Taupo Volcanic Zone (red polygon) (Wilson et al., 1995). Structure of the Hikurangi Plateau from Davy et al. (2008). (b) Simplified conceptual model for the structural and metamorphic evolution of Pacific plate lithosphere as it subducts beneath the North Island (after Ranero et al., 2003). Geometry of the slab, mantle wedge, and crust to scale. Distribution of relocated Benioff seismicity (black filled circles) considered a proxy for dehydration reaction rate (e.g. Hacker et al., 2003). Hydrated mantle wedge (in red) approximated by Vp/Vs ratio ≥ 1.8 from 3D velocity model of New Zealand (Eberhart-Phillips et al., 2010).

1. Introduction

The Taupo Volcanic Zone (TVZ) in the North Island, New Zealand is one of the most frequently active and productive silicic volcanic systems on Earth. Volcanic production rates and heat flow along a ~100 km section of this continental intra-arc rift (Fig. 1) are comparable to locations where mantle plumes intersect both continental and oceanic crust (e.g. Yellowstone and Iceland respectively) (Stern et al., 2006; Wilson et al., 2008) therefore questions remain as to the origin of the heat source driving this exceptional volcanism. A second related question that must also be considered is why arc volcanism extinguishes so abruptly to the south of the TVZ despite the continuity of a seismically active slab for a further ~350 km along strike (Fig. 1) (Reyners et al., 2006). As arc volcanism in the TVZ is ultimately an expression of processes occurring in the mantle wedge and underlying slab, understanding the factors that contribute to magma production at depth will enhance our understanding of subduction systems.

The subduction zone water cycle, i.e. the hydration and subsequent dehydration of oceanic lithosphere as it is recycled back into the mantle, is a key component of arc magma genesis (Gill, 1981; Kirby et al., 1996; Hacker et al., 2003; van Keken, 2003) (Fig. 1b). The depth to the subducting slab below volcanic arcs indicates their location relative to the trench is a function of the mantle wedge temperature and viscosity structure which is largely the product of three interdependent factors; the dip, convergence rate, and fluid flux of the subducting slab (England et al., 2004; Manea & Gurnis, 2007; Wada & Wang, 2009; England & Katz, 2010). Arc magmas are believed to be generated largely by ‘wet’ partial melting (Gill, 1981), melting due to the reduction of the mantle solidus through the addition of fluids into the hot core of the mantle wedge, and a general correlation between volcanic production rates and thermal parameter (φ) of the subducting slab is thought to reflect the greater ability of colder slabs to carry fluids to sub-arc depths (Kirby et al., 1996). Variations in the rate and distribution of fluid liberated from the subducting slab along an arc segment (where slab age, dip and convergence rate are approximately uniform) has important consequences for the thermal and viscosity structure of the mantle wedge (Billen & Gurnis, 2001; Hirth & Kohlstedt, 2003), which in turn influences the location and productivity of arc volcanism (Kirby et al., 1996; Hacker et al., 2003; England et al., 2004).

The frequency of Benioff-zone seismicity with depth (50-350 km) has been considered a proxy for the rate of dehydration embrittlement within the subducting

lithosphere (Hacker et al., 2003). If this intra-plate seismicity within the subducting slab is related to the volume of fluid fluxing the mantle wedge, this may have important consequences for volcanism at the surface. At present however, the rates of seismicity in the subducting plate along the Hikurangi Margin have not been quantified. Previous models accounting for the anomalous volcanic production and heat flow rates in the TVZ include; a deep plume source (Wilson et al., 1984), cooling intrusions (Stern, 1987), heat from plastic deformation (Hochstein, 1995), along strike mantle flow (Reyners et al., 2006), elevated slab fluid flux/arc-related hotspot (Reyners et al., 2006; Wilson et al., 2008), and delamination of the overriding plate mantle lithosphere (Stern, 2009). Recently our understanding of subduction processes occurring beneath the North Island has been greatly enhanced by the publication of three-dimensional Vp, Vs, Vp/Vs, and Qp tomography that map variations in the physical properties of rocks due, for example, to changes in composition, temperature, water and melt content (Reyners et al., 2006; Eberhart-Phillips et al., 2008; Eberhart-Phillips et al., 2010). These studies show variations in the seismic properties of the subducting slab and overlying mantle wedge along strike correlate with the distribution and style of volcanism at the surface.

In this paper I build on this recent work by investigating the spatial distribution of hydration and dehydration of the Pacific plate beneath the Hikurangi margin, specifically, quantifying the distribution of seismicity with depth in the slab. The Hikurangi margin is an ideal location to examine subduction related processes due to the emergent North Island (and regional seismic network) directly overlying the subducting Pacific plate. A robust 22 year long earthquake catalogue (www.GeoNet.org.nz) complemented by a subset of events relocated in the three-dimensional velocity model of New Zealand (Eberhart-Phillips et al., 2010) along with published (Dziewonski et al., 1981; Bannister et al., 1989) and unpublished focal mechanisms (Ristau, 2008) form the basis for the study. I find the highest rates of seismicity within the subducting slab are directly beneath/down dip from regions of highest volcanic productivity at the surface. Coincidence of the high rates of seismicity in the slab and volcanism at the surface is consistent with a model in which volcanism is driven by fluids fluxing from the slab (e.g. Hacker et al. 2003). These high rates of dehydration are along the plate motion path from a region of high seismicity in the subducting plate at the trench. The seismicity at the trench records normal faulting associated with bending of the plate. It supports the notion that this bending-related faulting increases permeability of the subducting plate (e.g. Peacock, 2001; Faccenda et

al, 2009) which, together with the availability of water from the ocean and subducting sediments, results in pervasive hydration of the downgoing plate.

2. North Island volcanism and tectonics

Arc volcanism has migrated progressively southeast across the North Island since the early Miocene (Fig. 2) (Stipp, 1968; Brothers, 1984; Adams et al., 1994; Houghton et al., 1995; King & Thrasher, 1996; Hayward et al., 2001; Briggs et al., 2005; Giba et al., 2010; Mortimer et al., 2010). The vast majority of volcanic centres across the North Island have island arc chemistries derived from mantle fluxed with fluids from a subducting slab i.e. the enrichment of large ion lithophile (e.g. Rb, Ba, and K) and relative depletion of high field strength (e.g. Nb and Ti) trace elements for example (Bergman et al., 1992; Black et al., 1992; Adams et al., 1994; Price et al., 1999). The present southern limit of volcanism in the North Island has been relatively stable since 14 Ma (relative to the strike of the subducting slab) (Giba, 2010) albeit ~150 km to the northwest of its present position (Fig. 2). Explosive rhyolitic caldera forming arc volcanism initiated contemporaneously with intra-arc rifting in the North Island around 12 Ma, and has increased in size and frequency towards the present (Carter et al., 2003; Giba et al., 2010). Increases in the size and frequency of rhyolitic eruptions, particularly from ~8 and ~2 Ma, are recorded in outcrop and deep sea drillholes east of the North Island (Adams et al., 1994; Carter et al., 2003). Hydrogen isotopes provide direct evidence for the presence of slab derived fluids in silicic magmas (Deering et al., 2012) from the onset of explosive rhyolitic volcanism in the TVZ ~1.6 Ma ago to the present (Houghton et al., 1995).

Rhyolitic caldera formation is a common feature of arc front volcanism along the Kermadec arc towards the North Island (Wright & Gamble, 1999; Campbell et al., 2007), however volcanic production rates associated with caldera formation in the TVZ appear exceptional (Wilson et al., 2008). Since ~1.6 Ma the TVZ has produced at least 25 predominantly ignimbrite caldera forming eruptions (ca. 6000 km^3 of magma) (Wilson et al., 2008). Volcanic production rates in the central North Island over this time are comparable to those of the Yellowstone volcanic province over the last ~ 2 Myr (3-4 km^3/kyr) (Wilson et al., 2008).

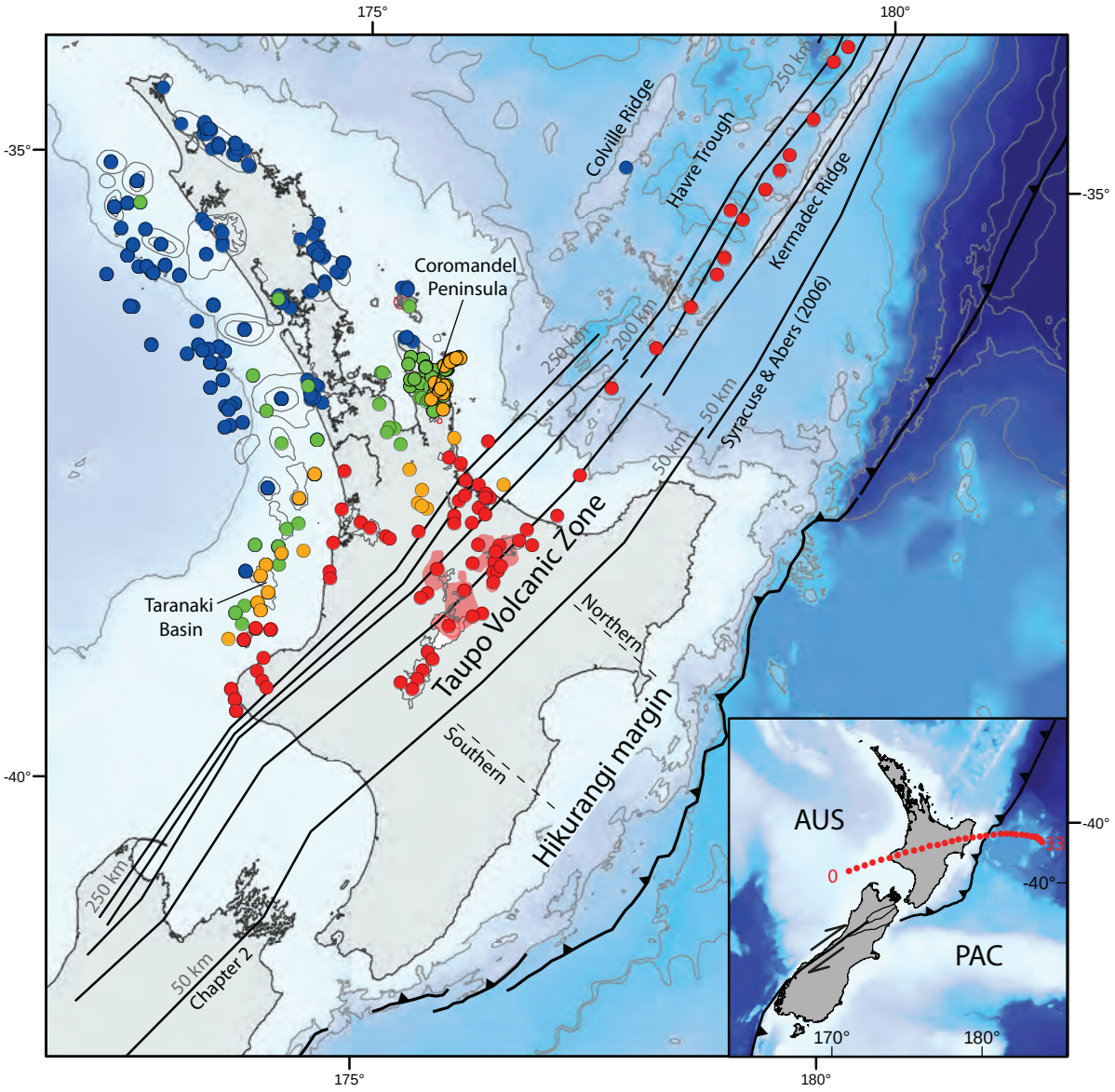

Figure 2. Onshore and offshore North Island arc volcanism since the Miocene. Present day slab geometry shown by 50 km depth contours on top of the slab. Maximum (oldest) age of arc volcanism from surficial radiometric dates onshore and stratigraphic correlation of seismic reflectors and rare radiometric dates offshore shown (see chapter 5 for references). Maximum age of volcanism; 0-4 Ma (red filled circles), 4-8 Ma (orange filled circles), 8-16 Ma (green filled circles), and 16-24 Ma (dark blue circles). Present geometry of the slab to 250 km defined by Benioff seismicity beneath the North Island (chapter 5) and Kermadec arc (Syracuse & Abers, 2006). Dashed lines show approximate boundaries for the northern and southern Hikurangi margin discussed in this study. Inset shows a horizontal Pacific plate motion vector relative to a fixed Australian plate from 33 Ma to the present through the Hikurangi margin (Cande & Stock, 2004).

At present, the average heat flux from localised high temperature geothermal systems in the TVZ (700 mW/km^3) (Bibby et al., 1995) is comparable to that of Iceland where hot spot volcanism and spreading coexist (Stern, 2009).

The age, geometry, and kinematics of the subducting slab are key parameters for the generation of arc volcanism (Hacker et al., 2003; England et al., 2004; Syracuse & Abers, 2006). Arc front volcanism in the central North Island lies 85 ± 10 km above the northeast (~040º) striking slab (Reyners et al., 2006) (Fig. 2). At present, the maximum depth of Benioff-zone seismicity shallows southward from depths of ~350 km beneath the north-eastern North Island to ~240 km beneath the northern South Island (Fig. 3) (Reyners et al., 2006; Eberhart-Phillips & Bannister, 2010). Deep earthquakes (Boddington et al., 2004) and positive mantle velocity anomalies (Li et al., 2008) infer a northeast striking slab to depths of at least 600 km beneath the North Island. At present, the Cretaceous (ca. 120 Ma) Hikurangi Plateau, a buoyant fragment (16-23 km thick) of a large igneous province (Davy et al., 2008), is subducting obliquely westward beneath the Hikurangi margin at rates of 42-48 mm/yr (Beavan et al., 2002). How much of the Hikurangi Plateau has been subducted is uncertain. Present estimates place the leading edge of the plateau at depths between 65-150 km beneath the North Island; the slab below these depths is inferred to be normal oceanic crust (Reyners et al., 2006; Reyners et al., 2011). The separation of the upper and lower Benioff-zones (seismicity in the slab crust and mantle, respectively) beneath the southern Hikurangi margin is also consistent with normal oceanic lithosphere 90-120 Ma in age (Brudzinski et al., 2007).

The southeast migration of arc volcanism normal to the present alignment of arc front volcanoes over the last 16 Ma indicate the geometry of the slab changed (Fig. 2). The southeast migration of the arc front across the North Island accelerated from rates of ~4 mm/yr between 16-7 Ma to ~18 mm/yr from ~7 Ma to the present (chapter 5). This increase in arc migration rates was associated with elevated mantle wedge temperatures adjacent to the slab from ~6 Ma (Booden et al., 2010) and the uplift of the central North Island from ~5 Ma (Pulford & Stern, 2004). To the north of the North Island from ~6 Ma, intra-arc rifting, attributed to rollback of the subducting slab, commenced along the length of the Tonga-Kermadec trench (van der Hilst, 1995; Taylor et al., 1996; Wright, 1997; Sdrolias & Muller, 2006). Over the last ~1.6 Myr, rates of extension across the North Island increase northwards to where they are comparable to rates of volcanic migration (chapter 5). This difference between the extension rate and arc migration rate indicates that arc migration patterns in the North

Island have been controlled by predominantly slab rollback beneath the region offshore of the northern TVZ and slab steepening towards the southern limit of volcanism (chapter 5).

3. Pacific plate seismicity

Benioff-zone seismicity provides important information about processes and deformation in the subducting Pacific plate beneath the North Island. The correlation between the distribution of intraplate seismicity and the predicted locations of hydrous phases within subducting lithosphere has led to the accepted view that Benioff-zone seismicity is facilitated by the reduction of the effective stress by high fluid pressures generated by the dehydration embrittlement (Fig. 1) (Kirby et al., 1996; Hacker et al., 2003). Earthquake catalogues have also been used to infer the degree of slab hydration/dehydration (Fig. 2) (Kirby et al., 1996; Peacock, 2001; Hacker et al., 2003; Brudzinski et al., 2007). As no one catalogue can provide a complete representation of the seismicity in the subducting slab due to strengths and weaknesses inherent in each (e.g. completeness or hypocentral accuracy) I use multiple, regional and global data sets. Where individual earthquakes occur in multiple catalogues, events have been compared to assess differences in hypocentre location and fault plane solutions.

3.1 Benioff-zone

The GeoNet earthquake catalogue has been used to evaluate the spatial distribution of Benioff-zone earthquake associated with the subducting slab (www.GeoNet.cri.nz) (Fig. 3). The minimum magnitude of completeness (M_C) for this catalogue has been estimated using ZMap, a suite of software tools designed for the spatial and temporal analysis of earthquakes (Wiemer, 2001), to ensure frequency-magnitude (F-M) and frequency-depth (F-D) relationships are meaningful. A complete earthquake catalogue above the M_C is required to ensure that sampling bias, due to station spacing or under reporting for example, does not significantly influence the spatial distribution of events (Wiemer & Wyss, 2000). Prior to 1988, the GeoNet catalogue shows under reporting in the total number of events with time and has been excluded. Prior to 2000, and the upgrade of the regional seismic network, $M_L \leq 3.6$ are under reported. Between M_C 3.6 and 4.5 no significant differences in b-value are observed and therefore the lower end of

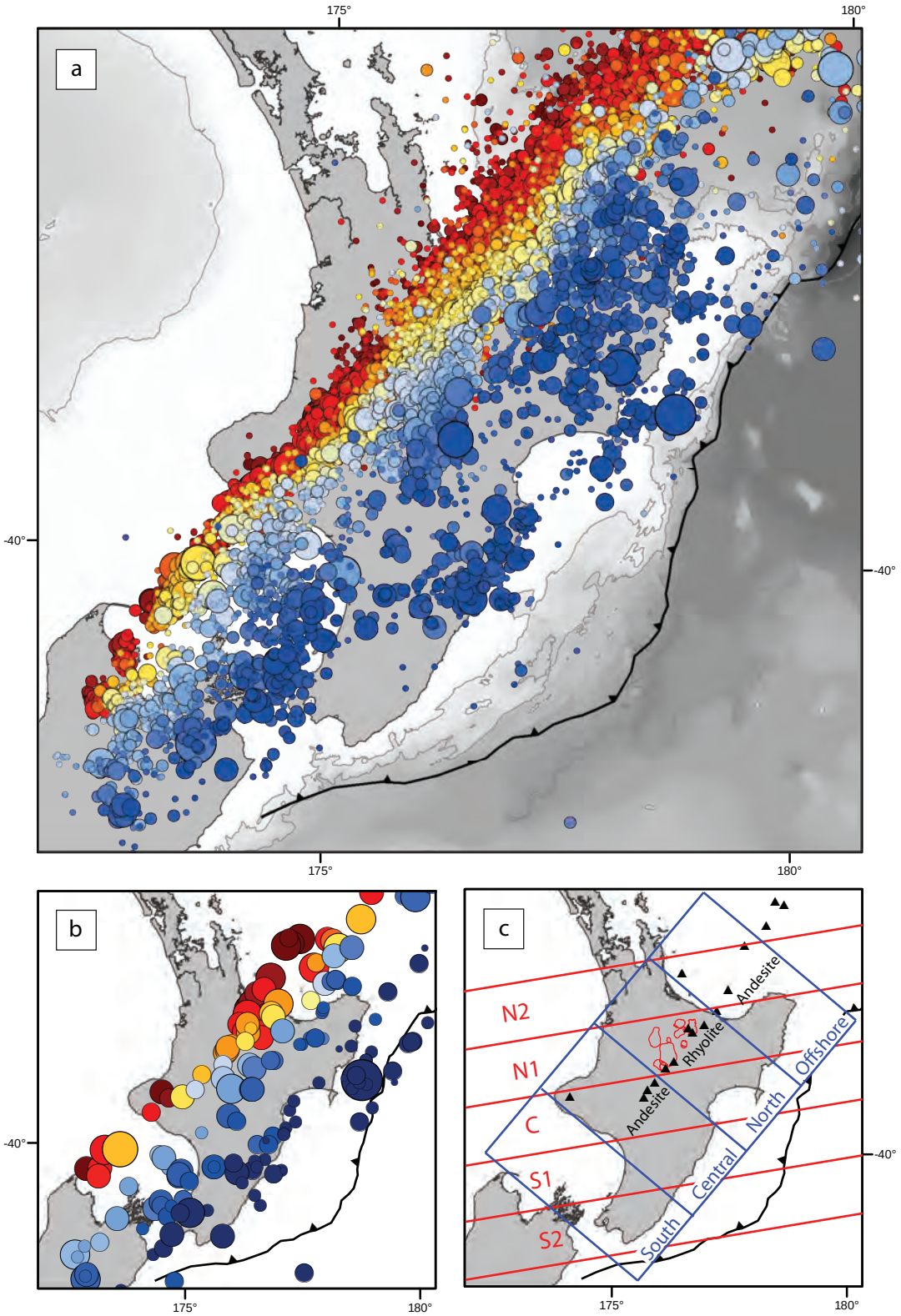

Figure 3. Intermediate depth seismicity along the Hikurangi subduction margin. (a) Intermediate depth (50-350 km) GeoNet earthquake catalogue $M_C \leq M_L$ 3.6 1988-2010. (b) Pacific Plate Regional Moment Tensor (RMT) focal mechanisms 2004-2010 (Ristau, 2008). (c) Seismicity sample sections in slab dip parallel (blue boxes) and Pacific Plate motion vector (red boxes) directions. Arc volcanoes (black filled triangles) and TVZ calderas (thin red line). Volcanic classification of Wilson et al. (1995) showing predominant volcanic composition; andesitic in Central (C) and Offshore (N2) sections, rhyolitic in North (N1) section.

the M_C range was used to provide the greatest number of earthquakes. The overriding crustal thickness is typically ≤ 40 km where M_C 3.6 is robust to depths of ~250 km beneath the majority of the North Island. First-order spatial variations previously interpreted beneath the North Island (Reyners, 1983) are observed over time window durations of varying length throughout the period of interest and are considered real features of the catalogue. The GeoNet catalogue (1988-2010) $M_L \geq 3.6$ at depths ≥ 50 km (N=11514, mean residual error 0.2 ± 0.9 s) is the principal dataset used for spatial analysis of Benioff-zone seismicity and is referred to hereafter as the GeoNet catalogue unless otherwise stated.

The GeoNet catalogue has been analysed in two ways to determine the spatial distribution of seismicity in the slab. 1) The first are adjacent 100 km wide along strike sections of Benioff-zone seismicity oriented parallel to the relative plate motion vector (260°), and 2) adjacent 150 km wide along strike sections oriented in a slab dip-parallel direction (310°) (Fig. 3c). The relative plate motion vector reflects the Pacific plate transport direction relative to a stable Australian plate over timescales of millions of years (Cande & Stock, 2004), while dip-parallel sections are parallel to the present plate convergence direction (Wallace et al., 2004). The two sample orientations have frequency-depth distributions for earthquakes that differ 2-25% for sections of comparable location. The sections are positioned in such a way as to sample the slab underlying different volcanic and tectonic regions in the overriding plate (e.g. rifted rhyolite dominated TVZ or contractional southern North Island) (Fig. 3c). The spatial distribution of seismicity in each section has been analysed over a range of bins 40 to 200 km in depth to ensure robust F-M relationships are observed throughout the slab. Where the M_C increases to M_L 3.8 > 100 km beneath the Bay of Plenty (offshore and N2 sections) correcting for the under sampling of low magnitude earthquakes would only further support the first-order conclusions presented here.

3.2 Velocity models

The structure of the subducting plate is investigated using the recently published three-dimensional velocity model of New Zealand (3DNZ) along with a relocated subset of the GeoNet catalogue (2001-2009) (Fig. 4) (for further detail on methods and data see Eberhart-Phillips et al., 2010 and references therein). Limitations of the tomographic method include an inability to model sharp velocity gradients, directional sampling bias,

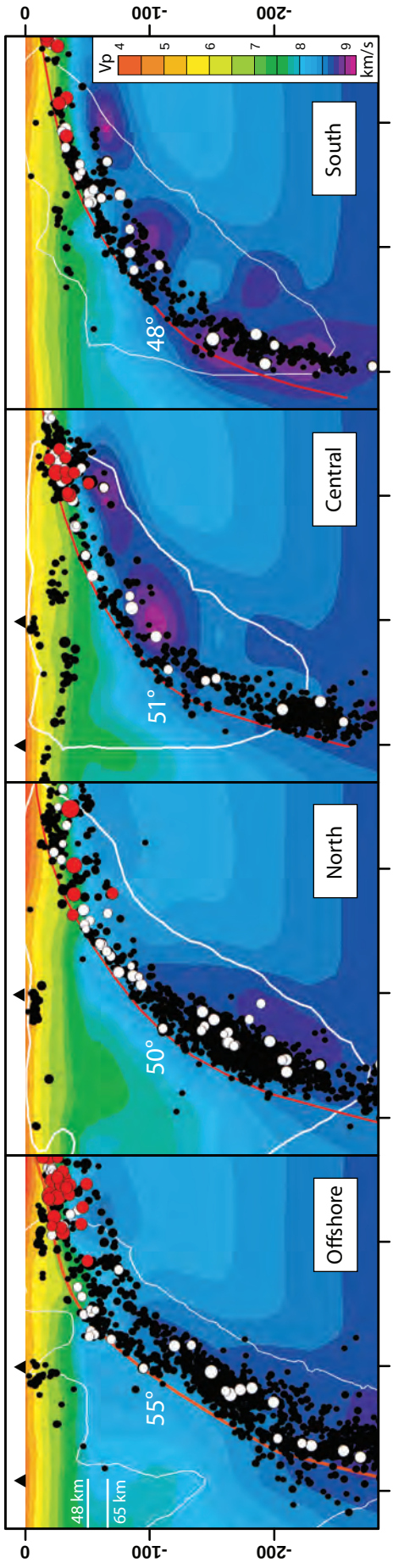

Figure 4. Curvature of the subducting slab. Relocated Benioff zone seismicity (black filled circles) superimposed on 3D P-wave velocity model of New Zealand (Eberhart-Phillips et al., 2010). RMT focal mechanisms (2004-2010) (Ristau, 2008) with relocated hypocentres where available (white filled circles). EHB catalogue (1977-2007) $\leq$ 50 km depth (red filled circles) (Engdahl et al., 1995). Meaningful velocity information inside spread function contour $<$ 3.0 (thin white line) (Eberhart-Phillips et al., 2010). Interpreted slab surface from Chapter 5 (red line) with mean dip between 50-200 km depth shown. Arc volcanoes $<$ 0.5 Ma (black triangles). Depth of Fig. 7 map sections at 48 and 65 km shown for reference.

and coarse spacing of the grid nodes (i.e. 30-50 km below 50 km depth), however the regional extent and internal consistency of the 3DNZ velocity model provide unparalleled detail of the location and geometry of the subducting plate along the Hikurangi margin (Eberhart-Phillips et al., 2010). The resolution of the tomographic model is measured by a spread function where ≤ 3 indicates regions with meaningful velocity information at or smaller than the grid spacing (i.e. < 50 km). All relocated GeoNet events have been recorded on ≥ 6 stations with travel time residuals ≤ 0.3 s and a distance of 2 focal lengths from the nearest station to ensure good depth control. Individual earthquakes are relocated with greater accuracy (lower residuals) using 3DNZ than the standard 1D GeoNet velocity model and can be clearly assigned to the subducting or overriding plate (Fig. 6) (Reyners & Eberhart-Phillips, 2009).

Deriving a meaningful spatial distribution of slab seismicity is dependent on accurate locations. Hypocentres derived from a 1D velocity model in the GeoNet catalogue were compared to their equivalent relocated in the 3DNZ velocity model by M. Reyners ($M_L \geq 3.6$, N=2879, 50-340 km depth). This comparison showed an average change in depth of -9 ± 12 km along a mean azimuth of 274 ± 25° by a mean distance of 96 ± 50 km with relocation. The systematic westward shift in hypocentres results in a minor shallowing of the slab dip below 100 km depth, while above 100 km the scatter associated with the GeoNet catalogue is significantly reduced. At the scale of sampling employed in this study the difference in location, and more importantly depth, between hypocentres derived from 1D and 3D velocity models is not significant. The use of relocated hypocenters makes only minor changes (± 10 km) to the depth of the maximum frequency peaks in either orientation of sample section (motion vector or dip-parallel) compared to the GeoNet catalogue. Due to its longer record and larger sample size I consider the GeoNet catalogue (1988-2010, $M_L \geq 3.6$, ≥ 50 km depth) to provide robust first-order estimates on the spatial distribution of Benioff-zone seismicity along the Hikurangi margin.

3.3 Focal mechanisms

Focal mechanisms provide information about the orientation and kinematics of faults that slip during earthquakes (Webb & Anderson, 1998). Focal mechanism solutions are widely available for events in the subducting plate between M_W 3.8 and 7.1 (Dziewonski et al., 1981; Ristau, 2008). To relate deformation in the subducting plate as

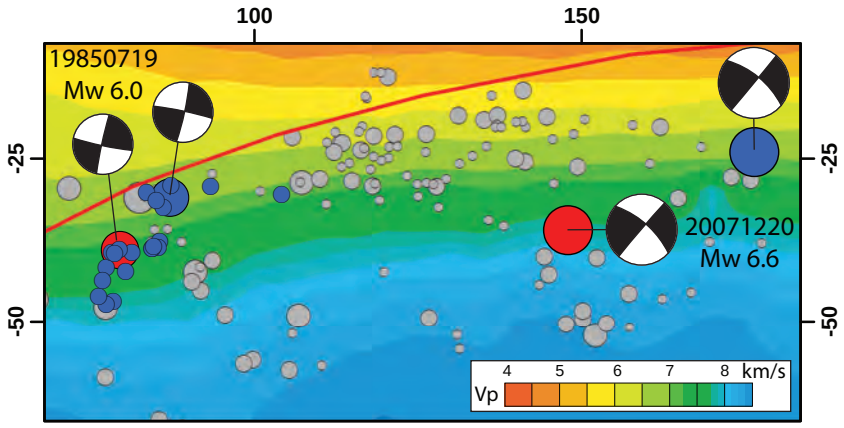

Figure 5. Normal-faulting earthquakes in the upper and lower seismic zones beneath the Hikurangi margin. See Fig. 1 for location. Comparison between focal mechanisms calculated from regional (blue filled circles) (Bannister et al., 1989; Ristau, 2008) and global (red filled circles) (Dziewonski et al., 1981; Engdahl et al., 1998) networks superimposed on 3D velocity model of New Zealand (Eberhart-Phillips et al., 2008). The majority of relocated GeoNet events (grey filled circles) < 50 km depth lie below the interpreted slab surface (red line).

it passes through the trench to beneath the active arc, I use Regional Moment Tensor (RMT) focal mechanism solutions along the Hikurangi margin (Fig. 3b). Since 2004, RMT focal mechanisms for earthquakes > Mw 3.8 have been routinely calculated from GeoNet hypocentre and waveform data (Ristau, 2008). As RMT solutions are typically insensitive to differences between GeoNet hypocenters calculated using a 1D velocity model and those relocated in the 3DNZ (Eberhart-Phillips et al., 2010) (i.e. ≤ -5% residual reduction), I use RMT solutions with relocated (3DNZ) hypocentres. To provide a regional context and comparison to previous studies of shallow slab faulting along the southern Kermadec trench and Hikurangi margin, I use relocated hypocentres from the EHB catalogue for depths ≤ 50 km and a majority of which have corresponding Centroid Moment Tensor (CMT) solutions (Fig. 1) (Dziewonski et al., 1981; Engdahl et al., 1998). The EHB catalogue provide more accurate locations (i.e. lower residuals) than those of the original CMT solutions and in some cases, such as that of the M_W 7.1 East Cape earthquake (5 February 1995), may be more reliable than those derived from the local network at the time (Glendhill pers. comm; 2011).

RMT solutions are entirely consistent with reference CMT solutions and well-constrained first-motion solutions for larger earthquakes and aftershock sequences (Ristau, 2008). For example, a M_W 6.6 normal faulting slab earthquake (20 December 2007) (Fig. 5) is reported at depths of 24 and 36 km in GeoNet and EHB catalogues respectively, the EHB catalogue location ~35 km to the west of the GeoNet location. Both hypocentres are located within the lower seismicity zone of the subducting slab and have near identical focal mechanism solutions, therefore using the EHB catalogue location and CMT focal mechanism solution does not significantly change the interpretation of the earthquake using local network solutions. Detailed relocation and long period body-wave modelling of a M_W 5.7 normal faulting slab earthquake (19 July 1985) (Fig. 5) by Bannister et al. (1989) has a near identical focal mechanism to the CMT solution. The hypocentre of both the CMT and EHB catalogue locations are within 20 km horizontally and 10 km vertically of the Bannister et al. (1989) hypocenter, with all hypocentres located within the upper seismic zone of the slab. These and others studies (Webb & Anderson, 1998) show the consistency between locally derived and global focal mechanism solutions. I therefore use RMT and CMT focal mechanism solutions in this study as these form the most complete and consistent data set with which to evaluate deformation in the subducting slab.

4. Hydration of the subducting slab

The spatial distribution and kinematics of seismicity beneath (and east of) the North Island provide information about the processes associated with the hydration of the lithosphere prior to and during subduction. The hydration of the subducting lithosphere is dependent on the plate age, spreading rate during formation (i.e. the depth and degree of hydrothermal alteration), and the degree of bending the plate experiences as it approaches the trench (Fig. 1) (Peacock, 2001; Hacker et al., 2003; Ranero et al., 2003; Faccenda et al., 2009). If the Hikurangi Plateau has subducted beneath the North Island (Reyners et al., 2011), hydration and/or hydrothermal alteration experienced during rifting and break-up of the Ontong Java-Manihiki-Hikurangi Plateau must also be considered (Taylor, 2006; Davy et al., 2008). Cretaceous rifting of the plateau parallel and perpendicular to the present dip direction of the slab along the Hikurangi margin appears extensive, particularly through the Central Basin and Northern Volcanic Region, where numerous pre-existing faults dissect volcanic basement (Fig. 1 and Appendix Fig. 4) (Davy et al., 2008). These faults were potential conduits for fluids migrating into and out of the plateau during the rifting process (Mancktelow, 2008).

4.1 Bending related faulting and slab curvature

Normal faults formed by bending of the slab as it enters the subduction system promote hydration of the subducting plate. The degree to which the slab bends in proximity to the trench determines the size and frequency of faults formed, or reactivated, to accommodate the flexure of the lithosphere (Chapple & Forsyth, 1979; Masson, 1991; Ranero et al., 2005). As faults are considered the primary pathway for fluids into and out of the slab, their size and frequency have important consequences for the amount of fluid liberated into the mantle wedge at sub-arc depths (Peacock, 2001; Hacker et al., 2003; Ranero et al., 2003; Faccenda et al., 2009). Displacement on bending related normal faults typically initiates $\leq$ 75 km from the trench (increasing significantly within 30 km) where faults may penetrate as deep as 15-30 km into the subducting lithosphere (Chapple & Forsyth, 1979; Masson, 1991; Ranero et al., 2003). Fault (re)activation due to bending typically starts with low displacements at shallow depths within the slab as it approaches the trench (Masson, 1991; Faccenda et al., 2009). As the faults move through trench and interplate zone they progressively increase in length and depth

(Masson, 1991; Ranero et al., 2003; Faccenda et al., 2009). As the cumulative seismic moment of normal faulting earthquakes in proximity to the trench exceeds the total extension predicted by elastic plate models, a large amount of permanent deformation must be accommodated by fault displacement (Chapple & Forsyth, 1979). Peacock (2001) proposed and Faccenda et al. (2009) demonstrated how normal faults in the fluid-saturated brittle crust permit hydration of the lower crust and mantle through percolation induced by the downward pumping of water driven by inverted (subhydrostatic or negative) vertical pressure gradients focused along the fault zones (Fig. 1). These models for the hydration of the subducting lithosphere via normal faults are supported by broad regions of steeply dipping seismic reflectors (interpreted as hydrated mantle shear zones) beneath normal fault scarps formed in the subducting plate approaching the Middle America trench (Ranero et al., 2003). These regions have low seismic velocities with respect to mature oceanic crust indicating up to 10-15% serpentinization of the mantle (equivalent to 4-5 wt% H_2O) (Grevemeyer et al., 2007).

The curvature of the subducting lithosphere as it bends and accumulates fault displacement depends on factors such as the composition and thickness of the overriding and subducting plates, the age and rate of the subduction plate, and whether or not the subduction hinge is rolling back, stable or advancing (Chapple & Forsyth, 1979; Masson, 1991; Lallemand et al., 2005; Royden & Husson, 2006). The maximum curvature of the slab and its location relative to the trench changes along the Hikurangi margin. Depth converted seismic-reflection lines indicate that the plate interface at depths of 5-18 km is steeper (~10-18°) in the northern Hikurangi margin than the southern margin (~6°) (Barker et al., 2009). The average dip of the slab between 50-200 km depth decreases southwards by ~7° from the northern (55°) to southern (48°) Hikurangi margin (Fig. 4). The steeper dips of the slab in the northern Hikurangi margin are a reflection of the fact that in this region it steepens more rapidly and has a greater curvature close to the trench than further south. The greater curvature of the slab at shallow depths (< 50 km) in the north produces high displacements on bending moment normal faults in this area. The total fault displacement of the slab accumulated at shallow depths (< 50 km) through bending decreases southwards along the Hikurangi margin (Fig. 1).

4.2 Normal faulting earthquakes

Medium to large magnitude earthquakes (M_W 4-7) and their associated focal mechanisms provide information on deformation of the Pacific plate as it subducts beneath the North Island. Normal faulting predominates in the shallow slab and is interpreted to mainly form due to slab bending (Fig. 6). Maximum bending strains and associated normal faulting (Chapple & Forsyth, 1979) are immediately adjacent to the trench (and beneath the accretionary prism) in the north of the Hikurangi margin and beneath the lower North Island in the south (distal to the trench and accretionary prism) (Fig. 1). The southward divergence of shallow slab normal-faulting earthquakes from the trench along the Kermadec trench is coincident with the transition from an oceanic to continental overriding plate where crustal thickness increases by ~10-15 km along the Hikurangi margin (Bassett et al., 2010).

Normal-faulting earthquakes and their aftershock sequences within the slab beneath the northern Hikurangi margin extend to mantle depths in the subducting lithosphere. The largest earthquake in the North Island region over the last 30 years occurred within the subducting slab at the transition from oceanic to continental overriding crust. The M_W 7.1 East Cape (05 February 1995) normal-faulting earthquake occurred close to the top of the subducting plate at a depth of 21 km and was followed by at least 14 normal faulting aftershocks > Mw 5.2 extending up to 20 km into the slab (Fig. 4) (Dziewonski et al., 1981). The detailed study of a M_W 5.7 normal faulting event (19 July 1985) and aftershock sequence by Bannister et al. (1989) showed that a main shock at a depth of 31 km also initiated close to the surface of the slab. The distribution of aftershocks suggest this event ruptured at least 16 km downwards into the slab (Bannister et al., 1989). These data are consistent with previous studies that suggest normal-faulting earthquakes of ~M_W 7.0 rupture oceanic lithosphere to depths of at least 25-30 km (Chapple & Forsyth, 1979) with relocated GeoNet catalogue events indicating depths up to 40 km within the slab beneath the northern Hikurangi margin (Fig. 6, 7). The close proximity of the M_W 5.7 (19 July 1985) event to a 5 km step in the plate interface imaged by seismic reflection has led to a hypothesis that the curvature of the slab in this region is accomplished by a series of long-lived steps in the subducting plate (Henrys et al., 2006).

Focal mechanisms at depths ≤ 50 km from within the slab show it to be in down dip tension. Principal strains within a slab are generally aligned parallel and normal to

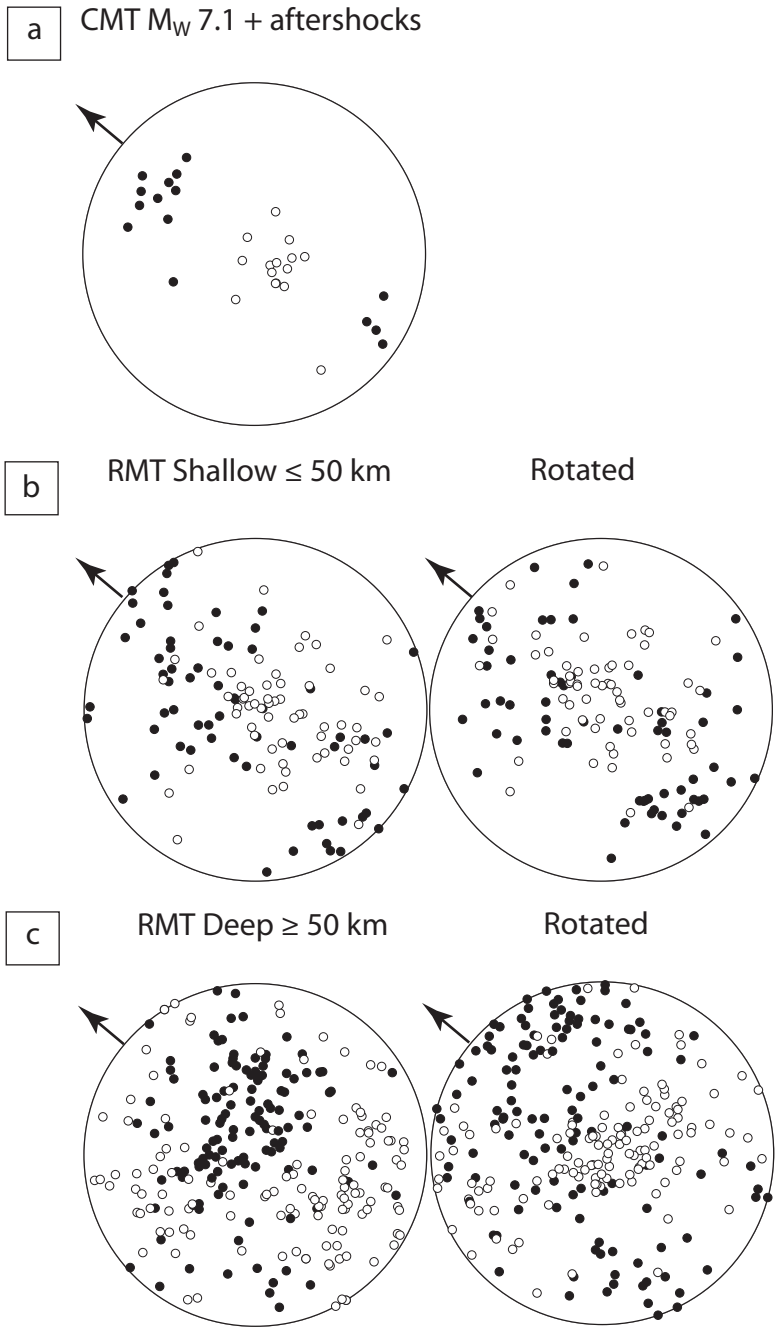

Figure 6. Kinematics of faulting in the subducting slab. Table 1 details mean P and T eigenvectors for each data set. (a) CMT P (white filled circles) and T (black filled circles) axes for East Cape (19950205) M_W 7.1 normal faulting earthquake and aftershock sequence (Dziewonski et al., 1981). (b) RMT P and T axes for events in the shallow slab ≤ 50 km depth (right), (Ristau, 2008) and same data rotated into slab reference frame (left). Rotation of P and T axes restores slab to horizontal, see Table 1 for details. Slab down dip direction 310º (arrow) for reference. (c) RMT P and T axes ≥ 50 km depth (right) and same data rotated into slab reference frame (left). For locations see Fig. 1 for CMT and Fig. 3 for RMT. Subhorizontal T and subvertical P axes in rotated plots indicate kinematics consistent with the reactivation of bending-related normal faults, i.e. (a).

its surface (Molnar & Atwater, 1978), and as this surface progressively curves with depth, direct comparison of focal mechanisms from different locations becomes problematic. To overcome this difficulty, RMT focal mechanisms ≤ 50 km (N = 62) have been rotated to remove the dip of the slab (Fig. 6). The distribution of unrotated and rotated P axes near vertical and subhorizontal T axes indicate normal faulting predominates shallow intraplate events (Table 2). The majority of slab focal mechanisms (84%) occur in the northern Hikurangi margin where the slab steepenening and rollback has occurred over the last ~7 Ma (Chapter 5). These data indicate that faults formed prior to subduction to accommodate lithospheric flexure are rotating with the slab through the interplate zone. The scatter in the P and T axes, however, reflect a complex deformation pattern associated with a full spectrum of slip from normal to strike slip to reverse on bending-related and reactivated faults (Ranero et al., 2005). Eigenvectors of these kinematic data, however, reflect a predominantly normal-faulting focal mechanism similar to the M_W 7.1 intraplate event (Fig. 6).

Location	Source	P	T	P(rot)	T(rot)	N	M_W
Slab ≤ 50 km	RMT	096/69	305/19	012/77	127/2	62	3.8-6.6
Slab ≥ 50 km	RMT	104/16	342/57	069/65	329/12	124	3.9-6.3
East Cape	CMT	301/63	122/26			15	5.1-7.1

Table 2: Mean P and T axes from Pacific intraplate RMT (Ristau, 2008) and CMT focal mechanisms (Dziewonski et al., 1981). Mean kinematic axes determined from the maximum eigenvalue for each group of P and T axes. P and T axes are rotated into slab reference frame about a horizontal axis trending 040º (i.e. strike of slab) by the dip of the slab at the earthquake focal depth (Fig. 4).

Seaward dipping (antithetic) bending-related faults are considered favourable locations for slab hydration below the over-riding plate where slab curvature and inverted fluid pressure gradients are high and downward fluid pumping is at a maximum (Faccenda et al., 2009). A number of RMT solutions originate from the lower zone of seismicity (depths of 20-40 km within the slab) and in particular the M_W 6.6 normal faulting earthquake of 20 December 2007 (Fig. 5). The main shock of this event, which occurred over an area of ~10 km^2 with a maximum displacement of ~2.6 m, a high stress drop (17 MPa) at depth of 40 km (~1 GPa) characteristic of an intraplate event, occurred well within the mantle of the subducting plate (Holden et al., 2008). Displacement occurred on a 45° east (seaward) dipping fault which in turn triggered

slow slip on the plate interface 25-30 km above (Holden et al., 2008). The observation that medium to large earthquakes ($\geq M_W$ 5.7) occurring near the top of the subducting plate rupture downwards at least the thickness of Hikurangi Plateau (16-23 km) and that normal faulting also occurs in the lower seismicity zone indicates that earthquakes provide a viable mechanism for hydrating the slab to mantle depths (~40 km) along the northern Hikurangi margin.

4.3 Slab hydration

In order for surface fluids to hydrate the mantle lithosphere, the fluids must be able to pass from the water saturated upper crust through an assumed anhydrous lower crustal layer to the mantle (Hacker et al., 2003). Normal faults in the subducting plate in the northern Hikurangi margin rupture to depths of at least 15 to 30 km within the slab and provide the potential fluid pathways required for deep water transport and hydration of the mantle. The crustal composition of the Hikurangi Plateau is largely unknown and assumed here to be similar to mid-ocean ridge basalts where the predominant hydrous phases are lawsonite (11.2 wt% H_2O), chlorite (12 wt% H_2O) and amphibole (2.1 wt% H_2O) which comprise 20-60 wt% of basalt (Schmidt & Poli, 1998). Serpentinite, together with chlorite, dominate the hydrous phases (12.3 and 13 wt% H_2O respectively) in fluid saturated peridotite and have previously been proposed as significant sources of water during sub-arc dehydration to depths of ca. 150 km (Schmidt & Poli, 1998; Peacock, 2001; Carlson & Miller, 2003; Rupke et al., 2004; Grevemeyer et al., 2007).

Seismic velocities are the best indicator for the degree of hydration that the lithosphere has undergone (Grevemeyer et al., 2007). For example, P-wave velocities (Vp) in partially serpentinized ultra-mafic rocks typically decrease by 1% per 2.4% increase in serpentine content (Carlson & Miller, 2003). The relative hydration of the incoming oceanic lithosphere can be estimated using the 3DNZ velocity model for the North Island (Fig. 8) (Eberhart-Phillips et al., 2010) in association with relocated intraplate seismicity (Fig. 7). Velocities within the subducting slab beneath the east coast of the North Island increase southward. High velocities (~9.25 km/s) in the slab mantle beneath the southern Hikurangi margin replicate those obtained from previous earthquake and seismic refraction studies but may also an artefact of coarse model parametrization (Reyners et al., 2006). However, as these high velocities occur along

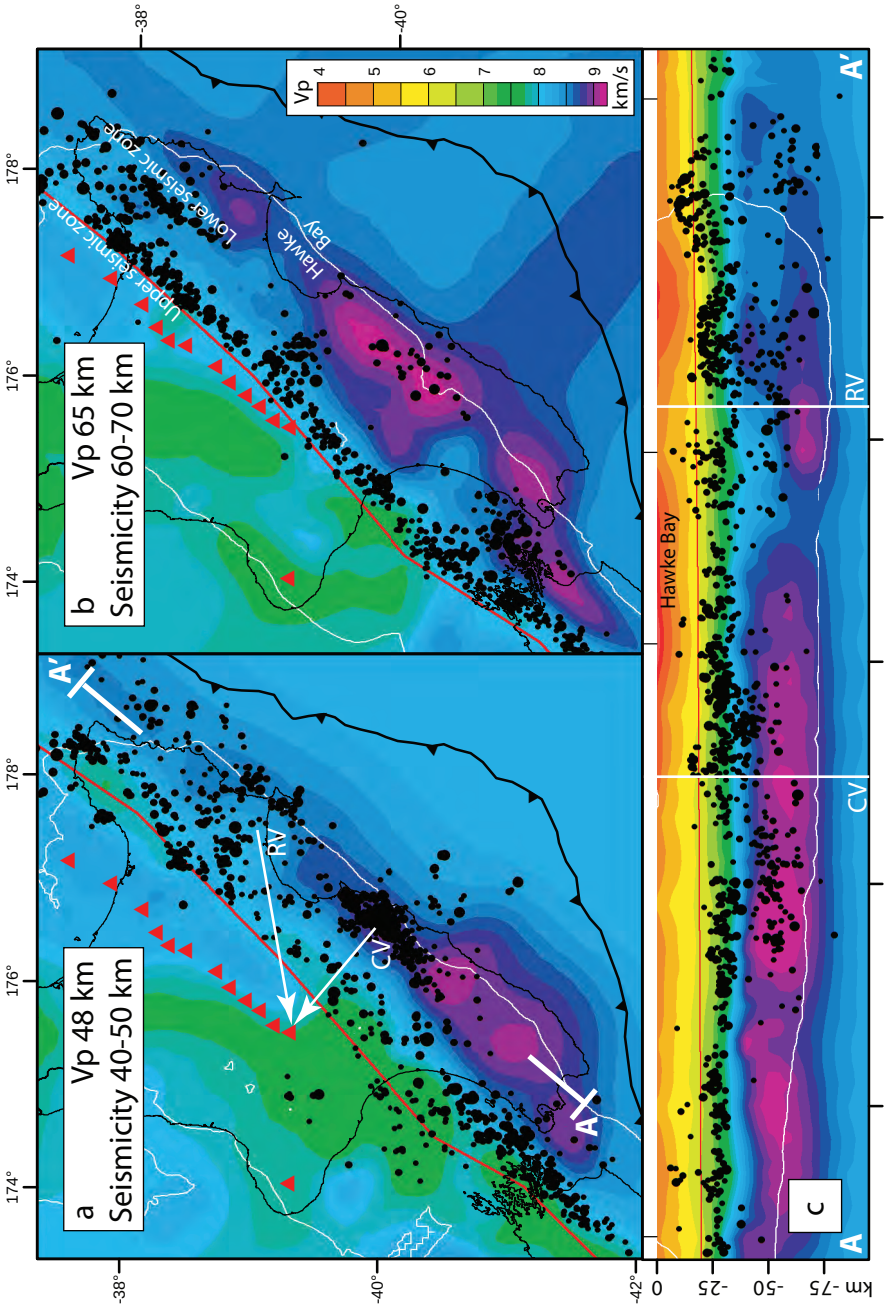

Figure 7. Seismicity and velocity structure of the subducting slab. Relocated seismicity (black filled circles) superimposed on 3D P-wave velocity (Vp) model of New Zealand (Eberhart-Phillips et al., 2010). (a) & (b) Depth slices showing sections of a curved slab (see Fig. 4 for location), interpreted slab surface (thin red line). (c) Along strike velocity profile (see A for location). Meaningful velocity information inside spread function contour < 3.0 (thin white line), arc volcanoes < 0.5 Ma (red triangles). Direction of Pacific motion (RV) and convergence vectors (CV) relative to southern limit of arc frontshown for reference.

the margin at many times the nodal grid spacing, the high velocities appear to be a real feature of the slab. A ~3% (0.25 km/s) increase in P-wave velocities at slab mantle depths occurs southwards across the transition between volcanic and non volcanic sections of the margin (Fig. 7). This increase in velocity may reflect a reduction in the degree of serpentinization towards the south (Carlson & Miller, 2003). Alternatively, high slab velocities in the south may represent an anhydrous eclogite root to the Hikurangi Plateau, created during formation of the plateau or later during failed Cretaceous subduction along the Gondwana subduction margin (Reyners et al., 2011).

The distribution of intraplate seismicity also indicate an along strike changes in the hydration of the slab. At depths of 40-50 km, relocated seismicity show a broad distribution (~100 km width) of earthquakes through the crust and mantle of the slab in the northern Hikurangi margin tapering to widths of 20-30 km toward the south (Fig. 7a). The southern limit of the lower seismic zone within the slab mantle (eastern-most events in this depth range) in the northern Hikurangi margin is associated with southward transition to a high velocity region. At 60-70 km depth, the distribution of earthquakes shows a clearly defined upper (western) and lower (eastern) Benioff-zone in the northern Hikurangi margin that does not continue toward the south (Fig. 7b). The presence or absence of seismicity in the slab mantle indicates differences in the degree of dehydration between the northern and southern Hikurangi margin and is discussed in section 5.

Differentiating between the origin of complementary changes in the velocity structure and curvature of the subducting plate from north (low velocities, high curvature) to south (high velocities, low curvature) along the Hikurangi margin makes little difference to the degree and depth extent of hydration interpreted along strike. For example, do high velocities reflect a lower fluid content due to less bending related faulting or do the high velocities reflect a stronger slab (i.e. with an eclogite root) that is less faulted and consequently contains less fluid? Either way, in the northern Hikurangi relatively low slab velocities, the presence of a double Benioff-zone and large magnitude (M_W 7) normal faulting earthquakes rupturing to mantle depths in close proximity to the trench would suggest hydration of the lithosphere could be pervasive. To the south of the southern limit of volcanism, high slab velocities, a weak to absent double Benioff-zone and lower maximum magnitude (M_W < 6.3) of bending related normal faulting earthquakes far from the trench would suggest slab hydration is limited in degree and depth extent. In the following section I examine the distribution of

Benioff-zone earthquakes at intermediate depths (50-350 km) along the Hikurangi margin for evidence that dehydration of the subducting lithosphere decreases southwards in concert with changes in hydration inferred near surface.

5. Dehydration of the subducting slab

Slab dehydration accompanies subduction which is generally associated with volcanic arc formation (Gill, 1981; McCulloch & Gamble, 1991). The release of fluids from the stepwise and continuous dehydration of hydrous phases throughout the crust and mantle of the subducting slab is believed to promote brittle failure (i.e. earthquakes) through elevated of pore fluid pressures (Kirby et al., 1996; Manning, 2004). The ascent of these fluids from the slab into the hot core of the mantle wedge (ca. 1300 °C) induces 'wet' partial melting and the formation of volcanic arcs (Gill, 1981; Schmidt & Poli, 1998). Dehydration of most of the hydrous phases in the subducting crust, such as amphibole, should occur at depths shallower (i.e. 65-90 km) than arc magma generation and therefore it has been proposed that the majority of fluids inducing 'wet' partial melting are likely to originate from a hydrated slab mantle (Schmidt & Poli, 1998; Hacker et al., 2003; Eberhart-Phillips & Bannister, 2010). The correlation between patterns of intermediate depth seismicity and the locations of predicted hydrous minerals led Hacker et al. (2003) to propose the hypothesis that the rate of Benioff-zone seismicity should be proportional to the degree to which the subducted lithosphere is hydrated. Benioff-zones have a number of universal features (for review see Hacker et al., 2003) which, important for this study, include the presence of distinct upper and lower seismic zones separated vertically by an aseismic or weakly seismic zone (Hacker et al., 2003; Brudzinski et al., 2007).

The rate of Benioff-zone earthquakes correlate with the location and productivity of volcanism along the Hikurangi margin. By far the greatest number of earthquakes in the slab occur over depths of 130-210 km at the latitude, and west of the central rhyolite dominated segment of the TVZ (sections N1 and North) (Fig. 8, see Fig. 3 for location of sections). This section of slab has at least twice the number of earthquakes as adjacent sections over the same depth range (Appendix 2). North of the central TVZ (section N2 and Offshore) a comparable number of earthquakes occur over a larger depth range (130-290 km) but with lower maximum frequencies than the central TVZ sections (e.g. < 125 verses 350-400). Immediately south of the central TVZ

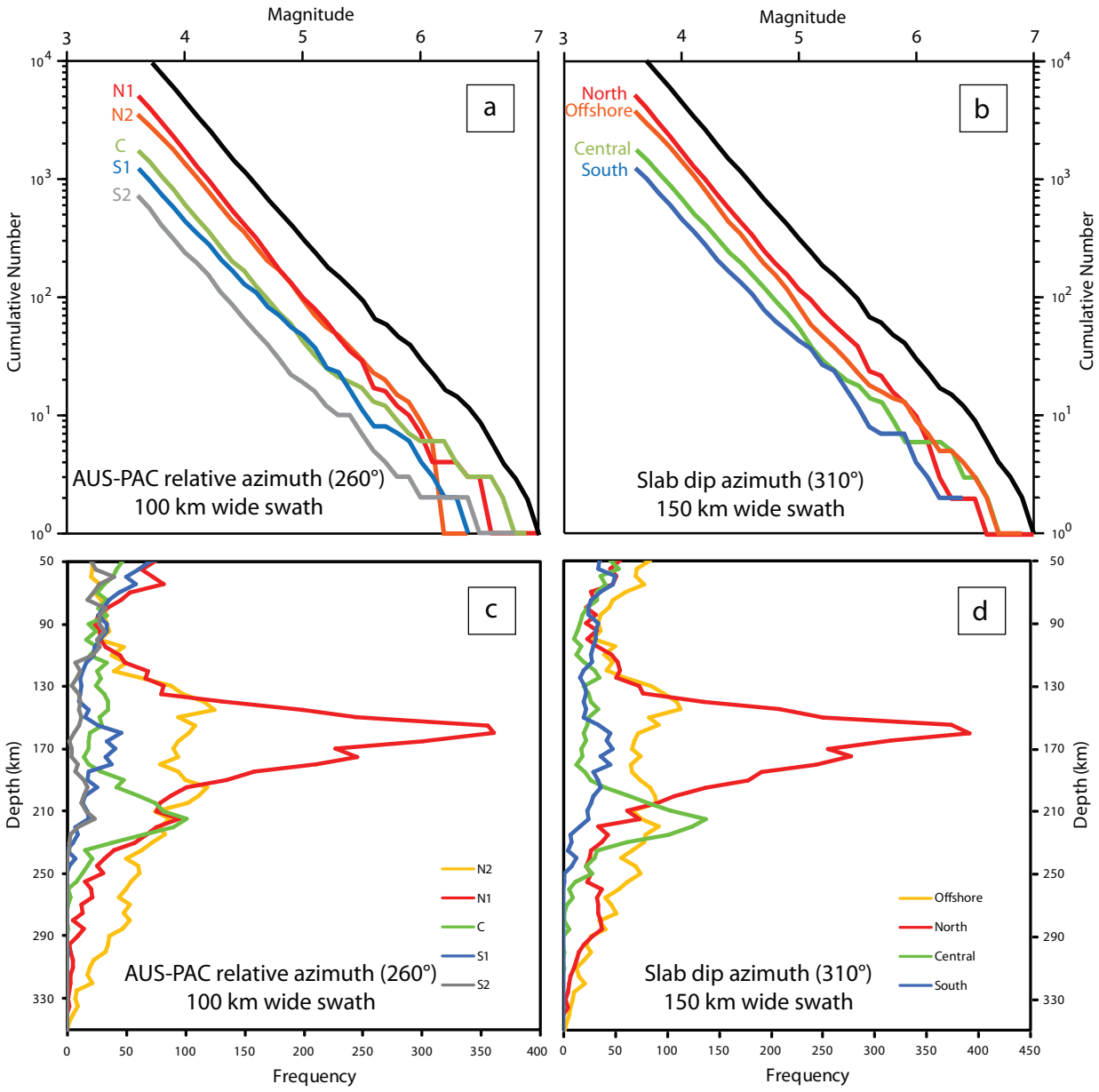

Figure 8. Intermediate depth seismicity frequency-magnitude and frequency-depth relations. See Fig. 3 for section locations. (a) & (b) Frequency-magnitude relations for sections oriented in relative motion vector and slab dip directions, respectively. (c) & (d) Frequency-depth relations for sections oriented in relative motion vector and slab dip directions, respectively. See Appendix 2 for statisitcs.

(section C1 or Central) a relatively small frequency peak in seismicity occurs between 180-230 km. Further to the south towards the end of the seismically active slab, no significant peaks in seismicity occur which is limited to depths of < 250 km.

The distribution of seismicity within the subducting lithosphere provides information about which hydrous minerals are most likely to be dehydrating. To investigate the depth distribution of earthquakes within the slab I perform a simple coordinate rotation of relocated seismicity (Brudzinski et al., 2007) in slab dip-parallel profiles that correspond to depth ranges where amphibole in the slab crust (50-90 km) and serpentinite in the slab mantle (130-210 km) predominantly dehydrate (Fig. 9) (Schmidt & Poli, 1998). Sections along the Hikurangi margin clearly show the dominance of dehydration of hydrous minerals in the crust (upper seismic zone) at depths of 50-90 km and serpentinite in the mantle (lower seismic zone) at depth of 130-210 km. Profiles from along the margin show a similar distribution and frequency of upper zone seismicity between depths of 50-90 km where maximum frequency peaks occur within 8 km of the interpreted slab surface (Fig. 7a). The Offshore and South sections have pronounced lower seismicity zones extending to depths ~40 and 30 km within the slab mantle, respectively. The separation between maximum frequency peaks of the upper and lower seismic zones in the Offshore and South sections is 24 ± 2 km, typical of normal oceanic slabs ~120 Myr in age (Brudzinski et al., 2007) and consistent with the age inferred for the Hikurangi Plateau (Taylor, 2006; Davy et al., 2008). The frequency of seismicity in the North section between 130-210 km indicates significant rates of dehydration (i.e. at least twice that of other sections) occur at depths of ~12-32 km within the mantle of 'normal' 120 Ma old oceanic lithosphere (Brudzinski et al., 2007) or the lower crust-upper mantle of the Hikurangi Plateau (Davy et al., 2008; Reyners et al., 2011).

Focal mechanisms from the slab at depth (50-350 km) show the slab is predominantly in down dip extension. Similar to the focal mechanism from the shallow slab, rotation of RMT focal mechanisms ≥ 50 km (N= 124) (Fig. 6) to remove the dip of the slab shows near vertical P axes (mean 069/65°) and horizontal T axes (mean 329/12°) (Fig. 6b). Again the majority of the data (79%) come from the volcanic portion of the margin. The kinematic extension direction (T axes) of intraplate faulting at depth is consistent with that at shallow depths (≤ 50 km) (127º), and coupled with near vertical kinematic shortening direction (P axes) normal to the slab surface, indicate normal faults forming to accommodate bending of the shallow slab near surface are

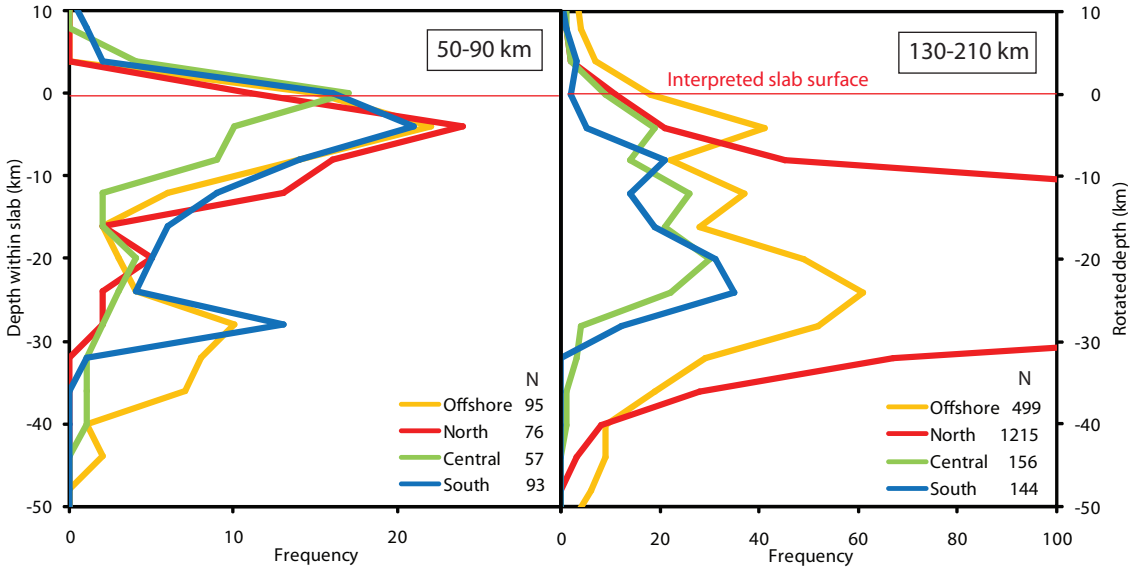

Figure 9. Seismicity structure of the subducting slab. Depth distribution of relocated earthquakes after a simple coordinate rotation to remove slab dip (e.g. Brudzinski et al., 2007). Interpreted slab surface (thin red line) from Fig. 4.

preferentially reactivated at depth. While the predominant deformation in the slab is extensional, similar to shallow intraplate earthquakes, the scatter of P and T axes indicates complex reactivation of pre-existing faults in a variety of orientations. These pre-existing faults may have formed by a number of mechanisms including rifting of the plateau (Appendix Fig. 4) and bending of the slab prior to subduction in the Cretaceous. Faults related to prior rifting of the Hikurangi Plateau approximately normal to the trench (parallel to the Raphuia Scarp) (Davy et al., 2008) (Appendix Fig. 4) are now being dissected by bending-related faults parallel to the trench which, dependent on their mutual spacing, may result in significant weakening of the crust allowing the free flow of fluids into and out of the mantle.

In summary, the distribution and rate of Benioff-zone seismicity below 50 km depth indicate that the depth and degree of dehydration in the subducting slab decreases southwards. While the frequency of earthquakes in the upper seismic zone (slab crust) are approximately equivalent along strike, the depth distribution of earthquakes in the lower seismic zone (slab mantle) contrasts between the northern and southern Hikurangi margin. These observations support the hypothesis that it is the degree and/or depth of hydration in the subducting mantle lithosphere that is the key factor in determining whether sufficient fluid is released to induce 'wet' partial melting in the mantle wedge and the formation of arc volcanoes (Hacker et al., 2003). In the next section, I examine how and why the hydration of the slab may vary along the Hikurangi margin.

6. Fluid flux and volcanism

Variability in the style and production rates of volcanism along the Hikurangi margin can be understood when the hydration (and subsequent dehydration) of the subducting slab is considered. In the northern Hikurangi margin, the highest rates of strain associated with the bending of the incoming plate are occurring beneath the accretionary prism in close proximity to the trench and the ocean (Fig. 1). Here abundant free fluids from subducted sediments (Eberhart-Phillips & Chadwick, 2002) and pervasively faulted crust of the subducting slab are available to be transported to mantle depths through large bending related normal faults (capable of M_W 7 earthquakes). While aftershock sequences of large normal faulting earthquakes beneath the shallow interplate zone (3-20 km depth) extend at least 20 km into the slab, seismicity indicates brittle deformation and potential for significant hydration to depths of at least 40 km

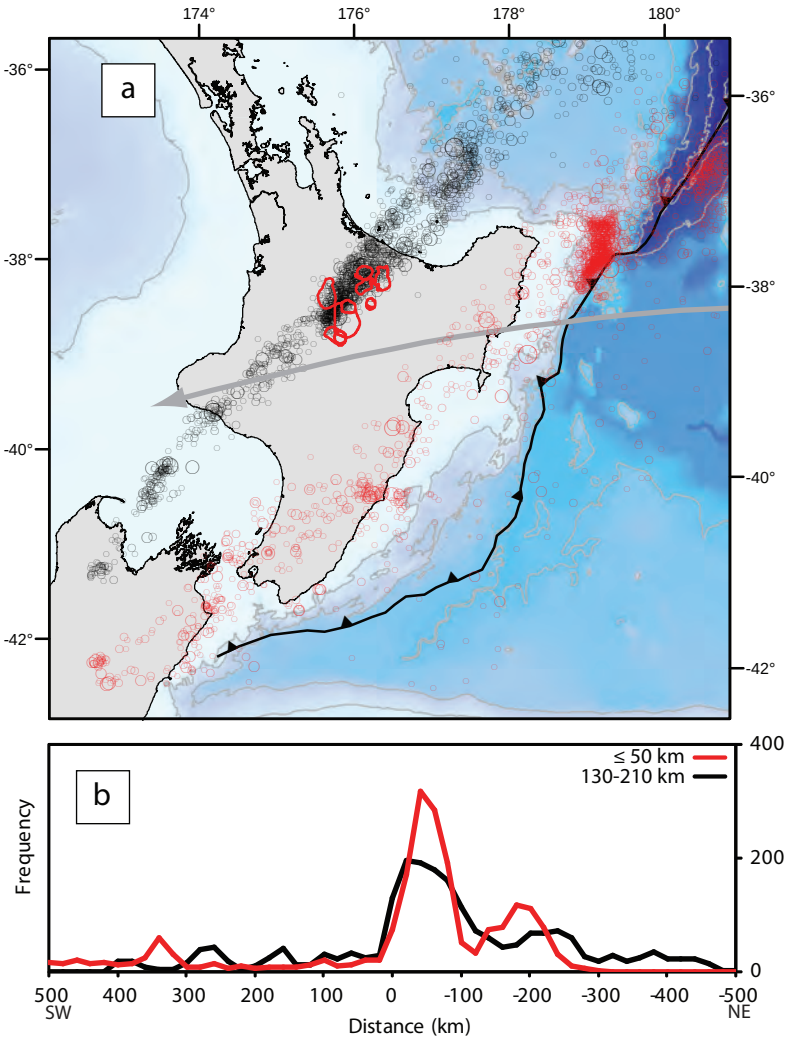

Figure 10. Relationship between shallow bending-related and deep dehydration-related seismicity. (a) GeoNet earthquake catalogue events (1988-2010, $M_L \geq 4$) ≤ 50 km (red circle outlines) through interplate zone and 130-210 km (black circle outlines) in slab. Vast majority of earthquakes in interplate zone are within subducting slab. TVZ calderas active in last 1.6 Ma shown by thick red lines (Wilson et al., 1995). Pacific plate motion vector relative to fixed Australian plate for last 16 Myr (grey arrow) (Cande & Stock, 2004). (b) Earthquake frequency along strike corrected for obliquity of Pacific Plate motion vector. Note the coincidence of modes for inferred hydration and dehydration seismicity.

(Fig. 9). Towards the southern Hikurangi margin bending of the slab does not occur until well beneath (> 20 km depth) the continental crust of the North Island where the availability of free fluids is reduced and the maximum magnitude of intraplate earthquakes ($M_W \leq 6.3$) is lower than the northern Hikurangi margin (Fig. 1).

The mantle of the subducting Pacific plate is the main source of fluids contributing to the 'wet' partial melting of the mantle wedge and arc volcanism in the North Island. The contribution of fluid from the slab mantle is illustrated by the location of back arc volcanism in the western North Island. Here, a high-K andesite stratovolcano (Mt. Taranaki) (Price et al., 1999) is located near vertically above anomalously high rates of seismicity (relative to the distribution up dip) in the slab mantle centred at a depth of ~215 km (Fig. 8, see Fig. 2c for location). If these high rates of seismicity in the mantle reflect dehydration embrittlement reactions (Schmidt & Poli, 1998; Hacker et al., 2003) then the partial melts for the high-K series magmas forming Mt. Taranaki have a slab mantle source. By contrast dehydration of the subducting Pacific plate crust at depths typically < 90 km (Fig. 9) is approximately uniform along strike and releases an insufficient volume of fluid to induce 'wet' partial melting of the mantle wedge and resultant arc volcanism. The relative paucity of slab mantle dehydration in the southern Hikurangi margin may account for the absence of volcanism in this region.

The high frequency of earthquakes beneath the central TVZ imply extensive and rapid dehydration of the crust and upper mantle of the Pacific plate is occurring at 2-3 times the rate of the slab section immediately to the north (between depths of 130-210 km) (Fig. 8) (Appendix 2). The maximum rate of seismicity (~160 km depth) occurs in the slab 25-35 km west of, and parallel to, active TVZ rhyolitic calderas which have produced at least 6000 km^3 of magma over the last ~1.6 (Fig. 10) (Wilson et al., 2008). These high rates of seismicity in the slab are associated with the lowest Qp in the mantle wedge which is indicative of high temperatures and fluid saturation (Eberhart-Phillips et al., 2008), and only occur over an along strike distance of ~100 km consistent with the dimensions of the rhyolite dominated section of the TVZ (Wilson et al., 1995). The correlation between high rates of slab seismicity and the spatial extent of rhyolitic volcanic systems suggest that elevated fluxes of slab-derived fluids into the mantle wedge is a key driver for the high volcanic production rates observed in the TVZ. High flux rates of fluids into the mantle wedge would also decrease its viscosity and increase

its temperature promoting the uplift of the central North Island associated with volcanism.

The highest frequency of plate bending earthquakes (interpreted to facilitate slab hydration) in the shallow slab sits on the same plate motion path as the high frequency of events beneath the central TVZ. I highlight the relationship between the frequency of shallow and deep slab seismicity by performing a static shift of earthquake frequency profiles along strike to account for the obliquity of the Australia-Pacific relative plate motion vector (Fig. 10). The spatial distribution of these shallow slab earthquakes is similar in extent to the dimensions of the slab section with high seismicity rates at depth and the rhyolitic segment of the TVZ (Fig. 10). The highest density of earthquakes in the subducting plate inferred to arise from bending occur in the northern Hikurangi margin where the subducting plate transitions from oceanic crust to Hikurangi Plateau and the overriding plate changes from oceanic to continental crust (Davy et al., 2008; Bassett et al., 2010). The spatial coincidence of seismicity and these mechanical boundaries is consistent with the notion that they focus faulting in the subducting plate.

The depth, location and degree of hydration in the subducting slab is a key determinant in the location and dehydration of the plate and productivity of arc volcanism in the North Island, New Zealand. For the slab hydration-dehydration cycle proposed the analysis of plate motion vectors of Cande & Stock (2004) indicates fluid residence time of 7 to 10 Ma. Hydration of the slab continues today and assuming that plate motions and subduction continue volcanism in the central North Island could be expected to continue to at least a further 7 Myr. By contrast the levels of slab hydration and dehydration in the southern Hikurangi margin provide little basis to suggest that volcanism will migrate southward into this area in the future.

7. Conclusions

The origin of the high rates of volcanic productivity and heat flow in the TVZ is an important question. A model associated with the subduction zone water cycle is advanced in which volcanism and high heat flow are promoted by high rates of dehydration of the slab mantle at depths of 130-210 km parallel with, and immediately to the west of, the TVZ. Benioff-zone seismicity is inferred to reflect dehydration embrittlement of the previously hydrated slab. The high rates of dehydration in the slab beneath the TVZ lie on a common plate motion path with high rates of seismicity and

normal faulting beneath the accretionary prism at the northern end of the Hikurangi margin. In this high strain zone where overriding and subducting plate crustal composition and thicknesses change, bending of the Pacific plate is accomplished by large (M_W > 7) normal-faulting earthquakes that rupture at least 20 km into the subducting lithosphere. The proximity of abundant oceanic fluids to the location of normal faulting decreases southward along the margin. In addition, the maximum magnitude of intraplate normal-faulting earthquakes, slab curvature and Benioff seismicity decrease south from the high strain zone in the northern Hikurangi margin. These decreases are inferred to limit slab hydration in the southern Hikurangi margin where insufficient water is liberated from the slab to promote melting in the mantle wedge and produce arc volcanism. The depth and extent of hydration in the slab mantle is a key determinant for the location and productivity of volcanic centres across the North Island.

References

Adams, C.J., Graham, I.J., Seward, D. & Skinner, D.N.B., 1994. Geochronological and geochemical evolution of late Cenozioc volcanism in the Coromandel Peninsula, New Zealand. *New Zealand Journal of Geology & Geophysics*, 37, pp.359-79.

Bannister, S.C., Perin, B.J. & Webb, T.H., 1989. Normal faulting through subducted oceanic crust: the 19 July 1985 earthquake of Hawke's Bay, New Zealand. *Tectonophysics*, 162, pp.303-13.

Barker, D., Sutherland, R., Henrys, S. & Bannister, S., 2009. Geometry of the Hikurangi subduction thrust and upper plate, North Island, New Zealand. *Geochemistry, Geophysics, Geosystems*, 10(2), p.Q02007. doi:10.1029/2008GC002153.

Bassett, D., Sutherland, R., Henrys, S., Stern, T., Scherwath, M., Benson, A., Toulmin, S. & Henderson, M., 2010. Three-dimensional velocity structure of the northern Hikurangi margin, Raukumara, New Zealand: Implications for the growth of continental crust by subduction erosion and tectonic underplating. *Geochemistry Gephysics Geosystems*, 11(10), p.Q10013. doi:10.1029/2010GC03137.

Beavan, J., Tregoning, P., Bevis, M., Kato, T. & Meertens, C., 2002. Motion and rigidity of the Pacific Plate and implications for plate boundary deformation. *Journal of Geophysical Research*, 107(B10), p.2261. doi:10.1029/2001JB000282.

Bergman, S.C., Talbot, J. & Thompson, P.R., 1992. The Kora Miocene submarine andesite stratovolcano hydrocarbon reservior. *Taranaki Basin 1991 New Zealand Oil Exploration Conference Proceedings*, pp.178-206.

Bibby, H.M., Caldwell, T.G., Davey, F.J. & Webb, T.H., 1995. Geophysical evidence on the structure of the Taupo Volcanic Zone and its hydrothermal circulation. *Journal of Volcanology & Geothermal Research*, 68, pp.29-58.

Billen, M. & Gurnis, M., 2001. A low viscosity wedge in subduction zones. *Earth & Planetary Science Letters*, 193, pp.227-36.

Black, P.M., Briggs, R.M., Itaya, T., Dewies, E.R., Dunbar, H.M., Kawasaki, K., Kuschel, E. & Smith, I.E.M., 1992. K-Ar age data and geochemistry of the Kiwitahi Volcanics, western Hauraki Rift, North Island, New Zealand. *New Zealand Journal of Geology & Geophysics*, 35, pp.403-13.

Boddington, T., Parkin, C.J. & Gubbins, D., 2004. Isolated deep earthquakes beneath the North Island of New Zealand. *Geophysics Journal International*, 158, pp.972-82.

Booden, M.A., Smith, I.E.M., Mauk, J.L. & Black, P.M., 2010. Evolving volcanism at the tip of a propagating arc: The earliest high-Mg andesities in northern New Zealand. *Journal of Volcanology & Geothermal Research*, 190, pp.83-96.

Briggs, R.M., Houghton, B.F., McWilliams, M. & Wilson, C.J.N., 2005. 40Ar/39Ar ages of silicic volcanic rocks in the Tauranga-Kaimai area, New Zealand: dating the transition between volcanism in the Coromandel Arc and Taupo Volcanic Zone. *New Zealand Journal of Geology & Geophysics*, 48, pp.459-69.

Brothers, R.N., 1984. Subduction regression and oceanward migration of volcanism, North Island, New Zealand. *Nature*, 309, pp.698-700.

Brudzinski, M.R., Thruber, C.H., Hacker, B.R. & Engdahl, E.R., 2007. Global Prevalence of Double Seismic Zones. *Science*, 316, p.1472. doi:10.1126/science.1139204.

Campbell, M.E., Rowland, J.V., Wright, I.C. & Smith, I.E.M., 2007. Obilque rifting along the central and southern Kermadec Arc front (30-36S), SW Pacific. *Geochemisrty Geophysics Geosystems*, 8(1). doi:10.1029/2006GC001504.

Cande, S.C. & Stock, J., 2004. Pacific-Antarctic-Australian motion and the formation of the Macquire Plate. *Geophysics Journal International*, 157, pp.399-414.

Carlson, R.L. & Miller, D.J., 2003. Mantle wedge water contents estimated from seismic velocities in partially serpentinized peridotites. *Geophysical Research Letters*, 30(5), p.1250. doi:10.1029/2002GL016600.

Carter, L., Shane, P., Alloway, B., Hall, I.R., Harris, S.E., Harris, S.E. & Westgate, J.A., 2003. Demise of one volcanic zone and the birth of another - a 12 m.y. record of rhyolitic eruptions from New Zealand. *Geology*, 31, pp.493-96.

Chapple, W.M. & Forsyth, D.W., 1979. Earthquakes and bending of plates at trenches. *Journal of Geophysical Research*, 84(B12), pp.6729-49.

Davy, B., Horernle, K. & Werner, R., 2008. Hikurangi Plateau: Crustal structure, rift formation, and Gondwana subduction history. *Geochemsitry, Geophysics, Geosystems*, 9, p.Q07004.

Deering, C.D., Horton, T.W., Gravely, D.M. & Cole, J.W., 2012. Hornblende, cummingtonite, and biotite hydrogen isotopes: Direct evidence of slab-derived fluid flux in silicic magmas of the Taupo Volcanic Zone, New Zealand. *Journal of Volcanology & Geothermal Research*, 233-234, pp.27-36. doi:10.1016/j.jvolgeores.2012.04.010.

Dziewonski, A.M., Chou, T.-A. & Woodhouse, J.H., 1981. Determination of earthquake source parameters from waveform data for studies of global and regional seismicity. *Journal of Geophysical Research*, 86, pp.2825-52.

Eberhart-Phillips, D. & Bannister, S., 2010. 3-D imaging of Marlborough, New Zealand, subducted plate and strike-slip fault systems. *Geophysics Journal International*, 182, pp.73-96. doi:10.1111/j.1365-246X.2010.04621.x.

Eberhart-Phillips, D. & Chadwick, M., 2002. Three-dimensional attenuation model of the shallow Hikurangi subduction zone in the Raukumara Peninsula, New Zealand. *Journal of Geophysical Research*, 107(B2), p.2033. doi:10.1029/2000JB00046.

Eberhart-Phillips, D., Reyners, M., Bannister, S., Chadwick, M. & Ellis, S., 2010. Establishing a versatile 3-D seismic velocity model for New Zealand. *Seismological Research Letters*, 81(6), pp.992-1000.

Eberhart-Phillips, D., Ryeners, R., Chadwick, M. & Stuart, G., 2008. Three-dimensional attenuation strucutre of the Hikurangi subduction zone in the central North Island, New Zealand. *Geophysics Journal International*, 174, pp.418-34.

Engdahl, E.R., van der Hilst, R. & Buland, R., 1998. Global teleseismic earthquake relocation with improved travel times and procedures for depth determination. *Bulletin of the Seismological Society of America*, 88(3), pp.722-43.

England, P., Engdahl, R. & Thatcher, W., 2004. Systematic variation in the depths of slabs beneath arc volcanoes. *Geophysics Journal International*, 156, pp.377-408. doi:10.1111/j.1365-246X.2003.02132.x.

England, P.C. & Katz, R.F., 2010. Melting above the anhydrous solidus controls the location of volcanic arcs. *Nature*, 467, pp.700-04. doi:10.1038/nature09417.

Faccenda, M., Gerya, T.V. & Burlini, L., 2009. Deep slab hydration induced by bending-related variations in tectonic pressure. *Nature Geoscience*, 2, pp.790-93. doi:10.1038/NGEO656.

Giba, M., 2010. *The evolution of Tertiary normal faults in the Taranaki Basin, New Zealand*. Dublin: University College Dublin. unpublished PhD thesis.

Giba, M., Nicol, A. & Walsh, J.J., 2010. Evolution of faulting and volcanism in a back-arc basin and its implications for subduction processes. *Tectonics*, TC4020. doi: 10.1029/2009TC002634.

Gill, J., 1981. *Orogenic Andesites and Plate Tectonics*. New York: Springer.

Grevemeyer, I., Ranero, C.R., Flueh, E.R., Klaschen, D. & Bialas, J., 2007. Passive and active seismological study of bending-related faulting and mantle serpentinization at the Middle America trench. *Earth & Planetary Science Letters*, 258, pp.528-42. doi:10.1016/j.epsl.2007.04.013.

Hacker, B.R., Peacock, S., Abers, G.A. & Holloway, S.D., 2003. Subduction factory, 2. Are intermediate-depth earthquakes in subducting slabs linked to metamorphic dehydration reactions? *Journal of Geophysical Research*, 108(B1), p.2030. doi:10.1029/2001JB001129.

Hayward, B.W., Black, P.M., Smith, I.E.M., Ballance, P.F., Itaya, T., Doi, M., Takagi, M., Bergman, S., Adams, C.J., Herzer, R.H. & Robertson, D.J., 2001. K-Ar ages of

Early Miocene arc-type volcanoes in northern New Zealand. *New Zealand Journal of Geology & Geophysics*, 44, pp.285-311.

Henrys, S., Reyners, M., Pecher, I., Bannister, S., Nishimura, Y. & Maslen, G., 2006. Kinking of the subducting slab by esclator normal faulting beneath the North Island of New Zealand. *Geology*, 34(9), pp.777-80. doi:10.1130/G22594.1.

Hirth, G. & Kohlstedt, D., 2003. Rheology of the Upper Mantle and the Mantle Wedge: A view from the Experimentalists. In J. Eiler, ed. *Inside the Subduction Facory*. Geophysical Monograph 138: AGU. pp.83-105. doi:10.1029/138GM06.

Hochstein, M.P., 1995. Crustal heat transfer in the Taupo Volcanic Zone (New Zealand): comparison with other volcanic arcs and explanatory heat source models. *Journal of Volcanology & Geothermal Research*, 68, pp.117-51.

Holden, C.F., Bannister, S., Beavan, J., Cousins, J., Field, B., McCaffrey, R., McVerry, G., Reyners, M., Ristau, J., Samsonov, S. & Wallace, L., 2008. The Mw 6.6 Gisborne earthquake of 2007: Preliminary records and general source charaterisation. *Bulletin of the New Zealand society for Earthquake Engineering*, 4(4), pp.266-77.

Houghton, B.F., N, W.C.J., McWilliams, M.O., Lamphere, M.A., Weaver, S.D., Briggs, R.M. & Pringle, M.S., 1995. Chronology and dynamics of a silicic magmatic system: Central Taupo Volcanic Zone, New Zealand. *Geology*, 23(1), pp.13-16.

King, P.R. & Thrasher, G.P., 1996. Cretaceous-Cenozoic geology and petroleum systems of the Taranaki Basin. In *Institute of Geological & Nuclear Sciences Monograph 13*. Lower Hutt, New Zealand: Institute of Geological & Nuclear Sciences.

Kirby, S.H., Engdahl, E.R. & Denlinger, R., 1996. Intermediate-depth intraslab earthquakes and arc volcanism as physical expressions of crustal and uppermost mantle metamorphism in subducting slabs. In G.E. Bebout, D. Scholl, S.H. Kirby & J.P. Platt, eds. *Subduction: Top to Bottom*. Geophysical Monograph 96, Washington DC: AGU. pp.195-214.

Lallemand, S., Heuret, A. & Boutelier, D., 2005. On the relationships between slab dip, back-arc stress, upper plate absolute motion, and crustal nature in subduction zones. *Geochemistry, Geophysics, Geosystems*, 6(Q09006). doi: 10.1029/2005GC000917.

Li, C., van der Hilst, R.D., Engdahl, E.R. & Burdick, S., 2008. A new global model for P wave speed variations in Earth's mantle. *Geochemsitry, Geophysics, Geosystems*, 9(Q05018). doi: 10.1029/2007GC001806.

Mancktelow, N., 2008. Tectonic pressure: theoretical concepts and modelled examples. *Lithos*, 103, pp.149-77.

Manea, V. & Gurnis, M., 2007. Subduction zone evolution and low viscosity wedges and channels. *Earth & Planetary Science Letters*, 264, pp.22-45. doi: 10.1016/j.epsl.2007.08.030.

Manning, C.E., 2004. The chemistry of subduction-zone fluids. *Earth & Planetary Science Letters*, 223, pp.1-16. doi:10.1016/j.epsl.2004.04.030.

Masson, D.G., 1991. Fault patterns at outer rise trench walls. *Marine Geophysical Researches*, 13, pp.209-25.

McCulloch, M.T. & Gamble, J.A., 1991. Geochemical and geodynamical constraints on subduction zone magmatism. *Earth & Planetary Science Letters*, 102, pp.358-74.

Molnar, P. & Atwater, T., 1978. Interarc spreading and Cordilleran tectonics as alternatives related to the age of subducted lithosphere. *Earth & Planetary Science Letters*, 41, pp.330-40.

Mortimer, N., Gans, P.B., Palin, J.M., Meffe, S., Herzer, R.H. & Skinner, D.N.B., 2010. Location and migration of Miocene-Quarternary volcanic arcs in the SW Pacific region. *Journal of Volcanology & geothermal Research*, 190, pp.1-10. doi: 10.1016/j.jvolgeores.2009.02.017.

Peacock, S.M., 2001. Are the lower planes of double seismic zones caused by serpentine dehydration in subducting oceanic mantle? *Geology*, 29, pp.299-302. doi:10.1130/0091-7613.

Price, R.C., Stewart, R.B., Woodhead, J.D. & Smith, I.E.M., 1999. Petrogenesis of high-K magmas: evidence from Egmont Volcano, North Island, New Zealand. *Journal of Petrology*, 40, pp.167-97.

Pulford, A. & Stern, T., 2004. Pliocene exhumation and landscape evolution of central North Island: the role of the upper mantle. *Journal of Geophysical Research*, 109, p.F01016. doi:10.1029/2003JF000046.

Ranero, C.R., Phipps Morgan, J., McIntosh, K. & Reichert, C., 2003. Bending-related faulting and mantle serpentinization at the Middle America Trench. *Nature*, 425, pp.367-73. doi:10.1038/nature01961.

Ranero, C.R., Villasenor, A., Phipps Morgan, J. & Weinrebe, W., 2005. Relationship between bend-faulting at trenches and intermediate-depth seismicity. *Geochemistry Geophysics Geosystems*, 6(12), p.Q12002. doi:10.1029/2005GC000997.

Reyners, M., 1983. Lateral segmentation of the subducted plate at the Hikurangi Margin, New Zealand: seismological evidence. *Tectonophysics*, 96, pp.203-23.

Reyners, M. & Eberhart-Phillips, D., 2009. Small earthquakes provide insight into plate coupling and fluid distribution in the Hikurangi subduction zone, New Zealand. *Earth & Planetary Science Letters*, 282, pp.299-305. doi:10.1016/j.epsl.2009.03.034.

Reyners, M., Eberhart-Phillips, D. & Bannister, S., 2011. Tracking repeated subduction of the Hikurangi Plateau beneath New Zealand. *Earth & Planetary Science Letters*, 311(1-2), pp.165-71. doi:10.1016/j.epsl.2011.09.011.

Reyners, M.E., Eberhart-Phillips, D., Stuart, G. & Nishimura, T., 2006. Imaging subduction from the trench to 300 km depth beneath the central North Island, New Zealand with Vp and Vp/Vs. *Geophysics Journal International,* 165, pp.565-83.

Ristau, J., 2008. Implementation of routine Regional Moment Tensor analysis in New Zealand. *Seismological Research Letters*, 79(3), pp.400-15. doi:10.1785/gssrl.79.3.400.

Ristau, J., 2009. Comparison of magnitude estimates for New Zealand earthquakes: Moment magnitude, local magnitude, and teleseismic body-wave magnitude. *Bulletin of the Seismological Society of America*, 99(3), pp.1841-52. doi:10.1785/0120080237.

Royden, L.H. & Husson, L., 2006. Trench motion, slab geometry, and viscous stresses in subduction systems. *Geophysics Journal International*, 167, pp.881-905. doi:10.1111/j.1365-246X.2006.03079.x.

Rupke, L.H., Phipps Morgan, J., Hort, M. & Connolly, J.A.D., 2004. Serpentine and the subduction water cycle. *Earth & Planetary Science Letters*, 223, pp.17-34. doi:10.1016/j.epsl.2004.04.018.

Schmidt, M.W. & Poli, S., 1998. Experimentally based water budgets for dehydrating slabs and consequences for arc magma generation. *Earth & Planetary Science Letters*, 163, pp.361-79.

Sdrolias, M. & Muller, R.D., 2006. Controls on back-arc basin formation. *Geochemistry, Geophysics, Geosystems*, 7, p.Q04016. doi:10.1029/2005GC001090.

Stern, T.A., 1987. Asymmetric back-arc spreading, heat flux and structure associated with Central Volcanic Region, New Zealand. *Earth & Planetary Science Letters*, 85, pp.265-76.

Stern, T.A., 2009. Reconciling short- and long-term measures of extension in continental back-arcs: heat flux, crustal structure and rotations within the central North Island, New Zealand. In U. Ring & B. Wernicke, eds. *Extending a Continent: Architecture, Rheology and Heat Budget*. London, Special Publications 321: Geological Society. pp.73-87. doi:10.1144/SP321.4.

Stern, T.A., Stratford, W.R. & Salmon, M.L., 2006. Subduction evolution and mantle dynamics at a continental margin: Central North Island, New Zealand. *Review of Geophysics*, 44, p.RG4002. doi:10.1029/2005RG000171.

Stipp, J.J., 1968. *The geochronology and petrogenesis of the Cenozoic volcanics of North Island, New Zealand*. Canberra, Australia: Australian National University. Unpublished PhD Thesis.

Syracuse, E.M. & Abers, G.A., 2006. Global compliation of variations in slab depth beneath arc volcanoes and implications. *Geochemistry, Geophysics, Geosystems*, 7, p.Q05017. doi:10.1029/2005GC001045.

Taylor, B., 2006. The single largest oceanic plateau: Ontong Java-Maihiki-Hikurangi. *Earth & Planetary Science Letters*, 241, pp.372-80. doi:10.1016/j.epsl.2005.11.049.

Taylor, B., Zellmer, K., Martinez, F. & Goodlife, A., 1996. Sea-floor spreading in the Lau back-arc basin. *Earth & Planetary Science Letters*, 144, pp.35-40.

van der Hilst, R.D., 1995. Complex morphology of subducted lithosphere in the mantle beneath the Tonga trench. *Nature*, 374, pp.154-57. doi:10.1038/374154a0.

van Keken, P.E., 2003. The structure and dynamics of the mantle wedge. *Earth & planetary Science Letters*, 215, pp.323-38. doi:10.1016/S0012-821X(03)00460-6.

Wada, I. & Wang, K., 2009. Commondepth of slab-mantle decoupling: Reconciling diversity and uniformity of subduction zones. *Geochemistry Geophysics Geosystems*, 10(10), p.Q10009. doi:10.1029/2009GC002570.

Wallace, L.M., Beavan, J., McCaffrey, R. & Darby, D., 2004. Subduction zone coupling and tectonic block rotations in the North Island, New Zealand. *Journal of Geophysical Research*, p.B12406. doi:10.1029/2004JB003241.

Webb, T.H. & Anderson, H., 1998. Focal mechanisms of large earthquakes in the North Island of New Zealand: slip partitioning at an oblique active margin. *Geophysics Journal International*, 134, pp.40-86.

Wiemer, S., 2001. A software package to analyze seismicity: ZMAP. *Seismological Research Letters*, 72(2), pp.374-82.

Wiemer, S. & Wyss, M., 2000. Minimum magnitude of completeness in Earthquake Catalogs: Examples from Alaska, the Western United states, and Japan. *Bulletin of the Seismological Society of America*, 90(4), pp.859-69.

Wilson, C.J.N., Gravely, D.M., Leonard, G.S. & Rowland, J.V., 2008. Volcanism in the central Taupo Volcanic Zone, New Zealand: tempo, styles and controls. In T. Thordarson et al., eds. *Studies in Volcanology: The Legacy of George Walker*. Special Publication of IAVCEI 2, London: Geological Society. pp.225-47.

Wilson, C.J.N., Houghton, B.F., McWilliams, M.O., Lanphere, M.A., Weaver, S.D. & Briggs, R.M., 1995. Volcanic and structural evolution of Taupo Volcanic Zone, New Zealand: a review. *Journal of Volcanology & Geothermal Research*, 68, pp.1-28.

Wilson, C.J.N., Rogan, A.M., Smith, I.E.M., Northey, D.J., Nairn, I.A. & Houghton, B.F., 1984. Caldera volcanoes of the Taupo Volcanic Zone, New Zealand. *Journal of Geophysical Research*, 89(B10), pp.8463-84.

Wright, I.C., 1997. Morphology and evolution of the remnant Colville and active Kermadec arc ridges south of 33 30'S. *Marine Geophysical Research*, 19, pp.177-93.

Wright, I.C. & Gamble, J.A., 1999. Southern Kermadec submarine caldera volcanoes (SW Pacific): Caldera formation by effusive and pyroclastic eruption. *Marine Geology*, 161, pp.207-27.

Chapter 5

Geometry of the subducting Pacific plate along New Zealand's Hikurangi subduction margin since 20 Ma

Abstract

Evolution of the subducting slab geometry beneath the North Island, New Zealand, has been investigated using a combination of published arc-type volcanic ages and the locations of earthquakes in the subducting Pacific plate. Present day arc-slab relations show the depth to the slab beneath active arc-front volcanoes is, on average, 85 km beneath the central North Island. Arc-front volcanoes have migrated southeast by 150 km in the last 8 Ma (185 km since 16 Ma) sub-parallel to the present active arc. Migration of the arc is interpreted to mainly reflect slab rollback northeast of New Zealand along the Tonga-Kermadec subduction system and fixed hinge slab steepening beneath the central North Island. The strike of the Pacific plate beneath the North Island, imaged by Benioff zone seismicity (50-200 km) and positive mantle velocity anomalies (200-600 km) is parallel to the northeast trend of arc-front volcanism. Arc parallelism since 16 Ma is consistent with the view that the subducting plate beneath the North Island has not rotated clockwise about vertical axes. The stability of arc-front trends and strike of the slab contrasts with clockwise vertical-axis rotations of $\geq 30^{o}$ over the last 10 Myr of the overriding plate along the eastern and southern Hikurangi margin. The variable rotation rates may be accounted for by differential interplate slip on the subduction thrust along the Hikurangi margin (higher in the north than the south). Acceleration of arc-front migration rates (~4 mm/yr to ~18 mm/yr), eruption of high Mg# andesites, increasing eruption frequency and size, and uplift of the over-riding plate indicate an increase in the hydration, temperature, and size of the mantle wedge beneath of the central North Island from ~7 Ma.

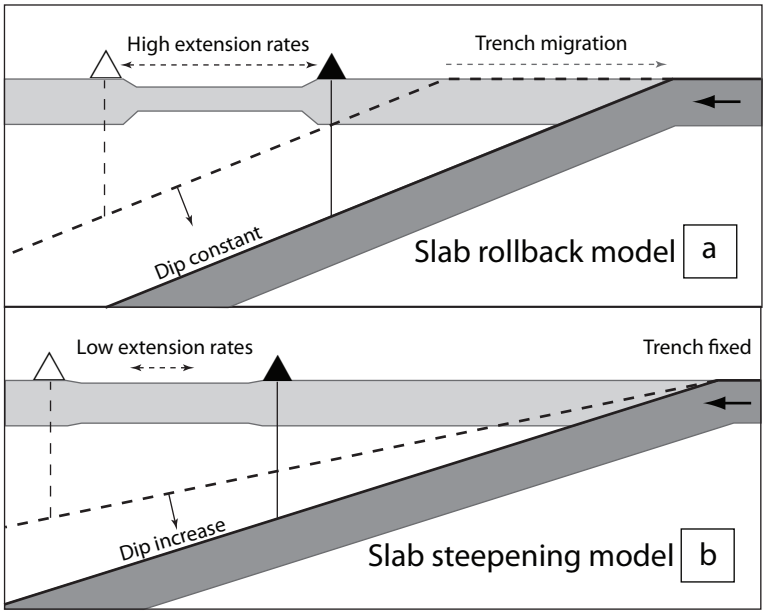

Figure 1. Schematic end-member models for the trenchward migration of arc volcanism through the evolution of subducting slab geometry. (a) Trenchward rollback of the subduction hinge (e.g. Molnar & Atwater, 1978; Schellart, 2005). (b) Slab steepening with fixed trench location.

1. Introduction

The geometry of plate boundaries and the relative motions of juxtaposed plates typically change on timescales of millions to tens of millions of years. Along many subduction margins, the strike and/or dip of the down-going plate has changed through time (Walcott, 1987; Gutscher et al., 2000; Sdrolias & Muller, 2006). Spatial and temporal changes in slab geometry have been attributed to a number of factors including variations in; the age, thickness and composition of the subducting plate, the rate and total amount of subduction, and the viscosity of the mantle wedge (Molnar & Atwater, 1978; Gutscher et al., 2000; Billen & Gurnis, 2001; Lallemand et al., 2005; Royden & Husson, 2006; Sdrolias & Muller, 2006; Manea & Gurnis, 2007). As the location of arc volcanism and style of upper plate deformation is dependent on the interplay between some or all of these factors (England et al., 2004; Syracuse & Abers, 2006; Wallace et al., 2009a), understanding how the slab geometry changes through time leads to a more complete understanding of mantle wedge processes and the underlying causes of upper plate deformation.

Slab rollback, the seaward migration of the subduction-hinge induced by the negative buoyancy and gravitational instability of the subducting plate as it founders and sinks into the mantle, is considered one of the principal mechanisms responsible for the migration of volcanic arcs and back-arc extension in over-riding plates at subduction margins (Fig. 1) (Molnar & Atwater, 1978; Lallemand et al., 2005; Schellart, 2005; Sdrolias & Muller, 2006; Manea & Gurnis, 2007). Back-arc extension and associated vertical-axis rotations have also been attributed to upper plate processes, including continental collision at subduction terminations (Wallace et al., 2009a), and questions remain as to how much upper-plate deformation can be directly attributed to changes in the geometry of the underlying plate? The locations and geometries of relict volcanic arcs preserve changes in the geometry of the subducting slab over time and provide a means of assessing to what extent changes in the slab geometry influence extension and vertical-axis rotation of the over-riding plate.

In this paper, we examine arc migration in relation to the geometry and kinematics of subduction over the last 20 Ma along the Hikurangi subduction margin, North Island, New Zealand (Fig. 2). The North Island is situated in a transition zone between oblique ocean-ocean subduction along the Tonga-Kermadec trench and continent-continent transpression along the Alpine Fault in the South Island. Presently,

the thickened oceanic crust (12-15 km) of the Hikurangi Plateau (Davy et al., 2008) is subducting obliquely westwards beneath the east coast of the North Island at rates of 39-47 mm/yr (Beavan et al., 2002; De Mets et al., 2010). The modern plate boundary configuration has formed since the Eocene through the partial reactivation of the extinct Gondwana subduction margin in the North Island and development of the Alpine Fault through the South Island (King, 2000). Paleomagnetic data from the emergent North Island forearc show clockwise vertical-axis rotations of up to 90° (relative to a stable Australian Plate) associated with subduction of the Pacific plate (Wright & Walcott, 1986; Nicol et al., 2007). Tectonic reconstructions of the Hikurangi margin, either implicitly or explicitly, suggest that the dip direction of Pacific plate also rotated clockwise over the last 20 Myr. Since the Early Miocene arc volcanism has migrated southeast across the North Island (Stipp, 1968; Brothers, 1984; Adams et al., 1994; Briggs et al., 2005), and while the migration of arc volcanism is generally accepted, the timing, orientation, and relationship to the trench has been widely debated (Ballance, 1976; Brothers, 1984; Kamp, 1984; Ballance, 1999; Kear, 2004; Stern et al., 2006; Booden et al., 2011; Schellart, 2012).

We present a synthesis of historical earthquake catalogue data, mantle tomography, and arc volcanism along the Hikurangi subduction margin to place constraints on the geometry of the slab since the early Miocene (~20 Ma). The distribution, age and composition of volcanism in the North Island are from published and unpublished data, the main additional contributions to previous studies coming from the Taranaki Basin. The data provide insights into the evolution of the slab geometry and mantle wedge beneath the North Island since the Early Miocene (~20 Ma). We show the first-order trend of arc volcanism and the strike of the interpreted slab to depths of 600 km vary little since 16 Ma and contrast with the ≥ 30° clockwise vertical-axis rotation of the central and southern Hikurangi forearc over this time. A rapid southeast parallel migration of volcanism indicates steepening and roll back of the slab since ~7 Ma accompanied by the development of a mantle wedge beneath the central North Island.

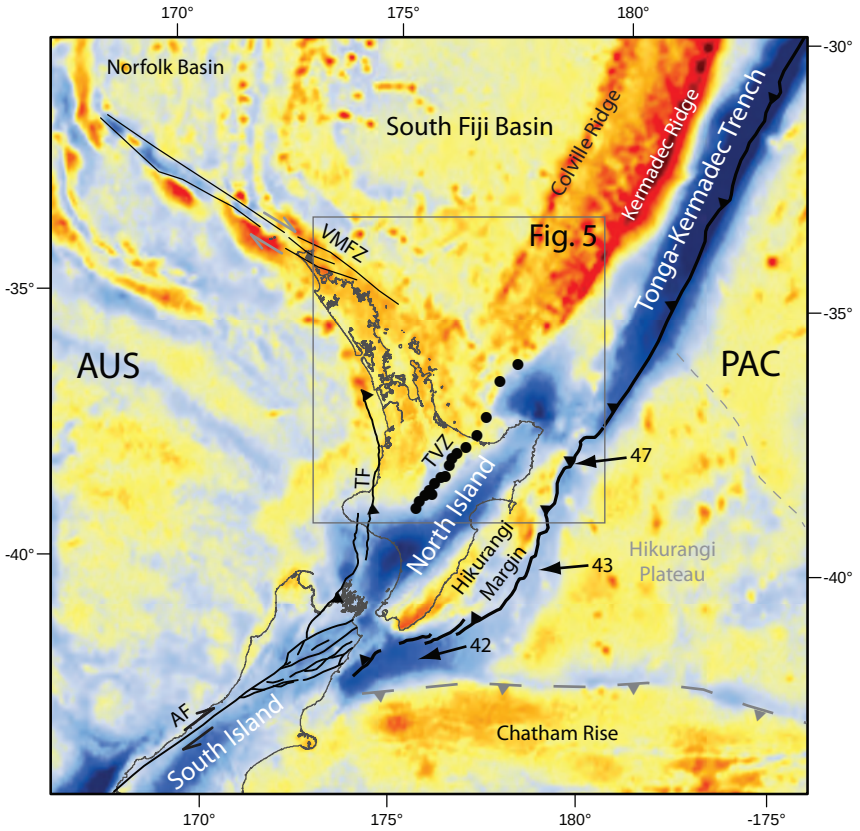

Figure 2. Present tectonics and arc-front volcanism of the New Zealand plate boundary superimposed on satellite Free Air gravity from Sandwell & Smith (2009). The Hikurangi subduction margin forms a transition from oblique westward ocean-ocean subduction along the Tonga Kermadec trench to continental collision and transform motion along the Alpine Fault. Main Miocene to Recent crustal scale faults (black lines); AF = Alpine Fault, TF = Taranaki Fault, VMFZ = Vening Meinesz Fracture Zone. Present arc front volcanic centres (black filled circles), TVZ = Taupo Volcanic Zone. Pacific plate motion relative to fixed Australian plate (black arrows) in mm/yr (Beavan et al., 2002).

2. Subduction geometry and arc volcanism

2.1 Contemporary geometry of the subducting Pacific plate

To establish the present relationship between arc volcanism and the geometry of the subducting slab we use the top of Benioff zone seismicity as a proxy for the top of the down going plate (Nakajima et al., 2001; England et al., 2004; Syracuse & Abers, 2006; Eberhart-Phillips et al., 2008). Contours of the top of the Benioff zone to 250 km beneath the North Island and northern South Island are based on hypocentres from the GeoNet earthquake catalogue (2001-2009) > 50 km in depth (N=32370) relocated using the three-dimensional velocity model of New Zealand (3DNZ) (Fig. 3a and b; Appendix Fig. 5) (Eberhart-Phillips et al., 2010). To ensure depth accuracy only GeoNet events recorded by ≥ 6 stations, with travel time residuals ≤ 0.3 s, and distances of 2 focal lengths from the nearest station were relocated (Reyners et al., 2006). A comparison between the original GeoNet catalogue (from which previous interpretations of slab geometry are based) and the relocated hypocentres ($M_L \geq 3.6$, N=3012) shows a systematic westward relocation (azimuth 274 ± 25°, mean distance 96 ± 50 km, mean depth -9 ± 12 km) resulting in a minor shallowing of the slab dip (~5º) below 100 km depth and, due to a reduction in scatter, an overall sharpening of the Benioff zone for relocated events. By comparison, the top of the slab inferred from the global EHB earthquake catalogue by Syracuse & Abers (2006) varies between 5 to 40 km deeper than the upper surface of the slab inferred with the local relocated GeoNet catalogue (e.g. Fig. 3d). Despite differences in depth, the interpreted top of the slab have similar dips over the depth range 50-200 km for different velocity models. For the relocated Geonet data used here we estimate uncertainties in the upper surface of the Benioff zone are ± 5 km to 100 km depth and ± 10 km at depths > 100 km.

To define the present along strike geometry of the slab the top of the northwest dipping Benioff zone is visually estimated in map view using 10 km thick seismicity slices, we locate the top of the slab by assuming that ~95% of events lie southeast of this surface and within the subducting plate (e.g. Fig. 3a; Appendix Fig. 5) (Syracuse & Abers, 2006). Seismicity 75 km either side of section lines perpendicular to the regional strike of the slab (040°) has been used to estimate changes in the mean dip of the slab along strike (Fig. 3b-d) (Eberhart-Phillips et al., 2010).

Seismicity in the slab which defines the geometry of the Benioff zone is generally limited to depths < 250 km beneath the North Island. At depths greater than

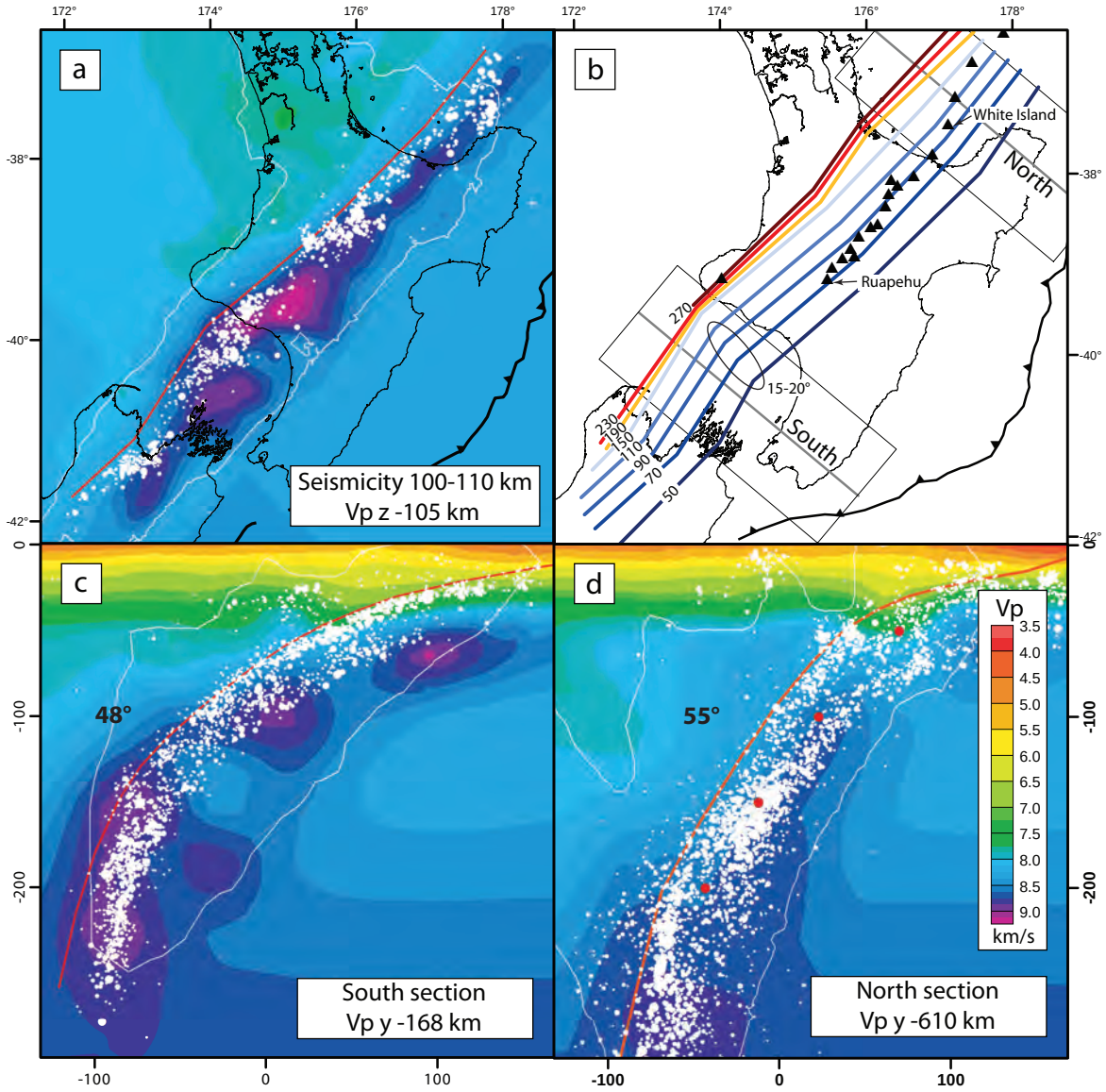

Figure 3. Subducted Pacific plate geometry from relocated Benioff zone seismicity. (a) Relocated seismicity (2001-2009 $M_L \geq 2.5$) (white filled circles) and P-wave velocity model of the subducting Pacific plate at a depth of ~110 km . The western limit of seismicity is used to approximate the upper surface of the slab (red line). P-wave velocity model (Vp) of Eberhart-Phillips et al. (2010) showing the high velocity slab, meaningful velocity information contained within spread function contour ≤ 3 (white lines). (b) Interpretation of slab contours (depth in km) (coloured lines) in relation to active arc volcanoes (black triangles). Sections of seismicity (thin black lines) and location of Vp section line (grey line) for (c) and (d). (c) South section showing seismicity with slab surface interpretation . (d) North section with key same as (c). The slab surface of Syracuse & Abers (2006) (red filled circles) projected from 60 km to south shown for comparison. Note the difference in slab curvature between southern and northern sections.

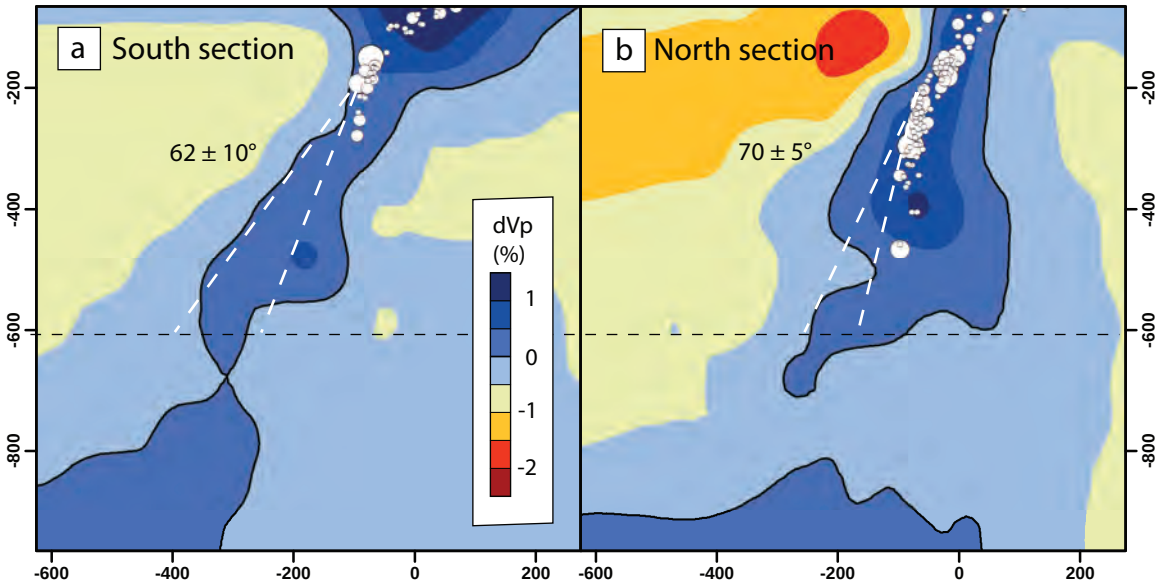

Figure 4. Mantle velocity anomaly sections through the North Island. Global mantle tomography (version MIT-P08) primarily incorporates data from the EHB catalogue and is inverted for 3D variations in P-wave velocity (dVp) resulting in a spatial resolution of ~100 km in well sampled regions (for details of the method and data used refer to Li et al., 2008). Sections (a) and (b) are vertical extensions of those shown in Fig. 3c-d, South and North, respectively (for location see Fig. 3b) and include relocated intermediate depth seismicity (white filled circles). Positive mantle anomalies (dVp $\geq$ 0 % deeper blue colours) are inferred to represent the aseismic slab at depth. Slab dips shown on each section were estimated from 200-600 km depth.

250 km the presence and geometry of an aseismic slab can be inferred from global mantle P-wave tomography (Li et al. 2008 version MIT-P08). We use the positive mantle velocity anomaly contour (dVp ≥ 0%) as a proxy for the aseismic portion of the subducted slab (Fig. 4). Velocities determined from global mantle P-wave tomography and local velocity model (3DNZ) (Eberhart-Phillips et al., 2010) are similar and support the use of this proxy. The Benioff zone beneath the North Island correlates well with the location of positive mantle velocity anomalies. The positive mantle velocity anomaly contour (dVp ≥ 0%) contain ≥85% of the EHB and ≥80% of the relocated GeoNet earthquake hypocentres from depths of ~70 to 350 km beneath the North Island and are here inferred to show the general strike, dip, and location of the slab beneath New Zealand in regions not associated with seismicity (e.g. Fig. 4b; Appendix Fig. 6). By combining the upper surface of the slab defined by the Benioff zone with the positive mantle velocity contour we show the distribution of the subducted slab beneath New Zealand over a greater length scale than previous studies, importantly inferring the presence of an aseismic slab beneath the South Island (Reyners et al., 2011) and showing the continuity of the slab to at least 600 km beneath the North Island (Fig. 4; Appendix Fig. 6).

2.2 Arc volcanism in the over-riding Australian Plate

To estimate the location, depth, and geometry of the subducting slab over the last 20 Myr we map the location and the maximum age of subduction-related volcanism onshore and offshore of the North Island (Fig. 5). To complement these volcanic age data from continental New Zealand, we also incorporate recent age data that place constraints on island arc and seafloor formation to the north of New Zealand (Mortimer et al., 2010).

Volcanic centres mapped and dated in this study mainly formed Island arcs above the subducting Pacific plate. The Island arc interpretation is supported by the observed incompatible trace element enrichment (e.g. Rb, Ba, and K), negative anomalies for the high field strength elements such as Nb and Ti, and the full spectrum of low- to high-K calc-alkaline basaltic to rhyolitic compositions commonly associated with subduction-related volcanism (Bergman et al., 1992; Price et al., 1999; Briggs et al., 2005; Booden et al., 2010). Island arc compositions presently sampled in the western North Island differ from those in the east by having more primitive Sr-Nd

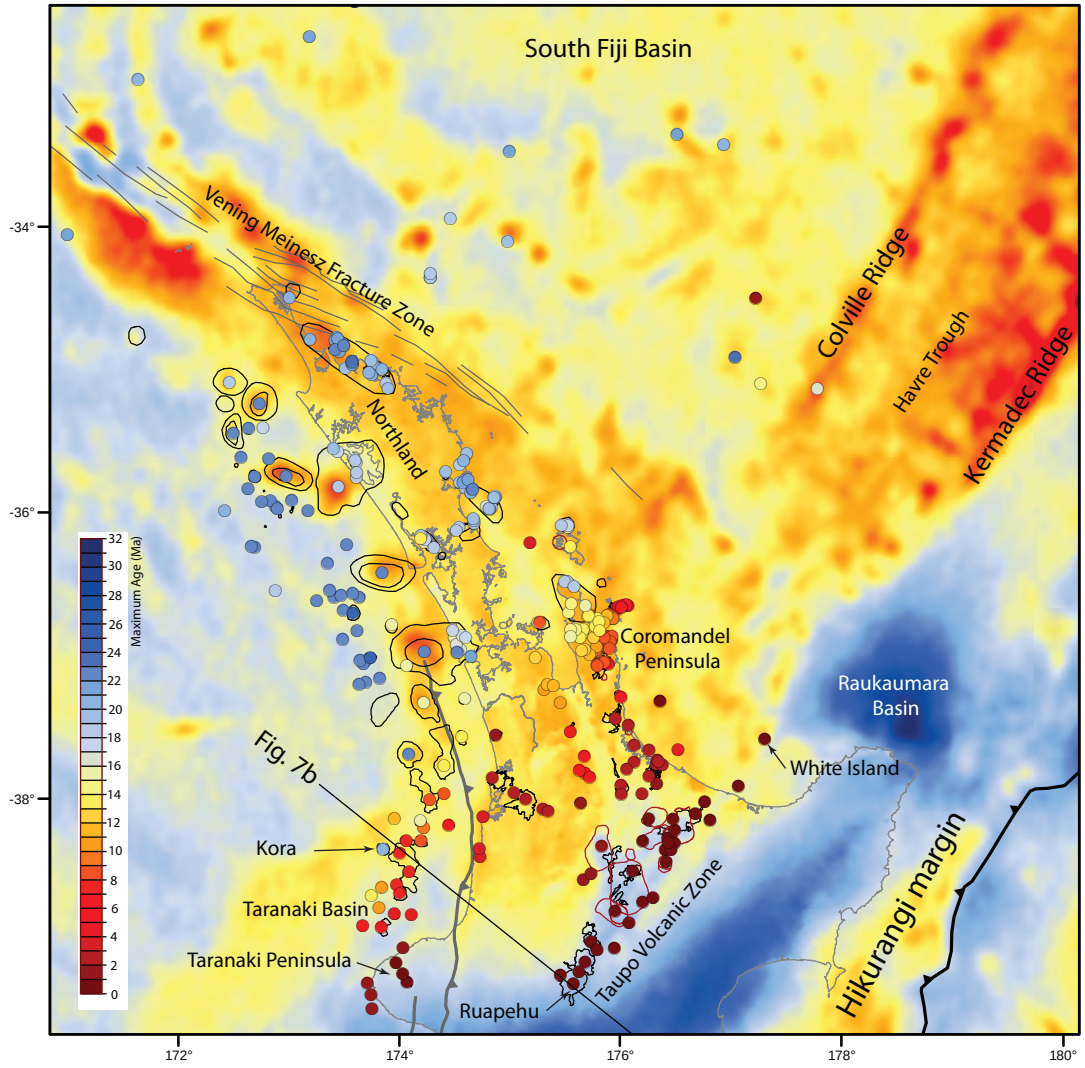

Figure 5. Maximum age of arc volcanism across onshore and offshore North Island. See main text for references. From ~20 Ma there is a southeastward younging in the maximum age of arc volcanism towards the Taupo Volcanic Zone (e.g. Brothers, 1984). Ages from seamounts in SW Fiji Basin cluster around ~20 Ma (Mortimer et al., 2007). Right lateral displacement along the Vening Meinesz Fracture Zone inferred to have emplaced Northland Plateau and Colville Ridge in current location by ~16 Ma (Mortimer et al., 2010; Herzer et al., 2011).

isotopic ratios, indicative of greater mantle source depletion and a lower degree of crustal contamination, the likely the result of decreases in crustal thickness from east to west (Bergman et al., 1992; Price et al., 1999; Booden et al., 2011). The most-recent back-arc volcanism in the western North Island is associated with eroded and active high-K calcalkaline stratovolcanoes of the onshore Taranaki Peninsula. Taranaki volcano compositions are consistent with lower degrees of partial melting and greater influence of slab fluids than those associated with the present arc-front ~130 km to the east (Price et al., 1999). These Taranaki volcanoes show distinctive Island arc chemistry (e.g. low Ce/Pb ratios and high Ba/Nb ratios relative to N-MORB) and do not appear to require more complex models involving crust or magmas derived from lithospheric mantle (Price et al., 1999). The presence of Island arc volcanism in the Taranaki Basin is also constrained by drillcore samples from a long-lived submarine low- to medium-K calcalkaline stratovolcano complex (Kora) (Fig. 5) (Bergman et al., 1992). Further north in offshore Northland, volcanic centres overlap in space and time with onshore volcanoes that also have Island arc compositions and are considered to be Island arc (Hayward et al., 2001).

The locations and ages of volcanoes have been used to track the migration of the arc across northern New Zealand since ~20 Ma. The temporal and spatial analysis of volcanic arc migration in relation to slab geometry assumes magma ascent from source to surface is effectively instantaneous over the million-year timescales investigated. This assumption is reasonable given U-Th isotope disequilibria from arc lavas indicate transport times from slab-fluid release to eruption can be less than a hundred thousand years (Turner & Hawkesworth, 1997). Individual volcanic centres (particularly in the Taranaki Basin and the northern Coromandel Peninsula) record sporadic episodes of eruption over periods as long as 12 Myr, though the majority were active for $\leq$ 3 Myr (Bergman et al., 1992; Adams et al., 1994; Houghton et al., 1995; Hayward et al., 2001; Briggs et al., 2005; Giba et al., 2010). The age data used in this study is from published (Briggs et al., 1989; Bergman et al., 1992; Black et al., 1992; Adams et al., 1994; Alloway et al., 1995; Burt et al., 1996; Herzer, 1995; Houghton et al., 1995; Wilson et al., 1995) (Hayward et al., 2001; Gamble et al., 2003; Briggs et al., 2005; Mortimer et al., 2007; Townsend et al., 2008; Cameron et al., 2010; Mortimer et al., 2010; Leonard et al., 2011) and unpublished sources (Stipp, 1968; Middleton, 1983; Robertson, 1983; Smith, 1986; Henry, 1991; Giba, 2010) (Fig. 5).

The majority of onshore samples have whole rock chemical analyses and radiometric dates (Ar-Ar, K-Ar) with mean standard errors < ± 0.6 Ma. Radiometric ages from volcanic centres in offshore Northland, offshore Taranaki Basin and the South Fiji Basins are rare. In the offshore Northland and Taranaki Basins the age of volcanic centres are mainly constrained by the age of sedimentary rocks that underlie, onlap, and drape volcanic centres imaged on 2D and 3D seismic-reflection lines (Herzer, 1995; Giba et al., 2010). The ages of stratigraphy that enclose the volcanic centres were determined by correlation of seismic reflectors to wells and typically have uncertainties of ±1-2 Myr (Giba et al., 2010). Where radiometric and stratigraphically correlated ages have been determined for the same location (e.g. Kora) (Fig. 5), the maximum age for the onset of volcanism is within error (Bergman et al., 1992; Giba, 2010). To be considered active over a particular time interval the age of a volcanic centre (including uncertainties) must be partly or entirely contained within the time interval of interest. Sensitivity tests suggest that varying the duration and absolute limits of these time windows down to as little as 1 Myr intervals does not significantly modify our first-order conclusions on the evolution of arc trends and plate geometry.

3. Contemporary slab geometry and arc volcanism

The relationship between the present geometry and motion of the slab and the distribution of arc volcanism provide information on the evolution of slab geometry and its relationship to upper plate deformation. The present geometry of the slab is defined by the Benioff zone and by positive mantle velocity anomalies. Consistent with previous studies (Eberhart-Phillips & Bannister, 2010), we interpret the slab as a continuous unbroken feature extending from the active subduction zone in the northern North Island to the southern limit of intermediate depth seismicity in the northern South Island (chapter 6). In map view, contours of the top of the Benioff zone beneath the northern and central North Island generally strike ~040-050°, sub-parallel to the ~036° trend of active arc-front volcanoes, and oblique to the 020-030° trend of the east coast and structural fabric of the upper plate in the southern North Island (Fig. 3b) (Mortimer, 2004). Lateral bends or segmentation of the subducting plate beneath the North Island have previously been inferred from the distribution and trend of seismicity in the Benioff zone (Fig. 3d) (Reyners, 1983; Robinson, 1986). A pronounced 15-20° trenchward inflection of the contoured slab surface is interpreted here in the southern

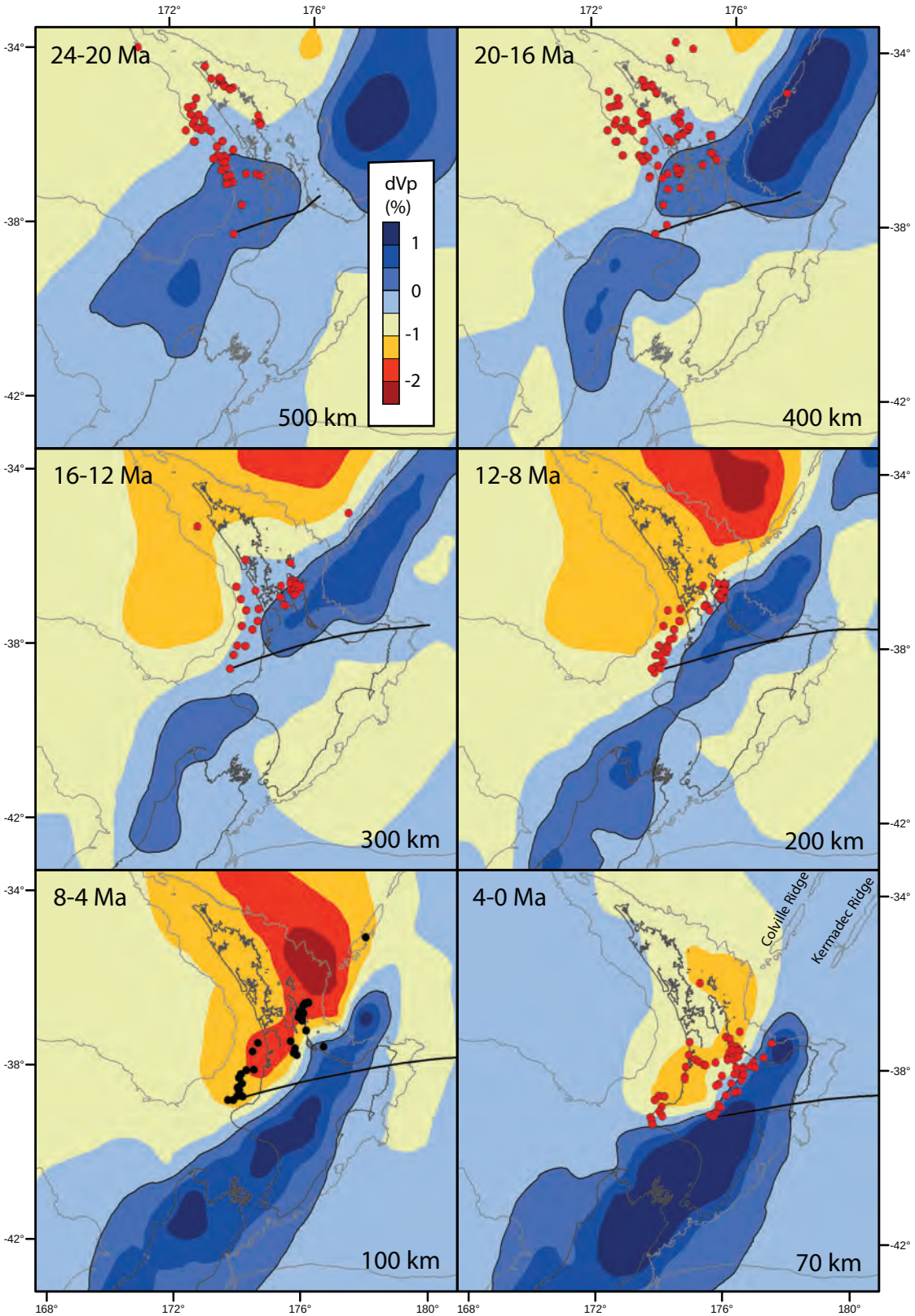

Figure 6. Active arc volcanism (red or black filled circles) across onshore and offshore North Island since the Early Miocene superimposed on mantle velocity anomalies (Li et al., 2008) at depth. See main text for volcanic age references. Alignment of eastern-most active arc volcanism trends sub-parallel to the underlying positive velocity anomalies (dVp ≥ 0%) (i.e. subducted slab). The trend of positive velocity anomalies (dVp ≥ 0%) (blue colours) in each depth slice approximate trend of trench during the associated time interval. Relative motion path of Pacific plate relative to a fixed Australian plate (black line) calculated from Cande & Stock (2004) from 33 Ma to youngest age in time interval indicates an approximate motion vector to sub-arc position.

North Island (~40°S). This inflection has been interpreted by Robinson (1986) to reflect a ~7 km downward step to the south in the top of the slab at a depth of ~50 km.

The average dip of the slab between 50-200 km depth (Syracuse & Abers, 2006), decreases southwards by ~7° from 55° in the north section to 48° in the south section (Fig. 3c,d) and is consistent with a southward increase in the radius of curvature for the slab between depths of 15 to 45 km (Ansell & Bannister, 1996). The along strike decrease in slab dip is also supported by depth-converted seismic reflection profiles of the shallow plate interface (5-18 km depth) beneath the accretionary prism where dips of ~10-18° in the northern Hikurangi margin shallow southwards to ~6° (Barker et al., 2009). This southward shallowing of the slab may be due to the presence of stronger, thicker lithosphere associated with the Hikurangi Plateau to the south and/or southward decreasing convergence rates (Wallace et al., 2009b).

Positive mantle velocity anomalies (dVp ≥ 0%) provide a first-order estimate of the location and trend of the subducted slab beneath the Benioff zone (van der Hilst, 1995). The aseismic slab extends to depths of at least 600 km beneath the North Island and to depths of ~250 km beneath the South Island, ≥ 200 km south of the southern limit of slab seismicity (Li et al., 2008) (Fig. 4 and 6). The depth extent and trend of the tomographically imaged slab is supported by deep earthquakes (~600 km) beneath the western North Island (Boddington et al., 2004) (Appendix Fig. 6), while the inference of an aseismic slab extending to at least 43°S beneath the South Island is consistent with the fossil Gondwana slab imaged by a deep seismic reflection line beneath the Chatham Rise at this latitude (Davy et al., 2008) (Appendix Fig. 4). The first-order strike of the slab to depths of 600 km is northeast, similar to the present day trend of the margin (Fig. 6). In cross section, positive mantle velocity anomalies indicate a general southward decrease in slab dip of up to ~20º (70 ± 5° to 62 ± 10° from northern to southern Hikurangi margin, respectively) along the margin between depths of 200 to 600 km (Fig. 4).

The active arc-front in the North Island is 85 ± 10 km vertically above the subducting slab, decreasing systematically from ~100 km beneath White Island to 75 km beneath Ruapehu (Fig. 3b). The depth to the slab in the North Island is consistent with global compilations where 50% of all arc volcanoes lie between 85 and 119 km above the subducting slab (median 100 km) (Syracuse & Abers, 2006). We therefore assume that a 90 ± 15 km vertical arc-front to slab separation has also applied for at least the last 16 Ma along the Hikurangi Margin and that arc-front locations at different

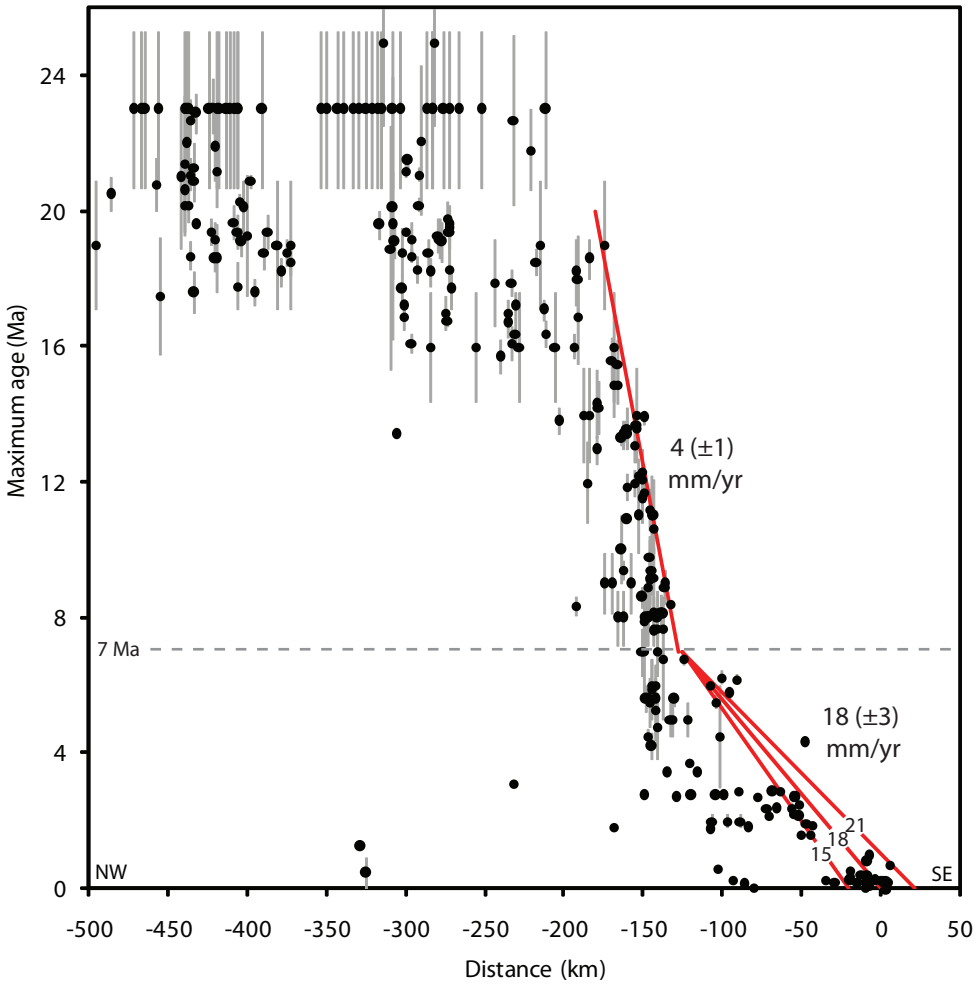

Figure 7. Maximum age of arc volcanism at distances normal to the strike of the active arc front. Migration rate of southeastern-most volcanic centres (red lines) accelerates from ~4 to 18 mm/yr at about 7 Ma (convergence of red lines and dashed grey line). Linear regression of arc front maximum ages from 7 Ma to present indicates a rate of ~19 mm/yr (R^2 0.92).

times provide a proxy for the ~90 km depth contour on top of the slab. Because of variations in the vertical arc-front to slab separation along the Hikurangi margin (± 10 km) and uncertainties in depth to the upper surface of the slab (± 5 km), the location of the ~90 km depth contour can only be considered first-order.

4. Arc migration

Volcanic arcs indicate the presence of an underlying subducting slab (Syracuse & Abers, 2006). The migration of arc volcanism indicates temporal changes in the slab geometry (dip and/or strike) and thermal structure of the mantle wedge. These changes have generally been related to changes in the geometry (dip and/or strike) of the underlying slab (Brothers, 1984; Gutscher et al., 2000b). Global compilation of arc-slab relations show the depth to the slab beneath arc-front volcanism systematically varies on average by less than a few ten's of kilometres within arc segments (Syracuse & Abers, 2006) and as the alignment of arc-front volcanoes is sub-parallel to the strike of the underlying slab, changes in the location and strike of arc-front volcanism over time can be used to infer changes in sub-arc slab geometry (Manea & Gurnis, 2007).

Previous studies have utilized the trend and southeast migration of North Island onshore volcanic arcs to infer evolution in geometry of the subducting slab since Early Miocene (e.g., Ballance, 1976; Brothers, 1984). These studies point to a general steepening of a westward dipping slab with time, however the narrow width of the northern North Island, combined with the limited number of offshore samples, resulted in ambiguous arc-front trends through the North Island prior to 2 Ma (Brothers, 1984; Stern et al., 2006). To overcome previous difficulties in defining ancient arc-front locations and trends since 20 Ma, we have collated a large data set of ages for offshore and onshore volcanic centres; importantly these include higher resolution age estimates for volcanism in the Taranaki Basin (Giba, 2010; Giba et al., 2010) than previously available and recently published radiometric ages and compositions from the South Fiji Basin and Colville Ridge (Mortimer et al., 2007, 2010) (Fig. 5). Prior to 20 Ma, there is on-going debate as to the polarity of subduction that resulted in the close spatial and temporal relationships between emplacement of allochthons across the north-eastern continental margin of the North Island and northwest-southeast aligned Northland arc in the Early Miocene (Herzer, 1995; Hayward et al., 2001; Mortimer et al., 2007; Booden

et al., 2011; Schellart, 2012). While outside the scope of this paper, we discuss subduction polarity and plate reconstructions on which they are based in Chapter 6.

The south-eastern margin of volcanic arcs trended approximately northeast over the last 20 Myr and migrated southeast with time. The arc locations and approximately constant arc trends are illustrated for 4 Myr time intervals in Fig. 6. For each time interval arc data are complemented by mantle velocity anomalies that show the present trend of the slab which was passing through the interplate zone when the youngest volcanoes in each time interval formed. For each of the time intervals over the last 16 Myr the trend of the slab (as determined from mantle velocity anomalies) and the volcanic arcs are approximately parallel. This parallelism supports the argument that the strike of the slab has not changed since it commenced subduction (i.e. steady-state) (Billen & Hirth, 2007) and travelled along the trajectories indicated by the thick black lines in Fig. 6. From 16 Ma to the present the sub-parallel eastern margin of arc volcanoes and the trend of the positive mantle velocity anomalies indicate the slab strike was approximately northeast (~036°) over this time interval. The available data provide no support for suggestions that the volcanic arc and/or the subducting plate rotated clockwise over the last 4 Myr (see Stern et al., 2006). Prior to 16 Ma the trends of volcanic arcs are ambiguous and do not provide conclusive evidence for the strike of the underlying slab. If, however, positive mantle velocity anomalies define the trend of the slab between 16 and 24 Ma (as they appear to do after 16 Ma), then the slab may also have had a northeast to north-northeast strike immediately to the north of the North Island continental margin. By 16 Ma relative plate motion rates had reached approximately 85% of the present day where subduction of slab to sub-arc depths takes 6-7 Myr (Cande & Stock, 2004; De Mets et al., 2010), therefore the eruption of arc volcanism along a northeast trend from 16-17 Ma would require subduction along a parallel trend from at least 22 Ma.

Well defined arc-front trends parallel to the present (030-040º) since 16 Ma (Fig. 6) are broadly consistent with previous studies (Brothers, 1984), and shows that ~185 km southeast migration of the arc-front was also parallel. The arc-front at 8 Ma is ~150 km from its present location in the TVZ, comparable to the distance between the extinct Colville and active Kermadec arcs to the northeast in the South Fiji Basin (130-140 km separation). Migration of the arc front indicates that the ~90 km depth contour of the subducting slab beneath the North Island has migrated southeast over time. The rate of south-eastward migration of the arc-front changed by a factor of three or more at about

7 Ma. The maximum age of all arc volcanic centres and their distances perpendicular to the present arc-front indicate average arc migration rates of 4 ± 1 mm/yr between 16-7 Ma accelerating to 18 ± 3 mm/yr from ~7 Ma to present (Fig. 7). The high migration rates since ~7 Ma estimated from all data in Fig.7 are, within the uncertainties, consistent with migration rates of 14-21 mm/yr estimated from individual volcanic centres in the North Island. On the Taranaki Pennisula, for example, volcanic centres < 2 Ma in age have migrated southeast at rates of ~15 mm/yr while migration rates of 21 ± 3 mm/yr have been estimated for volcanic centres in the central North Island since 6 Ma (Cole et al., 1995). Acceleration in the south-eastward arc migration rates point to an important increase in the rate of change in the geometry of the subducting plate and in the size and rheology of the mantle wedge beneath the North Island.

5. Evolution of slab geometry

The evolution of the slab location and geometry beneath the North Island has been inferred primarily using the migration of the active arc-front and its relation to the trench. Two end-member models for the evolution of slab geometry could account for the trenchward migration of arc volcanism within the Hikurangi margin. The first model involves steepening of slab dip with a fixed subduction-hinge location (Fig. 1a). In the slab steepening model the location of the trench is approximately fixed with respect to the over-riding plate and the predicted rates of extension in the over-riding plate are significantly less (≤ 30 %) than the rates of arc migration. In the second model the subduction-hinge migrates seaward with a constant slab dip to produce slab rollback (Fig. 1b). In the slab rollback model finite extension in the over-riding plate is approximate to the hinge and trench migration distances (Molnar & Atwater, 1978). Discriminating between these models using trench locations relative to the over-riding plate can be problematic. Along the Hikurangi margin, for example, although the deformation front at the trench does not appear to have migrated seaward more than 50 km since 20 Ma (Fig. 8) (Barnes et al., 2010), the accretion of sediments and clockwise rotation of the upper plate make it difficult to determine the precise location of the trench at any given time (Fig. 9). Where the amount of trench migration is ambiguous or unknown, the total amount or rate of extension in the over-riding plate can be used to differentiate between these end member models.

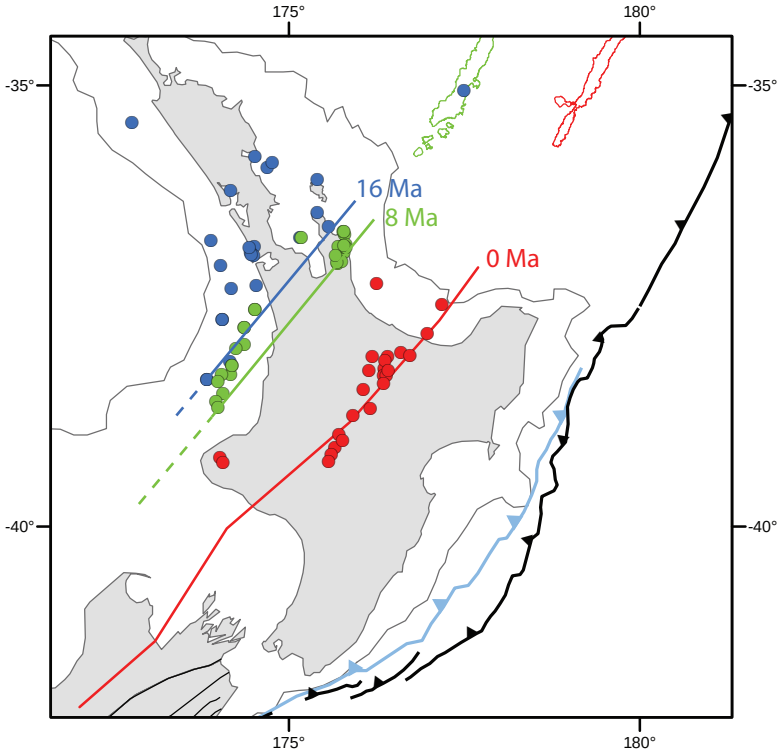

Figure 8. Schematic evolution of sub-arc plate geometry. Present day and inferred 90 km slab isobath (coloured lines) with associated active volcanism (± 0.5 Ma) (filled circles). For reference Kermadec Ridge approximates 100 km slab contour to northeast of North Island (Syracuse & Abers, 2006). Late Cenozoic trench location (light blue line) inboard of present deformation front is from Barnes et al. (2009). Note the southern limit of arc volcanism in each time interval is approximately stationary with respect to slab strike.

Despite our imprecise knowledge of paleo-trench preliminary reconstructions of the slab suggest it steepened since 8 Ma. The relative motion vector of the Pacific plate (with respect to a fixed Australian Plate) determines the long term passage of the slab to sub-arc depths (Fig. 9). At the southern limit of volcanism in the North Island, the distance from the present trench to the active arc-front is equivalent along relative plate motion and dip parallel vectors (~290 km) resulting in an average slab dip to sub-arc depths of ~15-17º in both orientations. From preliminary reconstructions of the Hikurangi margin at 8 Ma, the ~400 km distance along relative plate motion and dip parallel vectors to the southern-most volcanic centres indicates slab dips of ~11-13º. Comparison of slab dips at ~8 Ma and today indicates steepening of 2-6º over this time. If steepening of slab dip has been the only geometric change occurring over last 8 Ma, a ~4º increase in the average dip to sub-arc depth would be required to produce the observed arc migration. Therefore at the southern limit of volcanism slab steepening could account for at least two thirds of the arc migration. The remaining arc migration could be due to slab rollback and/or to southward movement of steeper slab arising from oblique subduction of the Pacific plate.

The inferred slab steepening is dependent on the ~400 km arc-trench separation distance at 8 Ma, however, questions remain whether this is unreasonably large. The modern Alaskan subduction system has a maximum arc-trench separation of ~460 km and demonstrates that our estimated ~400 km is possible (Syracuse & Abers, 2006). South-eastern Alaska also demonstrates that where collision and over-riding plate vertical-axis rotations are occurring (Wallace et al., 2009a), in particular towards the termination of subduction, the strike of the slab at sub-arc depths and trench need not be parallel (≥ 30° obliquity). Like the North Island, arc volcanism in south-eastern Alaska extinguishes hundreds of kilometres before the end of the seismically defined slab and the transition into a transform plate boundary (Syracuse & Abers, 2006; Wallace et al., 2009a). These relations suggest a common process is operating in both locations and is discussed further in section 6.

A slab steepening model would require that extension of the overriding plate was less than the rate of arc migration. At the latitude of Taranaki Peninsula extension in the upper plate since 2 Ma has been ≤ 3 mm/yr which is significantly less than the 18 ± 3 mm/yr arc migration rate over the last ~7 Myr (Wallace et al., 2004; Nicol et al., 2005; Villamor & Berryman, 2006; Giba et al., 2010). This disparity in rates shows that at the southern limit of volcanism increasing slab dip has been an important factor in arc

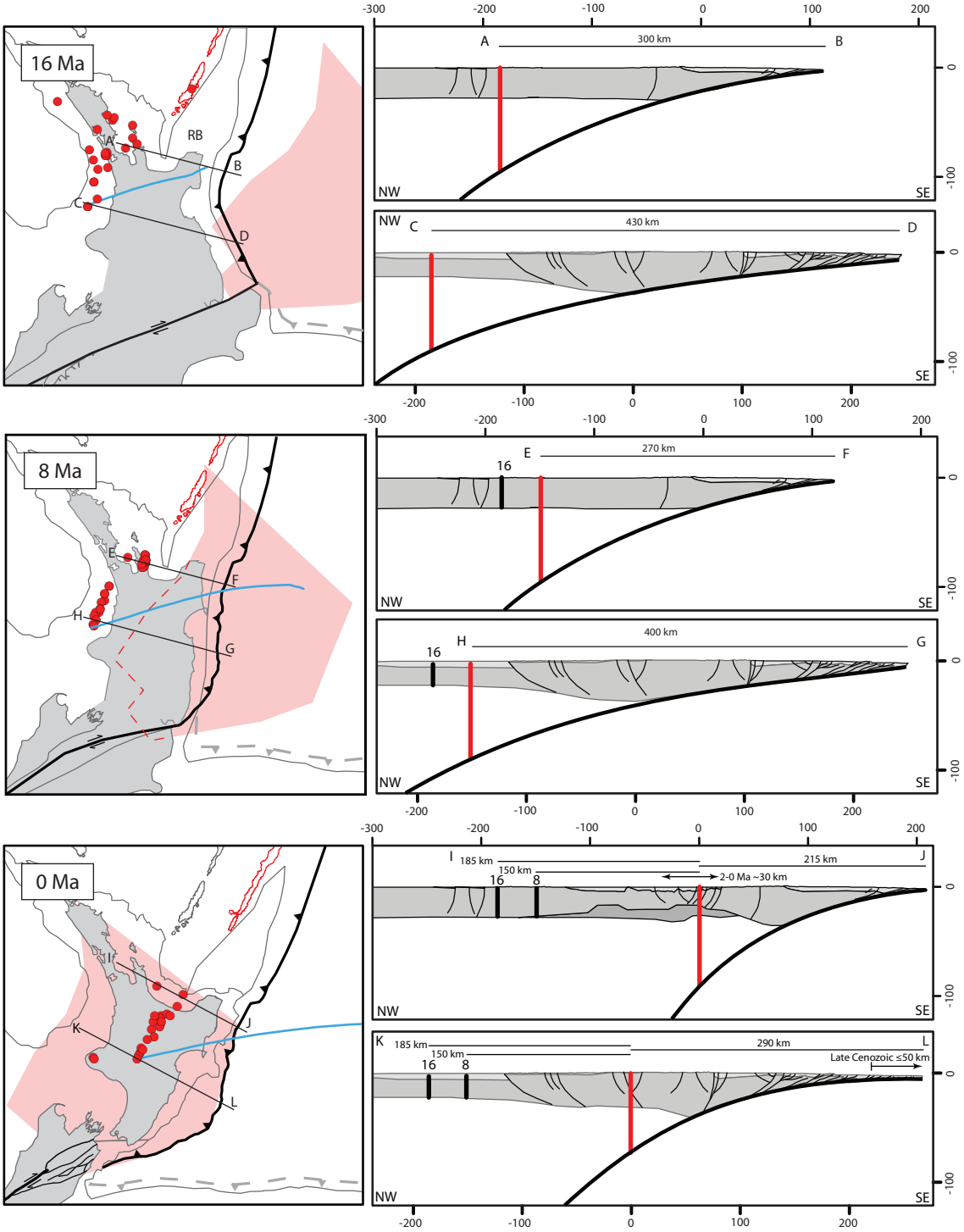

Figure 9. Tectonic model for the evolution of slab geometry beneath the North Island. Map view reconstructions for motion of the Pacific plate (PAC) relative to a fixed Australian plate (AUS) using total reconstruction poles of Cande & Stock (2004), see chapter 6 for details. To illustrate the passage of the slab the lower limit of Benioff zone seismicity is unfolded to horizontal extent (red shaded polygon) and motion path of slab from 33 Ma to southern arc volcano (blue lines) is shown. Cross-section at 0 Ma created using data from Eberhart-Phillips et al. (2010), Davey et al. (1995), Barker et al. (2009), Barnes et al. (2009) and volcanic age data detailed in Fig. 5 with references in text. Reconstruction of the Hikurangi margin based on King (2000) and Nicol et al. (2007) where the Raukumara Basin (RB) constrains the minimum arc trench distance approaching the North Island (Sutherland et al., 2009).

migration. By contrast, to the northeast of the TVZ in the offshore Bay of Plenty, the rate of extension is 13-20 mm/yr and comparable to the rate of arc migration (Davey et al., 1995; Wallace et al., 2004; Lamarche et al., 2006). The similarity of these values indicates that arc migration northeast of New Zealand was produced mainly by slab rollback. The gradual northeast increase in extension of the upper plate supports the view that the transition from slab steepening to slab rollback dominated systems is gradual.

The southeast migration of parallel arc trends over the last 16 Ma indicates that the strike of the subducting plate remained approximately constant with changes in slab dip and rollback. The uniformity of slab strike since 16 Ma is supported by the constant northeast trend of the slab at depths > 70 km (Fig. 6) and by the parallelism between the extinct Colville and active Kermadec arcs. The implications of uniform slab strike since 16 Ma are discussed in section 6.2.

6. Discussion

6.1 Mantle wedge development

The mantle wedge (the region of mantle lithosphere lying between the subducting and over-riding plates) is the locus of important processes in subduction zones, including arc magmatism and back-arc spreading. The dehydration and release of water from subducting oceanic lithosphere is mainly a temperature dependent process which lowers both the viscosity and solidus of the mantle wedge and promotes the formation of melt (Hirth & Kohlstedt, 2003; Billen, 2008; Wada & Wang, 2009; England & Katz, 2010). The mantle wedge beneath active arc volcanic centres in the central North Island is characterized by low seismic velocities and high attenuation (Qp), indicative of temperatures approaching the solidus and the presence of melt and slab-derived fluids (Wiens & Smith, 2003; Reyners et al., 2006; Eberhart-Phillips et al., 2008; Li et al., 2008; Seaward et al., 2008). Beneath the volcanic region in the central North Island, a strong seismic attenuation gradient (Qp) (approximated by the location of the volcanic front) separates relatively cold, dry and viscous mantle to the east from hot, hydrated and flowing mantle to the west (Eberhart-Phillips et al., 2008). Along strike, increasing mantle velocity and decreasing attenuation indicates a reduction in the temperature, water content, and corner flow of the mantle wedge south of the limit of arc volcanism

(Carlson & Miller, 2003; Reyners et al., 2006). The hydration and temperature of the mantle wedge appears to be a critical determinant for the location of arc volcanism in the North Island (see chapter 4).

The absence of arc volcanism in the central North Island prior to 6 Ma indicates the mantle wedge beneath this region was relatively cold, dry and viscous or not present (i.e. crust of the two plates was in contact across an interplate fault). The acceleration of southeast arc migration across the North Island commencing at about 7 Ma was approximately coincident in time with the initiation of back-arc rifting the length of the Tonga-Kermadec trench (Taylor et al., 1996; Wyzocanski et al., 2010). The acceleration of arc migration is here proposed to reflect an increase in the rates of slab rollback and steepening. These changes in the geometry of the subducting Pacific plate beneath the central North Island occurred in association an increase of plate convergence rates and reorganisation of plate boundaries in the southwest Pacific beginning ~10 Ma (Croon et al., 2008). Changes in plate rates included a 5-10% increase in spreading rates along the Pacific-Antarctic Ridge at ~7 Ma, initiation of subduction in southwest New Zealand (11-5 Ma), and an increase in convergence across the Alpine Fault at 6-8 Ma (Kamp & Tippet, 1993; Walcott, 1998; House et al., 2002; Cande & Stock, 2004; Croon et al., 2008; Giba et al., 2010). The temporal coincidence of these events may suggest that accelerated slab rollback and steepening was triggered by plate wide processes rather than processes confined to the Hikurangi margin (chapter 6).

The mantle beneath volcanic arcs can have viscosities up to an order of magnitude lower than normal oceanic lithosphere due to the flux of fluids from the dehydrating slab (Hirth & Kohlstedt, 2003; Manea & Gurnis, 2007). Numerical models indicate the viscosity of the mantle wedge is important for determining the style of upper plate deformation in collision zones where high viscosities are associated with tectonic escape via strike-slip faulting and low viscosities are associated with microplate vertical-axis rotation (Wallace et al., 2009a). Numerical models also indicate that the introduction of a low viscosity mantle wedge on top of a subducting slab results in a steepening of dip over million years, the magnitude of which is dependent on the maximum depth and magnitude of viscosity reduction (Manea & Gurnis, 2007). These studies suggest that the introduction of a low viscosity mantle wedge beneath the central North Island would facilitate vertical axis rotation of the overriding plate and a steepening of the subducting plate due through reduction of the viscous forces between the two.

A decrease in arc-trench distance associated with a steepening slab through time is predicted to increase the flux of slab-derived fluids and/or induce upwelling of hot asthenosphere into the mantle wedge (Tatsumi & Tsunakawa, 1992; Manea & Gurnis, 2007). Increasing the hydration and/or temperature will decrease the viscosity of the mantle wedge (Hirth & Kohlstedt, 2003; Billen, 2008). The acceleration of arc migration rates at ~7 Ma (Fig. 7), the eruption of high Mg# andesites at the north-western margin of the TVZ beginning ~6 Ma (Black et al., 1992; Booden et al., 2010), uplift of the central North Island since 5 Ma (Pulford & Stern, 2004), and increases in the frequency and size of eruptions from these times to the present (Adams et al., 1994; Houghton et al., 1995; Carter et al., 2003), are all consistent with an increase in the hydration and temperature (and decrease in the viscosity) of the mantle wedge beneath the central North Island at this time (~7 Ma).

Volcanism in the Taranaki Basin at 14 Ma reached within 75 km of the present southern extent of volcanism on the Taranaki Peninsula and indicates a low rate of arc migration (~5 mm/yr) parallel to the trend of the margin (Fig. 8) (Giba, 2010). This is in contrast to arc-parallel rates of relative plate motion of ~ 30 mm/yr (Cande & Stock, 2004). Volcanic age data imply a relatively stable south-western boundary exists between volcanic and non-volcanic regions of the over-riding plate and in turn separation between low to high relative velocities in the mantle wedge (75 km depth slice in Fig. 6). A simple mechanism for creating contrasting regions of hot, hydrated mantle producing arc volcanism adjacent to relatively cold, dry mantle producing insufficient melt to ascend through the crust are along strike variations in the flux of slab-derived fluids (chapter 4). In the North Island, inferred low mantle wedge viscosities are associated with steeper dips and rollback of the subducting slab along with arc volcanism, extension and vertical-axis rotation in the over-riding plate. Higher inferred mantle viscosities to the south are associated with shallower slab dips along with contraction and strike-slip faulting in the over-riding plate.

6.2 Vertical-axis rotations

Clockwise vertical-axis rotations of between $\geq 50^{o}$ have been widely reported for the over-riding plate along the central and southern Hikurangi margin since 30 Ma (Fig. 9) (Wright & Walcott, 1986; Walcott, 1987; Nicol et al., 2007; Rowan & Roberts, 2008). These rotations have been attributed to the differential rollback of the subducting plate

(e.g., Walcott, 1987), to collision of continental crust at the southern termination of subduction (e.g., Wallace et al., 2004) or to a combination of both (Wallace et al., 2009a). The analysis of volcanic arc trends in this paper appear to suggest that the rates of vertical-axis rotations in the over-riding plate and the subducting plate have been different since 16 Ma. The stability of the volcanic arc trends through the North Island since 16 Ma sub-parallel to the strike of the Colville and Kermadec Ridges can be interpreted to indicate that the strike of the subducting Pacific plate has not changed significantly in this time (Fig. 6). This contrasts with ≥~35º vertical-axis rotations that have been recorded by paleomagnetic and geological studies for the eastern and southern Hikurangi margin during the last 16 Ma (Wright & Walcott, 1986; Walcott, 1987; Little & Roberts, 1997; Nicol et al., 2007; Rowan & Roberts, 2008).

The disparity in vertical-axis rotations between the plates is consistent with upper plate deformation in that they both suggest that interplate slip has been substantial. GPS and geological data indicate that along the Hikurangi margin the majority of the relative plate motion (≥80%) has been accommodated on the subduction thrust (Wallace et al., 2004; Nicol & Beavan, 2003; Nicol et al., 2007). Slip on the subduction thrust at least partially decouples deformation between the plates, and provides a means for the over-riding plate to rotate about vertical axes independent of the subducting plate. Interplate slip is a key component of the block models of Wallace et al. (2004) and is consistent with the view that vertical-axis rotations of the upper plate since ~16 Ma cannot be attributed to clockwise rotation of the underlying subducting slab. Instead, the southward decrease in extension rates and eventual transition to shortening could indicate that vertical-axis rotations of the upper plate were induced by collision of continental crust at the southern termination of subduction and by extension associated with slab rollback at the southern end of the Tonga-Kermadec subduction system (Wallace et al., 2009a).

Rotation of the over-riding plate may have been facilitated by the development of a low viscosity mantle wedge beneath the central North Island since ~7 Ma. The relatively low viscosity of a hot mantle wedge would be expected to reduce the viscous forces between subducting and over-riding plates enabling margin-parallel relative plate motion to be accommodated by vertical-axis rotation of the forearc (Billen, 2008; Wallace et al., 2009a). Acceleration of vertical-axis rotations from ~6-5 Ma (Wright & Walcott, 1986; Rowan & Roberts, 2008), provides support for a model in which

introduction of a low viscosity mantle wedge promotes vertical-axis rotations in the over-riding plate.

Decoupling of plate vertical-axis rotations has important implications for Hikurangi margin evolution and how it should be presented. Tertiary reconstructions of the Hikurangi margin are generally presented in map-view and implicit in these models (although rarely explicitly stated) is the requirement that the rotation histories of the two plates are similar (Walcott, 1987; King, 2000; Nicol et al., 2007). For at least the last 16 Myr the slab strike has remained approximately fixed, while the slab dip steepened and the over-riding plate rotated clockwise across the top of the subducting plate. In this model the over-riding plate and trench rotate clockwise in unison, which is well represented by the map-view reconstructions. Temporal changes in the geometry of the subducting plate are less obvious in map view and future reconstructions offering a 3D perspective of plate boundary evolution will be required to chart the development of both subducting and over-riding plates throughout the Tertiary.

7. Conclusions

Active front volcanoes in the central North Island strike sub-parallel to Benioff zone earthquakes where the average depth to the slab beneath the active arc-front is ~85 km. Arc-front volcanism from 16 Myr has migrated southeast 185 km sub-parallel to the presently active arc and to the strike of the slab to depths of 600 km as inferred from positive mantle velocity anomalies. Arc migration rates accelerated from 4 ± 1 mm/yr between 16-7 Ma to 18 ± 3 mm/yr from ~7 Ma to present. The acceleration of arc migration rates, eruption of high Mg# andesites, increasing frequency and size of eruptions, and uplift of the central North Island from 7 Ma indicate the development of a hot, low viscosity mantle wedge beneath the central North Island that may have facilitated the vertical-axis rotation of the fore-arc. The consistent strike of the arc is in contrast to ≥ 30° clockwise vertical-axis rotations of the eastern and southern Hikurangi margin and suggests that the subducting plate is not rotating with the overriding plate. The increasing mismatch between arc migration and intra-arc extension rates suggest that changes in slab geometry transition southwards from being dominated by rollback to dip steepening processes.

References

Adams, C.J., Graham, I.J., Seward, D. & Skinner, D.N.B., 1994. Geochronological and geochemical evolution of late Cenozioc volcanism in the Coromandel Peninsula, New Zealand. *New Zealand Journal of Geology & Geophysics*, 37, pp.359-79.

Alloway, B., Neall, V.E. & Vucetich, C.G., 1995. Late Quarternary (post 28,000 BP) tephrostratigraphy of northeast and central Taranaki, New Zealand. *Journal of the Royal Society of New Zealand*, 25, pp.385-458.

Ansell, J.H. & Bannister, S.C., 1996. Shallow morphology of the subducted Pacific Plate along the Hikurangi Margin, New Zealand. *Physics of Earth & Planetary Interiors*, 93, pp.3-20.

Ballance, P.F., 1976. Evolution of the Upper Cenozoic magmatic arc and plate boundary in northern New Zealand. *Earth & Planetary Science Letters*, 28, pp.356-70.

Ballance, P.F., 1999. Simplification of the southwest Pacific Neogene arcs: inherited complexity and control by a retreating pole of rotation. *Geological Society of London Special Publication*, 164, pp.7-19.

Barker, D., Sutherland, R., Henrys, S. & Bannister, S., 2009. Geometry of the Hikurangi subduction thrust and upper plate, North Island, New Zealand. *Geochemistry, Geophysics, Geosystems*, 10(2), p.Q02007. doi:10.1029/2008GC002153.

Barnes, P.M., Lamarche, G., Bialas, J., Henrys, S., Pecher, I., Netzeband, G.L., Greinert, J., Mountjoy, J.J., Pedley, K. & Crutchley, G., 2010. Tectonic and geological framework for gas hydrates and cold seeps on the Hikurangi subduction margin, New Zealand. *Marine Geology*, 272(1-4).

Beavan, J., Tregoning, P., Bevis, M., Kato, T. & Meertens, C., 2002. Motion and rigidity of the Pacific Plate and implications for plate boundary deformation. *Journal of Geophysical Research*, 107(B10), p.2261. doi:10.1029/2001JB000282.

Bergman, S.C., Talbot, J. & Thompson, P.R., 1992. The Kora Miocene submarine andesite stratovolcano hydrocarbon reservior. *Taranaki Basin 1991 New Zealand Oil Exploration Conference Proceedings*, pp.178-206.

Billen, M.I., 2008. Modelling the dynamics of Subducting Slabs. *Annula Reviews of Earth & Planetary sciences*, 36, pp.325-56. doi:10.1146/annurev.earth.36.031207.124129.

Billen, M. & Gurnis, M., 2001. A low viscosity wedge in subduction zones. *Earth & Planetary Science Letters*, 193, pp.227-36.

Billen, M.I. & Hirth, G., 2007. Rheologic controls on slab dynamics. *Geochemistry, Geophysics, Geosystems*, 8(8), p.Q08012. doi:10.1029/2007GC001597.

Black, P.M., Briggs, R.M., Itaya, T., Dewies, E.R., Dunbar, H.M., Kawasaki, K., Kuschel, E. & Smith, I.E.M., 1992. K-Ar age data and geochemistry of the Kiwitahi Volcanics, western Hauraki Rift, North Island, New Zealand. *New Zealand Journal of Geology & Geophysics*, 35, pp.403-13.

Boddington, T., Parkin, C.J. & Gubbins, D., 2004. Isolated deep earthquakes beneath the North Island of New Zealand. *Geophysics Journal International*, 158, pp.972-82.

Booden, M.A., Smith, I.E.M., Black, P.M. & Maulk, J.L., 2011. Geochemistry of the Early Miocene volcanic succession of Northland, New Zealand, and implications for the evolution of subduction in the Southwest Pacific. *Journal of Volcanology & Geothermal Research*, 190, pp.25-37. doi:10.1016/j.jvolgeores.2010.10.006.

Booden, M.A., Smith, I.E.M., Mauk, J.L. & Black, P.M., 2010. Evolving volcanism at the tip of a propagating arc: The earliest high-Mg andesities in northern New Zealand. *Journal of Volcanology & Geothermal Research*, 190, pp.83-96.

Boyden, J.A., Muller, R.D., Gurnis, M., Torsvik, T.H., Clark, J.A., Turner, M., Ivey-Law, H., Watson, R.J. & Cannon, J.S., 2011. Next-generation plate-tectonic reconstructions using GPlates. In G.R. Keller & C. Baru, eds. *Geoinformatics: Cyberinfrastructure for the Solid Earth Sciences*. Cambride University Press. pp.95-114.

Briggs, R.M., Houghton, B.F., McWilliams, M. & Wilson, C.J.N., 2005. 40Ar/39Ar ages of silicic volcanic rocks in the Tauranga-Kaimai area, New Zealand: dating the transition between volcanism in the Coromandel Arc and Taupo Volcanic Zone. *New Zealand Journal of Geology & Geophysics*, 48, pp.459-69.

Briggs, R.M., Itaya, T., Lowe, D.J. & Keane, A.J., 1989. Ages of the Pliocene-Pleistocene Alexandra and Ngatutura Volcanics, western North Island, New Zealand, and some geological implications. *New Zealand Journal of Geology & Geophysics*, 32, pp.417-27.

Brothers, R.N., 1984. Subduction regression and oceanward migration of volcanism, North Island, New Zealand. *Nature*, 309, pp.698-700.

Burt, R.M., Cole, J.W. & Vroon, P.Z., 1996. Volcanic geology and geochemistry of Motuhora (Whale Island), Bay of Plenty, New Zealand. *New Zealand Journal of Geology & Geophysics*, 39, pp.565-80.

Cameron, E., Gamble, J., Price, R., Smith, I., McIntosh, W. & Gardner, M., 2010. The petrology, geochronology and geochemistry of Hauhungatahi Volcano, S.W. Taupo Volcanic Zone. *Journal of Volcanology & Geothermal Research*, 190, pp.179-91.

Cande, S.C. & Stock, J., 2004. Pacific-Antarctic-Australian motion and the formation of the Macquire Plate. *Geophysics Journal International*, 157, pp.399-414.

Carlson, R.L. & Miller, D.J., 2003. Mantle wedge water contents estimated from seismic velocities in partially serpentinized peridotites. *Geophysical Research Letters*, 30(5), p.1250. doi:10.1029/2002GL016600.

Carter, L., Shane, P., Alloway, B., Hall, I.R., Harris, S.E., Harris, S.E. & Westgate, J.A., 2003. Demise of one volcanic zone and the birth of another - a 12 m.y. record of rhyolitic eruptions from New Zealand. *Geology*, 31, pp.493-96.

Cole, J.W., Darby, D.J. & Stern, T.A., 1995. Taupo Volcanic Zone and Central Volcanic Region: Backarc structures of North Island, New Zealand. In B. Taylor, ed. *Back Arc Basins: Tectonics and Magmatism*. New York: Plenum Press. pp.1-28.

Croon, M.B., Cande, S.C. & Stock, J.M., 2008. Revised Pacific-Antarctic plate motions and geophysics of the Menard Fracture zone. *Geochemistry, Geophysics, Geosystems*, 9, p.Q07001.

Davey, F.J., Henrys, S.A. & Lodolo, E., 1995. Asymmtric rifting in a continental back-arc environment, North Island, New Zealand. *Journal of Volcanology and Geothermal Research*, 68, pp.209-38.

Davy, B., Horernle, K. & Werner, R., 2008. Hikurangi Plateau: Crustal structure, rift formation, and Gondwana subduction history. *Geochemsitry, Geophysics, Geosystems*, 9, p.Q07004.

De Mets, C., Gordon, R.G. & Argus, D.F., 2010. Geologically current plate motions. *Geophysics Journal International*, 181, pp.1-80.

Eberhart-Phillips, D. & Bannister, S., 2010. 3-D imaging of Marlborough, New Zealand, subducted plate and strike-slip fault systems. *Geophysics Journal International*, 182, pp.73-96. doi:10.1111/j.1365-246X.2010.04621.x.

Eberhart-Phillips, D., Reyners, M., Bannister, S., Chadwick, M. & Ellis, S., 2010. Establishing a versatile 3-D seismic velocity model for New Zealand. *Seismological Research Letters*, 81(6), pp.992-1000.

Eberhart-Phillips, D., Reyners, M., Chadwick, M. & Stuart, G., 2008. Three-dimensional attenuation strucutre of the Hikurangi subduction zone in the central North Island, New Zealand. *Geophysics Journal International*, 174, pp.418-34.

England, P., Engdahl, R. & Thatcher, W., 2004. Systematic variation in the depths of slabs beneath arc volcanoes. *Geophysics Journal International*, 156, pp.377-408. doi:10.1111/j.1365-246X.2003.02132.x.

England, P.C. & Katz, R.F., 2010. Melting above the anhydrous solidus controls the location of volcanic arcs. *Nature*, 467, pp.700-04. doi:10.1038/nature09417.

Gamble, J.A., Price, R.C., Smith, I.E.M., McIntosh, W.C. & Dunbar, N.W., 2003. 40Ar/39Ar geochronology of magmatic activity, magma flux and hazards at Ruapehu

Volcano, Taupo Volcanic Zone, New Zealand. *Journal of Volcanology & Geothermal Research*, 120, pp.171-87.

Giba, M., 2010. *The evolution of Tertiary normal faults in the Taranaki Basin, New Zealand*. Dublin: University College Dublin. unpublished PhD thesis.

Giba, M., Nicol, A. & Walsh, J.J., 2010. Evolution of faulting and volcanism in a back-arc basin and its implications for subduction processes. *Tectonics*, TC4020. doi: 10.1029/2009TC002634.

Gutscher, M.A., Maury, R., Eissen, J.-P. & Bourdon, E., 2000b. Can slab melting be caused by flat subduction? *Geology*, 28(6), pp.535-38.

Gutscher, M.A., Spakman, W., Bijwaard, H. & Engdahl, E.R., 2000. Geodynamics of flat subduction: Seismicity and tomographic constraints from the Andean margin. *Tectonics*, 9, pp.814-33.

Hayward, B.W., Black, P.M., Smith, I.E.M., Ballance, P.F., Itaya, T., Doi, M., Takagi, M., Bergman, S., Adams, C.J., Herzer, R.H. & Robertson, D.J., 2001. K-Ar ages of Early Miocene arc-type volcanoes in northern New Zealand. *New Zealand Journal of Geology & Geophysics*, 44, pp.285-311.

Henry, M.A.C., 1991. *The volcanic geology of Motiti Island*. Hamilton, New Zealand: University of Waikato. unpublished MSc Thesis.

Herzer, R.H., 1995. Seismic stratigraphy of a buried volcanic arc, offshore Northland, New Zealand and implications for Neogene subduction. *Marine & Petroleum Geology*, 12, pp.511-31.

Hirth, G. & Kohlstedt, D., 2003. Rheology of the Upper Mantle and the Mantle Wedge: A view from the Experimentalists. In J. Eiler, ed. *Inside the Subduction Facory*. Geophysical Monograph 138: AGU. pp.83-105. doi:10.1029/138GM06.

Houghton, B.F., N, W.C.J., McWilliams, M.O., Lamphere, M.A., Weaver, S.D., Briggs, R.M. & Pringle, M.S., 1995. Chronology and dynamics of a silicic magmatic system: Central Taupo Volcanic Zone, New Zealand. *Geology*, 23(1), pp.13-16.

House, M.A., Gurnis, M., Kamp, P.J.J. & Sutherland, R., 2002. Uplift in the Fiordland Region, New Zealand: Implications for incipent subduction. *Science*, 297, pp.2038-41.

Kamp, P.J.J., 1984. Neogene and Quarternary extent and geometry of the subducted Pacific Plate beneath North Island, New Zealand: implications for Kaikoura tectonics. *Tectonophysics*, 108, pp.241-66.

Kamp, P.J.J. & Tippet, J.M., 1993. Dynamics of Pacific plate continental crust in the South Island collision zone (New Zealand). *Journal of Geophysical Research*, 98, pp.16105-18.

Kear, D., 2004. Reassessment of Neogene tectonism and volcanism in North Island, New Zealand. *New Zealand Journal of Geology & Geophysics*, 47(3), pp.361-74.

King, P.R., 2000. Tectonic reconstructions of New Zealand: 40 Ma to present. *New Zealand Journal of Geology & Geophysics*, 43, pp.611-38.

Lallemand, S., Heuret, A. & Boutelier, D., 2005. On the relationships between slab dip, back-arc stress, upper plate absolute motion, and crustal nature in subduction zones. *Geochemistry, Geophysics, Geosystems*, 6(Q09006). doi: 10.1029/2005GC000917.

Lamarche, G., Barnes, P.M. & Bull, J.M., 2006. Faulting and extension rate over the last 20,000 years in the offshore Whakatane Graben, New Zealand continental shelf. *Tectonics*, 25, p.TC4005. doi:10.1029/2005TC001886.

Leonard, G.S., Begg, J.G. & Wilson, C.J.N., 2011. *Geology of the Rotorua area 1:250 000 geological map*. Lower Hutt, New Zealand: Institute of Geological & Nuclear Sciences. 1 sheet + 99p.

Little, T.A. & Roberts, A.P., 1997. Distribution and mechanism of Neogene to present-day vertical axis rotations, Pacific-Australian Plate boundary zone, South Island, New Zealand. *Journal of Geophysical Research*, 102, pp.20447-68.

Li, C., van der Hilst, R.D., Engdahl, E.R. & Burdick, S., 2008. A new global model for P wave speed variations in Earth's mantle. *Geochemsitry, Geophysics, Geosystems*, 9(Q05018). doi: 10.1029/2007GC001806.

Manea, V. & Gurnis, M., 2007. Subduction zone evolution and low viscosity wedges and channels. *Earth & Planetary Science Letters*, 264, pp.22-45. doi: 10.1016/j.epsl.2007.08.030.

Middleton, L.M.H., 1983. *The Whangeri Head Calc-alkaline Tertiary Volcanic Complex, Northland, New Zealand*. Auckland, New Zealand: University of Auckland. unpublished PhD Thesis.

Molnar, P. & Atwater, T., 1978. Interarc spreading and Cordilleran tectonics as alternatives related to the age of subducted lithosphere. *Earth & Planetary Science Letters*, 41, pp.330-40.

Mortimer, N., 2004. New Zealand's geological fondations. *Gondwana Research*, 7(1), pp.261-72.

Mortimer, N., Gans, P.B., Palin, J.M., Meffe, S., Herzer, R.H. & Skinner, D.N.B., 2010. Location and migration of Miocene-Quarternary volcanic arcs in the SW Pacific region. *Journal of Volcanology & geothermal Research*, 190, pp.1-10. doi: 10.1016/j.jvolgeores.2009.02.017.

Mortimer, N., Herzer, R.H., Gans, P.B., Laporte-Magoni, C., Clavert, A.T. & Bosch, D., 2007. Oligocene-Miocene tectonic evolution of the South Fiji Basin and Northland

Plateau, SW Pacific Ocean: evidence from petrology and dating of dredged rocks. *Marine Geology*, 237, pp.1-24.

Nakajima, J., Matsuzawa, T., Hasegawa, A. & Zhao, D., 2001. Three-dimensional structure of Vp, Vs, and Vp/Vs beneath northeastern Japan: Implications for arc magmatism and fluids. *Journal of Geophysical Research*, 106(B10), pp.21843-58.

Nicol, A. & Beavan, J., 2003. Shortening of an over-riding plate and its implication for slip on a subduction thrust, central Hikurangi Margin, New Zealand. *Tectonics*, 22(6), p.1070. doi:10.1029/2003TC001521.

Nicol, A., Mazengarb, C., Chanier, F., Rait, C., Uruski, C. & Wallace, L., 2007. Tectonic evolution of the active Hikurangi subduction margin, New Zealand, since the Oligocene. *Tectonics*, 26, p.TC4002. doi:10.1029/2006TC002090.

Nicol, A., Walsh, J., Berryman, K. & Nodder, S., 2005. Growth of a normal fault by the accumulation of slip over millions of years. *Journal of Structural Geology*, 27, pp.327-42. doi:10.1016/j.jsg.2004.09.002.

Price, R.C., Stewart, R.B., Woodhead, J.D. & Smith, I.E.M., 1999. Petrogenesis of high-K magmas: evidence from Egmont Volcano, North Island, New Zealand. *Journal of Petrology*, 40, pp.167-97.

Pulford, A. & Stern, T., 2004. Pliocene exhumation and landscape evolution of central North Island: the role of the upper mantle. *Journal of Geophysical Research*, 109, p.F01016. doi:10.1029/2003JF000046.

Reyners, M., 1983. Lateral segmentation of the subducted plate at the Hikurangi Margin, New Zealand: Seismological evidence. *Tectonophysics*, 96, pp.203-23.

Reyners, M., Eberhart-Phillips, D. & Bannister, S., 2011. Tracking repeated subduction of the Hikurangi Plateau beneath New Zealand. *Earth & Planetary Science Letters*, 311(1-2), pp.165-71. doi:10.1016/j.epsl.2011.09.011.

Reyners, M.E., Eberhart-Phillips, D., Stuart, G. & Nishimura, T., 2006. Imaging subduction from the trench to 300 km depth beneath the central North Island, New Zealand with Vp and Vp/Vs. *Geophysics Journal International*, 165, pp.565-83.

Robertson, D.J., 1983. *Paleomagnetism and geochronology of volcanics in the North Island, New Zealand*. Auckland, New Zealand: University of Auckland. Unpublished PhD Thesis.

Robinson, R., 1986. Seismicity, structure and tectonics of the Wellington region, New Zealand. *Geophysical Journal of the Royal Astromoical Society*, 87, pp.379-409.

Rowan, C.J. & Roberts, A.P., 2008. Widespread remagnetisations and a new view of Neogene tectonic rotations within the Australian-Pacific plate boundary zone, New Zealand. *Journal of Geophysical Research*, 113, p.B03103. doi:10.1029/2006JB004594.

Royden, L.H. & Husson, L., 2006. Trench motion, slab geometry, and viscous stresses in subduction systems. *Geophysics Journal International*, 167, pp.881-905. doi:10.1111/j.1365-246X.2006.03079.x.

Sandwell, D.T. & Smith, W.H.F., 2009. Global marine gravity from retracked Geosat and ERS-1 altimetry: Ridge segmentation verses spreading rate. *Journal of Geophysical Research*, 114, p.B01411. doi:10.1029/2008JB006008.

Schellart, W.P., 2005. Influence of the subducting plate velocity on the geometry of the slab and migration of the subduction hinge. *Earth & Planetary Science Letters*, 231, pp.197-219.

Schellart, W.P., 2012. Comment on "Geochemistry of the Early Miocene volcanic succession of Northland, New Zealand, and implications for the evolution of subduction in the Southwest Pacific" by M.A. Booden, I.E.M. Smith, P.M. Black and J.L. Mauk. *Journal of Volcanology & Geothermal Research*, 211-212, pp.112-17. doi:10.1016/j.jvolgeores.2011.10.010.

Sdrolias, M. & Muller, R.D., 2006. Controls on back-arc basin formation. *Geochemistry, Geophysics, Geosystems*, 7, p.Q04016. doi:10.1029/2005GC001090.

Seaward, A.M., Hendersn, C.M. & Smith, E.G.C., 2008. Models of the upper mantle beneath the central North Island, New Zealand, from speeds and anisotropy of sub-horizontal P waves (Pn). *Journal of Geophysical Research*, 114, p.B01301. doi:10.1029/2008JB005805.

Smith, D.M.J., 1986. *The petrology and geochemistry of the Orangiwhao Volcanics*. Hamilton, New Zealand: University of Waikato. Unpublished MSc Thesis.

Stern, T.A., Stratford, W.R. & Salmon, M.L., 2006. Subduction evolution and mantle dynamics at a continental margin: Central North Island, New Zealand. *Review of Geophysics*, 44, p.RG4002. doi:10.1029/2005RG000171.

Stipp, J.J., 1968. *The geochronology and petrogenesis of the Cenozoic volcanics of North Island, New Zealand*. Canberra, Australia: Australian National University. Unpublished PhD Thesis.

Syracuse, E.M. & Abers, G.A., 2006. Global compliation of variations in slab depth beneath arc volcanoes and implications. *Geochemistry, Geophysics, Geosystems*, 7, p.Q05017. doi:10.1029/2005GC001045.

Tatsumi, Y. & Tsunakawa, H., 1992. Cenozoic volcanism, stress gradient and back-arc opening, New Zealand: Origin of Taupo-Rotorua Depression. *The Island Arc*, 1, pp.40-50.

Taylor, B., Zellmer, K., Martinez, F. & Goodlife, A., 1996. Sea-floor spreading in the Lau back-arc basin. *Earth & Planetary Science Letters*, 144, pp.35-40.

Townsend, D., Vonk, A. & Kamp, P.J.J., 2008. *Geology of the Taranaki area 1:250 000 geological map*. Lower Hutt, New Zealand: Institute of Geological & Nuclear Sciences. 1 sheet + 77p.

Turner, S. & Hawkesworth, C., 1997. Constraints on flux rates and mantle dynamics beneath island arcs from Tonga-Kermadec lava geochemistry. *Nature*, 389, pp.568-73.

van der Hilst, R.D., 1995. Complex morphology of subducted lithosphere in the mantle beneath the Tonga trench. *Nature*, 374, pp.154-57. doi:10.1038/374154a0.

Villamor, P. & Berryman, K.R., 2006. Evolution of the southern termination of the Taupo Rift, New Zealand. *New Zealand Journal of Geology & Geophysics*, 49, pp.23-37.

Wada, I. & Wang, K., 2009. Common depth of slab-mantle decoupling: Reconciling diversity and uniformity of subduction zones. *Geochemsitry, Geophysics, Geosystems*, 10(10), p.Q10009. doi:10.1029/2009GC002570.

Walcott, R.I., 1987. Geodetic strain and the deformation history of the North island of New Zealand during the late Cainozoic. *Philosphical Transactions of the Royal Society London*, A321, pp.163-81.

Walcott, R.I., 1998. Modes of oblique compression: Late Cenozoic tectonics of the South Island of New Zealand. *Reviews of Geophysics*, 36(1), pp.1-26.

Wallace, L.M., Beavan, J., McCaffrey, R. & Darby, D., 2004. Subduction zone coupling and tectonic block rotations in the North island, New Zealand. *Journal of Geophysical Research*, p.B12406. doi:10.1029/2004JB003241.

Wallace, L.M., Ellis, S. & Mann, P., 2009a. Collisional model for rapid fore-arc block rotations, arc curvature, and episodic back-arc rifting in subduction settings. *Geochemistry, Geophysics, Geosystems*, 10, p.Q05001. doi:10.1029/2008GC0022200.

Wallace, L.M., Reyners, M., Cochran, U., Bannister, S., Barnes, P.M., Berryman, K., Downes, G., Eberhart-Phillips, D., Fagereng, A., Ellis, S., Nicol, A. & McCaffrey, R., 2009b. Characterizing the seismogenic zone of a major plate boundary subduction thrust: Hikurangi Margin, New Zealand. *Geochemistry, Geophysics, Geosystems*, 10(10), p.Q10006. doi:10.1029/2009GC002610.

Wiens, D.A. & Smith, G.P., 2003. Seismological constraints on Structure and Flow Patterns Within the Mantle Wedge. In J. Eiler, ed. *Inside the Subduction Factory*. Geophysical Monograph 138: AGU. pp.59-81. doi:10.1029/138GM05.

Wilson, C.J.N., Houghton, B.F., McWilliams, M.O., Lanphere, M.A., Weaver, S.D. & Briggs, R.M., 1995. Volcanic and structural evolution of Taupo Volcanic Zone, New Zealand: a review. *Journal of Volcanology & Geothermal Research*, 68, pp.1-28.

Wright, I.E.M. & Walcott, R.I., 1986. Large tectonic rotation of part of New Zealand in the last 5 Ma. *Earth & Planetary Science Letters*, 80, pp.348-52.

Wyzocanski, R.J., Todd, E., Wright, I.C., Leybourne, M.J., Hergt, J.M., Adam, C. & McKay, K., 2010. Back-arc rfiting, constructional volcanism and nascent disorganised spreading in the southern Havre trough back-arc rifts (SW Pacific). *Journal of Volcanology & Geothermal Research*, 190, pp.39-57.

Chapter 6

Motion of the Australian and Pacific plates in relation to North Island, New Zealand

Abstract

The tectonics of New Zealand is primarily controlled by the relative motions of the Pacific and Australian plates which are typically described by their finite poles of rotation. Finite poles of rotation for the last 38 Myr are used to track the evolution of subduction beneath the North Island, New Zealand. The location and timing of arc volcanism and deformation across the North Island are placed in context with Australia-Pacific relative motions to constrain better processes such as subduction initiation and rollback. Absolute motion of the Australian plate (in a hot-spot reference frame) at the termination of subduction along the Tonga-Kermadec-Hikurangi trench has been away from the Cretaceous age Pacific plate from 38 Ma, conditions conducive to rollback of the slab. Punctuated development of back arc basins adjacent to the North Island, however, indicate that no simple relationship exists between subducting plate age and absolute motion of the overriding plate with rollback of the slab in this region. Plate-normal convergence rates across the Hikurangi margin doubled from 11 to 23 mm/yr between 20 and 16 Ma, increasing again by approximately a third between 8 and 6 Ma. Plate-parallel rates steadily increased from ~15 mm/yr at 26 Ma to 32 ± 2 mm/yr at 16 Ma where they have remained to the present. Pacific plate motion in a west-dipping subduction model indicates a minimum horizontal transport distance of 285 km preceding the initiation of volcanism along the Northland arc, a distance more than sufficient for self-sustaining subduction to occur. Tracking the southern and down-dip limits of the seismically imaged Pacific slab beneath the New Zealand indicates subduction along the Northland margin from at least 38 Ma.

1. Introduction

The geometry and kinematics of subduction are driven by the relative motions of tectonic plates over millions of years. Relative motions of the Australian and Pacific plates are generally well constrained and form the basis for models of the development of New Zealand plate boundary from the Early Miocene (Walcott, 1987; Sutherland, 1995; King, 2000; Cande & Stock, 2004). What is less clear are relative plate motions and subduction polarity prior to the initiation of arc volcanism in the northern North Island in the Late-Oligocene-Early Miocene (Ballance, 1976; Brothers, 1984; Hayward et al., 2001; Schellart et al., 2006; Mortimer et al., 2007; Schellart, 2007; Booden et al., 2011). Through the Miocene, the geometry and kinematics of subduction controlled the location of arc volcanism and intra-arc rifting along the Hikurangi margin (chapter 5) though there is little consensus on the how these systems have evolved (King & Thrasher, 1996; Parson & Wright, 1996; Stern et al., 2006; Giba et al., 2010). Examining how arc volcanism and rifting onshore and offshore North Island has developed in response to relative plate motions will lead to an improved understanding of subduction processes along the Hikurangi margin.

In this chapter we use tectonic reconstructions between the Australian and Pacific plates to track the development of subduction beneath the North Island in relation to intra-rifting and arc volcanism. We use published finite poles of rotation (Cande et al., 2000; Cande & Stock, 2004; Croon et al., 2008) in association with present day slab geometry and volcanic arc age data (chapter 5) to examine models for subduction beneath the North Island. Absolute motion of the overriding Australian plate along the New Zealand plate boundary region has been away from the Cretaceous age Pacific plate since at least 38 Ma, providing conditions conducive for slab rollback. West-dipping subduction of the Pacific plate is a viable model for the development of the Northland arc which strikes normal to relative motion vectors. Arc volcanism from 23 to 11 Ma offshore North Island requires the continuation of the Pacific plate to at least its southern extent at ~43.5ºS where it is imaged by a seismic-reflection profile beneath the Chatham Rise (Davy et al., 2008). The west-dipping subduction model is also consistent with subduction along the northern North Island continental margin since 38 Ma.

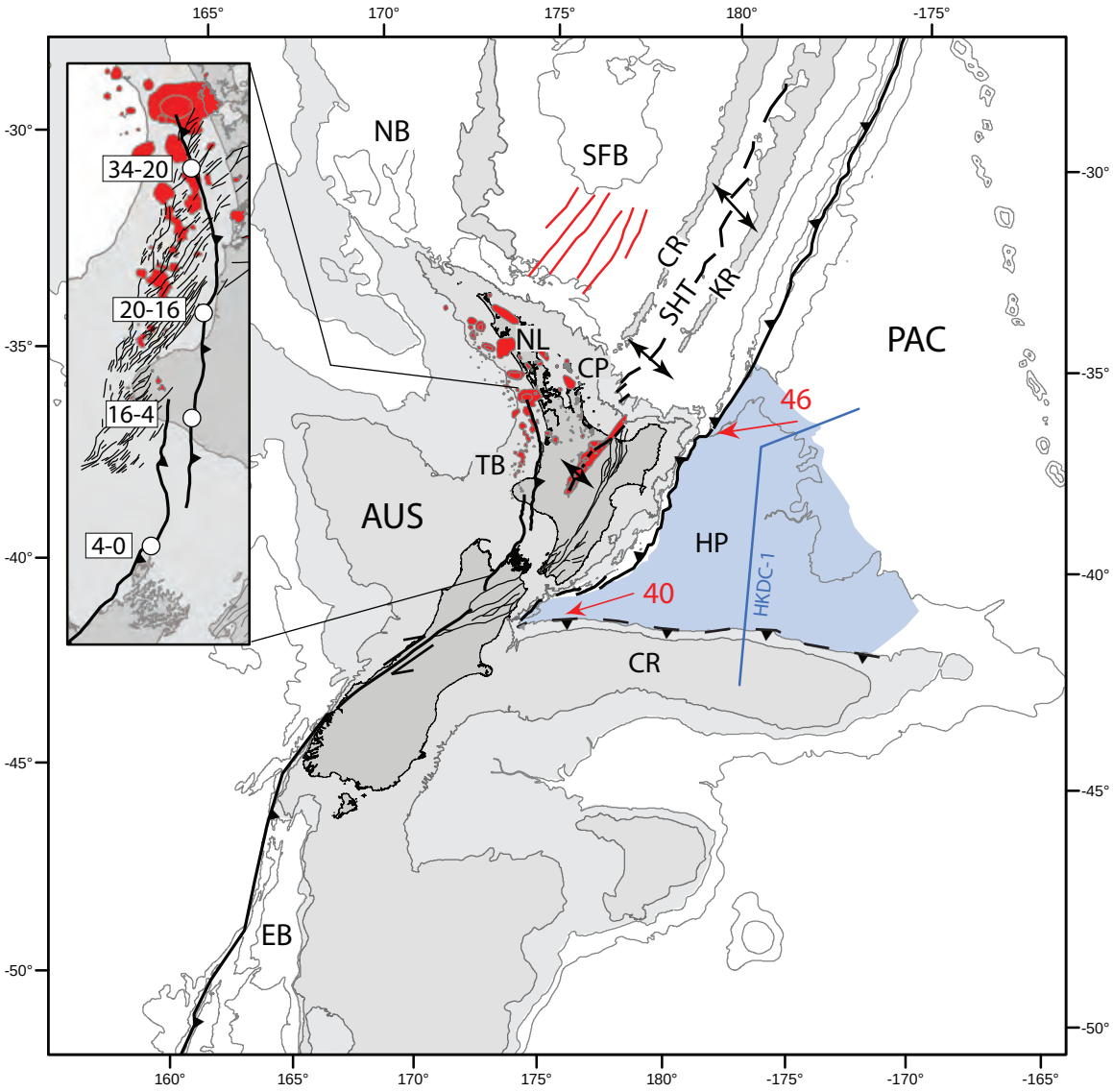

Figure 1. Tectonic setting of the New Zealand plate boundary. Oblique westward subduction of the Pacific plate is presently occurring beneath the Australian plate at rates of 40-46 mm/yr (red arrows) (De Mets et al., 2010). Miocene-Recent arc volcanic centres (red filled polygons) (see chapter 5 for full references), Emerald Basin (EB), Hikurangi Plateau (HP), Chaham Rise (CR), Taranaki Basin (TB), Coromandel Peninsula (CP), Northland (NL), South Fiji Basin (SFB), Norfolk Basin (NB), Colville Ridge (CR), and Kermadec Ridge (KR) shown for reference. Seismic line HKDC-1 (blue line) shows the Pacific plate extending beneath the Chatham Rise (Davy et al., 2008), see Appendix Fig. 4 for interpretation of seismic line. Magnetic anomaly trends (red lines) for the 23-18 Ma South Fiji Basin shown (Mortimer et al., 2007; Herzer et al., 2009). Inset shows the location of the northern active tip of the Taranaki Fault in millions of year (filled white circles) (Stagpoole & Nicol, 2008) and the Taranki Rift (thin black lines) (Giba et al., 2010).

2. North Island Subduction

The kinematics of subduction along the Hikurangi margin, North Island, New Zealand reflects its transitional location between ocean-ocean subduction along the Tonga-Kermadec trench and continental collision/transform motion in the South Island (Fig. 1). The oblique westward subduction of the Pacific plate beneath the Australian plate along the Hikurangi margin presently occurs at rates of 40-46 mm/yr (Fig. 1) (Beavan et al., 2002; De Mets et al., 2010). Plate convergence (i.e. arc-normal motion) is primarily accommodated on the subduction interface (≥ 80%) with the remainder of plate-normal motion and most of the plate-parallel motion (≥ 60%) accommodated by a combination of reverse and strike-slip faults, and by clockwise vertical-axis rotations of ~3°/Myr in the overriding plate (Webb & Anderson, 1998; Wallace et al., 2004; Nicol & Beavan, 2003; Nicol et al., 2007; Nicol & Wallace, 2007). At the southern termination of Hikurangi margin subduction convergence rates are low (< 6 mm/yr) with the majority of relative plate motion transferred onto strike-slip faults in the overriding plate (Wallace et al., 2012). Plate coupling along the Hikurangi margin increases southwards toward the termination of subduction and collision of the Chatham Rise with the Australian plate (Wallace et al., 2012). The latitude at which coupling on the plate interface deepens from ~10 to > 30 km coincides with the southern termination of the Taupo Rift and, at distances of 200-250 km from the trench, a change from extension to contraction and strike-slip in the overriding plate (Wallace et al., 2012). The Pacific plate presently subducting beneath the Hikurangi margin comprises a buoyant fragment of a thickened (12-15 km) oceanic large igneous province (Hikurangi Plateau) that partially subducted beneath the Chatham Rise during the Cretaceous along the Gondwana subduction margin (Fig. 1) (Davy et al., 2008). A seismic-reflection profile shows the Pacific plate extending to at least 43.5°S beneath the Chatham Rise (Davy et al., 2008), > 200 km beyond the southern limit of Benioff zone seismicity in the northern South Island (Eberhart-Phillips & Bannister, 2010). Beneath the North Island, deep earthquakes (Boddington et al., 2004) and mantle tomography (Li et al., 2008) indicate a continuous slab to depths of at least 600 km.

The geological history of the North and South Islands provide insights into the evolution of subduction along the Hikurangi margin. The evolution of the North Island is intimately tied to the reactivation of subduction along segments of the Gondwana subduction margin during a plate reorganisation around ~45 Ma (Stock & Molnar,

1982; Cande et al., 1995; Croon et al., 2008). Subduction has controlled both horizontal and vertical deformation, sedimentation patterns and the presence or absence of arc volcanism along the North Island plate boundary (Walcott, 1987; King & Thrasher, 1996; Stern et al., 2006; Nicol et al., 2007) (chapter 5). The Taranaki Fault, a 600 km long back thrust (antithetic to the Hikurangi subduction thrust) that runs nearly the entire length of the North Island, accrued at least 12-15 km of displacement since the middle Eocene (43-40 Ma) (Fig. 1) (Stagpoole & Nicol, 2008). Situated along the eastern margin of the Taranaki Basin and west of the Taupo Rift, the history of displacements on the Taranaki Fault are consistent with initiation of Hikurangi margin subduction during the middle Eocene (Stagpoole & Nicol, 2008). The development of a dextral transform plate boundary between the Australian and Pacific plates, the Alpine Fault, during the Late Oligocene-Early Miocene (~25-23 Ma) (Cooper et al., 1987) coincided with initiation of arc volcanism in the northern North Island. The development of the Alpine Fault between the Australian and Pacific plates was immediately preceded by and/or contemporaneous with the southwest directed emplacement of allochthons across the north-eastern North Island (Rait et al., 1991), widespread northwest-southeast trending arc volcanism in northern North Island (Herzer, 1995; Hayward et al., 2001), and 1.5 km subsidence of the Taranaki Basin (Stern & Holt, 1994).

By the end of the Early Miocene (~16 Ma) changing boundary conditions along the Hikurangi margin resulted in the northern active tip of the Taranaki Fault retreating ~300-400 km south of its Late Eocene location (Stagpoole & Nicol, 2008). This northern limit to reverse motion on the Taranaki Fault was ~50-150 km south of a northeast-southwest alignment of arc volcanic centres contiguous from the Taranaki Basin through the Coromandel Peninsula to the Colville Ridge (Bergman et al., 1992; Adams et al., 1994; Giba, 2010; Mortimer et al., 2010). Towards the end of the Middle Miocene (~12-11 Ma) intra-arc rifting in the Taranaki Basin (Giba et al., 2010) and explosive rhyolitic caldera-forming eruptions on the Coromandel Peninsula (Carter et al., 2003) in the North Island initiated contemporaneously with 2-3 mm/yr increases in the rate of convergence across the Alpine Fault in the South Island (Cande & Stock, 2004). This time also marks the beginning of subduction beneath south-western South Island (House et al., 2002) and vertical-axis rotations (3-14º/Myr) of the central and southern Hikurangi margin (Wright & Walcott, 1986; Nicol et al., 2007; Rowan &

Roberts, 2008), essentially establishing the boundary conditions for the modern plate boundary configuration through New Zealand.

Expansion of the southern and eastern margins of the Taranaki Rift (Giba et al., 2010) began around 8 Ma coinciding with increases in the size and frequency of explosive rhyolitic eruptions along the Coromandel Peninsula (Fig. 1) (Carter et al., 2003). Intra-arc rifting of the Colville-Lau and Kermadec-Tonga ridges to the northeast of New Zealand beginning around 6 Ma (Parson & Wright, 1996; Taylor et al., 1996) coincides with a further 2-3 mm/yr increase in convergence rates across the Alpine Fault (Walcott, 1998; Cande & Stock, 2004) and in uplift rates of the Southern Alps (Tippet & Kamp, 1993). To the southwest of New Zealand at this time a section of the Australian plate adjacent to the Australia-Pacific plate boundary, the Macquarie plate, began behaving as an independent plate (Cande & Stock, 2004). Across the North Island from ~7-5 Ma, increases in arc migration rates (chapter 5) and uplift (Pulford & Stern, 2004) are observed. From ~2 Ma to the present, intra-arc rifting migrated from the Taranaki Basin to the Taupo Rift (Giba et al., 2010).

These relations between intra-arc rifting and volcanism indicate regional changes in the kinematics of Australia-Pacific relative motions had significant influence on subduction processes and overriding plate deformation along the Hikurangi margin. Firstly, the contemporaneous initiation of intra-arc rifting in the North Island with subduction and contraction in the South Island at ~12-11 Ma mark a fundamental change in the kinematics of the New Zealand plate boundary. Secondly, the development of the Havre Trough-Lau Basin associated with rollback of the Pacific plate, increases in convergence across the Alpine Fault and the formation of the Macquarie plate to the southwest of New Zealand around ~8-6 Ma indicate that the southeast migration of arc volcanism/intra-arc rifting in the North Island was part of a regional reorganisation of the SW Pacific plate boundary.

3. Finite poles of rotation

The relative plate motions between the Australian and Pacific plates during the last 38 Myr are generally well constrained by seafloor spreading data. These data permit finite poles of rotation to be calculated which describe the relative motions between Pacific and Australian plates across the New Zealand plate boundary. Australia-Pacific relative motions are presently calculated using total reconstruction poles in circuits involving

two to four plates depending on the time of interest (Fig. 2) (Sutherland, 1995; Cande et al., 2000; Cande & Stock, 2004; Schellart et al., 2006; Furlong & Kamp, 2009). There are several different tectonic reconstructions for the southwest Pacific and New Zealand based on data from different regions and sources (Walcott, 1987; Sutherland, 1995; King, 2000; Schellart et al., 2006; Sdrolias & Muller, 2006; Mortimer et al., 2007). Two different plate circuits have been used to predict Australia-Pacific relative plate motion for the period 38-26 Ma during the formation of the modern plate boundary through New Zealand. The first circuit uses an Australia-Antarctica-Pacific plate circuit that includes the effects of East-West Antarctic motion for chron 13o (33.54 Ma) (Fig. 2) (Cande et al., 2000; Cande & Stock, 2004; Steinberger et al., 2004; Schellart et al., 2006). While it is generally accepted plate reorganisation around ~45 Ma initiated the formation of the modern New Zealand plate boundary, the most recent well constrained total reconstruction poles for Australia-Antarctic spreading (consistent with the methods defining the Pacific-Antarctic finite poles of rotation) begin at chron 17o (38.13 Ma) (Cande & Stock, 2004). The second plate circuit uses Australia-Pacific relative motion determined from seafloor spreading data from the Emerald Basin in southwest New Zealand for the period 40-30 Ma (see Fig. 1 for location and Fig. 2 for poles) (Sutherland, 1995; Keller, 2003; Furlong & Kamp, 2009). The proximity of finite rotation poles to the North Island prior to the initiation of the modern plate boundary configuration mean that differences in the location of these finite poles (and their associated stage poles) can result in large differences in the predicted relative motion between the Australian and Pacific plates in New Zealand at these times. In this section the methods and data that form the basis for this study are briefly described, and the predictions from both regional (Australia-Antarctica-Pacific) and local (Australia-Pacific) models currently in use.

Plate tectonics combines the concept of internally rigid tectonic plates with Euler's theorem to describe their relative motions across the surface of a sphere. The motion of a plate can be described by a rotation about a virtual axis that passes through the centre of the sphere (Euler's theorem). The most widespread parametrization of this plate rotation about a virtual axis uses latitude and longitude to describe the location where the rotation axis intersects the Earth's surface, and a rotation rate that corresponds to the magnitude of the angular velocity (in degrees per million years)

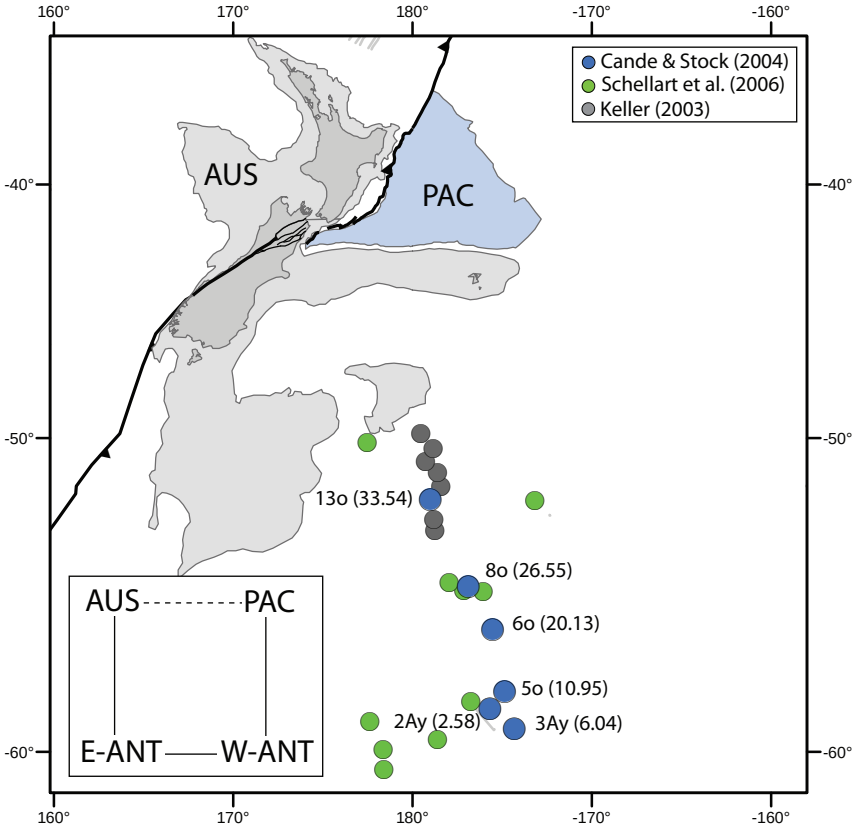

Figure 2. Total reconstruction poles for Pacific relative to Australia plate motion. Calculated total reconstruction poles for Pacific plate (PAC) motion relative to Australia (AUS). Chrons and corresponding ages (Ma) shown for finite rotation poles of Cande & Stock (2004) (blue filled circles). Finite poles of Schellart et al. (2006) (green filled circles) and Keller (2003) (grey filled circles) shown for reference, see Appendix 3 Tables 11-12. See text for details for each reconstruction model. Inset shows plate circuit used by Cande & Stock (2004), Schellart et al. (2006) and this study to calculate Australia-Pacific relative plate motions.

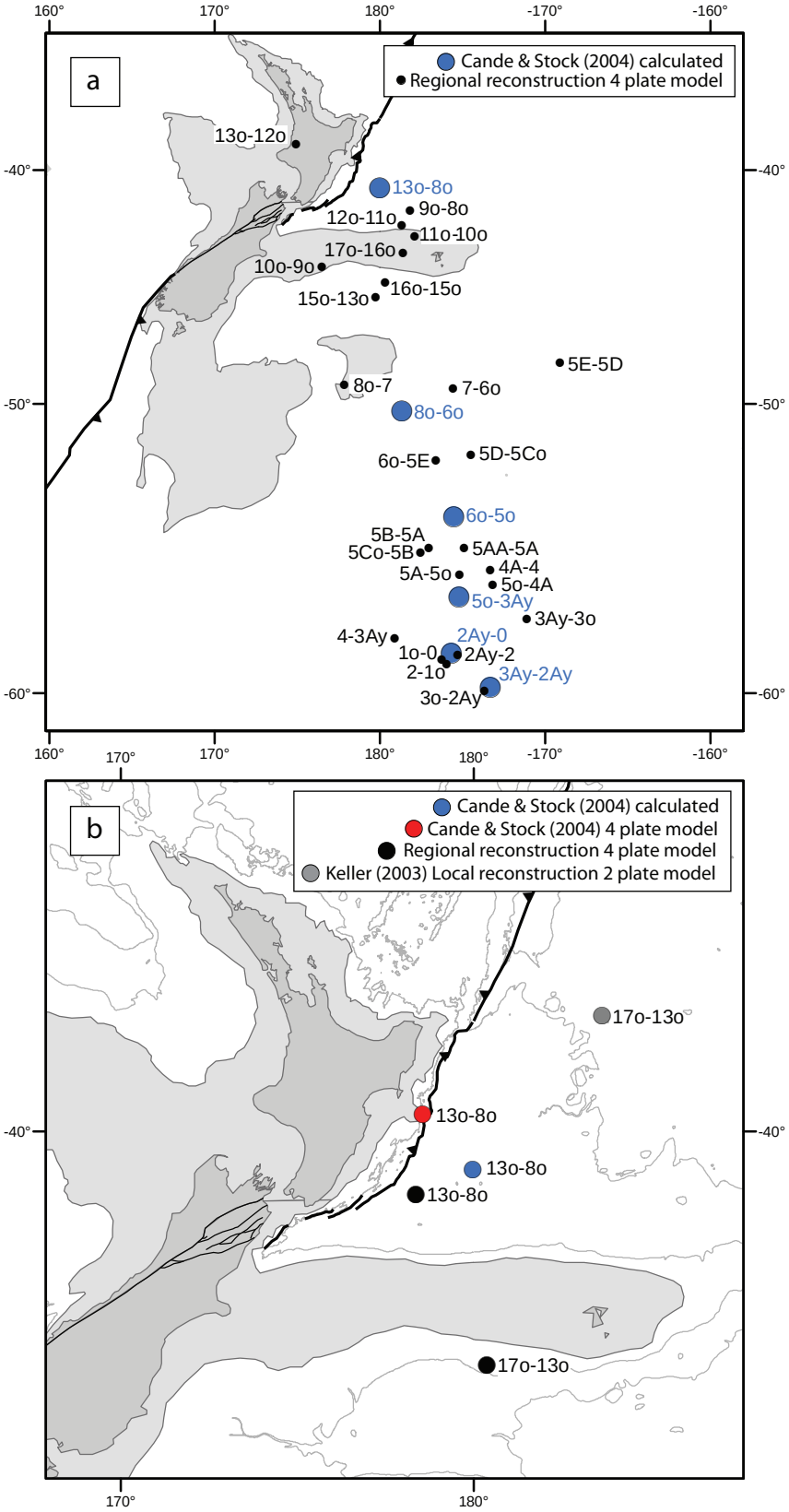

Figure 3. Stage poles for Pacific relative to Australia plate motion. (a) Stage poles for Pacific relative to Australia plate motion derived from Cande & Stock (2004) (blue filled circles) and regional reconstruction model (black filled circles), see text for details and Table 3 for chron ages. (b) Eocene-Oligocene stage poles associated with reactivation of subduction beneath the North Island. See text for details for each reconstruction model. The total reconstruction poles associated with the stage poles presented here can be found in Appendix 3.

(Wessel & Muller, 2007). The latitude and longitude of the angular velocity vector constitute the 'Euler pole'. The relative motion of adjacent plates are determined quantitatively, by the fitting of magnetic anomaly and fracture zone data on the ocean floor by matching conjugate isochrons for example, and are described using finite rotations. The finite rotations that displace a plate from its present-day position to its reconstructed position at some time in the past are called total reconstruction poles and are commonly published in the plate-tectonic literature (Cox & Hart, 1986). Total reconstruction poles are expressed as the combination of a "fixed" plate, a "moving" plate, a specific time in the past determined from sea-floor magnetic anomalies (chron) and a finite rotation. A sequence of total reconstruction poles generally define the motion of a "moving" plate averaged from a point in time and relative to a "fixed" plate across the surface of the Earth (e.g. Fig. 2). A stage is simply some interval of time in the history of a pair of plates (i.e. the interval of time between chrons in a sequence of total reconstruction poles), and a stage pole defines the amount of rotation that occurs during that stage (Cox & Hart, 1986). Total reconstruction poles describe the relative motion between plates which ultimately has to be tracked back to an "anchored" plate. This "anchored" plate can be a common plate in the circuit or an absolute reference frame such as hot-spot tracks (Muller et al., 1993; O'Neill et al., 2005) or GPS (Beavan et al., 2002). As is common in reconstructions of the New Zealand plate boundary, the "fixed" or "anchored" plate is often the Australian plate.

We use GPlates (Boyden et al., 2011) to reconstruct and compare Australia-Pacific relative motions from published total reconstruction poles. GPlates is a purpose built interactive plate tectonic reconstruction application that uses 3D unit-vectors and unit quaternions to model geological, geophysical and paleogeographic features providing an accessible and reproducible plate tectonic reconstruction framework (Boyden et al., 2011). Total reconstruction poles in GPlates are arranged in a hierarchy, or tree-like structure, with the top of the hierarchy being the "anchored" plate. Plates further down the chain from the "anchored" plate are linked by total reconstruction poles. GPlates calculates the rotation of a plate by starting at that point in a hierarchy and working its way to the top using rules for the calculation of finite rotations presented in Cox & Hart (1986).

Australia-Pacific relative motions in this study have been calculated from the relative motions between plate pairs in the Australia-East Antarctica-West Antarctica-Pacific plate circuit (see Fig. 3 for location of stage poles describing Pacific motion

relative to Australia from this model). While total reconstruction poles are associated with measurement and age uncertainties (Cande & Stock, 2004), tectonic reconstructions generally use the published location and rotation rate for these poles as we do here. Total reconstruction poles calculated for Australia-Pacific relative motions using this accepted four plate circuit (Australia-East Antarctica-West Antarctica-Pacific) (Cande et al., 2000; Cande & Stock, 2004; Steinberger et al., 2004; Schellart et al., 2006) can be compared to reconstructions using the original finite rotations between plate pairs within the circuit to help constrain the uncertainty between each type of model. Comparison of reconstructions based on calculated Australia-Pacific total reconstruction poles by Cande & Stock (2004) to a reconstruction based on total reconstruction poles between plate pairs in a four plate circuit detailed in Cande & Stock (2004), for example, show an ~20 km mismatch in the location of the Pacific plate in the New Zealand plate boundary at 33 Ma (with respect to a fixed Australian plate) (see Fig. 3 for comparison of stage poles). Considering the time and the distance of relative motion (> 1500 km) the difference between the two models is negligible. The advantage of using a four plate circuit is that reconstructions can be extended back to at least 38 Ma using the most recent and well-constrained West Antarctica-Pacific total reconstruction poles (Croon et al., 2008) and the absolute motion of plates (with reference to a hot-spot or common plate) can be tracked. We show comparisons of Pacific plate motion paths (with respect to a fixed Australian plate) over the last 33 Myr (Fig. 4) to highlight the similarities and differences between these and other models presently in the literature (Appendix 3). Motion paths are constructed using a point on the Pacific plate (with respect to a fixed Australian plate) reconstructed back in time for 1 Myr intervals. The path of this point over time forms a representation the direction and distance (i.e. vector) the moving plate has travelled with respect to the fixed plate over the time period of interest. Total reconstruction poles and associated references used in this study can be found in Appendix 3 Tables 7-13.

A motion path from calculated Antarctica-Pacific finite rotation poles of Cande & Stock (2004) (Appendix 3 Table 7) compared to one derived from a four plate circuit using the total reconstruction poles for plate pairs from Cande & Stock (2004) (Appendix 3 Table 8) are nearly identical (Fig. 4a), as is one from a four plate circuit using the most recent West Antarctica-Pacific finite rotations from Croon et al. (2008) (Appendix 3 Table 9). This updated model for Australia-Pacific relative motion based on Australia-East Antarctica finite rotations of Cande & Stock (2004), East Antarctic-

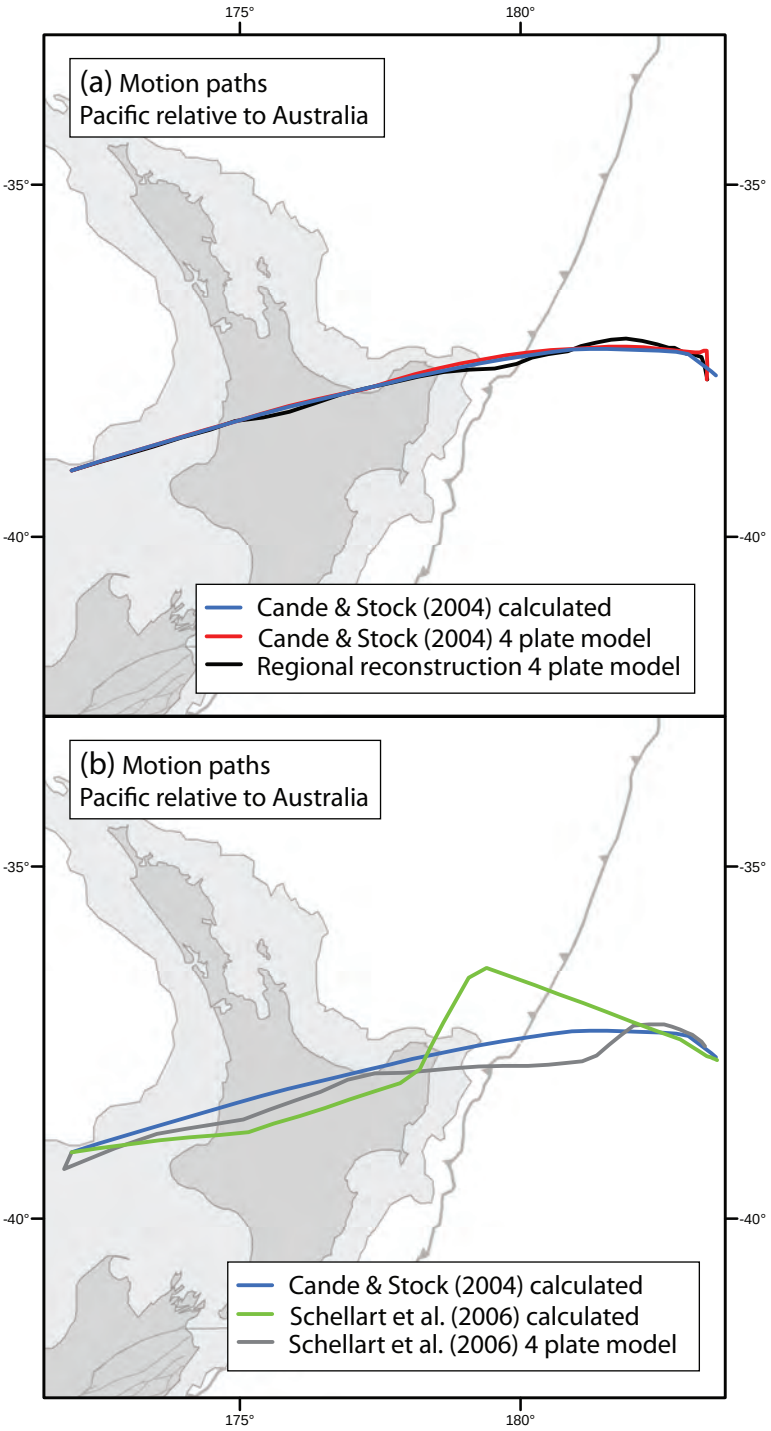

Figure 4. Comparison of Pacific motion paths relative to Australia for the last 33 Myr. See Appendix 3 Tables 4-9 for total reconstruction poles. (a) Comparison of Pacific plate motion paths from total reconstruction poles calculated for Australia-Pacific motion from Cande & Stock (2004), a 4 plate model using plate pairs detailed in Cande & Stock (2004), and a 4 plate regional reconstruction model using updated Pacific-West Antarctic total reconstruction poles from Croon et al. (2008). (b) Comparison of Pacific plate motion paths from total reconstruction poles calculated for Australia-Pacific motion from Cande & Stock (2004), Schellart et al. (2006) (Table 5) and a 4 plate model using plate pairs detailed in Schellart et al. (2006) (Table A1).

West Antarctic finite rotations of Cande et al. (2000) and West Antarctic-Pacific finite rotations of Croon et al. (2008) use the most recent data available for the period 38 Ma to present and are referred to here as the regional reconstruction model (Appendix 3 Table 9).

By comparison, Schellart et al. (2006) use older sources (Royer & Sandwell, 1989; Cande et al., 1995; Royer & Rollet, 1997) than Cande & Stock (2004) to calculate total reconstruction poles for Australia-Pacific relative motion using a four plate circuit (Fig. 4b) (Appendix 3 Table 10). A Pacific plate motion path (with respect to a fixed Australian plate) derived from a four plate circuit using the finite rotations from the original sources detailed in Schellart et al. (2006) has a broadly similar trend to the motion path derived from the calculated total reconstruction poles of Cande & Stock (2004) and the regional reconstruction model. The motion path derived from calculated Australia-Pacific total reconstruction poles detailed in Schellart et al. (2006) (Table 5 of Schellart et al., 2006) (Appendix 3 Table 11) departs significantly from all other motion paths between 24-12 Ma (Fig. 3b). It appears that the Australia-Pacific finite rotation pole for 17.6 Ma contains an error as the motion path does not match the predicted path using the finite rotations between plate pairs in the four plate model (Appendix 3 Table 10). These calculated Australia-Pacific total reconstruction poles of Schellart et al. (2006) have been used to support an argument that Australia-Pacific plate motions were insufficient to produce arc volcanism in a west-dipping subduction model beneath Northland initiating at 23 Ma (Schellart, 2007; Schellart, 2012); given the apparent errors in motions paths this assertion should be questioned. Reconstruction models relating to the initiation of arc volcanism in Northland are discussed further in following section 5.1.

The time interval between stage boundaries describing Australia-Antarctica and Pacific-Antarctica relative motions varies by up to an order of magnitude (Table 1). Revised Australia relative to Antarctica total reconstruction poles of Cande & Stock (2004) generally occur at intervals of 2-5 Ma, however, the longest stage duration is ~10 Ma (chron 6o to 5o). In contrast, revised Pacific relative to Antarctica total reconstruction poles of Croon et al. (2008) occur at approximately regular intervals of 0.9 ± 0.4 Ma. To determine Australia-Pacific relative plate motions at intervals less than those defined by stage boundaries in Cande & Stock (2004) previous studies (Furlong & Kamp, 2009) have interpolated stage poles linearly at 1 Myr intervals between chrons (as does GPlates when using Cande & Stock, 2004 stage boundaries), however, our

regional reconstruction model with a higher temporal resolution of Pacific-Antarctica total reconstruction poles show that stage pole locations do not follow a linear trend (Fig. 3a). The increased temporal resolution of Pacific-Antarctica relative motions, particularly between chrons 6o (20.13 Ma) and 5o (10.95 Ma), may help decrease uncertainties in Australia-Pacific relative motions during the longer Australia-Antarctica stage durations. While Australia-Antarctica relative motions between stage boundaries are interpolated, Pacific-Antarctica relative motions are well constrained. The overall effect of constraining Australia-Pacific plate motions in the regional reconstruction model with a higher resolution time sequence for Pacific-Antarctic motions is, however, minimal. This is demonstrated by comparison between Pacific plate motion paths (relative to a fixed Australian plate) calculated at 1 Ma intervals using the Cande & Stock (2004) stage durations to those in the regional reconstruction model (Fig. 4a).

A second set of reconstruction models for the New Zealand plate boundary are based on sea floor spreading data from the Emerald Basin in the southern South Island which record Australia-Pacific relative motions between 40 and 30 Ma (Fig. 2) (Sutherland, 1995; Keller, 2003). The finite rotations derived from the Emerald Basin are here referred to as the local reconstruction model. Recent reconstructions by Furlong & Kamp (2009) use updated and unpublished Australia-Pacific total reconstruction poles of Keller (2003) from the Emerald Basin in combination with those of Cande & Stock (2004) to chart the passage of the Pacific plate beneath the North Island. The location of the stage pole for the period 38-33 Ma differs significantly from the 4 plate model (by ~7.5º latitude or ~1100 km in a north-south direction) for the same time (Fig. 3b).

Pacific plate motion paths between 38-30 Myr predicted by the local and regional reconstruction models relative to Northland differ significantly. Due to the proximity of stage poles describing Pacific relative to Australia plate motions to Northland for this period (Fig. 3b), differences in their latitude (~7.5º or ~1100 km) result in contrasting motion vectors. Pacific plate motion paths predicted from each of these models during this time are essentially at right angles to one another (Fig. 5). This results in the amount of convergence prior to the initiation of the Northland arc predicted by either model varying by a factor of 2. It is difficult to reconcile such an abrupt change in relative motions at 30 Ma in the local reconstruction model across Northland. Both models accurately reflect the data they are based on, however, the relative motions they predict have different implications for the Northland plate

boundary during this period (i.e. convergence verses strike-slip). While beyond the scope for this study, geological constraints will be required to distinguish between these two models.

For plate reconstructions to be considered accurate, plate motions calculated by adding the motion of Australia-East Antarctica, East Antarctica–West Antarctica and West Antarctica-Pacific should predict a reasonable plate tectonic history for the Australia-Pacific plate boundary (Cande et al., 2000). Original reconstructions for the New Zealand region in the early Miocene predicted a large gap (~150 km) between the North and South Islands which could only be eliminated by including relative motions between East and West Antarctica (Stock & Molnar, 1982). Sutherland (1995) derived a total reconstruction pole for East-West Antarctica using data from the Emerald Basin by assuming this gap should be closed. The resulting total reconstruction pole predicted highly oblique dextral extension in the Ross Sea embayment the Cenozoic not supported by the geology (Cande et al., 2000). Total reconstruction poles derived from the Emerald Basin have not been widely adopted in the literature for Australia-Pacific relative motions during the period ~40 to 30 Ma.

Table 3. Total reconstruction poles for Australia and the Pacific relative to Antarctica.

Australia relative to Antarctica			Pacific relative to Antarctica			
Age (Ma)	Lat (ºN)	Long (º E)	Age (Ma)	Lat (ºN)	Long (º E)	Chron
			0.78	64.3	-81.21	1o
			1.86	64.9	-81.14	2
2.58	-11.16	-139.7	2.58	65.2	-81.23	2Ay
			3.58	65.9	-81.17	2Ao
			4.24	66.62	-80.53	3y
			5.11	66.91	-80.66	3o
6.04	-11.59	-139.2	6.04	67.09	-81.08	3Ay
			6.71	67.33	-81.2	3Ao
			7.86	68.16	-80.54	4
			8.86	68.83	-79.97	4A
			9.74	69.71	-78.57	5y
10.95	-11.9	-142.1	10.95	70.36	-77.81	5o
			12.29	71.29	-76.12	5A
			13.06	71.74	-75.12	5AA
			14.39	72.38	-73.58	5AD
			15.09	72.6	-73.18	5B
			16.15	72.97	-72.5	5Cy
			16.64	73.18	-72.03	5Co
			17.47	73.39	-71.58	5D
			18.28	73.62	-70.91	5E
			19.05	73.71	-70.94	6y
20.13	-13.39	-145.6	20.13	74.00	-70.16	6o
			21.16	74.13	-70.09	6A
			23.07	74.38	-69.73	6B
			24.06	74.48	-69.58	6C
			24.84	74.51	-69.66	7
			25.82	74.5	-69.84	8y
26.55	-13.8	-146.4	26.55	74.51	-69.81	8o
			27.03	74.45	-69.9	9y
			27.97	74.4	-69.75	9o
			28.28	74.41	-69.5	10y
28.74	-13.58	-146	28.75	74.33	-69.54	10o
			29.4	74.38	-68.71	11y
			30.1	74.33	-68.43	11o
			30.48	74.37	-67.75	12y
30.94	-13.4	-145.6	30.94	74.32	-67.59	12o
			33.06	74.44	-64.74	13y
33.54	-13.45	-146.6	33.55	74.48	-64.01	13o
			34.66	74.62	-61.89	15y
			34.94	74.63	-61.48	15o
			35.69	74.7	-60.18	16y
			36.34	74.75	-59.05	16o
			36.62	74.76	-58.64	17y
38.13	-14.65	-146.6	37.47	74.82	-57.44	17o
			38.43	74.85	-56.21	18y
			40.13	74.87	-54.46	18o
			41.39	74.86	-53.25	19
			42.54	74.85	-52.22	20y
			43.79	74.77	-51.61	20o

Australia relative to Antarctica from Cande & Stock (2004). Pacific relative to Antarctica from Croon et al. (2008). Ages are from Cande & Kent (1995) except for chrons 3Ay and 3Ao, which are from Krijgsman et al. (1999).

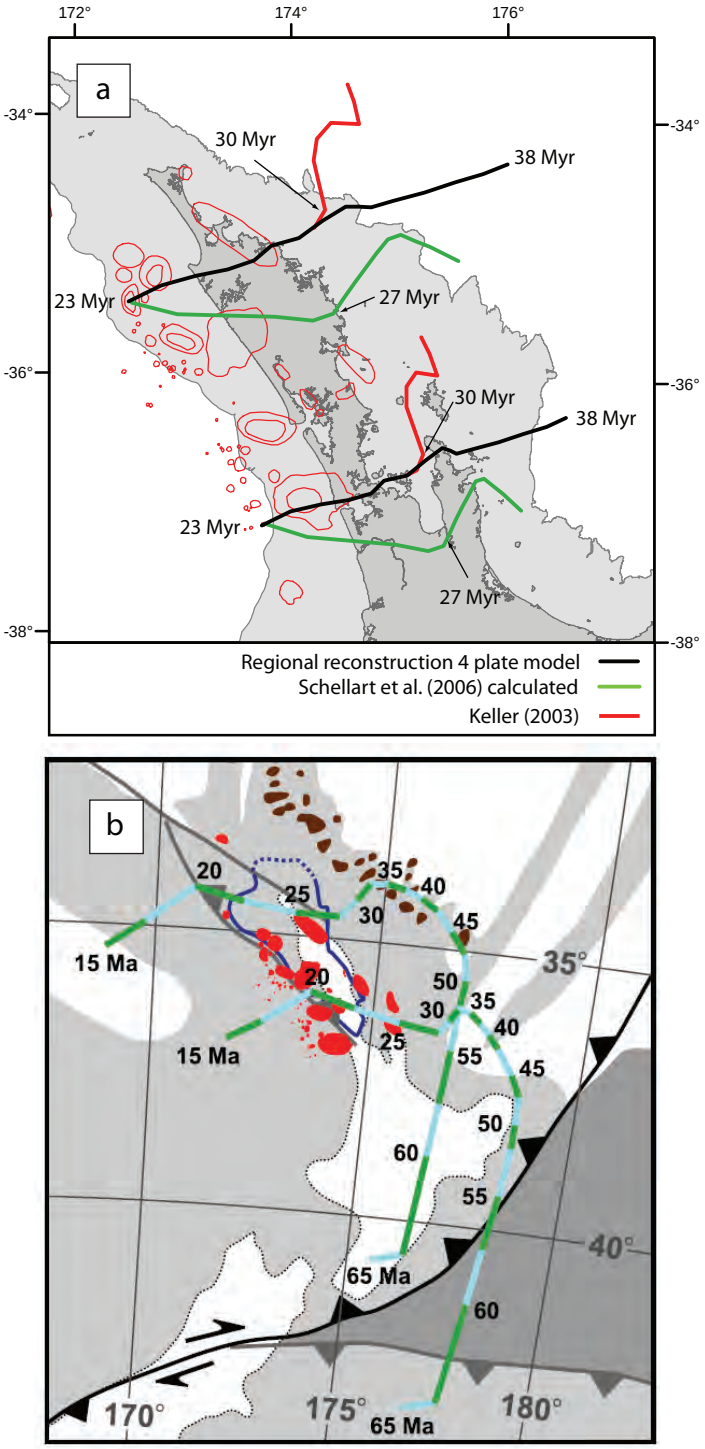

Figure 5. (a) Pacific plate motion paths relative to a fixed Australian plate for west dipping subduction models across Northland. Volcanic centres from Herzer (1995) and Hayward et al. (2001). (b) Pacific plate motion paths derived from Australia-Pacific total reconstruction poles calculated by Schellart et al. (2006) and detailed in Fig. 3 of Schellart (2007).

4. Absolute motions

The absolute motions of plates with respect to a fixed hot-spot reference frame or "anchored" plate may influence whether rollback of the subducting slab will occur (Lallemand et al., 2005; Sdrolias & Muller, 2006). Rollback of the slab is considered one of the primary mechanisms for extension in the overriding plate (Sdrolias & Muller, 2006). Slab rollback (or the seaward migration of the subduction hinge) causes upper plate extension by the negative buoyancy and gravitational instability of the subducting slab as it founders and sinks into the underlying asthenosphere (Molnar & Atwater, 1978; Sdrolias & Muller, 2006). Several studies have concluded that extension in the overriding plate associated with subduction correlates strongly with absolute motion of the overriding plate away from the trench where the age of the subducting lithosphere is > 55 Ma (Jarrard, 1986; Heuret & Lallemand, 2005; Lallemand et al., 2005; Sdrolias & Muller, 2006). Along the Tonga-Kermadec trench the subducting Pacific plate is Cretaceous in age (Downey et al., 2007) as is the Hikurangi Plateau presently subducting beneath the North Island (Davy et al., 2008). While the negative buoyancy of ~100 Myr old oceanic crust would be sufficient for rollback to occur, the presence of the buoyant Hikurangi Plateau towards the termination of subduction make these relationships less clear. The density of the lithosphere beneath, and adjacent to, the North Island should be sufficient for subduction of the Hikurangi Plateau to occur (Gutscher et al., 2000) even without consideration of an eclogite base to the shallow slab (Reyners et al., 2011). Whether a buoyant subducting plateau is capable of rollback is presently unknown.

In the North Island, the absolute motion of the Australian plate has been away from the Pacific plate relative to a hot-spot reference frame (Muller et al., 1993; O'Neill et al., 2005) (Fig. 6) or East Antarctica (not shown) from 38 Ma to the present. The absolute motion of the Australian and Pacific plates in the New Zealand region would be consistent with upper plate extension being driven by rollback of the Pacific plate. The formation of South Fiji Basin between ~23-18 Ma (Mortimer et al., 2007) and Havre Trough and Lau Basins since ~6 Ma (Parson & Wright, 1996; Taylor et al., 1996) indicate this process has been punctuated. At present there is no clear relationship between the absolute motion of the overriding plate and the timing of the most recent episode of Pacific plate rollback.

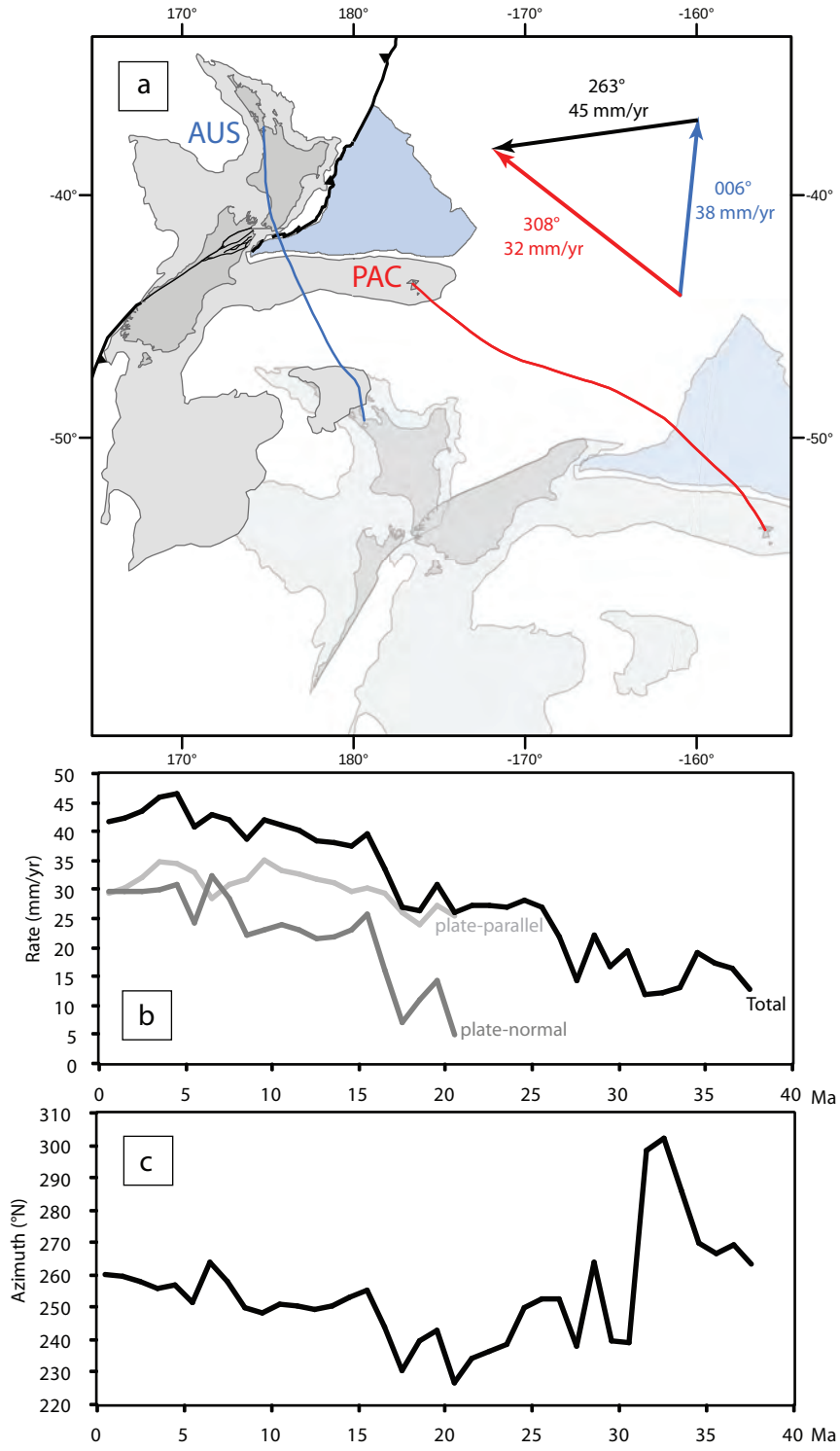

Figure 6. Absolute motion paths of the Pacific and Australian plates from 38 Ma. (a) Absolute plate motion paths of the Australian (blue line) and Pacific (red line) plates derived from the regional reconstruction model relative to a hot-spot reference frame (Muller et al., 1993; O'Neill et al., 2005), see text for details. Vector diagram shows contemporary absolute and relative plate vectors from GPS (Beavan et al., 2007). (b) Australia-Pacific relative plate motion rates calculated from absolute motion paths. Plate-normal and -parallel component of the relative motion vector calculated for an 035º striking plate. The alignment of arc volcanic centres through onshore and offshore North Island from ~16 Ma are approximately parallel to the present arc front (~035º) and the strike of the underlying slab (chapter 5). (c) The azimuth of the relative plate vector over the last 38 Myr.

Contemporary relative plate motion along the Hikurangi margin is accommodated by margin normal and parallel faults (i.e. the subduction thrust) and by vertical-axis rotations (Nicol & Wallace, 2007; Nicol et al., 2007). From ~16 Ma the strike of the subducting plate beneath the North Island - inferred from Benioff zone seismicity, mantle velocity anomalies, and the alignment of arc volcanoes - has been approximately parallel to present (chapter 5). To examine changes in the rate of plate-normal and plate-parallel motion over time, the relative motion vector resulting from the absolute motion of two points on stable portions of the Australian and Pacific plates (Beavan et al., 2002) is split into its respective components. Since arc volcanism along a trend similar to present (~035º) was established by 16 Ma through onshore and offshore North Island (chapter 5), plate-normal and -parallel components of the relative vector can be estimated from this time (Fig. 6b).

Immediately prior to 16 Ma (i.e. 20 to 16 Ma) the component of relative plate motion parallel to 305º doubles from ~11 mm/yr to ~23 mm/yr, increasing again by approximately a third (27%) between ~8-6 Ma. The component of relative plate motion parallel to 035º gradually increases from ~16 mm/yr at 26 Ma to 16 Ma where it has remained parallel to the plate and approximately constant at 32 ± 2 to the present. Between 8-6 Ma, plate-normal and -parallel rates become approximately equal for the first time since at least 26 Ma. Australia-Pacific motion vectors show a 50-60º counter-clockwise swing in direction between 33 and 26 Ma, an opposing 15-20º clockwise swing in direction from 20 to 16 Ma and a relatively constant azimuth of 254 ± 5º from 16 Ma to the present (Fig. 6b). By comparison, contemporary relative plate motion measured by GPS using the same stable locations on the Australian and Pacific plates is 263º (refer Fig. 3) (Beavan et al., 2002).

5. Relative plate motions

5.1 Initiation of arc volcanism in Northland

The evolution of the SW Pacific region during the Oligocene to Early Miocene is unresolved. In particular, the age of the South Fiji and Norfolk Basins has recently been revised to 23-18 Ma (Mortimer et al., 2007; Herzer et al., 2011) indicating back-arc opening occurred contemporaneously to the north of the North Island during widespread arc volcanism across Northland (Herzer, 1995; Hayward et al., 2001). The driving mechanism associated with southwest directed allochthon emplacement between ~25-22

Ma and the eruption of voluminous arc-type volcanism across Northland along a NW-SE trend from ~23 Ma is a matter of ongoing debate (Ballance, 1976; Brothers, 1984; Rait et al., 1991; Herzer, 1995; Hayward et al., 2001; Schellart et al., 2006; Mortimer et al., 2007; Schellart, 2007; Herzer et al., 2009; Mortimer et al., 2010) (Booden et al., 2011; Schellart, 2012). While we are primarily focussed on the geometric evolution of subduction and associated arc volcanism, accounting for the south-westward emplacement of allochthons across northeastern North Island is an important constraint for any subduction model.

Various models have been suggested for the evolution of subduction geometry beneath Northland in the Early Miocene (Fig. 7), and generally fall into two main categories; rollback of west-southwest-dipping Pacific plate as proposed by Mortimer et al. (2007) and slab detachment of northeast-dipping Australian plate as proposed by Crawford et al. (2003) and adapted and developed by Schellart et al. (2006) and Schellart (2007, 2012). At present, there is no spatial or temporal pattern to the development of arc volcanism across Northland that conclusively distinguishes between either northeast- or southwest-dipping subduction geometry (Hayward et al., 2001). Arc-type volcanic rocks across Northland contain comparable fractions of fluid mobile trace elements consistent with dehydration of an underlying slab (Booden et al., 2011). Arc-type trace element signatures are different between eastern and western volcanic belts in Northland although these differences are considered the result of crustal thickness variations and not subduction polarity (Booden et al., 2011).

Early models for the Northland arc involved progressive steepening of a north-westward dipping slab to explain an apparent south-eastward migration of the volcanism (Brother, 1984; Kamp, 1984) which are consistent with volcanic ages from 16 Ma to present (Fig. 7) (chapter 5). This model was rejected by Ballance et al. (1985), Herzer (1995), and Hayward et al. (2001) as volcanic ages show no age progression prior to 16 Ma (chapter 5). Schellart (2007) also considered the maximum distance between the Hikurangi trench and volcanism unrealistically large (750 km). It should be noted, however, that due to the obliquity of Australia-Pacific plate motions Miocene-Recent volcanism is no more than ~450 km from the northern and eastern continental margins of the North Island, the maximum distance presently observed for global compilations of arc volcanoes (Syracuse & Abers, 2006). Arc-type volcanism across Northland has been explained by west-southwest directed subduction of either the South Fiji Basin (Malpas et al., 1992; Herzer, 1995; Ballance, 1999; Whattam et al., 2005) or

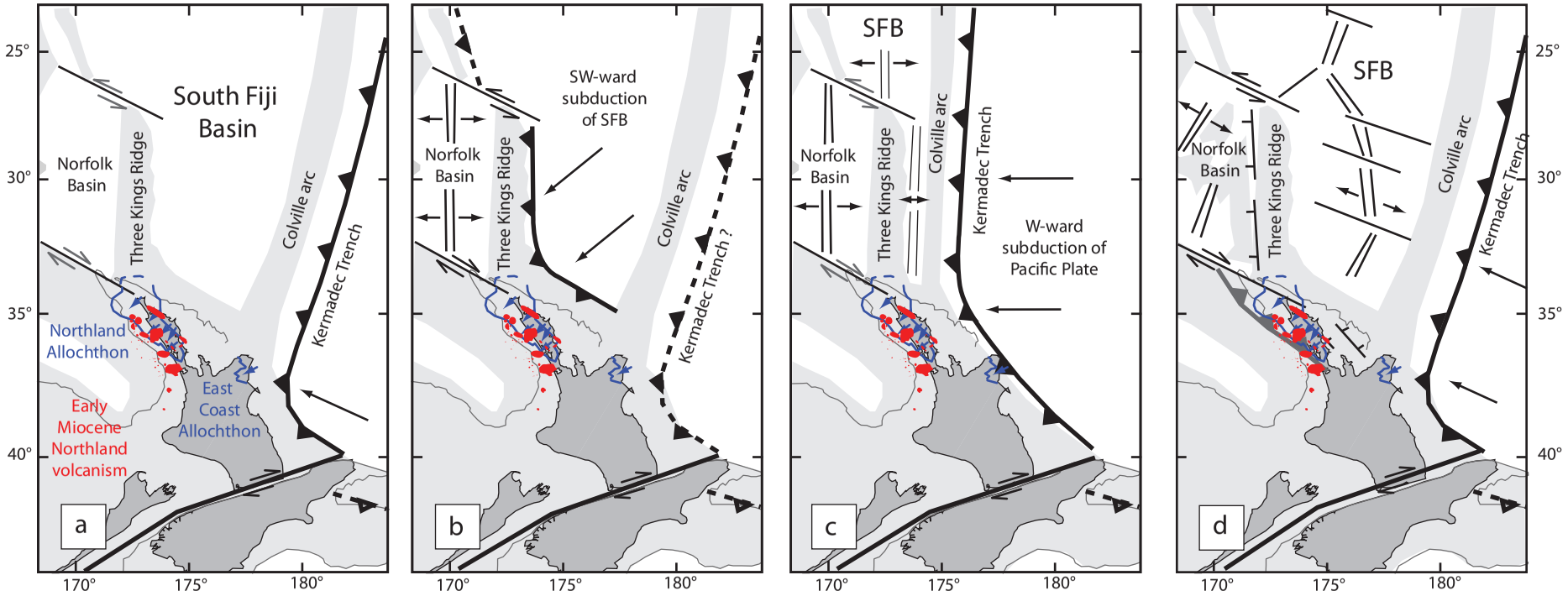

Figure 7. Schematic diagrams at 20 Ma for tectonic models relating to Northland arc volcanism (modified from Schellart, 2007). (a) West-northwestward subduction and progressive steepening of the Pacific plate (Brothers, 1984; Kamp, 1984). (b) Southwestward subduction of the South Fiji Basin (SFB) (e.g. Herzer, 1995; Ballance, 1999; Whattam et al., 2005). (c) West-southwestward subduction of the Pacific plate with simultaneous opening of Norfolk and South Fiji Basins (e.g. King, 2000; Mortimer et al. 2007; Herzer et al., 2011). (d) Northeastward subduction of the Australian plate and slab detachment and rollback of west dipping Pacific plate (Crawford et al., 2003; Schellart et al., 2006; Schellart, 2007; 2012). Extent of Northland and East Coast allochthons (blue lines) and Early Miocene transport directions (blue arrows) from Rait (2000), Herzer et al. (2009), and Sutherland et al. (2009). Arc volcanic centres active at 20 Ma (red polygons) from Bergman et al., (1992), Herzer (1995), Hayward et al., (2001). Hikurangi margin reconstruction after King (2000) and Nicol et al. (2007).

the Pacific plate (Mortimer et al., 1998; Herzer et al., 2000; King, 2000; Bradshaw, 2004; Mortimer et al., 2007). Recent revision of the South Fiji Basin to Oligocene and/or Early Miocene age precludes the subduction of young (probably < 10 Myr) buoyant oceanic lithosphere beneath Northland on geochemical grounds (i.e. absence of adakitic trace element signatures) (Mortimer et al., 2007; Booden et al., 2011). Reanalysis of lavas show a consistent Island-arc signature throughout Northland (Booden et al., 2011) favouring an origin in response to an actual, if short-lived subduction event, rather than slab detachment as proposed in some models (Schellart, 2007; Schellart, 2012).

At present, a west-dipping Pacific plate subduction model is consistent with geological evidence from New Zealand for the geometry of subduction beneath Northland (Fig. 8). An alternative hypothesis for the origin of arc volcanism across Northland, northeast-dipping subduction of the Australian plate followed by slab detachment (Fig. 7) (Crawford et al., 2003; Schellart, 2007), originates from obduction models for the emplacement of ophiolites by the northeast-dipping South Loyalty slab in New Caledonia (Schellart et al., 2006). The location of the trench associated with north-east dipping subduction model is shown southwest of Northland (Schellart et al., 2006; Schellart, 2007) in map view where seismic reflection lines provide no evidence for an accretionary prism or subduction thrust (Herzer, 1995), and to the northeast of Northland in cross-section (Schellart, 2012) which requires a ‘folded’ subduction geometry. In addition, the geometry and displacement history of the northeast- to east-dipping Taranaki Fault (Stagpoole & Nicol, 2008), and Late Eocene contraction across the Reinga Basin (Bache et al., 2012) are inconsistent with a northeast-dipping subduction model.

To place constraints on the timing and kinematics of west-dipping subduction we examine Pacific plate motion paths relative to a fixed Australian plate for the period 38-23 Ma across Northland. We show motion paths from three different models that finish at a common location for two points along the Northland arc (Fig. 5a). The Pacific plate motion paths of Schellart (2007, 2012) (Fig. 6b) – derived from Australia-Pacific total reconstruction poles of Schellart et al. (2006) - clearly deviate from those derived from the regional reconstruction model used in this study and are considered in error (see section 3 and Fig. 4b). I therefore consider the geodynamical arguments against a west-dipping Pacific plate subduction model (Schellart, 2012) - based on the Australia-Pacific total reconstruction poles calculated in Schellart et al. (2006) - that the

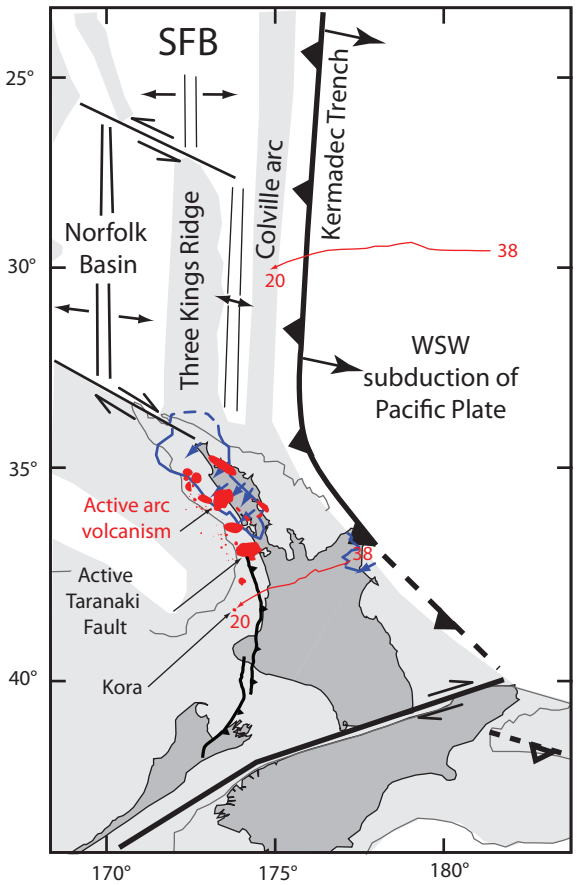

Figure 8. 20 Ma reconstruction of the North Island plate boundary (WSW dipping subduction model after Mortimer et al., 2007). Arc volcanic centres active at 20 Ma (red polygons) from Bergman et al., (1992), Herzer (1995), Hayward et al., (2001). Extent of Northland and East Coast allochthons (blue lines) and Early Miocene transport directions (blue arrows) from Rait (2000), Herzer et al. (2009), and Sutherland et al. (2009). Pacific plate motion path (thin red line) relative to fixed Australian plate. Northern active Taranaki Fault tip from Stagpoole & Nicol (2008). The location and trend of eastern-most active volcanic centers oshore and offshore North Island is consistent with the inferred location of the Colville Ridge at this time (Herzer et al., 2011). Reconstruction of Hikurangi margin after King (2000) and Nicol et al. (2007).

amount and direction of subduction was insufficient prior to allochthon emplacement and the initiation of arc volcanism are unsupported. Pacific plate motion relative to Australia between 38 to 23 Ma derived from the regional reconstruction model (Appendix 3 Table 9) trend approximately perpendicular to the Northland arc (~250º) and moderately oblique (34º clockwise) to allochthon emplacement beginning ~25 Ma (refer Fig. 8) (Rait, 2000). The distance the Pacific plate travelled between 38 and 23 Ma in a west-dipping subduction model is ~350 km and ~285 km at northern and southern ends of the arc respectively. The Pacific plate at sub-arc depths beneath Northland at the initiation of arc volcanism at 23 Ma in the regional reconstruction model had travelled from (or beyond) the North Island continental margin (refer Fig. 5). Numerical models indicate that self sustaining subduction could occur after approximately 100-150 km of convergence (Hall et al., 2003; Gurnis et al., 2004) and therefore the transport distance associated with our west-dipping Pacific plate subduction model is feasible as the source of Northland arc volcanism and as a mechanism for allochthon emplacement.

The generation of arc volcanism requires a hydrated slab sufficiently out of equilibrium with its surroundings to dewater, fluxing the mantle wedge with sufficient volumes of fluid to lower the solidus and generate melt (Gill, 1981; Kirby et al., 1996; Hacker et al., 2003b). The local reconstruction model indicates a Pacific plate beneath Northland at the initiation of subduction at 38 Ma (refer Fig. 5a). However, this slab was partially subducted beneath Northland in the Cretaceous and would have reached equilibrium with its surroundings, as it has beneath the Chatham Rise (Davy et al., 2008). Therefore it is suggested that for arc volcanism to have initiated in Northland at 23 Ma, a west-dipping Pacific plate model requires subduction of hydrated slab during the Cenozoic. A Cretaceous age plate subducting through a trench, hydrated through bending-related normal faults (Ranero et al., 2003; Faccenda et al., 2009) during the Cenozoic, could be expected to dehydrate sufficiently resulting in arc volcanism (chapter 4). The regional reconstruction model indicates the Pacific plate subduction would have occurred from at least (or beyond) the northern Northland continental margin where a trench may have been positioned (refer Fig. 5a). In order for the subducting Pacific plate to first hydrate and then dehydrate during the Cenozoic requires at least 285-300 km of subduction which at the rates of relative plate motion normal to the Northland margin (estimated from the regional reconstruction model) would indicate that subduction commenced no later than 38 Ma (e.g. Bache et al., 2012).

5.2 Pacific plate subduction

The present Hikurangi subduction margin has evolved since at least the Eocene as a result of relative motions between the Australian and Pacific plates. The southern and lower limits of the Benioff zone and the slab as defined by positive mantle anomalies are used as passive markers to track the evolution of subduction. These passive markers are easily defined and represent spatial and temporal scales of sufficient length with which to reconstruct subduction over the last 38 Myr. Tracking the subduction of the Pacific plate beneath the North Island is key to understanding the initiation and evolution of arc volcanism and rifting in the North Island since the Miocene. We use the regional reconstruction model to reconstruct the horizontal extent of the presently imaged slab through time. The location of arc volcanism constrains possible slab geometries prior to the reactivation of subduction. These plate reconstructions and relative plate motions indicate that slab hydrated beyond the northern North Island continental margin, though not at present seismically imaged, was the fluid source contributing to arc volcanism in Northland at 23 Ma and the Taranaki Basin between ~20 and 11 Ma.

The southern limit of intermediate depth seismicity (50-240 km) forms a sharp boundary beneath the northern South Island (Fig. 9). Eberhart-Phillips & Bannister (2010) interpret the slab as a continuous unbroken feature extending from the active subduction zone to the north (i.e. beneath the North Island) to the southern limit of Benioff zone seismicity beneath the South Island (Fig. 9a and c). The abrupt cessation of Benioff seismicity beneath the northern South Island is interpreted as an anhydrous/hydrous boundary within the slab (Eberhart-Phillips & Bannister, 2010). To the north of this boundary, Benioff seismicity defines a variably hydrated slab out of equilibrium with the temperature and pressure conditions of the surrounding mantle, whereas to the south of this boundary, an anhydrous slab in equilibrium with its surroundings is unlikely to be seismically active and therefore unlikely to be identified as subducted lithosphere (Kirby et al., 1996; Hacker et al., 2003b; Eberhart-Phillips & Bannister, 2010). The southern limit to Benioff seismicity extends vertically to ~240 km depth (representing a horizontal length of ~300 km). The lower limit of Benioff zone seismicity, also an inferred boundary between hydrous and anhydrous slab, varies in depth along the Hikurangi margin from ~240 km in the south (Fig. 9b) to ~350 km in the north (chapter 4).

To extend the length of the slab used in the reconstructions beyond the Benioff zone we use constraints from mantle tomography and the trend of deep earthquakes. The Pacific plate extends continuously to depths of at least 600 km beneath the North Island (chapter 5), ~300 km deeper than the slab defined by Benioff seismicity (Fig. 10). Deep earthquakes (Boddington et al., 2004) and positive mantle velocity anomalies (Li et al., 2008) are consistent with a northeast trending slab representing ~750 km of subducted Pacific plate. The southern limit of positive mantle velocities extends to at least ~43.5°S at depths < 250 km and to the hydrous/anhydrous boundary interpreted beneath the northern South Island at depths > 250 km.

Reconstructions were selected at times that reflect key points in the development of volcanism across the North Island to highlight the location of the presently imaged Pacific slab unfolded to its horizontal extent at the surface (Fig. 11). It is possible to infer the first-order geometry of the subducting plate through time using the general relationship between location and trend of arc volcanism to the underlying slab. The alignment of arc front volcanism generally approximates the 90-100 km depth contour of the underlying slab in the North Island (chapter 5) and global compilations of arc-slab relations (Syracuse & Abers, 2006). While this depth to slab beneath arc volcanism may not reflect the precise value of past depths it can be considered a first-order approximation. It is noted that the absence of arc volcanism does not imply the absence of an underlying slab as the present relationships between the slab and volcanism along the Hikurangi margin show (chapter 4), however, the presence of arc volcanism does require an underlying slab as it is fluid mobile elements from the subducting slab and mantle wedge that ultimately determine the provenance of Island arc volcanism (Gill, 1981).

The reconstruction of the horizontal or unfolded extent of the seismically imaged slab indicates its present southern edge began subducting beneath the continental margin of the North Island at around 20 Ma (not shown). The present southern and lower limits of the Benioff zone beneath the North Island and southern South Island represent slab subducting for ≤ 17 Myr. Slab subducting for more than 17 Myr is no longer seismically active. What is apparent is that the seismically imaged slab (i.e. either associated with Benioff zone seismicity or positive mantle anomalies) does not lie beneath either the northwest-southeast trending Northland arc at 23 Ma or the northeast-southwest trending Colville-Coromandel-Taranaki arc from ~20 to 11 Ma (16 Ma shown in Fig. 11). By 8 Ma the present lower limit of seismicity was approaching

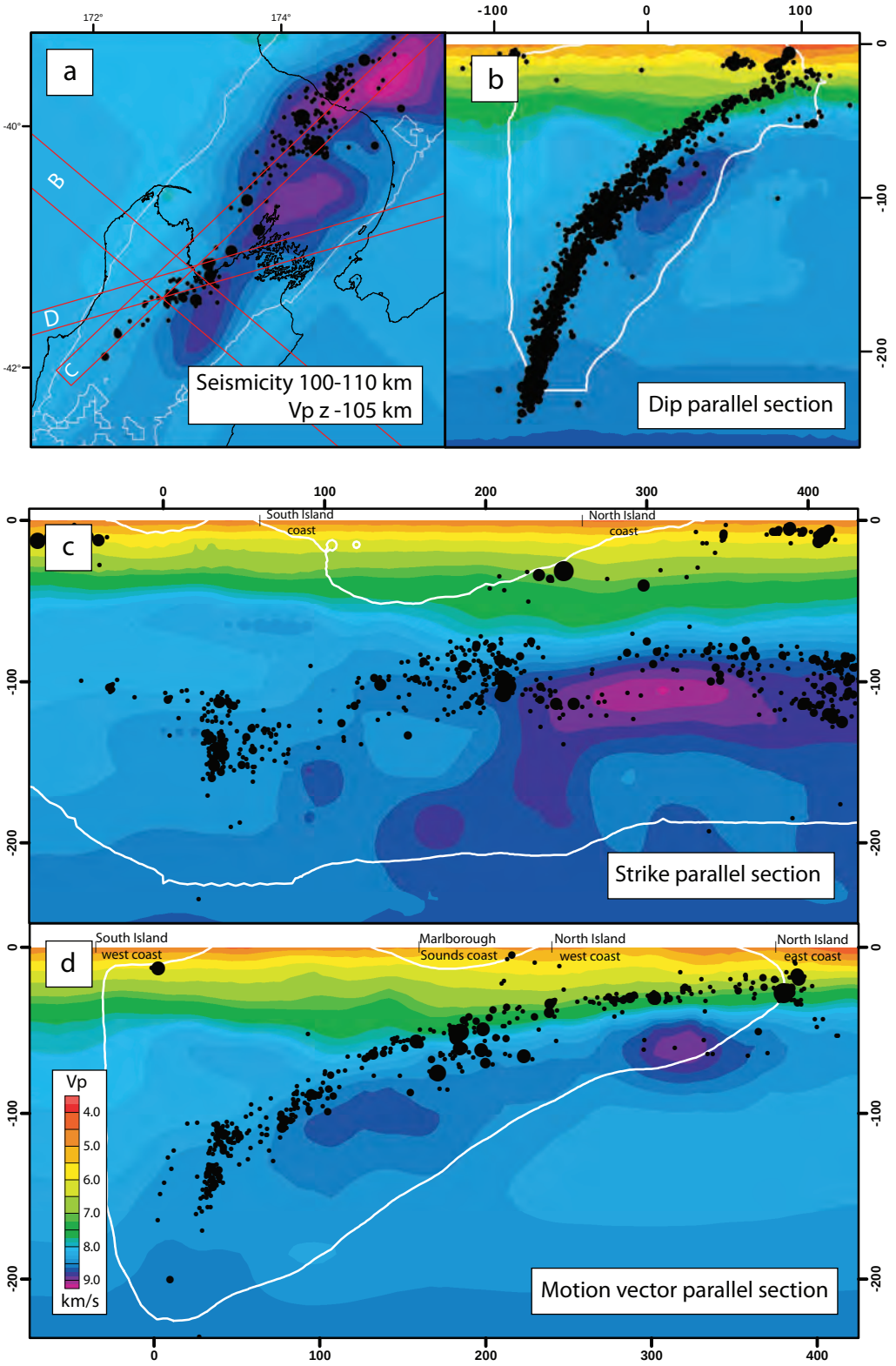

Figure 9. Seismicity and velocity sections of the subducting slab beneath northern South Island. Seismicity relocated using 3D velocity model of New Zealand (2001-2009 $M_L > 3$) (black filled circles). P-wave velocity (Vp) sections from 3D velocity model of New Zealand (Eberhart-Phillips et al., 2010). Meaningful velocity data lies within spread function < 3 (white line). (a) Seismicity sections (red lines) superimposed over 105 km Vp depth slice. (b) Dip-parallel profile showing curvature of slab. (c) Along strike section. (d) Section parallel to the relative plate motion vector. Coastline in A shown as black ticks in sections for reference.

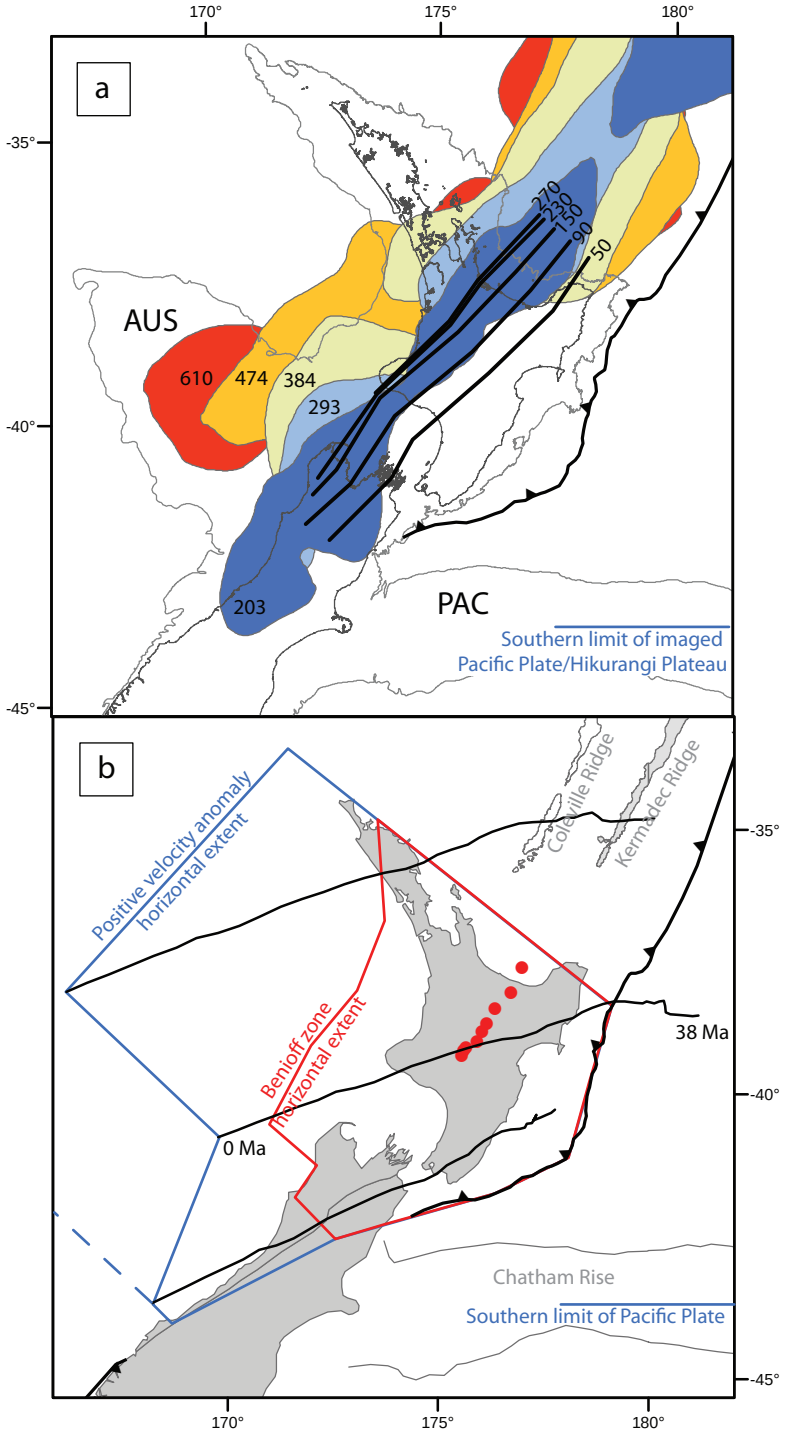

Figure 10. Depth extent of subducted Pacific plate. (a) Slab geometry beneath the New Zealand derived from Benioff zone seismicity (thick black lines) and positive velocity anomaly contours (coloured polygons) (Li et al., 2008). See chapter 5 for details. Numbers indicate depth in km. (b) Unfolded horizontal extent of the subducted slab from intermediate depth seismicity (red line) and positive mantle velocities (blue line) from (a). Southern limit of Pacific plate beneath Chatham Rise from seismic reflection profile HKDC-1 (Davy et al., 2008) (Fig. 1). Motion path of Pacific Plate relative to a fixed Australian Plate (black line) from 38 Myr derived from regional reconstruction model. Contemporary arc-front volcanism (red filled circles) approximates the 90 km depth contour on the subducting slab.

sub-arc depths parallel to the alignment of active arc volcanic centres through the onshore and offshore North Island.

These reconstructions imply that either volcanism in the Taranaki Basin between ~20-11 Ma was either not subduction related or that the slab at depth extends further to the southwest than presently imaged using positive mantle anomalies (e.g. slab extent marked by dashed line in Fig. 11). A subduction origin for volcanism in the Taranaki Basin is constrained by the arc-type trace element signature of a ~20-8 Ma (K-Ar dated samples and seismic stratigraphic constraints), low-med-K andesite submarine volcano (Kora) (Fig. 7) (Bergman et al., 1992; Giba, 2010). The southern extent of the slab required to produce arc volcanism between ~20-11 Ma in the Taranaki Basin would require the presence of a subducted slab to at least ~43.5°S at present - i.e. the southern limit of the slab imaged beneath the Chatham Rise (Davy et al., 2008) and/or its southern extent defined by positive mantle anomalies < 250 km depth (Li et al., 2008) (Fig. 11) – at least ~200 km south beyond the end of the seismically active slab.

The hypothesis that an anhydrous Pacific plate continues southwest beneath the central South Island (Eberhart-Phillips & Bannister, 2010; Reyners et al., 2011) to at least its southern limit observed in a seismic-reflection line across the Chatham Rise (~43.5°S) (Davy et al., 2008) is supported by the decreasing frequency of Benioff zone seismicity southwards along the Hikurangi margin (chapter 4). Rates of slab seismicity at sub-arc depths (90-170 km), considered a proxy for rates of dehydration embrittlement (Hacker et al., 2003b), in proximity to the southern limit of the Benioff zone are approximately 20% of those in the slab beneath the northern Hikurangi margin. This southward decrease in seismicity rates are therefore consistent with the southern boundary to Benioff seismicity being a transition from hydrous to anhydrous subducted lithosphere (Eberhart-Phillips & Bannister, 2010) rather than the edge to the slab, for example (Fig. 9). Interpretation of seismic velocities beneath the South Island may indicate the Pacific plate extends to latitudes of ~45°S (Reyners et al., 2011). The lower limit of Benioff seismicity also supports a model for the southern continuation of an aseismic slab. Subducted Pacific plate ≥ 17 Ma at depth is no longer seismically active, the slab inferred beneath the Taranaki Basin and Northland must have begun subducting no later than 20 Ma.

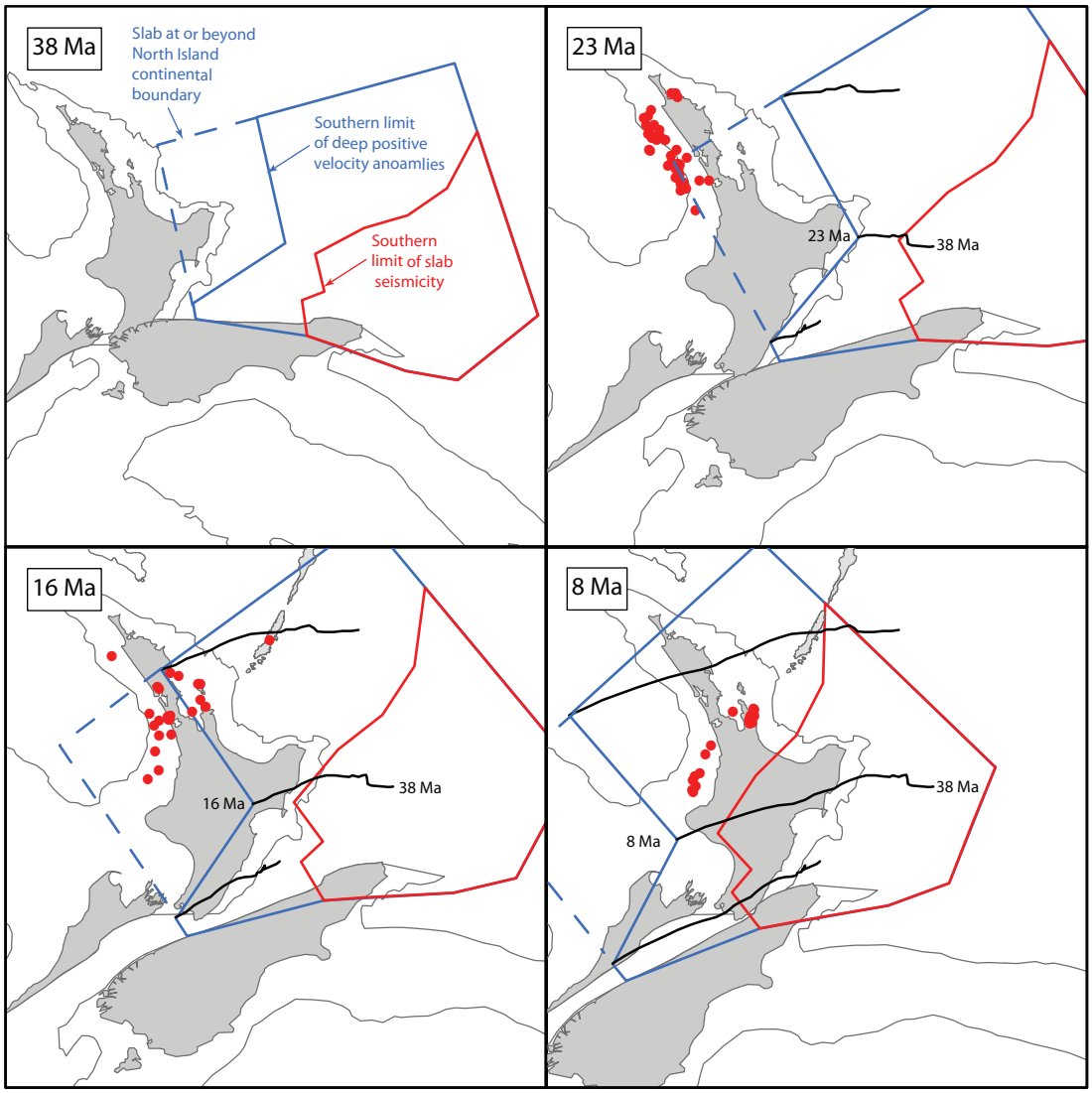

Figure 11. Reconstruction of the unfolded Pacific slab over the last 38 Ma. Refer to Fig. 10 for details of unfolded slab extent. Pacific plate relative to a fixed Australian plate reconstructions based on finite rotations from the regional reconstruction model. Trend of active eastern arc volcanism at 8 and 16 Ma approximates 90 km depth contour of subducting slab (see chapter 5 for details and references). Note that the Hikurangi margin is shown in its present position. Schematic reconstruction of Hikurangi margin shown in Fig. 8. Southern limit of seismically active slab and deep positive velocity anomalies began subducting beneath North Island around 20 Ma. Prior to this time the seismically defined subducted plate is inferred to lie east of trench in a west dipping Pacific plate subduction model (e.g. Mortimer et al. 2007). Slab at (or beyond) the northern North Island continental margin at 38 Ma (dotted blue line) is required to produce arc volcanism between 23 and 11 Ma offshore North Island for a west-southwest dipping subduction model.

6. Discussion

The time periods 12-10 Ma and 8-6 Ma mark fundamental plate motion changes across the New Zealand plate boundary and throughout SW Pacific. These changes arise in part due to rotation in the direction of spreading along the Pacific-Antarctic Ridge around ~11 and ~6 Ma (Croon et al., 2008). The spreading directions of ridge segments near the Menard fracture zone (50ºS) remained fairly constant between 23 and 5 Ma (3º clockwise rotation) which is in contrast to fracture zones along the south-western section of the Pacific-Antarctic Ridge that lie closer to Pacific-Antarctic stage poles and have undergone a 30º clockwise rotation since 10 Ma (Croon et al., 2008). This clockwise rotation in the direction of spreading along the south-western segment of the Pacific-Antarctic Ridge coincides with the initiation of subduction in the south-western South Island (House et al., 2002), increased convergence across the Alpine Fault (Tippet & Kamp, 1993; Walcott, 1998; Cande & Stock, 2004), and initiation of intra-arc extension in offshore western North Island (Giba et al., 2010). These contrasting styles of deformation along the New Zealand plate boundary indicate the existence of a local pole of rotation, possibly in proximity to the collision point of the Chatham Rise with the Australian plate.

Significant increases in margin normal motion coincide in time with the end of extension in the South Fiji Basin (Mortimer et al., 2010) at ~18 Ma and the initiation of extension along the Havre-Lau intra-arc rifts at ~6 Ma (Parson & Wright, 1996; Taylor et al., 1996). Intuitively, arresting the development of an extending ocean basin through an increase in margin normal convergence seems plausible, initiating a second phase of overriding plate extension with a further increase does not. Collision models for the formation of overriding plate extension may be consistent with the opening of the Havre Trough. Increased margin normal convergence would have increased torque on the eastern North Island possibly driving rollback of the slab through the seaward advance of the Hikurangi fore-arc (Wallace et al., 2009). The advance of a fore-arc over a subduction hinge may also involve uplift. Basin subsidence in the Taranaki Basin associated with subduction occurred around 25 Ma whereas major infilling of the basin did not occur until 17 Ma with the emergence of the Taranaki Fault above sea level (Stern & Holt, 1994). Widespread contraction of the Hikurangi fore-arc also occurred between 8-6 Ma (Nicol et al., 2002; Nicol et al., 2007) consistent with the acceleration of margin normal plate motion shown here.

7. Conclusions

The most recent and well constrained Australia-Antarctica-Pacific plate motions have been used to track the absolute and relative motions of the overriding and subducting plates along the North Island continental margin for the last 38 Myr. The absolute motion of the overriding Australian plate away from the subducting Cretaceous Pacific plate since the reorganisation of plate motions around 45 Ma is conducive for rollback to occur along the Hikurangi margin. The punctuated development of extensional basins adjacent to the North Island, however, show no simple correlation between the absolute motion of the overriding plate, subducting plate age and rollback. Plate-normal rates doubled from ~20 to 16 Ma, increasing further by approximately a third between ~8-6 Ma to their present values of ~30 mm/yr. In contrast, plate-parallel rates steadily increased from ~15 mm/yr at 26 Ma to 32 ± 2 mm/yr from 16 Ma to the present. Tracking the presently imaged southern extent of the Pacific plate prior to initiation of arc volcanism across Northland at 23 Ma and the Taranaki Basin between 20 and 11 Ma shows that west-dipping subduction models are viable and that subduction from 38 Ma is required to transport a sufficiently hydrated slab to sub-arc depths.

References

Adams, C.J., Graham, I.J., Seward, D. & Skinner, D.N.B., 1994. Geochronological and geochemical evolution of late Cenozioc volcanism in the Coromandel Peninsula, New Zealand. *New Zealand Journal of Geology & Geophysics*, 37, pp.359-79.

Bache, F., Sutherland, R., Stagpoole, V., Herzer, R., Collot, J. & Rouillard, 2012. Stratigraphy of the southern Norfolk Ridge and the Reinga Basin: A record of initiation of Tonga-Kermadec-Northland subduction in the southwest Pacific. *Earth & Planetary Science Letters*, 321-322, pp.41-53. doi:10.1016/j.epsl.2011.12.041.

Ballance, P.F., 1976. Evolution of the Upper Cenozoic magmatic arc and plate boundary in northern New Zealand. *Earth & Planetary Science Letters*, 28, pp.356-70.

Ballance, P.F., 1999. Simplification of the southwest Pacific Neogene arcs: inherited complexity and control by a retreating pole of rotation. *Geological Society of London Special Publication*, 164, pp.7-19.

Ballance, P.F., Hayward, B.W. & Brook, F.J., 1985. Subduction regression of volcanism in New Zealand. *Nature*, 313, p.820.

Beavan, J., Tregoning, P., Bevis, M., Kato, T. & Meertens, C., 2002. Motion and rigidity of the Pacific Plate and implications for plate boundary deformation. *Journal of Geophysical Research*, 107(B10), p.2261. doi:10.1029/2001JB000282.

Bergman, S.C., Talbot, J. & Thompson, P.R., 1992. The Kora Miocene submarine andesite stratovolcano hydrocarbon reservior. *Taranaki Basin 1991 New Zealand Oil Exploration Conference Proceedings*, pp.178-206.

Boddington, T., Parkin, C.J. & Gubbins, D., 2004. Isolated deep earthquakes beneath the North Island of New Zealand. *Geophysics Journal International*, 158, pp.972-82.

Booden, M.A., Smith, I.E.M., Black, P.M. & Maulk, J.L., 2011. Geochemistry of the Early Miocene volcanic succession of Northland, New Zealand, and implications for the evolution of subduction in the Southwest Pacific. *Journal of Volcanology & Geothermal Research*, 190, pp.25-37. doi:10.1016/j.jvolgeores.2010.10.006.

Booden, M.A., Smith, I.E.M., Mauk, J.L. & Black, P.M., 2010. Evolving volcanism at the tip of a propagating arc: The earliest high-Mg andesities in northern New Zealand. *Journal of Volcanology & Geothermal Research*, 190, pp.83-96.

Boyden, J.A., Muller, R.D., Gurnis, M., Torsvik, T.H., Clark, J.A., Turner, M., Ivey-Law, H., Watson, R.J. & Cannon, J.S., 2011. Next-generation plate-tectonic reconstructions using GPlates. In G.R. Keller & C. Baru, eds. *Geoinformatics: Cyberinfrastructure for the Solid Earth Sciences*. Cambride University Press. pp.95-114.

Bradshaw, J.D., 2004. Northland Allochthon: an alternative hypothesis of origin. *New Zealand Journal of Geology & Geophysics*, 47, pp.375-82.

Brothers, R.N., 1984. Subduction regression and oceanward migration of volcanism, North Island, New Zealand. *Nature*, 309, pp.698-700.

Cande, S.C. & Kent, D.V., 1995. Revised calibration of the geomagnetic polarity timescale for the Late Cretaceous and Cenozoic. *Journal of Geophysical Research*, 100(B4), pp.6093-95. doi:10.1029/94JB03098.

Cande, S., Raymond, C.A., Stock, J.M. & Haxby, W.F., 1995. Geophysics of the Pitman Fracture Zone and Pacific-Antarctic plate motions during the Cenozoic. *Science*, 947-953, p.270.

Cande, S.C. & Stock, J., 2004. Pacific-Antarctic-Australian motion and the formation of the Macquaire Plate. *Geophysics Journal International*, 157, pp.399-414.

Cande, S., Stock, J.M., Muller, R.D. & Ishihara, T., 2000. Cenozoic motion between East and West Antarctica. *Nature*, 404, pp.145-50.

Carter, L., Shane, P., Alloway, B., Hall, I.R., Harris, S.E., Harris, S.E. & Westgate, J.A., 2003. Demise of one volcanic zone and the birth of another - a 12 m.y. record of rhyolitic eruptions from New Zealand. *Geology*, 31, pp.493-96.

Cooper, A.F., Barreiro, B.A., Kimbrough, D.L. & Mattinson, J.M., 1987. Lamprophyre dike intrusion and the age of the Alpine fault, New Zealand. *Geology*, 15, pp.941-44.

Cox, A. & Hart, R.B., 1986. *Plate Tectonics: How it Works*. Oxford: Blackwell Scientific Publications.

Crawford, A.J., Meffre, S. & Symonds, P.A., 2003. 120 to 0 Ma tectonic evolution of the southwest Pacific and analogous geological evolution of the 600 to 220 Ma Tasman Fold Belt System. In R.R. Hillis & R.D. Muller, eds. *Evolution and Dynamics of the Australian Plate*. Geological Society of Australia Special Publication 22. pp.377-97.

Croon, M.B., Cande, S.C. & Stock, J.M., 2008. Revised Pacific-Antarctic plate motions and geophysics of the Menard Fracture zone. *Geochemistry, Geophysics, Geosystems*, 9, p.Q07001.

Davy, B., Horernle, K. & Werner, R., 2008. Hikurangi Plateau: Crustal structure, rift formation, and Gondwana subduction history. *Geochemsitry, Geophysics, Geosystems*, 9, p.Q07004.

De Mets, C., Gordon, R.G. & Argus, D.F., 2010. Geologically current plate motions. *Geophysics Journal International*, 181, pp.1-80.

Downey, N.J., Stock, J.M., Clayton, R.W. & Cande, S.C., 2007. History of the Cretaceous Osborn spreading center. *Journal of Geophysical Research*, 112, p.B4102. doi:10.1029/2006JB004550.

Eberhart-Phillips, D. & Bannister, S., 2010. 3-D imaging of Marlborough, New Zealand, subducted plate and strike-slip fault systems. *Geophysics Journal International*, 182, pp.73-96. doi:10.1111/j.1365-246X.2010.04621.x.

Faccenda, M., Gerya, T.V. & Burlini, L., 2009. Deep slab hydration induced by bending-related variations in tectonic pressure. *Nature Geoscience*, 2, pp.790-93. doi:10.1038/NGEO656.

Furlong, K.P. & Kamp, P.J.J., 2009. The lithospheric dynamics of plate boundary transpression in New Zealand: Initiating and emplacing subduction along the Hikurangi margin, and the tectonic evolution of the Alpine Fault system. *Tectonophysics*, 474, pp.449-62. doi:10.1016/j.tect.2009.04.023.

Giba, M., 2010. *The evolution of Tertiary normal faults in the Taranaki Basin, New Zealand*. Dublin: University College Dublin. unpublished PhD thesis.

Giba, M., Nicol, A. & Walsh, J.J., 2010. Evolution of faulting and volcanism in a back-arc basin and its implications for subduction processes. *Tectonics*, TC4020. doi: 10.1029/2009TC002634.

Gill, J., 1981. *Orogenic Andesities and Plate Tectonics*. New York: Springer.

Gurnis, M., Hall, C. & Lavier, L., 2004. Evolving force balance during incipient subduction. *Geochemsitry, Geophysics, Geosystems*, 5(Q07001). doi: 10.1029/2003GC000681.

Gutscher, M.A., Spakman, W., Bijwaard, H. & Engdahl, E.R., 2000. Geodynamics of flat subduction: Seismicity and tomographic constraints from the Andean margin. *Tectonics*, 9, pp.814-33.

Hacker, B.R., Peacock, S., Abers, G.A. & Holloway, S.D., 2003b. Subduction factory, 2. Are intermediate-depth earthquakes in subducting slabs linked to metamorphic dehydration reactions? *Journal of Geophysical Research*, 108(B1), p.2030. doi:10.1029/2001JB001129.

Hall, C.E., Gurnis, M., Sdrolias, M., Lavier, L.L. & Muller, R.D., 2003. Catastrophic initiation of subduction following forced convergence across fracture zones. *Earth & Planetary Science Letters*, 212, pp.15-30.

Hayward, B.W., Black, P.M., Smith, I.E.M., Ballance, P.F., Itaya, T., Doi, M., Takagi, M., Bergman, S., Adams, C.J., Herzer, R.H. & Robertson, D.J., 2001. K-Ar ages of Early Miocene arc-type volcanoes in northern New Zealand. *New Zealand Journal of Geology & Geophysics*, 44, pp.285-311.

Herzer, R.H., 1995. Seismic stratigraphy of a buried volcanic arc, offshore Northland, New Zealand and implications for Neogene subduction. *Marine & Petroleum Geology*, 12, pp.511-31.

Herzer, R.H., Barker, D.H.N., Roest, W.R. & Mortimer, N., 2011. Oligocene-Miocene spreading history of the northern South Fiji Basin and implications for the evolution of the New Zealand plate boundary. *Geochemistry Geophysics Geosystems*, 12(2), p.Q02004. doi:10.1029/2010GC003291.

Herzer, R.H., Davy, B.D., Mortimer, N., Quilty, P.G., Chaproniere, G.C.H., Jones, C.M., Crawford, A.J. & Hollis, C.J., 2009. Seismic stratigraphy and structure of the Northland Plateau and the development of the Vening Meinesz transform margin, SW Pacific Ocean. *Marine Geophysical Researches*, 30, pp.21-60. doi:10.1007/s11001-009-9065-1.

Herzer, R.H., Mascle, J., Davy, B.W., Ruellan, E., Mortimer, N., Laporte, C. & Duxfield, A., 2000. New constraints on the New Zealand-South fiji Basin continent-back-arc margin. *Comptes Rendus Acad Sci Paris Sci Terre Planetes*, 330, pp.701-08.

Heuret, A. & Lallemand, S., 2005. Plate motions, slab dynamics and back-arc deformation. *Physics of the Earth and Planetary Interiors*, 149, pp.31-51. doi:10.1016/j.pepi.2004.08.022.

House, M.A., Gurnis, M., Kamp, P.J.J. & Sutherland, R., 2002. Uplift in the Fiordland Region, New Zealand: Implications for incipent subduction. *Science*, 297, pp.2038-41.

Jarrard, R.D., 1986. Relations among subduction parameters. *Reviews of Geophysics*, 24(2), pp.217-84.

Keller, W.R., 2003. *Cenozoic plate tectonic reconstructions and plate boundary processes in the Southwest Pacific*. Unpub. PhD Thesis: California Institute of Techology. Pasadena.

King, P.R., 2000. Tectonic reconstructions of New Zealand: 40 Ma to present. *New Zealand Journal of Geology & Geophysics*, 43, pp.611-38.

King, P.R. & Thrasher, G.P., 1996. Cretaceous-Cenozoic geology and petroleum systems of the Taranaki Basin. In *Institute of Geological & Nuclear Sciences Monograph 13*. Lower Hutt, New Zealand: Institute of Geological & Nuclear Sciences.

Kirby, S.H., Engdahl, E.R. & Denlinger, R., 1996. Intermediate-depth intraslab earthquakes and arc volcanism as physical expressions of crustal and uppermost mantle metamorphism in subducting slabs. In G.E. Bebout, D. Scholl, S.H. Kirby & J.P. Platt, eds. *Subduction: Top to Bottom*. Geophysical Monograph 96, Washington DC: AGU. pp.195-214.

Krijgsman, W., Hilgen, F.J., Raffi, I., Sierro, F.J. & Wilson, D.S., 1999. Chronolgy, cauese and progression of the Messinian salinity crisis. *Nature*, 400(6745), pp.652-55. doi;10.1038/23231.

Lallemand, S., Heuret, A. & Boutelier, D., 2005. On the relationships between slab dip, back-arc stress, upper plate absolute motion, and crustal nature in subduction zones. *Geochemistry, Geophysics, Geosystems*, 6(Q09006). doi: 10.1029/2005GC000917.

Li, C., van der Hilst, R.D., Engdahl, E.R. & Burdick, S., 2008. A new global model for P wave speed variations in Earth's mantle. *Geochemsitry, Geophysics, Geosystems*, 9(Q05018). doi: 10.1029/2007GC001806.

Malpas, J., Sporli, K.B., Black, P.M. & Smith, I.E.M., 1992. Northland ophiolite, New Zealand, and implications for plate-tectonic evolution of the southwest Pacific. *Geology*, 20, pp.149-52.

Molnar, P. & Atwater, T., 1978. Interarc spreading and Cordilleran tectonics as alternatives related to the age of subducted lithosphere. *Earth & Planetary Science Letters*, 41, pp.330-40.

Mortimer, N., Gans, P.B., Palin, J.M., Meffe, S., Herzer, R.H. & Skinner, D.N.B., 2010. Location and migration of Miocene-Quarternary volcanic arcs in the SW Pacific region. *Journal of Volcanology & geothermal Research*, 190, pp.1-10. doi: 10.1016/j.jvolgeores.2009.02.017.

Mortimer, N., Herzer, R.H., Gans, P.B., Laporte-Magoni, C., Clavert, A.T. & Bosch, D., 2007. Oligocene-Miocene tectonic evolution of the South Fiji Basin and Northland Plateau, SW Pacific Ocean: evidence from petrology and dating of dredged rocks. *Marine Geology*, 237, pp.1-24.

Mortimer, N., Herzer, R.H., Gans, P.B., Parkinson, D.L. & Seward, D., 1998. Basement geology from Three Kings Ridge to West Norfolk Ridge, Southwest Pacific Ocena: evidence from petrology, geochemistry and isotopic dating of dredge samples. *Marine Geology*, 148, pp.135-62.

Muller, R.D., Royer, J.-Y. & Lawver, L.A., 1993. Revised plate motions relative to the hotspots from combined Atlantic and Indian Ocean hotspot tracks. *Geology*, 21, pp.275-78.

Nicol, A. & Beavan, J., 2003. Shortening of an overriding plate and its implication for slip on a subduction thrust, central Hikurangi Margin, New Zealand. *Tectonics*, 22(6), p.1070. doi:10.1029/2003TC001521.

Nicol, A., Mazengarb, C., Chanier, F., Rait, C., Uruski, C. & Wallace, L., 2007. Tectonic evolution of the active Hikurangi subduction margin, New Zealand, since the Oligocene. *Tectonics*, 26, p.TC4002. doi:10.1029/2006TC002090.

Nicol, A., Van Dissen, R., Vella, P., Alloway, B. & Melhuish, A., 2002. Growth of contractional structures during the last 10 m.y. at the southern end of the emergent Hikurangi forearc basin, New Zealand. *New Zealand Journal of Geology & Geophysics*, 45, pp.365-85.

Nicol, A. & Wallace, L.M., 2007. Temporal stability of deformation rates: Comparison of geological and geodetic observations, Hikurangi subduction margin, New Zealand. *Earth & Planetary Science Letters*, 258, pp.397-413. doi:10.1016/j.epsl.2007.03.039.

O'Neill, C., Muller, D. & Steinberger, B., 2005. On the uncertainites in hot spot reconstructions and significance of moving hot spot reference frames. *Geosystems Geophysics Geochemistry*, 6(4), p.Q04003. doi:10.1029/2004GC000784.

Parson, L.M. & Wright, I.C., 1996. The Lau-Havre-Taupo back-arc basin: A southward-progating, multi-stage evolution from rifting to spreading. *Tectonophysics*, 263, pp.1-22.

Pulford, A. & Stern, T., 2004. Pliocene exhumation and landscape evolution of central North Island: the role of the upper mantle. *Journal of Geophysical Research*, 109, p.F01016. doi:10.1029/2003JF000046.

Rait, G.J., 2000. Thrust transport directions in the Northland Allochthon, New Zealand. *New Zealand Journal of Geology & geophysics*, 43, pp.271-88.

Rait, G.J., Waters, D.W. & Chanier, F., 1991. Landward- and seaward-directed thrusting accompanying the onset of subduction beneath New Zealand. *Geology*, 19, pp.230-33.

Ranero, C.R., Phipps Morgan, J., McIntosh, K. & Reichert, C., 2003. Bending-related faulting and mantle serpentinization at the Middle America Trench. *Nature*, 425, pp.367-73. doi:10.1038/nature01961.

Reyners, M., Eberhart-Phillips, D. & Bannister, S., 2011. Tracking repeated subduction of the Hikurangi Plateau beneath New Zealand. *Earth & Planetary Science Letters*, 311(1-2), pp.165-71. doi:10.1016/j.epsl.2011.09.011.

Rowan, C.J. & Roberts, A.P., 2008. Widespread remagnetisations and a new view of Neogene tectonic rotations within the Australian-Pacific plate boundary zone, New Zealand. *Journal of Geophysical Research*, 113, p.B03103. doi:10.1029/2006JB004594.

Royer, J.-Y. & Rollet, N., 1997. Plate-tectonic setting of the Tasmanian region. *Australian Journal of Earth Sciences*, 44, pp.543-60.

Royer, J.-Y. & Sandwell, D.T., 1989. Evolution of the eastern Indian Ocean since the Late Cretaceous; constraints from Geosat altimetry. *Journal of Geophysical Research*, 94, pp.13755-82.

Sandwell, D.T. & Smith, W.H.F., 2009. Global marine gravity from retracked Geosat and ERS-1 altimetry: Ridge segmentation verses spreading rate. *Journal of Geophysical Research*, 114, p.B01411. doi:10.1029/2008JB006008.

Schellart, W.P., 2007. Northeastward subduction followed by slab detachment to explan ophiolite obduction and Early Miocene volcanism in Northland, New ZEaland. *Terra Nova,* 19, pp.211-18. doi:10.11/j1365-3121.2007.00736.x.

Schellart, W.P., 2012. Comment on "Geochemistry of the Early Miocene volcanic succession of Northland, New Zealand, and implications for the evolution of subduction in the Southwest Pacific" by M.A. Booden, I.E.M. Smith, P.M. Black and J.L. Mauk. *Journal of Volcanology & Geothermal Research*, 211-212, pp.112-17. doi:10.1016/j.jvolgeores.2011.10.010.

Schellart, W.P., Lister, G.S. & Troy, V.G., 2006. Cretaceous and Cenozoic reconstruction of the Pacific region: Tectonics controlled by subduction and slab rollback processes. *Earth-Science reviews*, 76(3-4), pp.191-233.

Sdrolias, M. & Muller, R.D., 2006. Controls on back-arc basin formation. *Geochemistry, Geophysics, Geosystems*, 7, p.Q04016. doi:10.1029/2005GC001090.

Stagpoole, V. & Nicol, A., 2008. Regional structure and kinematic history of a large subduction back thrust: Taranaki Fault, New Zealand. *Journal of Geophysical Research*, 113, p.B01403. doi:10.1029/2007JB005170.

Stagpoole, V. & Nicol, A., 2008. Regional structure and kinematic history of a large subduction back thrust: taranaki Fault, New Zealand. *Journal of Geophysical Research*, 113, p.B01403. doi:10.1029/2007JB005170.

Steinberger, B., Sutherland, R. & O'Connell, R.J., 2004. Prediction of Emperor-Hawaii seamount locations from a revised model of global plate motion and mantle flow. *Nature*, 430, pp.167-73.

Stern, T.A. & Holt, W.E., 1994. Platform subsidence behind an active subduction zone. *Nature*, 368, pp.233-36.

Stern, T.A., Stratford, W.R. & Salmon, M.L., 2006. Subduction evolution and mantle dynamics at a continental margin: Central North Island, New Zealand. *Review of Geophysics*, 44, p.RG4002. doi:10.1029/2005RG000171.

Stock, J. & Molnar, P., 1982. Uncertainties in the relative positions of the Australia, Antarctica, Lord Howe, and Pacific plates since the late Cretaceous. *Journal of Geophysical Research*, 87(B6), pp.4697-717.

Sutherland, R., 1995. The Australia-Pacific boundary amd Cenozoic plate motions in the SW Pacific: Some constraints from Geosat data. *Tectonics*, 14(4), pp.819-31.

Sutherland, R., Stagpoole, V., Uruski, C., Kennedy, C., Bassett, D., Henrys, S., Scherwath, M., Kopp, H., Field, B., Toulmin, S., Barker, D., Bannister, S., Davey, F., Stern, T. & Flueh, E.R., 2009. Reactivation of tectonics, crustal underplating, and uplift after 60 Myr of passive subsidence, Ruakumara Basin, Hikurangi-Kermadec fore arc,

New Zealand: Implications for growth and recycling of continents. *Tectonics*, 28, p.TC5017. doi:10.1029/2008TC002356.

Syracuse, E.M. & Abers, G.A., 2006. Global compliation of variations in slab depth beneath arc volcanoes and implications. *Geochemistry, Geophysics, Geosystems*, 7, p.Q05017. doi:10.1029/2005GC001045.

Taylor, B., Zellmer, K., Martinez, F. & Goodlife, A., 1996. Sea-floor spreading in the Lau back-arc basin. *Earth & Planetary Science Letters*, 144, pp.35-40.

Tippet, J.M. & Kamp, P.J.J., 1993. Fission track analysis of the Late Cenozoic vertical kinematics of continental Pacific crust, South Island, New Zealand. *Journal of Geophysical Research*, 98(B9), pp.16119-48.

Walcott, R.I., 1987. Geodetic strain and the deformation history of the North Island of New Zealand during the late Cainozoic. *Philosphical Transactions of the Royal Society London*, A321, pp.163-81.

Walcott, R.I., 1998. Modes of oblique compression: Late Cenozoic tectonics of the South Island of New Zealand. *Reviews of Geophysics*, 36(1), pp.1-26.

Wallace, L.M., Barnes, P., Beavan, J., Van Dissen, R., Litchfield, N., Mountjoy, J., Langridge, R., Lamarche, G. & Pondard, N., 2012. The kinematics of a transition from subduction to strike-slip: An example from the central New Zealand plate boundary. *Journal of Geophysical Research*, 117, p.B02405. doi:10.1029/2011JB008640.

Wallace, L.M., Beavan, J., McCaffrey, R. & Darby, D., 2004. Subduction zone coupling and tectonic block rotations in the North Island, New Zealand. *Journal of Geophysical Research*, p.B12406. doi:10.1029/2004JB003241.

Wallace, L.M., Ellis, S. & Mann, P., 2009. Collisional model for rapid fore-arc block rotations, arc curvature, and episodic back-arc rifting in subduction settings. *Geochemistry, Geophysics, Geosystems*, 10, p.Q05001. doi:10.1029/2008GC0022200.

Webb, T.H. & Anderson, H., 1998. Focal mechanisms of large earthquakes in the North Island of New Zealand: slip partitioning at an oblique active margin. *Geophysics Journal International*, 134, pp.40-86.

Wessel, P. & Muller, R.D., 2007. Plate Tectonics. In *Treatise on Geophysics Volume 6*. Amsterdam: Elsevier. pp.49-98.

Whattam, S.A., Malpas, J., Ali, J.R., Lo, C.H.- & Smith, I.E.M., 2005. Formation and emplacement of the Northland ophiolite, northern New Zealand: SW Pacific tectonic implications. *Journal of the Geological Society London*, 162, pp.225-41.

Wright, I.E.M. & Walcott, R.I., 1986. Large tectonic rotation of part of New Zealand in the last 5 Ma. *Earth & Planetary Science Letters*, 80, pp.348-52.

Chapter 7

Conclusions and future research

1. Introduction

The origins of continental intra-arc rifting and associated volcanism and the impact of normal faults on fluid flow are the focus of this thesis. Normal faulting and its control on fluid flow provide a common theme relating diverse processes such as intra-arc rifting, deep mantle hydration, explosive caldera-forming arc volcanism and near surface migration of water filled fault-zones. Rifting and arc volcanism are controlled by subduction processes and a key goal of this thesis has been to cast light on the evolution of subduction beneath the North Island of New Zealand. This improved understanding of subduction is important because it provides insights into first-order processes associated with the tectonics, sedimentation patterns, and land mass evolution of the North Island for at least the last 30 Myr. In addition to investigating regional plate boundary and subduction processes, generic studies of faults and their role in the flow of fluids have been considered. Faults are widely considered to both enhance and retard fluid flow and I have examined factors associated with the highly variable nature of fluid-flow and flow-rates from fault-zones *in situ* to understand better the hydraulic properties of fault and fracture systems. Conclusions drawn from this thesis are applicable to a wide range of industries and fields of research including; geothermal, oil and gas, CO_2 storage, ground water, subduction zones, earthquake mechanics, and basin analysis. In this chapter I outline the main conclusions of thesis study and make some recommendations for future work.

2. Conclusions

Each chapter in this thesis has a list of conclusions and the most important of these are outlined below. These conclusions are deliberately brief to minimise repetition and the reader is referred to the individual chapters for more detailed summaries.

Faults are known to profoundly influence the migration of fluids in the sub-surface. Understanding how faults impact on fluid flow has both academic interest and industrial application as important water, hydrocarbon, and geothermal resources are extracted from the sub-surface. The relationships between faulting and fluid flow are examined in chapter 2 where the geometry and hydraulic properties of fault-zones in Mesozoic basement and Miocene strata intersected by the tunnels of the Tongariro Power Development in the southern Taupo Rift are investigated. Observations and analysis shows that:

- Fault-zone thickness varies by several orders of magnitude approximating power-law distributions where the dimensions and architecture of these zones are dependent on many factors including displacement, host-rock type and fault geometries.
- Despite fault-zones accounting for a small proportion of the total sample length (<15%), localised flow of groundwater into the tunnels occurs almost exclusively (≥ 91%) within, and immediately adjacent to, these zones.
- The distribution and rate of flow from fault-zones are highly variable with typically ≤ 50% of fault-zones in any given orientation flowing. No simple relationships between fluid-flow and either or, fault strike, hydraulic head and flow-rate are observed.
- A general positive relationship between fault size (e.g., fault-zone thickness) and maximum flow rate is found. The entire basement dataset, for example, shows that 81% of the flow rate occurs from fault-zones ≥ 10 m wide, with a third of the total flow rate originating from a single fault-zone (i.e. the golden fracture).

The Taupo Rift accommodates intra-arc extension in the central North Island of New Zealand. A number of plate boundary processes, including slab rollback and continental collision at the southern termination of subduction, have been proposed to account for the formation of the Taupo Rift. Discriminating between these models and placing constraints on the origins of the rift requires information on the structural geometry and kinematics of rifting. The kinematics of the continental intra-arc Taupo Rift was investigated mainly using a large catalogue of new and published focal mechanisms and geological fault-slip data. This information together with mapping of the rift demonstrates that:

- The average extension direction is approximately orthogonal to the average trend of the rift and its constituent faults (α=76-84°).
- Comparison of contemporary fault geometry and kinematics of the Taupo Rift with intra-arc rifting in the Taranaki Basin and southern Havre Trough show that for ≥ 4 Myr, the slab and the associated changes in its geometry have exerted a first-order control on the location, geometry, and extension direction of intra-arc rifting in the North Island.
- Second-order features of rifting include a clockwise ~20° northwards change in the strike of normal faults and trend of the extension direction that indicates a relationship between fault orientation and extension direction. In the southern rift normal faults are parallel to, and probably reactivate, Mesozoic basement fabric (e.g., faults and bedding) which is in contrast to the northern rift faults that may have formed since rift initiation 1-2 Ma ago and which diverge from basement fabric by up to 55°.
- Focal mechanisms indicate third-order features of rifting include oblique to right lateral strike-slip along basement fabric and dip slip on newly formed rift faults.

The Taupo Volcanic Zone, which coincides spatially with the Taupo Rift, is one of most volcanically productive systems on Earth. The mechanisms proposed to account for the location and productivity of the TVZ include deep plumes, cooling intrusions, along strike mantle flow and an arc related hotspot. The location and high volcanic productivity of the TVZ is linked to the subduction water cycle, where hydration and subsequent dehydration of the subducting oceanic lithosphere is primarily accomplished by earthquakes. This conclusion is based on analysis of regional and global earthquake catalogues for the subducting Pacific plate. These data indicate that:

- The anomalously high heat flow and volcanic productivity of the TVZ is spatially associated with high rates of seismicity in the underlying slab mantle at depths of 130-210 km.
- The sub-arc region of anomalously high seismicity correlates with the transition from oceanic to continental overriding crust along a relative motion vector where high frequencies of large shallow normal faulting intraplate earthquakes occur due to bending of the slab. These bending-related earthquakes rupture

deep into the mantle of the subducting lithosphere potentially hydrating it to depths of up to 40 km.

- Hydration of the subducting plate decreases to the south where arc volcanism extinguishes and 'bending' earthquakes occur mainly beneath continental crust of the North Island, 100-200 km west of and distal from oceanic fluids.

Subduction systems evolve in space and time. Numerous studies have suggested a progressive change in the location of the subducted Pacific plate beneath the North Island of New Zealand(Ballance, 1976; Brothers, 1984; Kamp, 1984; Hayward et al., 2001; Mortimer et al., 2007; Giba, 2010). In chapter 5 evidence for rollback and/or steepening of the slab beneath the North Island has been re-examined. Evolution of the subducting slab geometry beneath the North Island has been investigated using a combination of published arc-type volcanic ages and the locations of earthquakes in the subducting Pacific plate. The data reveal that:

- Arc front volcanoes have migrated southeast by 150 km in the last 8 Ma (185 km since 16 Ma) sub-normal to the present active arc. Migration of the arc is interpreted to mainly reflect slab rollback northeast of New Zealand along the Tonga-Kermadec subduction system and fixed hinge slab steepening beneath the central North Island.
- The strike of the Pacific slab beneath the North Island, imaged by Benioff zone seismicity (50-200 km) and positive mantle velocity anomalies (200-600 km) is parallel to the northeast trend of arc front volcanism. Arc parallelism since 16 Ma is consistent with the view that the strike of the subducting plate has not changed significantly. In particular over this time, the subducting plate has not rotated clockwise about vertical axes in unison with rotation of the overriding plate.
- Acceleration of arc front migration rates (~4 mm/yr to ~18 mm/yr), eruption of high Mg# andesites, increasing eruption frequency and size, and uplift of the over-riding plate indicate an increase in the hydration, temperature, and size of the mantle wedge beneath of the central North Island from ~7 Ma.

Deformation of New Zealand continental crust (both terrestrial and marine) has been controlled over the last 38 Myr by the relative motions of the Pacific and Australian

plates. Relative plate motions on timescales of millions of years are estimated using seafloor spreading data to determine total reconstruction poles of plate rotations. These poles provide constraints for, and can be tested by, deformation of the Hikurangi margin over the last 38 Myr. Published total reconstruction poles for Australia-Pacific relative plate motions for the last 38 Myr were used in chapter 6 to track the evolution of subduction beneath the North Island and show that:

- Plate convergence rates doubled between 20 and 16 Ma from 11 to 23 mm/yr, increasing again by approximately a third between 8 and 6 Ma. Plate parallel rates steadily increased from ~15 mm/yr at 26 Ma to 32 ± 2 mm/yr at 16 Ma where they have remained to the present.
- Pacific plate motion in a west dipping subduction model shows a minimum horizontal transport distance of 285 km preceding the initiation of arc volcanism along the Northland arc normal to the motion vector, a distance more than sufficient for self-sustaining subduction to occur.
- Tracking the southern and down dip limits of the presently imaged Pacific slab beneath the North Island indicates arc volcanism in the Taranaki Basin at 16 Ma and Northland at 23 Ma requires the Pacific plate to have extend as far south as its present position beneath the Chatham Rise (~43.5ºS), ~200 km beyond the seismically imaged slab, prior to the reactivation of subduction.

3. Future research

The processes and relationships identified between faulting, earthquakes and fluid-flow in chapters 2-6 are first-order and many warrant further detailed investigation. In addition, during the course of work several avenues of research were discovered which could not be pursued due to time and financial constraints of the project. Below I list some potential questions and avenues for future research.

3.1 Fault systems and their earthquakes

- In chapter 2 I show that the distribution of fault-zone sizes and associated fluid-flow have power-law distributions with exponents ranging from ~0.5 to 1. Preliminary analysis of earthquakes in the southern Taupo Rift have *b*-values of 1.08 which are comparable to fault-zone thickness distributions from well

constrained tunnel sections that have exponents of ~1.03 (Fig. 1). While speculative, these data suggest that earthquake magnitude-frequency relations are similar to the size distribution of faults they are occurring on, a conclusion drawn for control on flow rates entering the tunnel. Relating basement fault-zone distributions to earthquake swarms occurring in the mid-crust immediately to the south of the eastern tunnels may provide insight into earthquake processes and the nature of deformation in the TVZ.

- Utilising estimates of the stress field and fault orientations to perform fault reactivation, slip tendency or dilation tendency are tools often used to predict which faults or parts of faults are likely to enhance fluid flow. In this study these tools appear to provide a poor basis from which to predict which faults will flow. Further examples of *in situ* fault-fluid flow relations are required to examine whether the predictions were poor because the regional stress and fault data do not accurately describe local conditions and/or because the theory relating stress conditions to fluid flow is incorrect.

3.2 Slab dehydration and arc volcanism

- The hydration and subsequent dehydration of subducting lithosphere have important implications for the Hikurangi margin (chapter 4). In particular, the distribution of fluid flux from the slab has important consequences for the viscosity of the mantle wedge (chapter 5) which in turn influences deformation in the overriding plate and the geometry of the subducting plate (Billen & Gurnis, 2001; Manea & Gurnis, 2007; Wallace et al., 2009a). Numerical modelling of the Hikurangi margin using presently available geophysical, geochemical, and geological constraints to understand the influence of mantle viscosity on deformation in the North Island or fluid-flow pathways within the mantle wedge, for example, may lead to widely applicable insights into subduction processes.

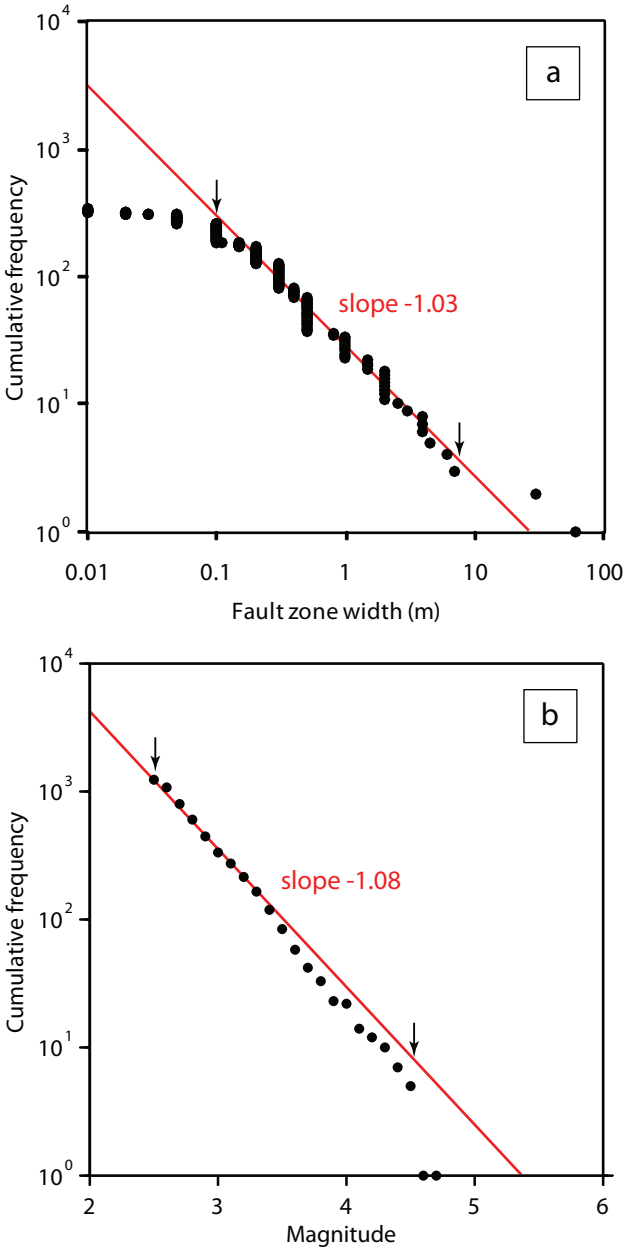

Figure 1. Fault size and earthquake magnitude-frequency relations in the southern Taupo Rift. (a) One-dimensional fault-zone thickness population from well constrained 5 km Tongariro Power Development tunnel section. See chapter 2 for details. (b) Magnitude-frequency relations for southern Taupo Rift earthquakes (GeoNet catalogue 2001-2009 M_C 2.5). Note the power-law exponents or the slope of the curves are similar between the width of the fault zone, which has a general positive relationship with fault length and displacement, and earthquake size.

- Chapter 3 focuses on regional patterns of fault geometry and kinematics, while most previous geological studies have focussed on near-surface faulting. Marrying sub-surface gravity, MT and focal mechanism data with surface mapping of the faults may offer the potential to improve understanding of the evolution of faulting, relationships between faulting and volcanism and crustal-scale controls on location changes in fault orientation and location.
- The largest earthquakes recorded on Earth are associated with subduction zones. Recent geodetic and seismological observations reveal that a large area of the subduction interface along the Hikurangi margin is interseismically coupled, along which stress could be released in an earthquake ≥ magnitude 8(Wallace et al., 2009b). The spatial extent of the likely seismogenic zone associated with a large subduction earthquake along the Hikurangi margin is considered a complex interplay between overriding and subducting plate structure, subducting sediment, thermal effects, regional tectonic stress regime and fluid pressure (Wallace et al., 2009b). While speculative, I would suggest that the locked region of the southern Hikurangi margin is the direct result of the relatively strong and dry subducting plate underlying this interseismically coupled zone. In chapter 4 I discuss the relative hydration of the slab along strike of the Hikurangi margin with relation to volcanism, however, the spatial correlation between the high velocity section of the slab, the distribution of intraplate earthquakes and the interseismically coupled zone indicates slab hydration may also provide first-order control on subduction zone earthquakes (Fig. 3). The high velocity section of the southern slab is interpreted to be eclogite created during either the formation or partial subduction of the Hikurangi Plateau in the Cretaceous(Reyners et al., 2011). This relatively dense anhydrous region of the slab is characterised by shallow interplate and intermediate dips relative to the northern Hikurangi margin which, in combination with the maximum magnitude of earthquakes, indicates lower magnitudes of bending and normal faulting (chapter 4). These features, a pre-existing anhydrous composition and low degrees of bending and normal-faulting, may result in lower fluid fluxes at the plate interface resulting in increased frictional resistance to slip relative to the northern Hikurangi margin. Reprocessing of existing offshore seismic reflection data to emphasise the structure of the subducting plate could test the hypothesis that bend-related faulting decreases southward. Large-scale geophysical

transects along the margin (i.e. seismic and/or magnetotelluric) could also test how and where the properties of the slab change along strike.

- Rates of SE arc migration in chapter 5 indicate a rapid increase at about ~7 Ma. Presently available data are consistent with the view that the increase in arc migration was associated with increases in the rate of relative plate motion. Analysis of melt inclusions from volcanic samples spanning this time interval might, for example, provide a test of the hypothesis that increases in subduction rate leads to increases in volatiles entering the mantle wedge (Manea & Gurnis, 2007). Defining better the changing location of the convecting portion of mantle wedge through uplift patterns across the North Island and the implications for upper-plate deformation associated with changes in mantle wedge viscosity are both avenues for future research.

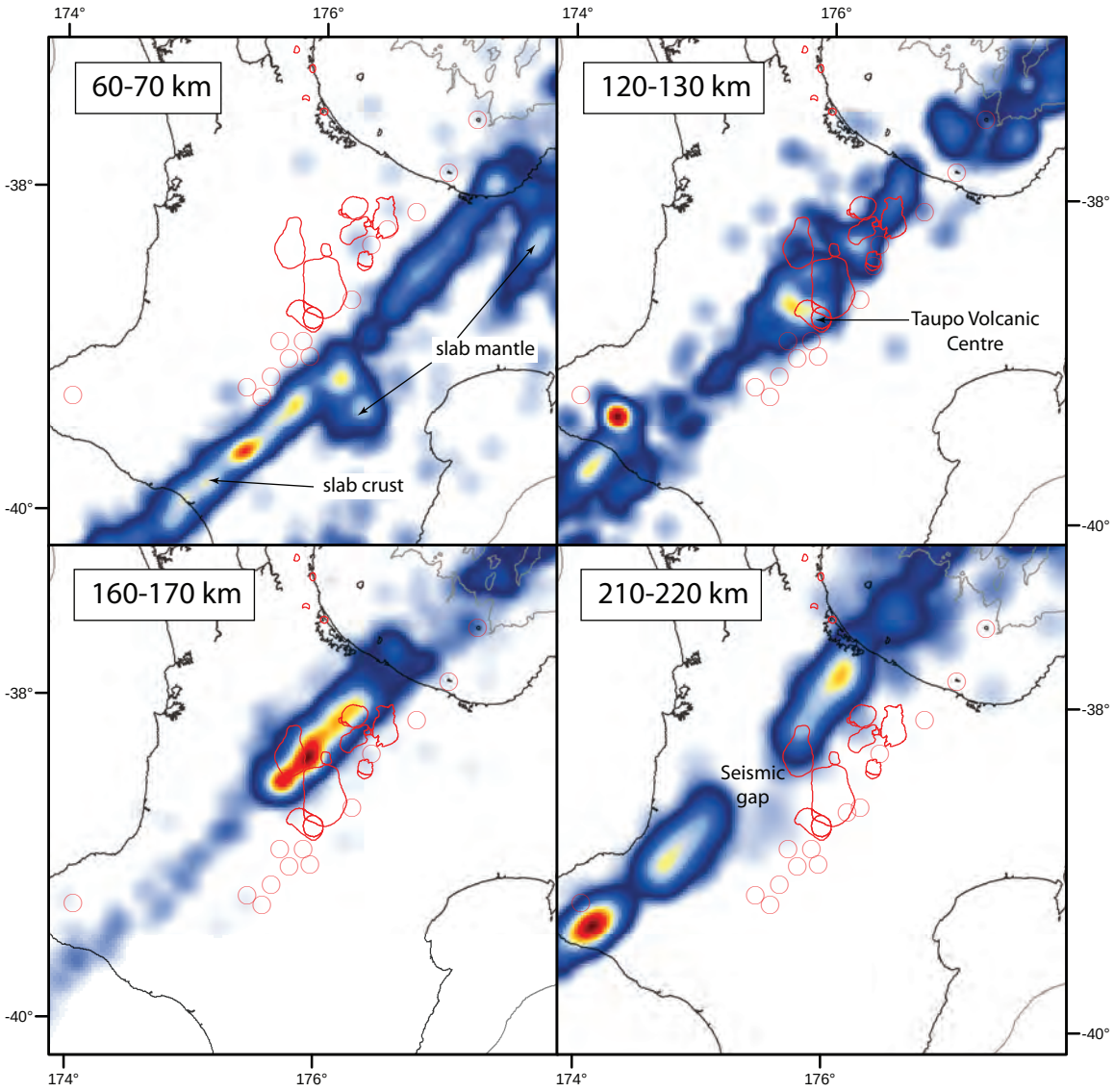

Figure 2. Earthquake densities in the subducting slab beneath active arc volcanoes. Contouring of relocated earthquake densities in 10 km deep horizontal slices of Benioff zone seismicity highlights the close spatial relationships between slab deydration and overlying arc volcanism (volcanoes = red open circles and calderas = red polygons). Note the approximately uniform density of earthquakes in the slab crust at 60-70 km compared with the variability in densities at greater depths. Warm colours represent high densities of earthquakes.

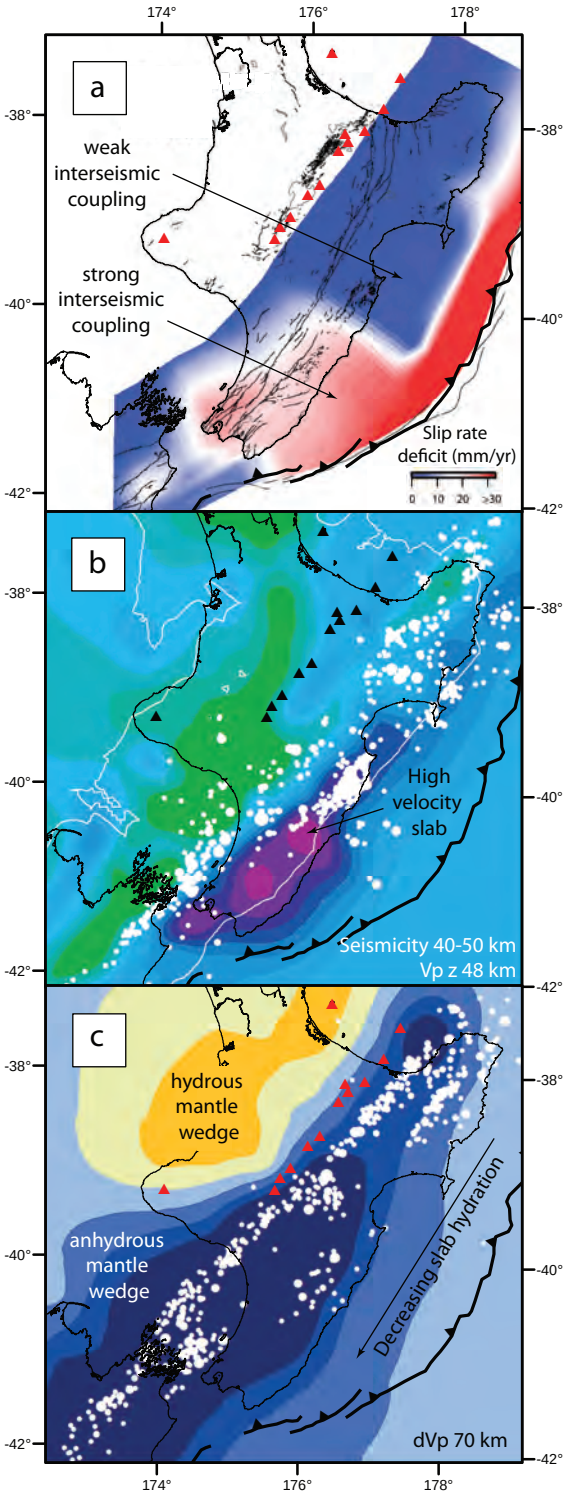

Figure 3. Interseismic locking of the plate interface and slab hydration along the Hikurangi margin. (a) Interseismic slip deficit on the Hikurangi margin subduction thrust (Wallace et al., 2012) in relation to arc volcanism (red and black triangles). Note the relationship between the termination of arc volcanism and the locked portion of the subduction interface. (b) P-wave velocity of the subducting slab at 48 km depth (Eberhart-Phillips et al., 2010) and the distribution of intraplate seismicity between 40-50 km depth (white filled circles). (c) Mantle velocity anomalies at 70 km depth (Li et al., 2008) showing the distribution of relatively hydrated (warm colours) and anhydrous (cool colours) mantle wedge west of Benioff zone seismicity (depth range 60-70 km) (white filled circles). See chapter 5 for details. Velocity models are consistent with decreasing slab and mantle wedge hydration to the south (chapter 4)

References

Ballance, P.F., 1976. Evolution of the Upper Cenozoic magmatic arc and plate boundary in northern New Zealand. *Earth & Planetary Science Letters*, 28, pp.356-70.

Billen, M. & Gurnis, M., 2001. A low viscosity wedge in subduction zones. *Earth & Planetary Science Letters*, 193, pp.227-36.

Brothers, R.N., 1984. Subduction regression and oceanward migration of volcanism, North Island, New Zealand. *Nature*, 309, pp.698-700.

Eberhart-Phillips, D. & Bannister, S., 2010. 3-D imaging of Marlborough, New Zealand, subducted plate and strike-slip fault systems. *Geophysics Journal International*, 182, pp.73-96. doi:10.1111/j.1365-246X.2010.04621.x.

Eberhart-Phillips, D., Reyners, M., Bannister, S., Chadwick, M. & Ellis, S., 2010. Establishing a versatile 3-D seismic velocity model for New Zealand. *Seismological Research Letters*, 81(6), pp.992-1000.

Giba, M., 2010. *The evolution of Tertiary normal faults in the Taranaki Basin, New Zealand*. Dublin: University College Dublin. unpublished PhD thesis.

Hayward, B.W., Black, P.M., Smith, I.E.M., Ballance, P.F., Itaya, T., Doi, M., Takagi, M., Bergman, S., Adams, C.J., Herzer, R.H. & Robertson, D.J., 2001. K-Ar ages of Early Miocene arc-type volcanoes in northern New Zealand. *New Zealand Journal of Geology & Geophysics*, 44, pp.285-311.

Kamp, P.J.J., 1984. Neogene and Quarternary extent and geometry of the subducted Pacific Plate beneath North Island, New Zealand: implications for Kaikoura tectonics. *Tectonophysics*, 108, pp.241-66.

Li, C., van der Hilst, R.D., Engdahl, E.R. & Burdick, S., 2008. A new global model for P wave speed variations in Earth's mantle. *Geochemsitry, Geophysics, Geosystems*, 9(Q05018). doi: 10.1029/2007GC001806.

Manea, V. & Gurnis, M., 2007. Subduction zone evolution and low viscosity wedges and channels. *Earth & Planetary Science Letters*, 264, pp.22-45. doi: 10.1016/j.epsl.2007.08.030.

Mortimer, N., Herzer, R.H., Gans, P.B., Laporte-Magoni, C., Clavert, A.T. & Bosch, D., 2007. Oligocene-Miocene tectonic evolution of the South Fiji Basin and Northland Plateau, SW Pacific Ocean: evidence from petrology and dating of dredged rocks. *Marine Geology*, 237, pp.1-24.

Reyners, M., Eberhart-Phillips, D. & Bannister, S., 2011. Tracking repeated subduction of the Hikurangi Plateau beneath New Zealand. *Earth & Planetary Science Letters*, 311(1-2), pp.165-71. doi:10.1016/j.epsl.2011.09.011.

Reyners, M.E., Eberhart-Phillips, D., Stuart, G. & Nishimura, T., 2006. Imaging subduction from the trench to 300 km depth beneath the central North Island, New Zealand with Vp and Vp/Vs. *Geophysics Journal International,* 165, pp.565-83.

Wallace, L.M., Barnes, P., Beavan, J., Van Dissen, R., Litchfield, N., Mountjoy, J., Langridge, R., Lamarche, G. & Pondard, N., 2012. The kinematics of a transition from subduction to strike-slip: An example from the central New Zealand plate boundary. *Journal of Geophysical Research*, 117, p.B02405. doi:10.1029/2011JB008640.

Wallace, L.M., Ellis, S. & Mann, P., 2009a. Collisional model for rapid fore-arc block rotations, arc curvature, and episodic back-arc rifting in subduction settings. *Geochemistry, Geophysics, Geosystems*, 10, p.Q05001. doi:10.1029/2008GC0022200.

Wallace, L.M., Reyners, M., Cochran, U., Bannister, S., Barnes, P.M., Berryman, K., Downes, G., Eberhart-Phillips, D., Fagereng, A., Ellis, S., Nicol, A. & McCaffrey, R., 2009b. Characterizing the seismogenic zone of a major plate boundary subduction thrust: Hikurangi Margin, New Zealand. *Geochemistry, Geophysics, Geosystems*, 10(10), p.Q10006. doi:10.1029/2009GC002610.

Appendix

Appendix 1: Gravity

This appendix contains information on gravity methods and data that have been conducted during this thesis. Appendix 1 supplements information presented in chapter 3.

Gravity surveying is used to investigate subsurface geology using the variations in the Earth's gravitational field arising from density contrasts between subsurface rocks. Rocks with densities different to their surroundings represent zones of anomalous mass that cause local perturbations in the gravitational field termed gravity anomalies. Due to the generally high density contrast between volcanoclastic deposits overlying basement ($\leq$ 670 kg/m^3), delineation of subsurface structure using gravity in the Taupo Rift and Taupo Volcanic Zone has been particularly successful. Gravity surveying has been used to map top basement and caldera collapse structures in the central North Island that underlie thick (e.g. > 2 km) accumulations of Late Quaternary (< 400 ka) low-density volcanic products (Wilson et al., 1984; Stern et al., 2006; Seebeck et al., 2010).

A1. Survey methodology

Field observations in the Taupo Rift were undertaken by the author during two surveys between the 10th February 2009 and the 5^{h} February 2010 using a Lacoste and Romberg gravimeter (serial number G106). The calibration of the gravimeter is maintained by Trevor Hunt, GNS Science Wairakei. The location and height of each observation was established with a Leica Real-Time Kinematic (RTK) differential GPS system in both real-time and post-processing mode using the New Zealand Geodetic Datum 2000 trig point Waimangu.

During the survey 130 new gravity stations were established (Fig. A1) and tied to Reporoa gravity station 156 (E2801549 N6302170 height 295 m (MSL) 979976.414 mGal), which is part of the New Zealand Primary Network (Robertson & Reilly, 1960). The daily determination of instrumental drift included the occupation of the Primary Gravity Network station at the beginning and end of each day and by looping to local

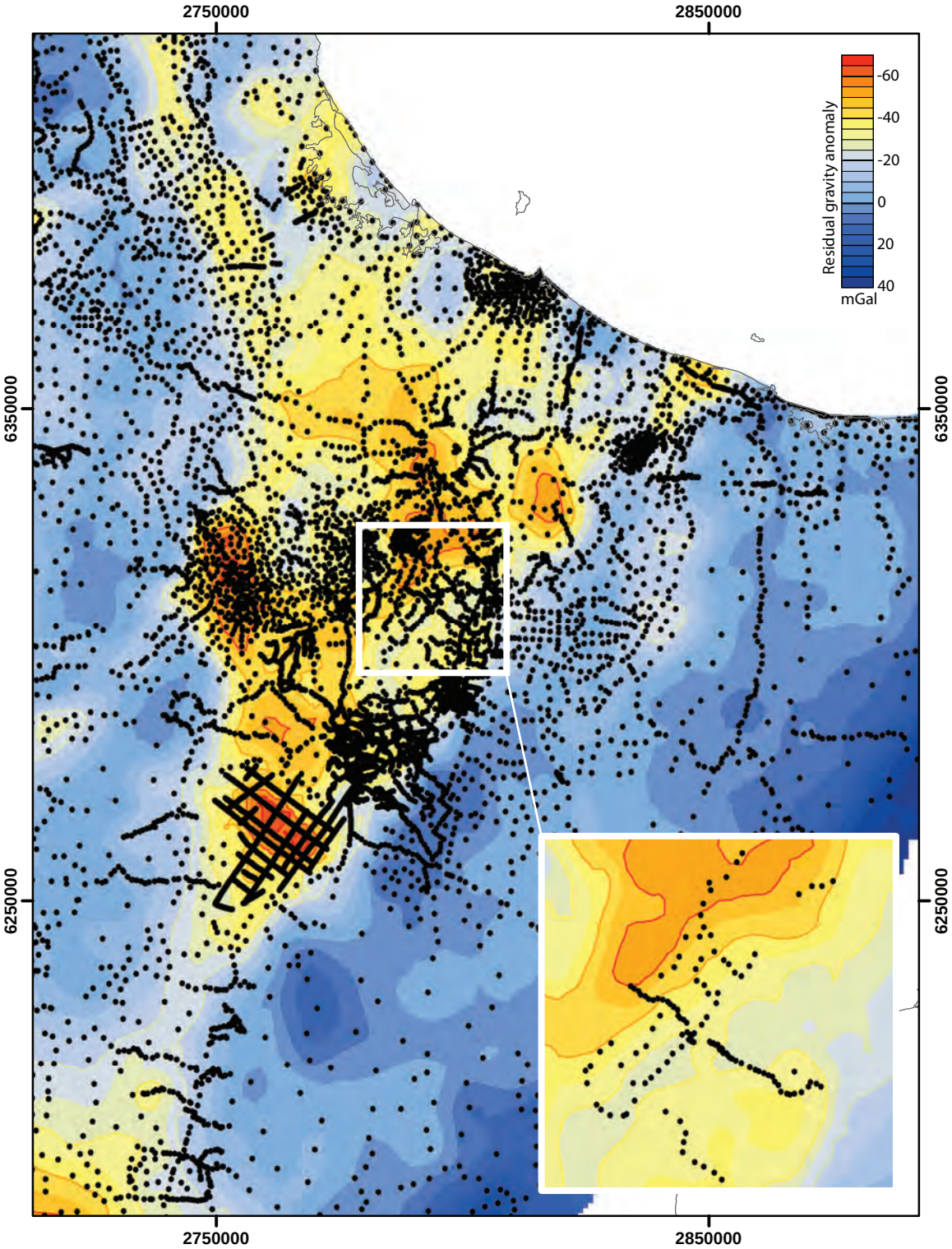

Appendix Figure 1. Gravity stations and residual gravity of the central North Island. See text for methods. Gravity data from the New Zealand Gravity Station Network with additional data from Davy & Caldwell (1998), Stagpoole & Beetham (2005), Mouslopoulou et al. (2008), Seebeck et al. (2010) and this study along the axis of rifting. See Appendix Fig. 2 for locations of additional studies. Inset shows gravity stations occupied during this study.

base stations (i.e. repeat readings of previously measured stations). Observations were made along public and private roads. The design of the surveys was based around two objectives: filling gaps in the New Zealand Gravity Station Network along the Taupo Rift axis (1-2 km spacing) and a detailed survey normal to the rift axis across the Paeroa Fault (0.25-0.5 km spacing).

A2. Data Reduction

The gravimeter observations were corrected for tidal effects of the Sun and Moon before solving for the instrumental drift and detection of any jumps or tares in the observations. The corrected gravity values have a standard error of approximately ±0.02 mGal. No instrument tares were recorded during either of the survey periods. The tying of each survey to the Primary Gravity Network Station at Reporoa ensures the gravity values are compatible with historical data within the New Zealand Gravity Station Network.

Free-air and Bouguer anomalies have been calculated using the method described in Reilly (1970, 1972 and references therein). Using the 1960 International formula for the external gravity field, the Free-air anomaly Δg_F is found from the observed gravity g at latitude φ and height h (km) by:

$$\Delta g_F = g - \gamma_h$$

Where

$\gamma_h = 978\ 049 + 5149.34\sin^2\varphi + 22.83\sin^4\varphi + 0.12\sin^6\varphi + h(-308.777 + 0.452\sin^2\varphi) + h^2(0.0727\text{-}0.0002\sin^2\varphi)$ mGal

The Bouguer anomaly Δg_B is found from

$$\Delta g_B = g - \gamma_B$$

γ_B is calculated by the addition of the gravitational effect of topography (i.e. departure of the physical surface from the geoid) to γ_h out to a radius of 166.7 km for each station. Densities of 2670 kg/m^3 and 1030 kg/m^3 are assumed for the topography (rock) and water respectively.

$$\gamma_B = \gamma_h + b(h) + \Delta b_1 + \Delta b_2 + c$$

Where $b(h)$ is the attraction of a circular plate of rock with a radius of 21.944 km and thickness h equal to the height of the station above sea level. The terms Δb_1 and Δb_2 are the inner (Hammer zone B-D) and outer terrain corrections (Hammer zone E-M),

respectively and c is the complete topographic correction from 21.944 km (Hammer zone M) to 166.7 km after Reilly (1970).

The correction for nearby topography out to Hammer D zone (170 m), or the inner terrain correction, was determined in the field by visual estimation of the height of the terrain relative to each observation point. The outer terrain corrections (Hammer E-M) were computed in the reduction stage using a 10 m digital terrain model and range in magnitude from 0.1 mGal in relatively flat areas to 2.75 mGal in locations with steep topography. The average terrain correction for the 130 measurements approaches 1 mGal due to the highly variable and often steep volcanic terrain.

A3. Sources of Error

Three main sources of error in the gravity observations have been identified; observational, elevation, and terrain estimation. Observational error for the calculated gravity at each station is a function of the gravimeter dial reading and the time of measurement. Time observations are used for calculating instrumental drift and the diurnal gravity variation. The LaCoste and Romberg gravity meter dial divisions represent approximately 0.01 mGal per division, repeat readings at stations typically produced residuals with standard deviation of ±0.02 mGal.

The elevation above sea-level of each gravity station was measured by a Leica SR530 Real-Time Kinematics Global Positioning system. An orthometric height for each gravity station was established using the New Zealand Geodetic Datum 2000 trig point Waimangu (Geodetic code 3073) NZMG E2806294.38 N6318297.52 orthometric height 467.75 m). This geodetic mark has a 3rd order control on both horizontal and vertical axes on the order of ±0.01 m. Coordinate quality is typically of the order of ±0.05 m for well resolved stations ranging to ±0.5 m for stations with limited satellite coverage. The uncertainty in the gravity arising from errors altitude is ±0.1 mGal.

Terrain estimation is potentially the largest and least quantifiable error in the calculation of Bouguer gravity anomalies. For each station, the terrain in a 170 m radius (Hammer zone D) was estimated in the field. Terrain corrections to a radius of 21.944 km (Hammer zones E-M) are calculated from a 10 m digital terrain model derived from Land Information New Zealand 1:50 000 topographic map sheets assuming a density of 2670 kg/m^3 for the topography. All terrain corrections for topography were calculated using GNS Science programs NEAR_TERRAIN and TERRAIN.

The effect of a topographic feature on any gravity observation is inversely proportional to the distance from the observation point. For example, an error in estimate of 50 m in elevation of a compartment in Hammer zone H (1530-2615 m) will result in an error in the terrain correction of 0.005 mGal, whereas an error in the elevation estimate of 50 m for Hammer zone C (16.6-53.3 m) will result in an error of ~0.25 mGal. Errors in terrain correction for the outer Hammer zones will tend to cancel one another out, while consistent over or under estimation in near zone elevation variation will produce estimated terrain correction errors of approximately ±0.3 mGal.

A4. GNS Land Gravity Database

Gravity data collected as part of this thesis was complemented with existing data from the New Zealand Gravity Station Network (http://maps.gns.cri.nz/website/gravity/). An existing onshore gravity dataset covering an area of 60 x 10^3 km^2 (13560 stations) has been extracted from the New Zealand Gravity Station Network for the central North Island (Fig. A1). These gravity data, collected over the past 60 years by numerous workers, are tied to the New Zealand Primary Gravity Network and reduced to Bouguer anomalies using the method of Reilly (1972) and a crustal density of 2670 kg/m^3. The principal source of error between existing and recent datasets is the method of altitude determination. The majority of the pre-existing gravity data have elevations derived from barometric levelling. All station altitudes in the New Zealand Gravity Station Network are checked against a digital elevation model with a 10 m cell size resolution and those station altitudes that differ from the model >20 m excluded from this study. Manual inspection of the data identified that station 2411 of the NZ Land Gravity Database has a recorded height of 55.7 m whereas the altitude of the topography and adjacent gravity stations is ~320 m above sea-level and is excluded as an erroneous station for this reason.

In addition to the data collected in this study, published (Davy & Caldwell, 1998; Mouslopoulou et al., 2008; Seebeck et al., 2010) and unpublished (Stagpoole et al., 2005) gravity data have been included with the New Zealand Gravity Station Network to increase the data density along the Taupo Rift axis (Fig. A2). These data were collected and reduced consistent with the methods outlined above and with the NZ Land Gravity database. Comparison of Bouguer anomalies in the same location show typical variations of < 2 mGal between pre-existing and new data sets. As interpolation

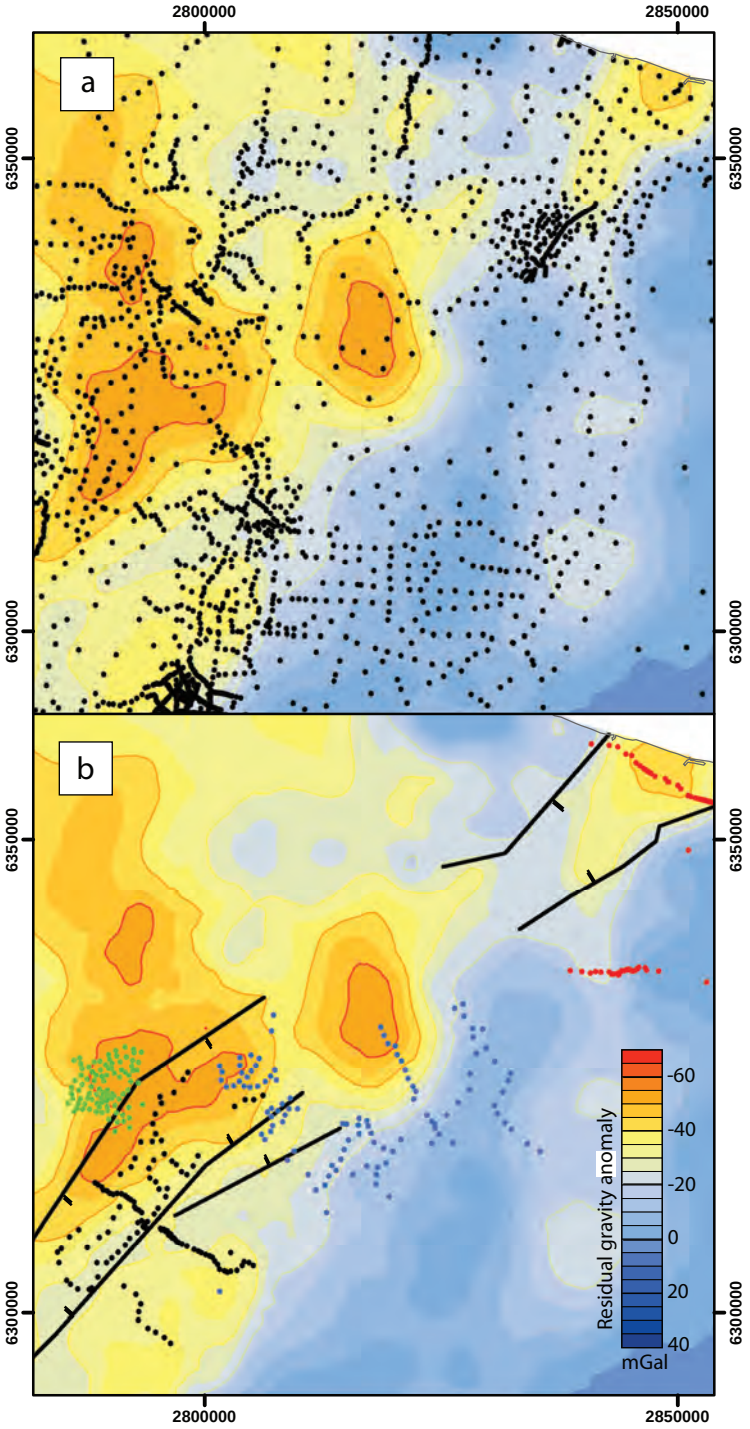

Appendix Figure 2. Residual gravity maps and station locations. (a) New Zealand Gravity Station Network locations (black filled circles) and associated residual gravity map. See text for methods. (b) Additional gravity stations used to constrain basement geometry in the Taupo Rift (black lines) with updated residual gravity map. Gravity stations from Davy & Caldwell (1998) across Lake Taupo (not shown), Stagpoole & Beetham (2005) (filled green circles), Mouslopoulou et al. (2008) (red filled circles), Seebeck et al. (2010) (light blue filled circles), and this study (black filled circles).

functions are generally used to contour the gravity data (Stagpoole & Bibby, 1999) these errors become insignificant, particularly when first order trends are being considered as they are here.

A5. Residual Gravity

Gravity anomalies represent the departure of the observed gravity field from a standard uniform Earth model. The effect of low density material in the upper crust combined with density variations in the deeper structure of the Earth result in the gravity anomalies observed along the Taupo Rift (Bibby et al., 1995). Long wavelength gravity anomalies (e.g. > 100 km) from the deep structure within the Earth (i.e. the subducting plate beneath the North Island) are considered part of the regional gravity field. A third-order, two-way, regional gravity field for the central North Island calculated by Stern (1979) is used here. Stern's long wavelength signal is derived from Bouguer gravity anomalies observed either side of the central North Island on a geologically uniform Mesozoic greywacke basement. Following the method of Stagpoole & Bibby (1999) this regional gravity field has been subtracted from the combined Bouguer gravity anomaly data to provide a residual gravity anomaly dataset from which the location and trend of rift and/or volcanic depressions can be interpreted (Fig. 4).

Table 4. Summary of Gravity data acquired during this study. Header information: Station number; X and Y, NZMG East and North coordinates; Height, metres above sea-level; Gravity, Absolute gravity minus 975000 in μN/kg; Date, yy mm dd; Inner Terrain, Hammer zone B-D; Outer Terrain, Hammer zone E-M; FAA; Free-air Anomaly; BA, Bouguer Anomaly; ISO, Isostatic Anomaly; Regional, calculated regional anomaly of Stern (1979); Residual, BA-Regional. Note all gravity reported in μN/kg. 1 μN/kg = 0.1 mGal.

STATION	X	Y	HEIGHT	GRAVITY	METER	DATE_	TER_IN	TER_OUT	FAA	BA	ISO	REGIONAL	RESIDUAL
7200	2802355	6304217	296.5	49745.5	106	90210	0.1	2.3	253	-60.2	138.9	305.8	-366.0
7201	2802075	6304325	296.5	49751.9	106	90210	0	2.4	260.2	-53.1	144.8	307.9	-361.0
7202	2801544	6304500	297.7	49763.8	106	90210	0.1	2.6	277	-37.3	160.3	311.6	-348.9
7203	2801333	6305029	299.2	49775.3	106	90210	0.1	2.8	297.3	-18.5	177.7	316.5	-335.0
7204	2801039	6305378	304.3	49773.2	106	90210	0.2	3.1	313.6	-7.6	187.8	320.4	-328.0
7205	2800810	6305776	309.2	49775	106	90210	0.1	3.4	333.6	7.1	201.5	324.3	-317.2
7206	2800471	6305920	311.7	49780	106	90210	0.1	3.8	347.3	18.4	212.5	326.8	-308.4
7207	2800071	6306093	316.9	49779.9	106	90210	0.1	4.5	364.5	30.5	224.4	329.7	-299.2
7208	2799617	6306292	318.7	49783.1	106	90210	0.1	5.5	374.7	39.8	233.3	333.1	-293.3
7209	2799326	6306425	325.3	49773.3	106	90210	0.1	6.3	386.2	44.7	237.9	335.2	-290.5
7210	2798853	6306629	365.9	49679.3	106	90210	0.1	6.3	418.9	32.2	224.9	338.6	-306.4
7211	2802723	6304320	296.5	49746.9	106	90210	0	2.3	255.4	-58.1	140.6	305.0	-363.1
7212	2803373	6304422	296.8	49763.9	106	90210	0.1	2.4	274.3	-39.3	158.5	302.8	-342.1
7213	2803952	6304919	298.4	49765.6	106	90210	0	2.6	285	-30.3	165.4	304.1	-334.4
7214	2804155	6305293	299.7	49759.9	106	90210	0	2.7	286.4	-30.4	163.8	306.0	-336.4
7215	2804663	6305201	300.3	49768.1	106	90210	0	2.8	295.8	-21.4	172.8	303.0	-324.4
7216	2805085	6304917	303.7	49774.8	106	90210	0.1	3.1	310.9	-9.8	186.1	298.9	-308.7
7217	2802722	6306255	304.6	49751.3	106	90210	0.1	2.8	300	-22.1	170	319.7	-341.8
7218	2793906	6308821	465.4	49462.2	106	90211	0.7	57.7	524.8	79.7	267.7	372.3	-292.6
7219	2793876	6308847	455.5	49485.9	106	90211	0.5	53.2	518.1	79.2	267.3	372.6	-293.4
7220	2793805	6308870	446.1	49510.4	106	90211	0.3	47.3	513.8	79.2	267.2	373.0	-293.8
7221	2793708	6308926	438.6	49532.7	106	90211	0.1	38.1	513.4	77.8	265.7	373.7	-295.9
7222	2793601	6308980	438	49542.4	106	90211	0.2	30.1	521.6	78.8	267.1	374.4	-295.6
7223	2793471	6309058	440.8	49547	106	90211	0	23.6	535.5	82.9	271	375.4	-292.5
7224	2792898	6309469	512.7	49416.8	106	90211	0.1	11.3	630.2	85.8	273.5	380.1	-294.3
7225	2793339	6309684	463.5	49514.9	106	90211	0.3	13.3	578.2	90.5	277.1	380.0	-289.5

STATION	X	Y	HEIGHT	GRAVITY	METER	DATE_	TER_IN	TER_OUT	FAA	BA	ISO	REGIONAL	RESIDUAL
7226	2793589	6309480	425.7	49591.6	106	90211	0.1	21.1	536.8	98.6	285.1	377.8	-279.2
7227	2793686	6309356	417.3	49600.4	106	90211	0.1	25	518.7	93.6	280.5	376.7	-283.1
7228	2793943	6309601	413.6	49599.6	106	90211	0.1	24.2	508.6	86.9	273	377.4	-290.5
7229	2792548	6311164	393.6	49587.8	106	90211	0.2	11	447	34.1	215.8	392.3	-358.2
7230	2792509	6311646	373.8	49621.3	106	90211	0.1	7.4	423.1	28.5	209.1	395.5	-367.0
7231	2788384	6313687	308.2	49632.7	106	90212	0.1	3.2	247.2	-79.1	97.3	420.4	-499.5
7232	2788711	6313476	316	49631.6	106	90212	0.3	3.3	268.5	-66.1	110.6	418.2	-484.3
7233	2789110	6313248	290.5	49683.1	106	90212	0	3.8	239.6	-66.5	110.9	415.7	-482.2
7234	2789250	6312929	292.3	49690.6	106	90212	0.1	4.3	250.2	-57.2	120.9	413.4	-470.6
7235	2789675	6312807	294.9	49702.8	106	90212	0.5	4.6	269.5	-40.1	138.2	411.4	-451.5
7236	2789970	6312565	300.8	49703.9	106	90212	0.3	6	287.1	-27.9	150.9	409.1	-437.0
7237	2790356	6312464	305	49711	106	90212	0.2	5.2	306.4	-14	164.8	407.3	-421.3
7238	2790760	6312589	320.9	49690.2	106	90212	0.5	6.4	335.8	-0.7	177	406.9	-407.6
7239	2791209	6312510	338	49677.2	106	90212	0.6	6.8	375.1	20	197.7	405.0	-385.0
7240	2791618	6312333	354.6	49651.5	106	90212	1.2	10.1	399.4	29.7	207.7	402.7	-373.0
7241	2791845	6312110	361.4	49648.5	106	90212	0.3	9.6	415.6	37	215.4	400.5	-363.5
7242	2792171	6311917	366.1	49637.5	106	90212	0.1	6.2	417.7	30.4	209.1	398.3	-367.9
7243	2797058	6307452	492.4	49476.6	106	90212	0.3	20.3	612.6	99.8	290.9	351.5	-251.7
7244	2796136	6308293	761.6	48857.8	106	90212	0.1	46	830.7	47.5	235.8	360.8	-313.3
7245	2796185	6308160	747.2	48893.3	106	90212	0.2	46.2	820.8	53.7	242.3	359.7	-306.0
7246	2796330	6308284	709.3	48992.7	106	90212	0.2	35	804.2	67.3	255.7	360.0	-292.7
7247	2796430	6308203	687.4	49059.6	106	90212	0.5	31.1	802.9	86.4	275	359.1	-272.7
7248	2796416	6308039	641	49138.6	106	90212	0.5	29	737.5	69.7	259	358.0	-288.3
7249	2796522	6307862	608	49212.8	106	90212	0.6	24.2	708.5	72.4	262.2	356.3	-283.9
7250	2796753	6307840	578	49293.2	106	90212	0.5	22	696.3	90.9	280.8	355.3	-264.4
7251	2796889	6307668	542.7	49366.6	106	90212	0.5	19.2	659.5	90.2	280.6	353.6	-263.4

STATION	X	Y	HEIGHT	GRAVITY	METER	DATE_	TER_IN	TER_OUT	FAA	BA	ISO	REGIONAL	RESIDUAL
7252	2797242	6307363	482.8	49494.1	106	90212	0.3	17.5	599.8	94.8	286.2	350.1	-255.3
7253	2797604	6307191	451	49533	106	90212	0.1	12.2	539.3	64.1	255.9	347.5	-283.4
7254	2798089	6306975	411.7	49599.7	106	90212	0.1	8.4	483.2	47.7	239.7	344.1	-296.4
7255	2792737	6310951	446	49494.6	106	90212	0.3	14.3	513.8	46.2	229.7	390.3	-344.1
7256	2793039	6310793	494.5	49415.7	106	90212	0.5	14.6	583.4	62.6	246.3	388.3	-325.7
7257	2793311	6310537	509.9	49398.4	106	90212	0.2	12.1	611.7	71.2	255.3	385.7	-314.5
7260	2796029	6313062	358.2	49680.3	106	100202	0	6.3	446.2	67.5	243	393.4	-325.9
7261	2795880	6312211	364.4	49677.1	106	100202	0	9.4	455.4	73	250.1	388.2	-315.2
7262	2795050	6310997	374.8	49673.8	106	100202	0	16.1	474.4	87.3	268.4	382.9	-295.6
7263	2794635	6310382	382.6	49654.1	106	100202	0	22.4	473.8	84.3	268.7	380.2	-295.9
7264	2793919	6309576	414.1	49598.2	106	100202	1	24.4	508.5	87.3	273.5	377.3	-290.0
7265	2792858	6308432	471.1	49495.8	106	100202	3	19.6	572.6	85.4	275.3	373.4	-288.0
7266	2792056	6307797	477.8	49496	106	100202	8	20.8	588.2	99.8	291.7	371.9	-272.1
7267	2791607	6307072	456.5	49532.1	106	100202	1	29.4	552.7	89.5	283.6	368.7	-279.2
7268	2790837	6306343	402.7	49640.9	106	100202	1	22.2	489.5	78.8	275.2	366.6	-287.8
7269	2790203	6305723	403.6	49655	106	100202	1	13.4	501.4	80.9	279.2	364.7	-283.8
7270	2789640	6305216	405.2	49648.7	106	100202	0	9.9	495.9	69.2	268.9	363.3	-294.1
7271	2788725	6303705	430.7	49603.4	106	100202	1	9	517	62.3	266.1	356.7	-294.4
7272	2788050	6302525	445	49582.5	106	100202	2	6.8	530.7	59.2	266.7	351.3	-292.1
7273	2786571	6302409	362.2	49770.8	106	100202	7	14.6	462.1	95.3	302.6	355.9	-260.6
7274	2785820	6302913	438.9	49591	106	100202	2	6.6	522.8	57.9	263.6	361.7	-303.8
7275	2785402	6303318	388.4	49693.3	106	100202	3	7.7	472.4	65.6	271.2	365.7	-300.1
7276	2787774	6302371	445.8	49597.6	106	100202	0	7.9	546.9	73.6	280.5	351.3	-277.7
7277	2784582	6305205	398.2	49624.7	106	100202	4	10.4	448.7	34.2	235.2	380.2	-346.0
7278	2784450	6306305	324.2	49742	106	100202	8	12.6	346.3	20.3	218	387.4	-367.1
7279	2784868	6306738	312.2	49767	106	100202	2	11.2	337.9	17.8	214.3	388.7	-370.9

STATION	X	Y	HEIGHT	GRAVITY	METER	DATE_	TER_IN	TER_OUT	FAA	BA	ISO	REGIONAL	RESIDUAL
7280	2785698	6307977	320.6	49718.2	106	100202	6	6.5	325	-5.2	188	393.7	-398.9
7281	2786681	6308737	327.3	49702.2	106	100202	4	5.6	335.9	-4.7	186.3	395.3	-400.0
7282	2795171	6313021	363.4	49658.9	106	100203	0	6	440.4	55.6	231.6	395.9	-340.3
7283	2794823	6313794	362.2	49611.6	106	100203	0	3	395.4	8.9	182.9	402.1	-393.2
7284	2794181	6314189	384.1	49563.4	106	100203	1	3.2	417.7	8.1	181.7	406.6	-398.5
7285	2794092	6315197	410.2	49497.6	106	100203	4	3.5	440.3	5	174.1	413.4	-408.4
7286	2794595	6316083	371.2	49585.4	106	100203	2	4	414.9	21	188.2	417.5	-396.5
7287	2795695	6316724	357	49608.5	106	100203	1	3.8	399.6	20.4	185.6	418.3	-397.9
7288	2796534	6315977	377.7	49563.9	106	100203	0	3.1	413.2	9.4	176.1	411.0	-401.6
7289	2796976	6315606	378	49584.1	106	100203	0	3.5	431.5	27.7	195.2	407.2	-379.5
7290	2797524	6314862	381	49614.6	106	100203	0	3.7	465.6	58.7	228	400.5	-341.8
7291	2798105	6314569	375.8	49629.6	106	100203	0	5.3	462.4	62.9	232.1	396.7	-333.8
7292	2794457	6318039	316.2	49645.4	106	100203	1	7.4	320.6	-10.4	151.3	430.2	-440.6
7293	2798180	6325372	404.1	49392.2	106	100203	1	3.9	397.7	-35.6	103.8	466.0	-501.6
7294	2797707	6324597	428	49373.1	106	100203	4	3.4	446	-11.1	129.8	462.4	-473.5
7295	2796751	6323256	411.9	49366	106	100203	2	3.9	378.4	-62.3	82.8	456.5	-518.8
7296	2795416	6322112	363.6	49470.9	106	100203	0	8.2	324.8	-59.4	89.4	452.8	-512.2
7297	2794767	6320935	390.7	49412.7	106	100203	3	3.1	340.7	-75.5	77.4	447.3	-522.8
7298	2794520	6319933	367.7	49483.9	106	100203	2	3.5	333	-58.3	97.9	441.8	-500.1
7299	2794792	6318873	331.6	49591.9	106	100203	1	7.9	321.4	-26.4	132.7	434.5	-460.9
7300	2795264	6322770	431.3	49313.3	106	100203	2	3.6	381.3	-80.4	66.1	457.2	-537.6
7301	2793225	6318015	311.3	49632.4	106	100203	1	3.4	292	-37.6	125.7	433.5	-471.1
7302	2795415	6318152	378.5	49521.9	106	100203	4	5.7	390.6	-8.4	152.2	428.2	-436.6
7303	2799293	6316523	434.5	49496	106	100203	2	5.1	525.7	62.4	226	405.9	-343.5
7304	2798785	6315465	404.2	49561.4	106	100203	1	4.2	489.1	58	224	400.4	-342.4
7305	2806113	6322929	532	49207.9	106	100203	4	10.9	591.1	27.2	165.1	427.8	-400.6

STATION	X	Y	HEIGHT	GRAVITY	METER	DATE_	TER_IN	TER_OUT	FAA	BA	ISO	REGIONAL	RESIDUAL
7306	2805149	6322465	577.2	49097.5	106	100203	4	12	616.1	3.5	143.8	427.7	-424.2
7307	2804261	6322460	612.9	49006.4	106	100203	1	10.3	634.8	-21.2	119.8	430.4	-451.6
7308	2803145	6321778	568.7	49091.6	106	100203	10	9.4	578	-21.7	122.2	429.2	-450.9
7309	2788858	6307877	379.1	49680.9	106	100204	3	6.8	468.3	70.1	262.7	383.1	-313.0
7310	2789754	6308477	359.4	49725.4	106	100204	11	11.6	457	93.6	284.4	384.0	-290.4
7311	2790329	6310002	366.3	49659.3	106	100204	2	8.7	424.4	41.4	228	391.9	-350.5
7312	2790985	6311130	346.6	49681.5	106	100204	5	8.5	394.9	36.5	218.4	397.0	-360.5
7313	2792639	6316279	299.4	49692.1	106	100204	3	5	301	-11	157.1	424.4	-435.4
7314	2792205	6315368	297.2	49713	106	100204	2	6.3	307.9	-1.2	169.3	419.9	-421.1
7315	2791073	6314601	296.7	49693.1	106	100204	2	5.7	280	-29.1	143.4	418.4	-447.5
7316	2787566	6306823	429.2	49591.2	106	100204	9	8.1	524.5	78.2	273.7	380.7	-302.5
7317	2788588	6305223	432.9	49599.9	106	100204	13	5.8	532.3	83.7	283.1	367.0	-283.3
7318	2791452	6302729	561.7	49286.3	106	100204	7	9	597.1	3.6	209.1	340.1	-336.5
7319	2792726	6301869	461	49489.3	106	100204	21	8.1	483	13.9	221.8	329.2	-315.3
7320	2793200	6300855	424.9	49552.1	106	100204	30	9.3	426.5	7.6	219	320.2	-312.6
7321	2793023	6300027	414.9	49579.4	106	100204	2	6.2	416.4	-22.4	192.4	315.0	-337.4
7322	2792954	6299169	407.1	49590.9	106	100204	9	7.2	397	-24.9	192.2	309.2	-334.1
7323	2793993	6298295	391.4	49613.9	106	100204	10	8.4	365	-37.2	182.3	298.4	-335.6
7324	2794774	6297895	374.6	49645.8	106	100204	21	6.4	342.1	-32.4	188	292.0	-324.4
7325	2795718	6297362	326.6	49721.2	106	100204	11	3.6	265.5	-68.2	153.7	283.8	-352.0
7326	2796358	6296735	301.1	49766.1	106	100204	0	2.6	226.9	-90.3	132.6	276.2	-366.5
7327	2795311	6308855	881.8	48546.9	106	100205	5	80.6	894.9	20.8	207.4	367.6	-346.8
7328	2795433	6308719	866.7	48589.8	106	100205	5	67.7	890.1	19.6	206.6	366.2	-346.6
7329	2795648	6308744	846.5	48641.7	106	100205	4	62.4	879.9	25.1	212	365.6	-340.5
7330	2795810	6308587	799.7	48761	106	100205	13	49.6	853.7	45.9	233.3	364.0	-318.1
7331	2796009	6308614	765.1	48849.9	106	100205	12	39.9	836.1	55.3	242.7	363.4	-308.1

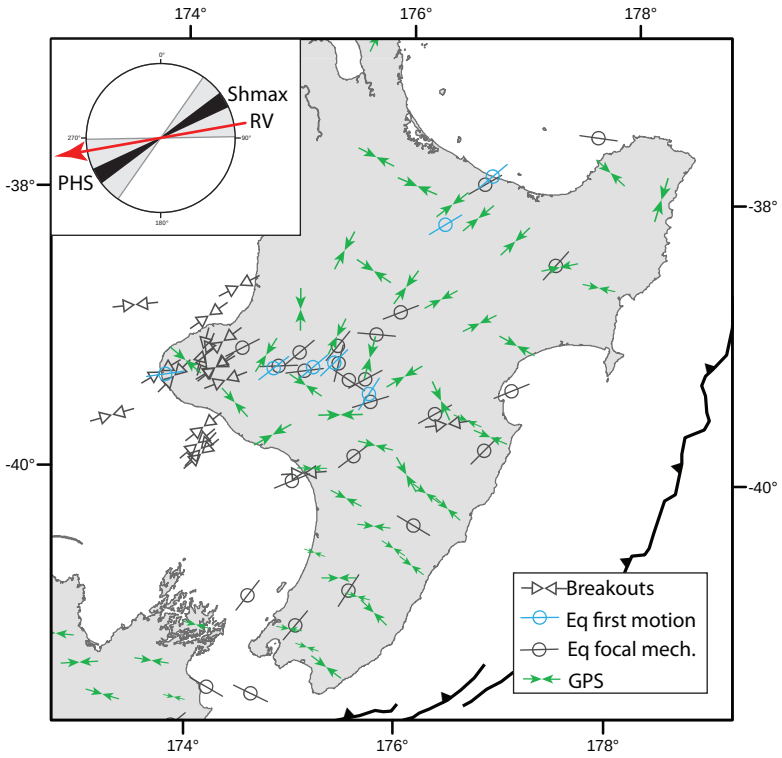

Appendix Figure 3. North Island regional stress and strain orientations. Orientation of Shmax derived from focal mechanisms (Sherburn et al., 2009) and first motions (Hurst et al., 2002; Hayes et al., 2004; Sherburn & White, 2005; Hurst et al., 2008; Reyners, 2010) from mid-crustal earthquakes with bore hole breakouts from the Australasia stress map (www.asprg.adelaide.edu.au/asm/). Principal shortening directions from GPS inversion (Beavan et al., 2007).

Appendix 2: Earthquake statistics

Appendix 2 supplements information presented in chapter 4. Appendix Tables 2 and 3 detail the statistics of earthquakes from the GeoNet catalogue (www.GeoNet.org.nz) 1988-2010 analysed in chapter 4. See chapter 4 Fig. 3 for the location of sections detailed in each table. The statistics for 40 and 200 km deep intervals through the subducting slab for each section are shown where N is the number of earthquakes in each interval and M_O is the approximate seismic moment. The approximate seismic moment M_O is based on M_L where M_L = (1.09 ± 0.10) M_W + (0.05 ± 0.06)(Ristau, 2009). The constant a is a measure of the seismicity rate ($a*$ is the annual seismicity rate) and the constant b is the ratio of large to small earthquakes (generally in the interval 0.8 < b > 1.2). The constants a and b are from the Gutenberg-Richter frequency-magnitude relation where the number N of earthquakes of size greater than m in a specific area follow:

$$logN = a - bm$$

The intervals highlighted in red are considered anomalous due to high numbers of earthquakes compared with adjacent sections. These seismicity rate anomalies are clearly seen in depth distribution profiles shown in chapter 4 Fig. 8.

Table 5. GeoNet catalogue (1988-2010) 150 km wide dip-parallel sections.

$M_L \geq 3.6$		South	Central	North	Offshore
Catalogue	N	1166	1680	4668	3362
	Mo	2.242×10^{26}	5.264×10^{26}	8.047×10^{26}	7.567×10^{26}
	a	6.63	6.79	7.47	7.06
	a*	5.28	5.44	6.12	5.71
	b	0.99 ± 0.03	0.99 ± 0.02	1.05 ± 0.01	0.98 ± 0.01
50-90 km	N	270	255	277	438
	Mo	7.699×10^{25}	8.72×10^{25}	2.278×10^{25}	1.428×10^{25}
	a	5.74	5.87	5.99	6.29
	a*	4.4	4.53	4.65	4.95
	b	0.918 ± 0.05	0.962 ± 0.06	0.985 ± 0.05	1.01 ± 0.04
90-130 km	N	202	160	361	391
	Mo	5.112×10^{25}	1.073×10^{25}	2.477×10^{25}	2.928×10^{25}
	a	5.78	5.94	6.69	6.42
	a*	4.45	4.62	5.53	5.08
	b	0.965 ± 0.07	1.04 ± 0.07	1.15 ± 0.06	1.06 ± 0.05
130-170 km	N	255	187	2021	691
	Mo	6.364×10^{25}	1.222×10^{25}	47.36×10^{25}	5.258×10^{25}
	a	6.09	6.36	7.33	6.55
	a*	4.75	5.05	5.99	5.21
	b	1.02 ± 0.06	1.13 ± 0.08	1.12 ± 0.02	1.03 ± 0.03
170-210 km	N	272	360	1290	607
	Mo	2.154×10^{25}	10.78×10^{25}	8.556×10^{25}	10.6×10^{25}
	a	6.46	6.33	6.84	6.6
	a*	5.12	5	5.5	5.26
	b	1.12 ± 0.06	1.05 ± 0.05	1.04 ± 0.03	1.06 ± 0.04
210-250 km	N	84	544	279	602
	Mo	0.503×10^{25}	29.28×10^{25}	1.337×10^{25}	6.828×10^{25}
	a	5.42	6.01	6.37	5.98
	a*	4.09	4.67	5.03	4.64
	b	0.97 ± 0.09	0.91 ± 0.03	1.09 ± 0.06	0.888 ± 0.03
50-250 km	N	1083	1506	4228	2729
	Mo	2.183×10^{26}	5.108×10^{26}	6.201×10^{26}	2.704×10^{26}
	a	6.62	6.72	7.52	7.05
	a*	5.28	5.38	6.18	5.71
	b	0.997 ± 0.03	0.984 ± 0.02	1.08 ± 0.01	1.0 ± 0.02

Table 6. GeoNet catalogue (1988-2010) 100 km wide relative motion vector parallel sections.

$M_L \geq 3.6$		S2	S1	C	N1	N2
Catalogue	N	655	1097	1597	4599	3166
	Mo	2.726×10^{26}	2.02×10^{26}	6.821×10^{26}	7.87×10^{26}	3.915×10^{26}
	a	6.58	6.54	6.93	7.5	6.95
	a*	5.24	5.2	5.59	6.16	5.61
	b	1.05 ± 0.04	0.97 ± 0.03	1.03 ± 0.02	1.07 ± 0.01	0.96 ± 0.01
50-90 km	N	225	326	266	397	158
	Mo	24.72×10^{25}	5.64×10^{25}	4.512×10^{25}	2.646×10^{25}	0.451×10^{25}
	a	5.61	5.99	5.92	6.28	6.37
	a*	4.2	4.65	4.58	4.94	5.04
	b	0.90 ± 0.06	0.97 ± 0.05	0.97 ± 0.05	1.02 ± 0.04	1.14 ± 0.09
90-130 km	N	145	166	216	384	355
	Mo	1.647×10^{25}	4.186×10^{25}	2.108×10^{25}	2.539×10^{25}	2.791×10^{25}
	a	6.14	5.54	6.15	6.72	6.33
	a*	4.81	4.21	4.82	5.38	4.99
	b	1.11 ± 0.09	0.92 ± 0.07	1.06 ± 0.07	1.15 ± 0.05	1.05 ± 0.05
130-170 km	N	72	209	221	1985	751
	Mo	0.135×10^{25}	6.397×10^{25}	1.221×10^{25}	4.53×10^{25}	7.399×10^{25}
	a	6.89	5.7	6.65	7.25	6.74
	a*	5.59	4.37	5.31	5.91	5.4
	b	1.4 ± 0.2	0.93 ± 0.06	1.19 ± 0.08	1.01 ± 0.02	1.07 ± 0.03
170-210 km	N	96	183	391	1159	731
	Mo	0.217×10^{25}	$1.93x\ 10^{25}$	10.8×10^{25}	7.025×10^{25}	5.121×10^{25}
	a	6.5	6.32	6.52	6.82	6.62
	a*	5.18	4.98	5.19	5.48	5.28
	b	1.25 ± 0.1	1.13 ± 0.08	1.09 ± 0.05	1.04 ± 0.03	1.04 ± 0.03
210-250 km	N	84	50	403	393	567
	Mo	0.054×10^{25}	0.41×10^{25}	21.44×10^{25}	8.896×10^{25}	6.861×10^{25}
	a	6.97	4.77	6.02	6.3	5.99
	a*	5.69	3.46	4.68	4.96	4.65
	b	1.48 ± 0.2	0.853 ± 0.1	0.95 ± 0.04	1.03 ± 0.05	0.89 ± 0.03
50-250 km	N	583	934	1497	4318	2562
	Mo	2.677×10^{26}	1.856×10^{26}	4.008×10^{26}	2.704×10^{26}	2.262×10^{26}
	a	6.63	6.45	6.9	7.5	7.01
	a*	5.29	5.1	5.55	6.16	5.67
	b	1.07 ± 0.04	0.97 ± 0.03	1.03± 0.02	1.07 ± 0.01	1.0 ± 0.02

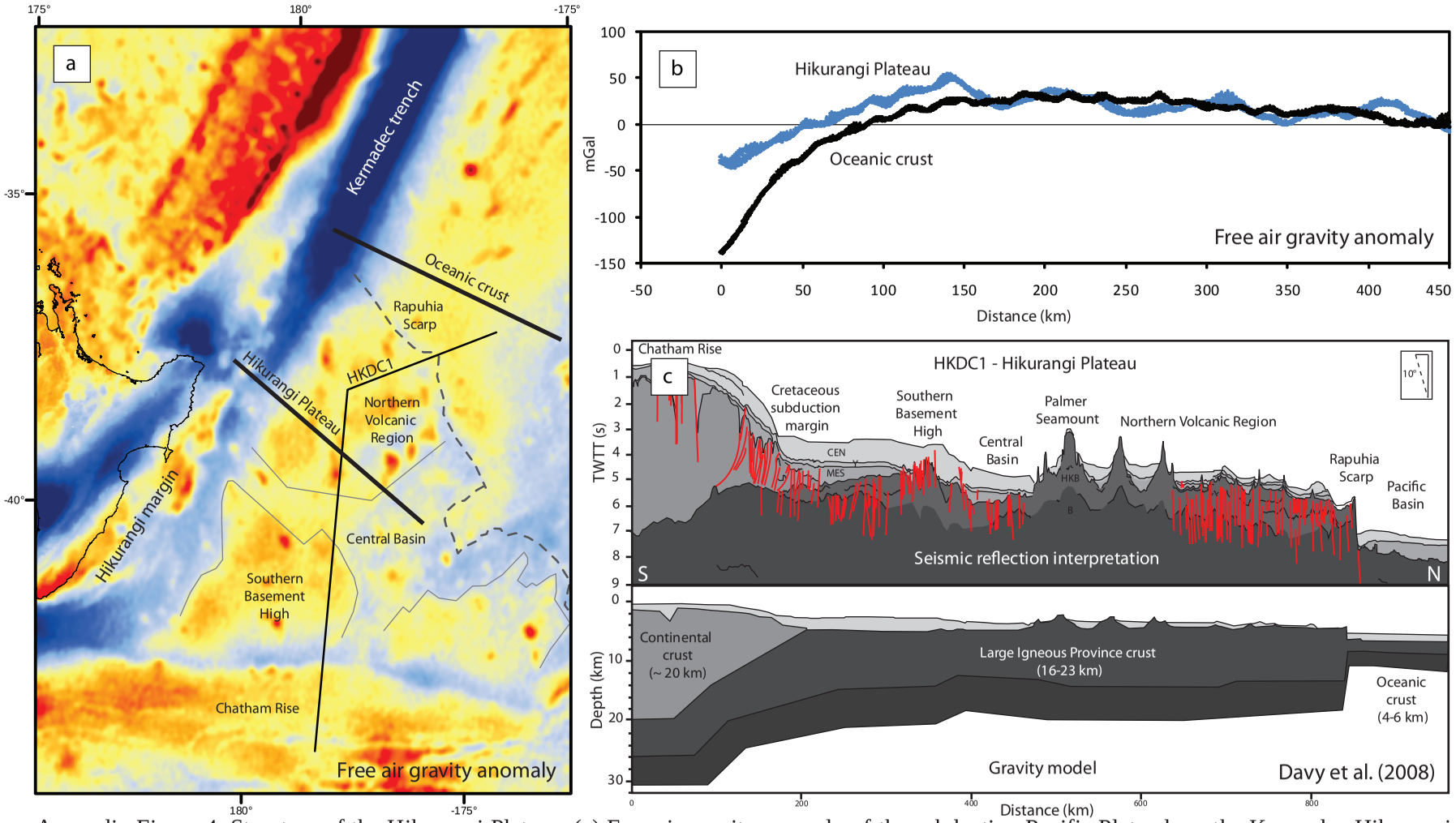

Appendix Figure 4. Structure of the Hikurangi Plateau. (a) Free air gravity anomaly of the subducting Pacific Plate along the Kermadec-Hikurangi trench (Sandwell & Smith, 2008). Location of gravity profiles in (b) and seismic reflection interpretation and gravity model along HKDC-1 in (c). (b) Free air gravity anomaly profiles of Cretaceous oceanic crust and Hikurangi Plateau showing curvature of lithosphere due to bending associated with subduction. (c) Structure of the Hikurangi Plateau interpreted from seismic reflection profile HKDC-1 and associated gravity model from Davy et al. (2008)

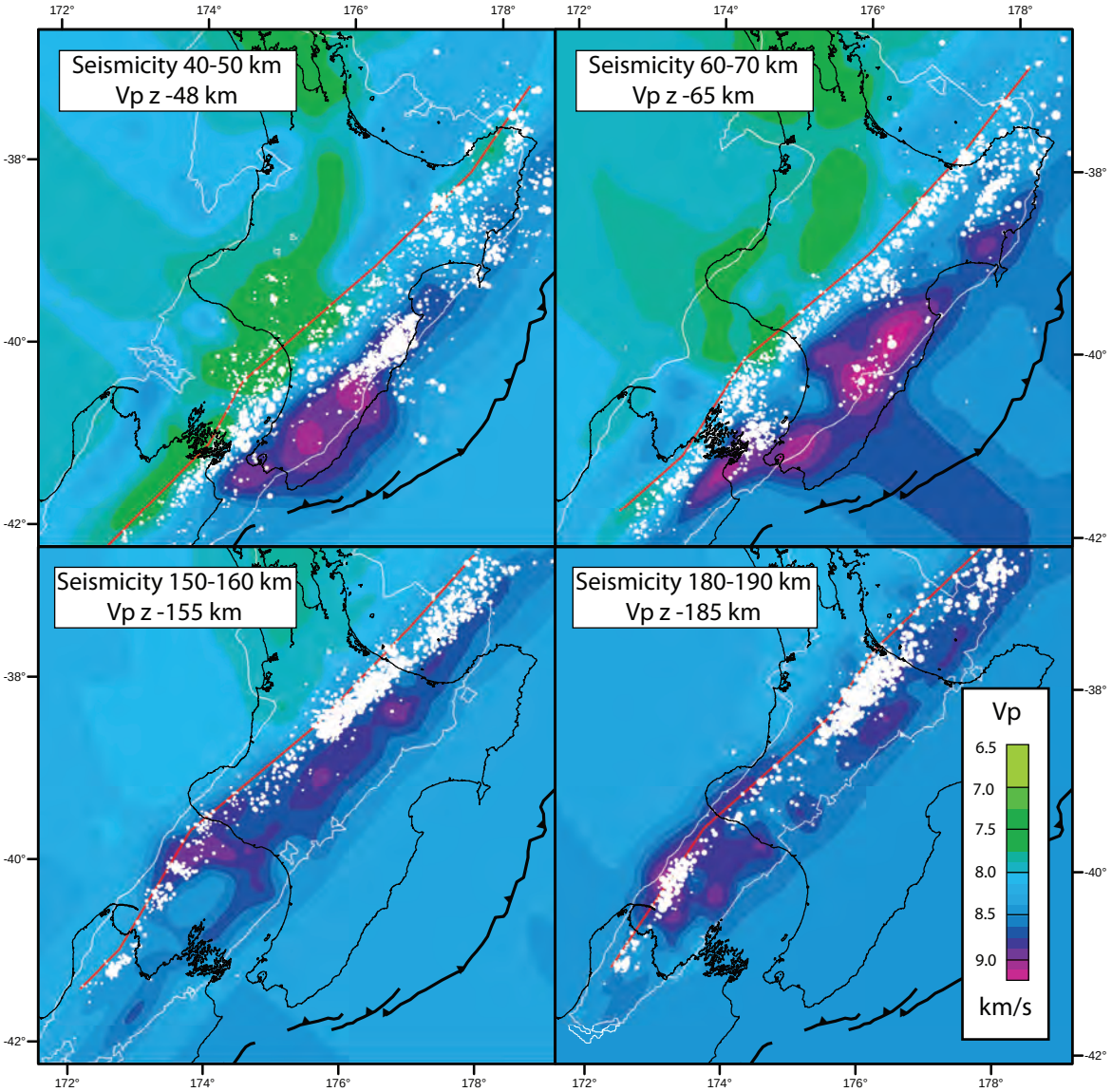

Appendix Figure 5. Pacific plate geometry from relocated Benioff zone seismicity. Relocated seismicity (2001-2009 $M_L \geq 2.5$) (white filled circles) and P-wave velocity model of the subducting Pacific plate at various depths. The western limit of seismicity is used to approximate the upper surface of the slab (red line). P-wave velocity model (Vp) of Eberhart-Phillips et al. (2010) showing the high velocity slab, meaningful velocity information contained within spread function contour ≤ 3 (white lines).

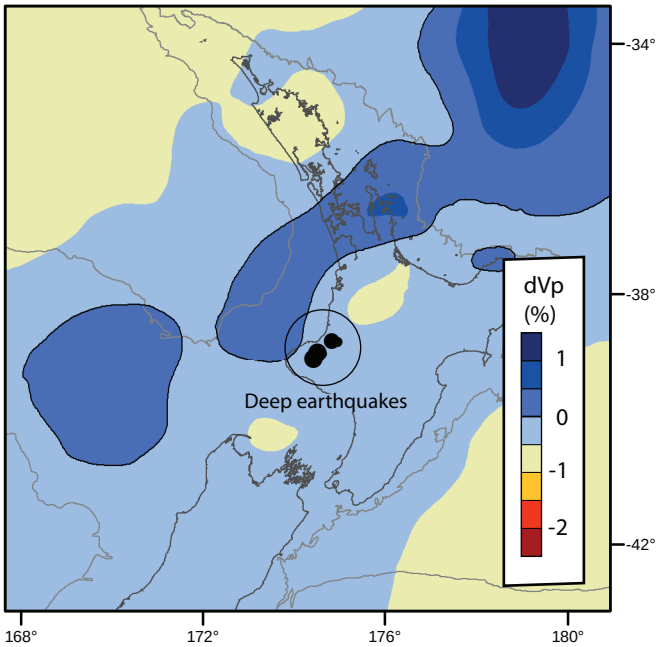

Appendix Figure 6. Mantle velocity anomalies at 600km depth (Li et al., 2008). See chapter 5 for details. Alignment of deep earthquakes beneath Taranaki at ~600 km (black filled circles) (Boddington et al., 2004) consistent with strike of positive mantle velocity anomaly.

Appendix 3: Finite poles of rotation

Appendix 3 supplements information presented in chapter 6.

Key to Appendix Tables

Plate ID	Plate	#	References
901	Pacific	1	Cande & Stock (2004)
801	Australia	2	Cande et al. (2000)
802	East Antarctica	3	Croon et al. (2008)
804	West Antarctica (Marie Byrd Land)	4	Schellart et al. (2006)
		5	Royer & Sandwell (1989)
		6	Royer & Rollet (1997)
		7	Cande et al. (1995)
		8	Keller (2003)

Table 7. Calculated Australia-Pacific Finite rotations from Cande & Stock (2004)

Moving Plate ID	Age (Ma)	Latitude (°N)	Longitude (°E)	Angle(°)	Fixed Plate ID	#
901	2.58	-58.761	-175.666	-2.766	801	1
901	6.04	-59.347	-174.331	-6.385	801	1
901	10.95	-58.244	-174.873	-11.933	801	1
901	20.13	-56.392	-175.556	-22.217	801	1
901	26.55	-55.03	-176.889	-29.232	801	1

Table 8. 4 Plate model Australia-Antarctica-Pacific finite rotations from Cande & Stock (2004)

Moving Plate ID	Age (Ma)	Latitude (°N)	Longitude (°E)	Angle(°)	Fixed Plate ID	#
801	2.58	-11.16	-139.7	1.65	802	1
801	6.04	-11.59	-139.2	3.83	802	1
801	10.95	-11.9	-142.1	6.79	802	1
801	20.13	-13.39	-145.6	12.05	802	1
801	26.55	-13.8	-146.4	15.92	802	1
801	28.74	-13.58	-146	17.32	802	1
801	30.94	-13.4	-145.6	18.89	802	1
801	33.54	-13.45	-146.6	20.49	802	1
801	38.13	-14.65	-146.6	22.88	802	1
804	33.55	-18.15	-17.85	0.7	802	2
804	43.8	-18.15	-17.85	1.7	802	2
901	2.58	65.532	-79.484	2.259	804	1
901	6.04	66.988	-81.949	5.195	804	1
901	10.95	70.335	-77.855	9.479	804	1
901	20.13	74.202	-69.52	16.87	804	1
901	26.55	74.773	-66.94	21.826	804	1
901	33.54	74.399	-64.556	27.36	804	1

Table 9. Regional reconstruction model –
4 Plate model Australia-Antarctica-Pacific finite rotations

Moving Plate ID	Age (Ma)	Latitude (°N)	Longitude (°E)	Angle(°)	Fixed Plate ID	#
801	2.58	-11.16	-139.7	1.65	802	1
801	6.04	-11.59	-139.2	3.83	802	1
801	10.95	-11.9	-142.1	6.79	802	1
801	20.13	-13.39	-145.6	12.05	802	1
801	26.55	-13.8	-146.4	15.92	802	1
801	28.74	-13.58	-146	17.32	802	1
801	30.94	-13.4	-145.6	18.89	802	1
801	33.54	-13.45	-146.6	20.49	802	1
801	38.13	-14.65	-146.6	22.88	802	1
801	40.1	17.1	30.6	-23.68	802	1
804	33.55	-18.15	-17.85	0.7	802	2
804	43.8	-18.15	-17.85	1.7	802	2
901	0.78	64.3	-81.21	0.67	804	3
901	1.86	64.9	-81.14	1.61	804	3
901	2.58	65.2	-81.23	2.23	804	3
901	3.58	65.9	-81.17	3.11	804	3
901	4.24	66.62	-80.53	3.7	804	3
901	5.11	66.91	-80.66	4.48	804	3
901	6.04	67.09	-81.08	5.21	804	3
901	6.71	67.33	-81.2	5.81	804	3
901	7.86	68.16	-80.54	6.83	804	3
901	8.86	68.83	-79.97	7.64	804	3
901	9.74	69.71	-78.57	8.42	804	3
901	10.95	70.36	-77.81	9.48	804	3
901	12.29	71.29	-76.12	10.63	804	3
901	13.06	71.74	-75.12	11.28	804	3
901	14.39	72.38	-73.58	12.42	804	3
901	15.09	72.6	-73.18	13.01	804	3
901	16.15	72.97	-72.5	13.95	804	3
901	16.64	73.18	-72.03	14.34	804	3
901	17.47	73.39	-71.58	14.93	804	3
901	18.28	73.62	-70.91	15.42	804	3
901	19.05	73.71	-70.94	15.95	804	3
901	20.13	74	-70.16	16.78	804	3
901	21.16	74.13	-70.09	17.38	804	3
901	23.07	74.38	-69.73	18.67	804	3
901	24.06	74.48	-69.58	19.35	804	3
901	24.84	74.51	-69.66	19.92	804	3
901	25.82	74.5	-69.84	20.62	804	3
901	26.55	74.51	-69.81	21.17	804	3
901	27.03	74.45	-69.9	21.53	804	3
901	27.97	74.4	-69.75	22.23	804	3
901	28.28	74.41	-69.5	22.57	804	3
901	28.75	74.33	-69.54	22.95	804	3
901	29.4	74.38	-68.71	23.66	804	3
901	30.1	74.33	-68.43	24.23	804	3

Table 9. Regional reconstruction model – 4 Plate model Australia-Antarctica-Pacific finite rotations continued

Moving Plate ID	Age (Ma)	Latitude (°N)	Longitude (°E)	Angle(°)	Fixed Plate ID	#
901	30.48	74.37	-67.75	24.71	804	3
901	30.94	74.32	-67.59	25.06	804	3
901	33.06	74.44	-64.74	26.97	804	3
901	33.55	74.48	-64.01	27.39	804	3
901	34.66	74.62	-61.89	28.39	804	3
901	34.94	74.63	-61.48	28.61	804	3
901	35.69	74.7	-60.18	29.23	804	3
901	36.34	74.75	-59.05	29.81	804	3
901	36.62	74.76	-58.64	30.05	804	3
901	37.47	74.82	-57.44	30.68	804	3
901	38.43	74.85	-56.21	31.41	804	3
901	40.13	74.87	-54.46	32.62	804	3

Table 10. 4 Plate model Australia-Antarctica-Pacific finite rotations from Schellart et al. (2006)

Moving Plate ID	Age (Ma)	Latitude (°N)	Longitude (°E)	Angle(°)	Fixed Plate ID	#
801	10.5	-12.5	-143.3	6.62	802	5
801	20.5	-14.5	-147.2	11.98	802	5
801	33	-13.696	-146.025	20.485	802	5
801	40.1	-14.32	-148.25	23.77	802	6
804	33	-18.146	-17.847	0.696	802	2
804	43	-18.146	-17.847	1.7	802	2
901	0.8	4.25	-79.06	0.68	804	7
901	2.6	67.03	-73.72	2.42	804	7
901	5.9	67.91	-77.93	5.42	804	7
901	8.9	69.68	-77.06	7.95	804	7
901	12.3	71.75	-73.77	10.92	804	7
901	17.5	73.68	-69.85	15.17	804	7
901	24.1	74.72	-67.28	19.55	804	7
901	28.3	74.55	-67.38	22.95	804	7
901	33.5	74.38	-64.74	27.34	804	7
901	42.5	74.9	-51.31	34.54	804	7

Table 11. Calculated Australia-Pacific finite rotations of Schellart et al. (2006)

Moving Plate ID	Age (Ma)	Latitude (°N)	Longitude (°E)	Angle(°)	Fixed Plate ID	#
901	0.8	-59.144	177.613	-0.83	801	4
901	2.6	-59.913	178.363	-2.94	801	4
901	5.9	-60.483	178.384	-6.57	801	4
901	9	-59.639	-178.627	-9.82	801	4
901	12.6	-58.538	-176.756	-13.85	801	4
901	17.6	-52.164	-173.169	-22.15	801	4
901	24.1	-55.199	-176.071	-26.397	801	4
901	26.1	-55.155	-177.133	-28.958	801	4
901	27.4	-54.89	-177.963	-30.632	801	4
901	33.5	-52.155	-179.042	-37.074	801	4
901	42.5	-50.148	177.464	-47.381	801	4

Table 12. Local reconstruction model-
Calculated Australia-Pacific finite rotations of Keller (2003)

Moving Plate ID	Age (Ma)	Latitude (°N)	Longitude (°E)	Angle(°)	Fixed Plate ID	#
901	30.1	-53.19	-178.74	-33.73	801	8
901	30.94	-52.83	-178.81	-34.58	801	8
901	33.55	-51.7	-178.45	-35.99	801	8
901	34.94	-51.19	-178.62	-37.49	801	8
901	36.34	-50.82	-179.3	-39.61	801	8
901	37.47	-50.36	-178.87	-39.62	801	8
901	40.13	-49.81	-179.55	-41.77	801	8

References

Beavan, J., Ellis, S., Wallace, L. & Denys, P., 2007. Kinematic constraints from GPS on oblique convergence of the Pacific and Australian Plates, Central South Island, New Zealand. In D. Okaya, T. Stern & F. Davey, eds. *A Continental Plate Boundary: Tectonics at South Island, New Zealand*. Geophysical Monograph 175, Washington DC: American Geophysical Union. pp.75-95.

Bibby, H.M., Caldwell, T.G., Davey, F.J. & Webb, T.H., 1995. Geophysical evidence on the structure of the Taupo Volcanic Zone and its hydrothermal circulation. *Journal of Volcanology & Geothermal Research*, 68, pp.29-58.

Boddington, T., Parkin, C.J. & Gubbins, D., 2004. Isolated deep earthquakes beneath the North Island of New Zealand. *Geophysics Journal International*, 158, pp.972-82.

Cande, S., Raymond, C.A., Stock, J.M. & Haxby, W.F., 1995. Geophysics of the Pitman Fracture Zone and Pacific-Antarctic plate motions during the Cenozoic. *Science*, 947-953, p.270.

Cande, S.C. & Stock, J., 2004. Pacific-Antarctic-Australian motion and the formation of the Macquire Plate. *Geophysics Journal International*, 157, pp.399-414.

Cande, S., Stock, J.M., Muller, R.D. & Ishihara, T., 2000. Cenozoic motion between East and West Antarctica. *Nature*, 404, pp.145-50.

Croon, M.B., Cande, S.C. & Stock, J.M., 2008. Revised Pacific-Antarctic plate motions and geophysics of the Menard Fracture zone. *Geochemistry, Geophysics, Geosystems*, 9, p.Q07001.

Davy, B.W. & Caldwell, T.G., 1998. Gravity, magnetic and seismic surveys of the caldera complex, Lake Taupo, North Island, New Zealand. *Journal of Volcanology & Geothermal Research*, 81, pp.69-89.

Eberhart-Phillips, D., Reyners, M., Bannister, S., Chadwick, M. & Ellis, S., 2010. Establishing a versatile 3-D seismic velocity model for New Zealand. *Seismological Research Letters*, 81(6), pp.992-1000.

Hayes, G., Reyners, M. & Stuart, G., 2004. The Waiouru. New Zealand, earthquake swarm: Persistent mid-crustal activity near an active rift. *Geophysical Research Letters*, 31, p.L19613. doi:10.1029/2004GL020709.

Hurst, A.W., Bibby, H.M. & Robinson, R., 2002. Earthquake focal mechanisms in the Taupo Volcanic Zone and their relation to faulting and deformation. *New Zealand Journal of Geology & Geophysics*, 45, pp.527-38.

Keller, W.R., 2003. *Cenozoic plate tectonic reconstructions and plate boundary processes in the Southwest Pacific*. Unpub. PhD Thesis: California Institute of Techology. Pasadena.

Li, C., van der Hilst, R.D., Engdahl, E.R. & Burdick, S., 2008. A new global model for P wave speed variations in Earth's mantle. *Geochemsitry, Geophysics, Geosystems*, 9(Q05018). doi: 10.1029/2007GC001806.

Mouslopoulou, V., Nicol, A., Walsh, J.J., Beetham, D. & Stagpoole, V., 2008. Quaternary temporal stability of a regional strike-slip and rift intersection. *Journal of Structural Geology*, 30(4), pp.451-63.

Reilly, W.I., 1970. *Topographic-isostatic Gravity Corrections for New Zealand*. Department of Scientific and Industrial Reseach Bulletin 203. Wellington: Department of Scientific and Industrial Reseach.

Reilly, W.I., 1972. New Zealand Gravity Map series. *New Zealand Journal of Geology & Geophysics*, 15(1), pp.3-15.

Reyners, M., 2010. Stress and strain from earthquakes at the southern termination of the Taupo Volcanic Zone, New Zealand. *Journal of Volcanology & Geothermal Research*, 190(1-2), pp.82-88.

Ristau, J., 2009. Comparison of magnitude estimates for New Zealand earthquakes: Moment magnitude, local magnitude, and teleseismic body-wave magnitude. *Bulletin of the Seismological Society of America*, 99(3), pp.1841-52. doi:10.1785/0120080237.

Robertson, E.I. & Reilly, W.I., 1960. The New Zealand Primary Gravity Network. *New Zealand Journal of Geology & Geophysics*, 3, pp.41-68.

Royer, J.-Y. & Rollet, N., 1997. Plate-tectonic setting of the Tasmanian region. *Australian Journal of Earth Sciences*, 44, pp.543-60.

Royer, J.-Y. & Sandwell, D.T., 1989. Evolution of the eastern Indian Ocean since the Late Cretaceous; constraints from Geosat altimetry. *Journal of Geophysical Research*, 94, pp.13755-82.

Schellart, W.P., Lister, G.S. & Troy, V.G., 2006. Cretaceous and Cenozoic reconstruction of the Pacific region: Tectonics controlled by subduction and slab rollback processes. *Earth-Science reviews*, 76(3-4), pp.191-233.

Seebeck, H.C., Nicol, A., Stern, T.A., Bibby, H.M. & Stagpoole, V., 2010. Fault controls on the geometry and location of the Okataina Caldera, Taupo Volcanic Zone, New Zealand. *Journal of Volcanology & Geothermal Research*, 190, pp.136-51. doi:10.1016/j.jvolgeores.2009.04.011.

Sherburn, S. & White, R.S., 2005. Crustal seismicity in Taranaki, New Zealand using accurate hypocentres from a dense network. *Goephysics Journal International*, 162, pp.494-506. doi:10.1111/j.1365-246X.2005.02667.x.

Stagpoole, V. & Bibby, H.M., 1999. *Residual gravity anomaly map of the Taupo Volcanic Zone, New Zealand, 1:250 000*. Institute of Geological & Nuclear Sciences Geophysical Map 13. Lower Hutt: Institute of Geological & Nuclear Sciences Ltd.

Stagpoole, V., Woodward, D. & Beetham, R., 2005. *Gravity Survey at the Horohoro geothermal prospect, Taupo Volcanic Zone*. Institute of Geological & Nuclear Sciences Client Report 2005/32. Lower Hutt: Institute of Geological & Nuclear Sciences.

Stern, T.A., 1979. Regional and Residual gravity fields, Central North Island, New Zealand. *New Zealand Journal of Geology & Geophysics*, 479-485, p.22.

Stern, T.A., Stratford, W.R. & Salmon, M.L., 2006. Subduction evolution and mantle dynamics at a continental margin: Central North Island, New Zealand. *Review of Geophysics*, 44, p.RG4002. doi:10.1029/2005RG000171.

Wilson, C.J.N., Rogan, A.M., Smith, I.E.M., Northey, D.J., Nairn, I.A. & Houghton, B.F., 1984. Caldera volcanoes of the Taupo Volcanic Zone, New Zealand. *Journal of Geophysical Research*, 89(B10), pp.8463-84.